Title
A Study of Gold(I/III) Redox Events by Means of Photredox Catalysis

Author
Kim, Suhong

Publication Date
2019

Peer reviewed|Thesis/dissertation

A Study of Gold(I/III) Redox Events by Means of Photredox Catalysis

By

Suhong Kim

A dissertation submitted in partial satisfaction of the

requirements for the degree of

Doctor of Philosophy

in

Chemistry

in the

Graduate Division

of the

University of California, Berkeley

Committee in charge:

Professor F. Dean Toste, Chair
Professor Thomas J. Maimone
Professor Alexander Katz

Fall 2019

Abstract

A Study of Gold(I/III) Redox Events by Means of Photredox Catalysis

by

Suhong Kim

Doctor of Philosophy in Chemistry

University of California, Berkeley

Professor F. Dean Toste, Chair

Chapter 1. Photoredox Catalysis Unlocks Single-Electron Elementary Steps in Transition Metal Catalyzed Cross-Coupling

A brief survey of photoredox/transition metal dual catalysis is provided. The central message of this chapter is that the photoredox catalysis enables transition metal catalysts to access open-shell intermediates that could rapidly undergo desired elementary steps such as oxidative addition, transmetallation, and reductive elimination.

Chapter 2. Visible light-mediated gold-catalysed carbon(sp^2)-carbon(sp) cross-coupling

A dual photoredox and gold-catalysed cross-coupling reaction of alkynyltrimethylsilanes and aryldiazonium tetrafluoroborates is described. The reaction proceeds through visible-light mediated oxidative addition of aryldiazoniums, transmetalation of alkynyltrimethylsilanes and aryl-alkynyl reductive elimination. Exclusive selectivity for silyl-substituted alkynes is observed, with no reactivity observed for terminal alkynes.

Chapter 3. The Mechanism of Photoredox-Catalyzed C−C and C−N Bond Formation by Arylation of IPrAu(I)−CF_3 and IPrAu(I)−Succinimide

Herein we report on the photoredox-catalyzed gold-mediated C(sp^2)−CF_3 and C(sp^2)−N coupling reactions. By adopting gold as a platform for probing metallaphotoredox catalysis, we demonstrate that cationic gold(III) complexes are the key intermediates of the C−C and C−N coupling reactions. The high-valent gold(III) intermediates are accessed by virtue of photoredox catalysis through a radical chain process. In addition, the bond-forming step of the coupling reactions is the reductive elimination from cationic gold(III) intermediates, which is supported by isolation and crystallographic characterization of key Au(III) intermediates.

A Study of Gold(I/III) Redox Events by Means of Photredox Catalysis

Table of contents

List of Figures

List of Schemes

List of Tables

Acknowledgement

First, I want to thank Prof. Chulbom Lee for his excellent mentorship and all of the support during my undergraduate research at Seoul National University. He had introduced me to the world of synthetic organic chemistry and taught me the joy of solving chemistry problems. The experience I had under his guidance was crucial to my decision of pursuing chemistry Ph. D. degree at UC Berkeley.

Most importantly, I was able to complete the Ph. D. program because of the scientific and emotional support of my Ph. D. advisor, Prof. F. Dean Toste. He was the only reason why I have not withdrawn the Ph. D. program, although I struggled with various severe challenges during the past five years. He advocated me on behalf of my parents before the surgery with general anesthesia at the hospital and gave me a chance to retry the qualifying exam. All scientific discussions I have had with him so far have served as nutrients of my intellectual growth. It is unimaginable how big his influence on me. I decided to continue studying synthetic organic chemistry because I enjoyed researching and discussing chemistry in his group. In the retrospective view, I was so fortunate that I was able to work with Prof. Toste.

I also thank all the individuals I met during my time in the Toste group, especially senior members and postdoc of the group who was involved in my scientific development. I sincerely appreciate all the help I received from the gold(III) subgroup members, Dr. Matt Winston, Dr. Willie Wolf, and Dr. Mark Levin during my earlier years of graduate school. I want to thank my classmates Dr. John Lee, Dr. Patrick Bohan, and Dr. Alec Chirstian, for their friendship and support. I also thank Dr. Souvagya Biswas, Edward Miller, and all visiting students and undergraduates who I have worked together in a team.

Finally, I would like to thank my parents, Seungil Kim and Miock Bang, and my brother, Minkyu Kim, for support and love during my entire life.

Chapter 1.

Photoredox Catalysis Unlocks Single-Electron Elementary Steps in Transition Metal Catalyzed Cross-Coupling

1.1 Introduction

The ability for transition metal catalysts to forge bonds between ligated fragments has become a cornerstone of modern synthetic chemistry. Cross-coupling methodologies allow access to a variety of carbon-carbon and carbon-heteroatom coupled products via straightforward retrosynthetic disconnections, and the systematic exploration of this paradigm has expanded the canon of accessible reactivity to cover a wide swath of chemical space.[1]

The vast majority of these methodologies rely on the same three two-electron elementary steps as a means to accomplish their target transformation: oxidative addition, transmetallation, and reductive elimination (Figure 1). The centrality of these reactions is underscored by the numerous mechanistic studies conducted which outline the influence of the metal catalyst and its ligand environment. Unfortunately, despite the attention given to these polar mechanisms, many worthwhile challenges in this field remain.[2]

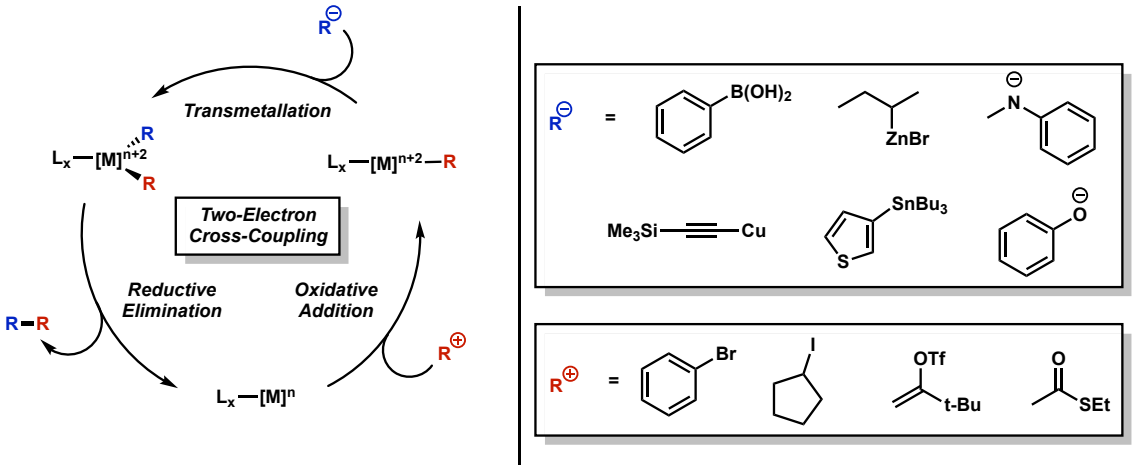

Figure 1.1 Generalized Mechanism for Cross Coupling and Representative Nucleophiles and Electrophiles

Meanwhile, it has long been known that the chemistry of 17- and 19-electron transition metal complexes is marked by dramatically faster rates compared to their even-electron congeners for virtually all elementary transformations.[3] Despite the wealth of stoichiometric precedent in this area, translation of odd-electron organometallic reactivity into mild catalytic reactions remained, until recently, far rarer than the two-electron analogues.

The key development in recent reports has been the implementation of visible-light photocatalysts as a means to induce the desired redox processes in a mild and selective manner. Examination of a generalized photoabsorption scheme reveals that such an activation mode is a natural means of accessing odd-electron intermediates (Figure 2). As noted by early studies on these photoredox catalysts, excited states become both stronger single-electron oxidants and single-electron reductants.[4–6] By employing

catalysts with absorption bands in the visible region of the spectrum (rather than in the ultraviolet), the source of open shell intermediates can be effectively controlled.[7,8]

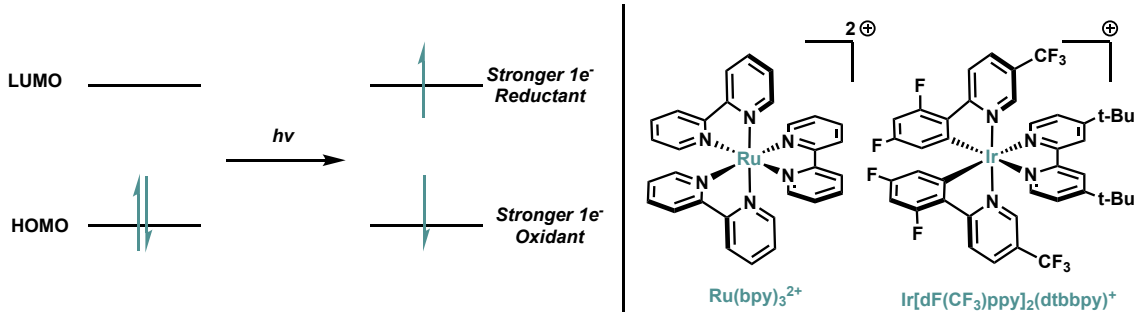

Figure 1.2 Simplified Photoabsorption Scheme and Commonly Employed Photoredox Catalysts

The rapid pace of recent developments combining photocatalysis with transition metal catalysis has prompted a survey of the field.[9] We have endeavored here, for instructive purposes, to organize these landmark examples by virtue of the elementary step in which the photocatalyst is engaged, as the guiding principles and mechanistic homologies of this new field are clearer when the catalyzed elementary steps are delineated. In each case, we aim to tie these novel catalytic methodologies back to their prior stoichiometric analogues as a means to both rationalize the observed reactivity and to inspire the next generation of technologies.

It is prudent to note that in many cases, the photocatalysts may serve as chain-initiators, with chain lengths measured for many photoredox processes exceeding one.[10] As such, we have chosen to abstract the involvement of these catalysts to the level of a photoinduced electron transfer (signified by an electron), rather than imply the specific species involved in any given reduction or oxidation event.[11] This Outlook is not meant as a comprehensive review[12–15] but rather as a tutorial, and the lessons involved do not hinge on the presence or absence of chain processes.[16]

1.2 Photocatalysis of Oxidative Addition

Oxidative addition involves the formation of bonds between a metal and an electrophilic substrate concomitant with the formal two-electron oxidation of the metal center.[2] In cross-coupling this step typically involves concerted oxidative addition of a carbon-halogen or carbon-pseudohalogen bond to generate the oxidized organometallic species. However, many metals and electrophiles undergo prohibitively slow reactions by this mechanism.

On the other hand, the facile addition of alkyl radicals to transition metals in both chain and non-chain processes has been studied in detail for a variety of complexes (Figure 3).[17] For example, photochemical initiation to generate isopropyl radical was shown to accelerate the oxidative addition of isopropyl iodide to Pt(II) via a radical chain

process.[18] Fluoroalkyl iodides similarly undergo radical chain oxidative additions to Au(I).[19,20] These precedents highlight the ability of otherwise sluggish oxidative addition processes to be facilitated by injection into a radical manifold.

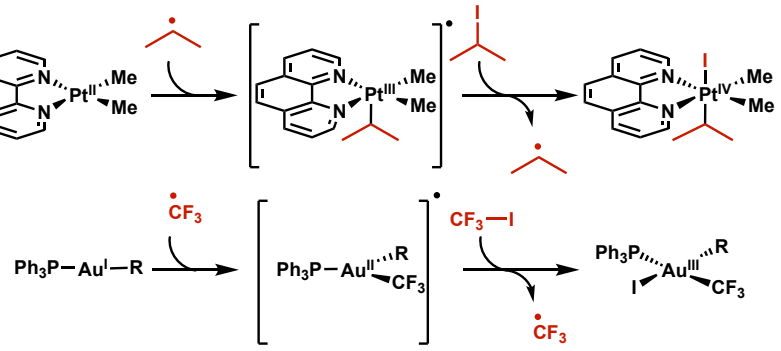

Figure 1.3 Stoichiometric Precedent: Radical Chain Oxidative Addition to Pt(II) and Au(I)

With a photoredox catalyst, the involvement of a photochemical process allows for the generation of the intermediate radical species in milder fashion and with transition metal catalysts kinetically incompetent for such an initiation on their own. In the most general scheme, an electrophilic reagent is reduced by a photoexcited species, leading to its radical congener. Subsequent addition to the metal species followed by oxidation yields the net oxidative addition product. In this way, the photocatalyst catalyzes the oxidative addition (Figure 4).

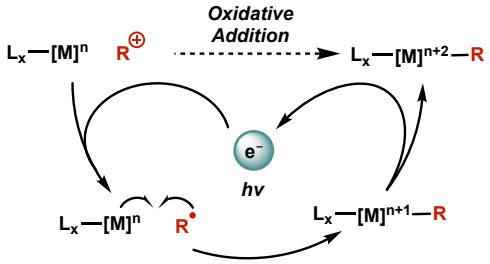

Figure 1.4 Generalized Scheme for Photoredox Catalysis of Oxidative Addition

One of the earliest examples of this activation mode in the context of catalysis is in Pd-catalyzed directed C-H functionalization (Figure 5).[21] Sanford and co-workers showed that in contrast to much harsher methods for accessing Pd(IV), which require elevated temperature, the use of aryldiazonium cations in combination with a photoredox catalyst allows the generation of the high-valent intermediate at room temperature. This was found to be broadly applicable with respect to the directing group employed and to the diazonium structure. Subsequent studies expanded this manifold to diaryliodonium electrophiles.[22]

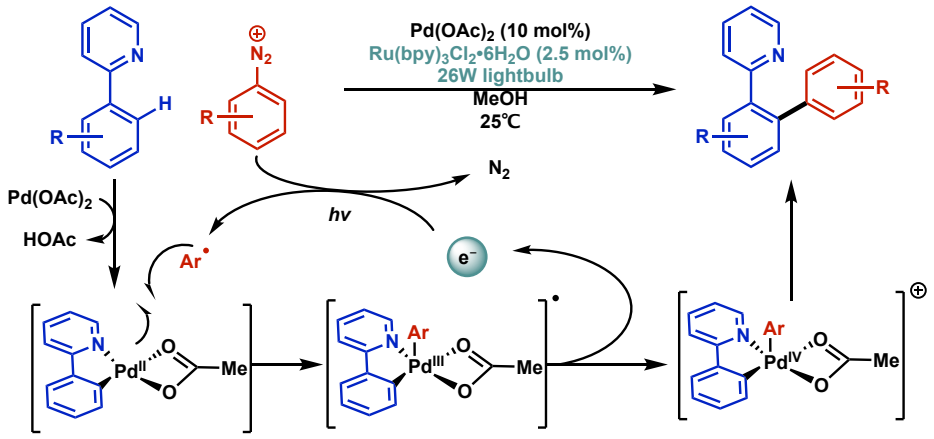

Figure 1.5 Catalytic Application: Palladium catalyzed C-H functionalization at room temperature via Pd(IV) intermediates generated by photoredox catalysis

This same strategy employing diazonium electrophiles was subsequently applied in the context of gold catalysis by the Glorius and Toste groups, providing access to highly reactive Au(III) intermediates in a straightforward fashion.[23,24] Initial studies focused on the activation of alkenes to provide oxy- and aminoarylated as well as ring expanded products (Figure 6).[25] Mechanistic investigations including time-resolved FT-IR, labelling studies, and DFT support a mechanism in which photocatalysis generates the Au(III)-aryl intermediate prior to intervention of the unsaturated substrate.[23,26] Subsequent studies have expanded the scope to a wide variety of Au-catalyzed reactions of alkynes[27–30], allenes[31], and heteroatom nucleophiles[32] allowing arylation to terminate catalytic cycles typically closed via protodeauration.

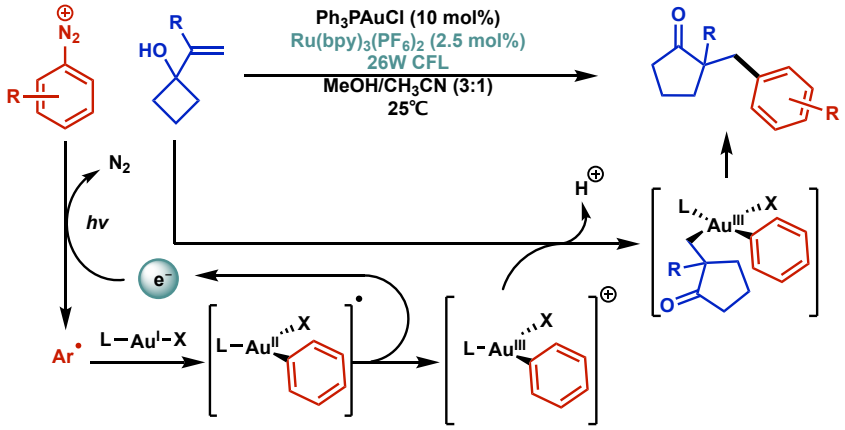

Figure 1.6 Catalytic Application: Gold catalyzed arylative ring expansion of vinylcyclobutanols via aryl-Au(III) intermediates generated by photoredox catalysis

Finally, a variant on this activation mode was demonstrated by Fu and Peters in which a copper catalyst serves as both the photocatalyst and ultimate bond-forming agent, albeit with UV rather than visible light in most cases. These processes vary in their nucleophiles and electrophiles, encompassing both aryl and alkyl halide substrates in C-

S[33], C-N[34–37], C-C[38,39], and C-O[40] forming reactions. Recent mechanistic studies have shown that the copper-mediated pathway involves photoinduced electron transfer from the nucleophile-cuprate complex followed by in-cage radical recombination to afford the coupled product, though oxidative addition and outer-sphere recombination could not be distinguished (Figure 7).[41] As such, it remains unclear the extent to which these precedents are analogous to other photoredox catalyzed oxidative additions. Nonetheless, a recent study demonstrated an enantioselective variant of this process for C-N bond formation.[42]

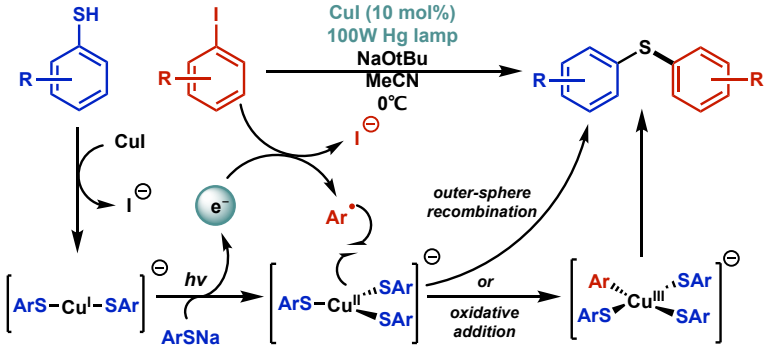

Figure 1.7 Catalytic Application: Copper catalyzed C-S bond formation via photoinduced electron transfer. Mechanistic experiments have not distinguished the two potential pathways

In addition to these illustrative examples, several other reports have emerged utilizing photoredox catalysis to enable oxidative addition. Notably, the combination of photoredox catalysts with copper has enabled mild C-fluoroalkyl and C-N coupling reactions to occur.[43,44]

1.3 Photocatalysis of Reductive Elimination

Reductive elimination involves the formation of a new bond between ligands bound to a metal with concomitant 2-electron reduction of the metal center.[2] As the key bond forming step in cross coupling reactions, this process has been widely explored for diverse combinations of metals and ligands, and virtually all classes of reductive elimination are precedented in the literature. Nonetheless, there remain examples for which bond formation is prohibitively slow.

Again, the literature surrounding single-electron processes provides a potential solution[45,46]; seminal studies by Kochi and Hillhouse show that complexes which are inert to reductive elimination or which undergo unselective decomposition can be coaxed to perform the desired bond-forming process by single-electron oxidation with a diverse array of oxidants (Figure 8).[47,48]

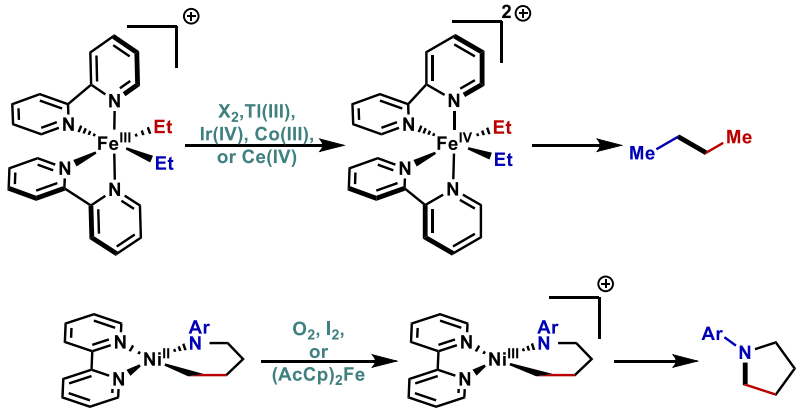

Figure 1.8 Stoichiometric Precedent: Oxidatively Induced Reductive Elimination from Fe(IV) and Ni(III).

It is not a far cry, then, to imagine application of a photoredox catalyst to accomplish such a transformation in a dual catalytic process. "Temporary" oxidation of the metal catalyst followed by re-reduction following the desired reductive elimination allows photocatalysis of this elementary step, as outlined in Figure 9.

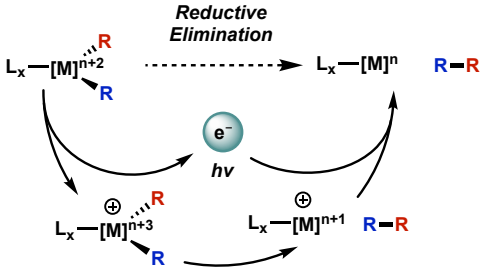

Figure 1.9 Generalized Scheme for Photoredox Catalysis of Reductive Elimination

A powerful realization of this activation strategy was employed by the Macmillan group in a nickel-catalyzed C-O coupling aided by an iridium photocatalyst (Figure 10).[49] In addition to demonstrating the scope of this process for a range of coupling partners, stoichiometric experiments on an isolated Ni(II)-aryl alkoxide complex clearly demonstrate the crucial influence of the photoredox catalyst on the desired reductive elimination process.

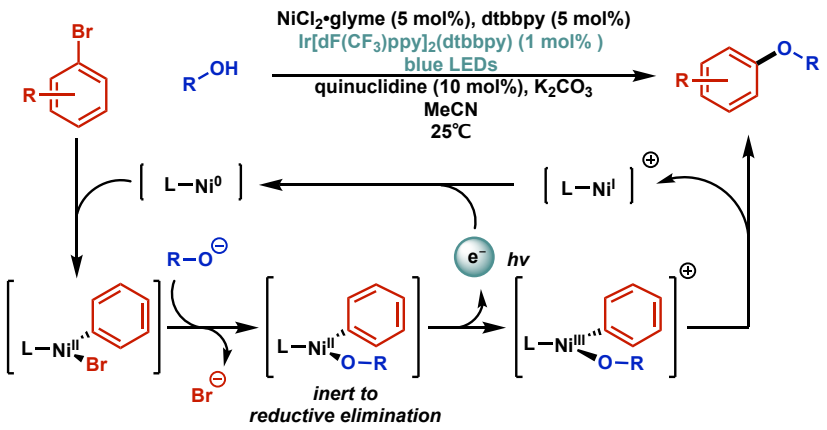

Figure 1.10 Catalytic Application: Nickel catalyzed etherification with C-O reductive elimination enabled via photoredox catalysis

A second example from Jamison and coworkers concerns the synthesis of indolines via the coupling of ortho-iodoaniline derivatives with alkenes (Figure 11).[50] Having observed that small amounts of the desired indoline product were formed upon exposure of the reaction mixture to air, they employed a photoredox catalyst to serve as a reversible means to access the requisite Ni(III) intermediate. The proposed mechanism bears many similarities to the example in Figure 10.

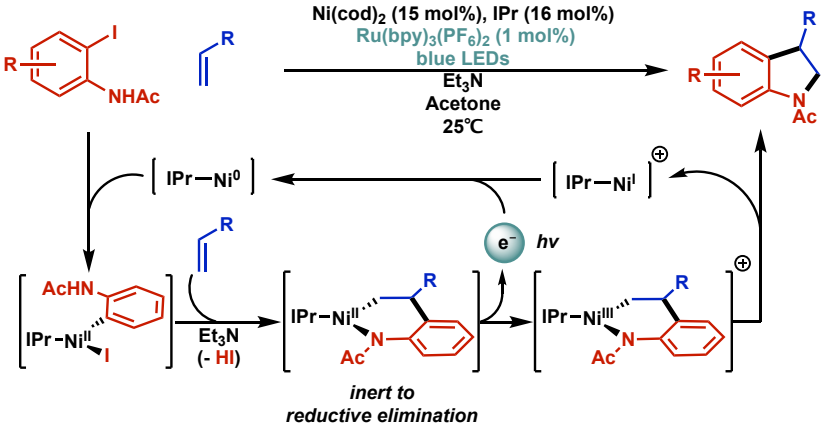

Figure 1.11 Catalytic Application: Nickel catalyzed Larock-type indoline synthesis with C-N reductive elimination enabled via photoredox catalysis

1.4 Photocatalysis of Transmetallation

Transmetallation involves the formation of a bond between a nucleophilic substrate and a metal, with no change in formal oxidation state of the metal.[2] These reactions typically involve displacement of a metal halide, and are by far the most complex mechanistically. Despite several in-depth studies into the underlying elementary steps, many transmetallation processes remain poorly understood.[51–53] Worse yet,

transmetallation of sp^3 alkyl fragments is typically challenging, requiring the use of sensitive reagents or harsh conditions.

In this arena, limited stoichiometric precedent employing open-shell intermediates has been reported; as such, the simultaneous discovery by the Macmillan, Doyle, and Molander groups that photoredox catalysis can be used to enable mild transmetallation from otherwise weakly nucleophilic coupling partners is perhaps even more impressive.[54,55]

Though many mechanisms have been proposed, the general scheme for such a photocatalyzed transmetallation can be conceived as follows: single electron oxidation of a nucleophile and subsequent reduction of a transition metal complex generates complementary odd-electron species which can then efficiently undergo recombination (Figure 12). The order of these two steps can likely be inverted, and other elementary steps can intervene, but the sense of redox is likely maintained regardless of the conditions employed.

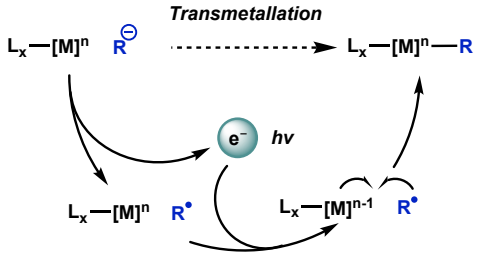

Figure 1.12 Generalized Scheme for Photoredox Catalysis of Transmetallation

Beyond the mechanistic novelty in these processes, a striking feature of all systems developed to date is that the nucleophiles employed are all air-stable, easily prepared, and yet still capable of effectively delivering sp^3 nucleophiles to transition metal centers. Four main classes of photoredox-activated alkyl nucleophiles have been developed: Carboxylates[54,56–59], Alkyl Trifluoroborates[55,60–65], Alkyl Silicates[66–70], and □-heteroatom C-H bonds[54,71,72]. In each, oxidation generates an alkyl radical via a subsequent fragmentation process, generating CO_2, BF_3, bis(catecholato)silane, or acid, respectively.

The most comprehensive mechanistic experiments and DFT calculations have been carried out for the nickel-catalyzed variants of these processes, and the studies support a process in which a Ni(0) intermediate combines with the nascent radical species to generate the corresponding Ni(I) alkyl.[73,74] The overall cycle is then closed via oxidative addition of the sp^2 halide coupling partner, reductive elimination from Ni(III), and single electron reduction to regenerate the Ni(0) complex. Two representative examples are shown in Figure 13, including a recently reported enantioselective method leveraging this protocol to generated enantioenriched benzylic amines in a stereoconvergent fashion[75].

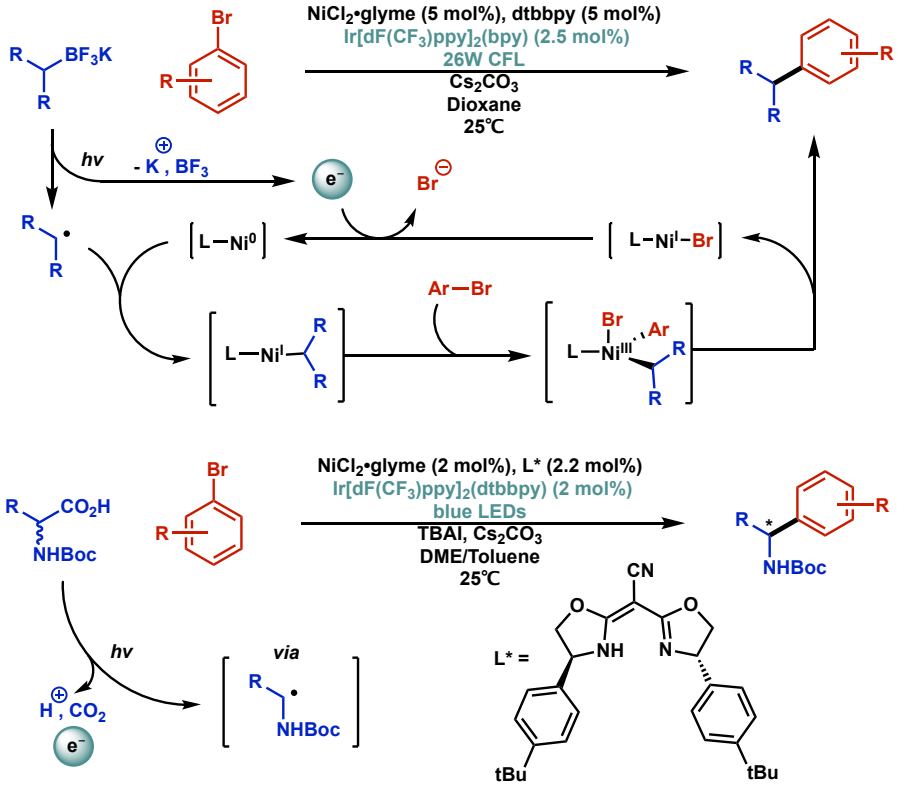

Figure 1.13 Catalytic Applications: Nickel catalyzed Csp^3-Csp^2 coupling reactions of alkyltrifluoroborates (racemic) and amino acids (enantioselective)

An interesting application of the carboxylate nucleophiles has been reported in which the carboxylate moiety is generated by oxidative addition to palladium forming a π-allyl intermediate.[76,77] Other photoredox-facilitated transmetallations in cross-coupling have also been reported.[78–80]

1.5 Conclusions and Outlook

The leveraging of single-electron chemistry via the enabling technology of photoredox catalysis has clearly opened new doors in the realm of transition metal catalyzed cross-coupling. The motifs outlined herein are only some of the powerful new strategies accessed by this fruitful marriage of catalytic modes.[81–85] For example, several reports have employed photoredox catalysts to access oxidative cross-couplings with a variety of transition metals.[86–93]

Moreover, there still exist stoichiometric precedents in single-electron acceleration of reactivity which have yet to be realized in a catalytic sense. One potentially instructive example of an accelerated migratory insertion is the documented catalysis of alkyl carbonylation at iron via single electron oxidation (Figure 14); a dual

catalytic coupling reaction making use of this behavior is likely possible by some combination of photoredox and transition metal catalysts.[94]

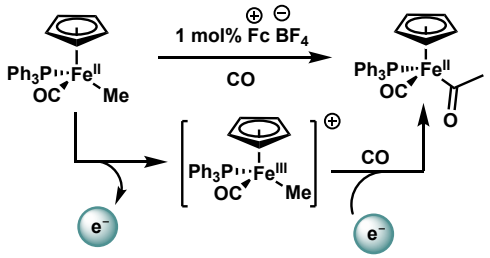

Figure 1.14 Redox Catalysis of Migratory Insertion

Though the power of open-shell intermediates to provide rapid turnover has evidently been demonstrated, there are a number of challenges that lie ahead. For one, while the stereoconvergent nature of radical addition to transition metals has allowed the development of enantioselective processes[75], it also imposes limitations in the diastereoselection process for radical transmetallation[62], making the synthesis of mismatched stereoisomers a more complex problem (Figure 15).[95]

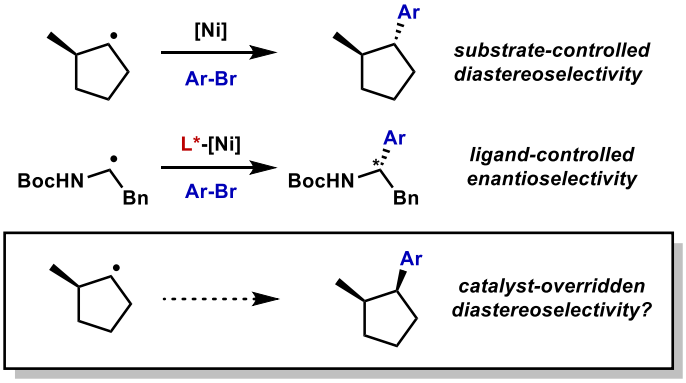

Figure 1.15 Stereoconvergence and Diastereoselectivity in Nickel Catalyzed Radical Cross Coupling

These challenges should be taken as a call to action, as the power demonstrated in the reports thus far suggests a wealth of untapped reactivity. Most tantalizingly, the involvement of a photoprocess suggests that endergonic transformations may be possible in these catalytic reactions.[96]

Additionally, there are a wide variety of photoredox catalysts and metals yet to be engaged in dual catalytic reactions. Recent reports of photoinduced electron transfer from supramolecular host complexes[97] is particularly intriguing given the synergy displayed between transition metal catalysts and supramolecular catalysts.[98]

Furthermore, the combination of more than one of the activation modes presented herein, though challenging, promises to enable progressively more complex transformations to be developed. To date, no sp^3-sp^3 C-C coupling protocols have taken

advantage of the newly discovered photoredox manifolds, but such an advance, not to mention many others, is undoubtedly on the horizon.

1.6 References and Notes

(1) Johansson Seechurn, C. C. C.; Kitching, M. O.; Colacot, T. J.; Snieckus, V. *Angew. Chem., Int. Ed.* **2012**, *51*, 5062–5085.

(2) Hartwig, J. F. *Organotransition Metal Chemistry: From Bonding to Catalysis*; University Science Books, 2010.

(3) Stiegman, A. E.; Tyler, D. R. *Comments Inorg. Chem.* **1986**, *5*, 215–245.

(4) Gafney, H. D.; Adamson, A. W. *J. Am. Chem. Soc.* **1972**, *94*, 8238–8239.

(5) Lowry, M. S.; Goldsmith, J. I.; Slinker, J. D.; Rohl, R.; Pascal, R. A. Jr.; Malliaras, G. G.; Bernhard, S. *Chem. Mater.* **2005**, *17*, 5712–5719.

(6) Slinker, J. D.; Gorodetsky, A. A.: Lowry, M. S.; Wang, J.; Parker, S.; Rohl, R.; Bernhard, S.; Malliaras, G. G. *J. Am. Chem. Soc.* **2004**, *126*, 2763–2767.

(7) Yoon, T. P.; Ischay, M. A.; Du, J. *Nat. Chem.* **2010**, *2*, 527–532.

(8) Prier, C. K.; Rankic, D. A.; MacMillan, D. W. C. *Chem. Rev.* **2013**, *113*, 5322–5363.

(9) Hopkinson, M. N.; Sahoo, B.; Li, J.; Glorius, F. *Chem. – Eur. J.* **2014**, *20*, 3874–3886.

(10) Cismesia, M. A.; Yoon, T. P. *Chem. Sci.* **2015**, *6*, 5426–5434.

(11) Studer, A.; Curran, D. P. *Nat. Chem.* **2014**, *6*, 765–773.

(12) We have elected not to discuss examples of photoredox and transition metal dual catalysis (ref 13,14) and sequential, photoredox and metal catalyzed steps (ref 15,16).

(13) Huo, H.; Shen, X.; Wang, C.; Zhang, L.; Rose, P.; Chen, L.; Harms, K.; Marsch, M.; Hilt, G.; Meggers, E. *Nature* **2014**, *515*, 100–103.

(14) Du, J.; Skubi, K. L.; Schultz, D. M.; Yoon, T. P. *Science* **2014**, *344*, 392–396.

(15) Rueping, M.; Koenigs, R. M.; Poscharny, K.; Fabry, D. C.; Leonori, D.; Vila, C. *Chem. – Eur. J.* **2012**, *18*, 5170–5174.

(16) Two mechanistic possibilities not discussed herein include photoinduced energy transfer and outer-sphere free radical coupling. Where possible we have relied on studies where mechanistic experiments discount these alternatives.

(17) Halpern, J. *Acc. Chem. Res.* **1970**, *3*, 386–392.

(18) Hill, R. H.; Puddephatt, R. J. *J. Am. Chem. Soc.* **1985**, *107*, 1218–1225.

(19) Johnson, A.; Puddephatt, R. J. *J. Chem. Soc. Dalton Trans.* **1976**, 1360–1363.

(20) Winston, M. S.; Wolf, W. J.; Toste, F. D. *J. Am. Chem. Soc.* **2014**, *136*, 7777–7782.

(21) Kalyani, D.; McMurtrey, K. B.; Neufeldt, S. R.; Sanford, M. S. *J. Am. Chem. Soc.* **2011**, *133*, 18566–18569.

(22) Neufeldt, S. R.; Sanford, M. S. *Adv. Synth. Catal.* **2012**, *354*, 3517–3522.

(23) Shu, X.; Zhang, M.; He, Y.; Frei, H.; Toste, F. D. *J. Am. Chem. Soc.* **2014**, *136*, 5844–5847.

(24) Sahoo, B.; Hopkinson, M. N.; Glorius, F. *J. Am. Chem. Soc.* **2013**, *135*, 5505–5508.

(25) Hopkinson, M. N.; Sahoo, B.; Glorius, F. *Adv. Synth. Catal.* **2014**, *356*, 2794–2800.

(26) Zhang, Q.; Zhang, Z.; Fu, Y.; Yu, H. *ACS Catal.* **2016**, *6*, 798–808.

(27) Tlahuext-Aca, A.; Hopkinson, M. N.; Garza-Sanchez, R. A.; Glorius, F. *Chem. – Eur. J.* **2016**, *22*, 5909–5913.

(28) Tlahuext-Aca, A.; Hopkinson, M. N.; Sahoo, B.; Glorius, F. *Chem. Sci.* **2016**, *7*, 89–93.

(29) Um, J.; Yun, H.; Shin, S. *Org. Lett.* **2016**, *18*, 484–487.

(30) Kim, S.; Rojas-Martin, J.; Toste, F. D. *Chem. Sci.* **2016**, *7*, 85–88.

(31) Patil, D. V.; Yun, H.; Shin, S. *Adv. Synth. Catal.* **2015**, *357*, 2622–2628.

(32) He, Y.; Wu, H.; Toste, F. D. *Chem. Sci.* **2015**, *6*, 1194–1198.

(33) Uyeda, C.; Tan, Y.; Fu, G. C.; Peters, J. C. *J. Am. Chem. Soc.* **2013**, *135*, 9548–9552.

(34) Bissember, A. C.; Lundgren, R. J.; Creutz, S. E.; Peters, J. C.; Fu, G. C. *Angew. Chem., Int. Ed.* **2013**, *52*, 5129–5133.

(35) Ziegler, D. T.; Choi, J.; Muñoz-Molina, J. M.; Bissember, A. C.; Peters, J. C.; Fu, G. C. *J. Am. Chem. Soc.* **2013**, *135*, 13107–13112.

(36) Do, H.; Bachman, S.; Bissember, A. C.; Peters, J. C.; Fu, G. C. *J. Am. Chem. Soc.* **2014**, *136*, 2162–2167.

(37) Creutz, S. E.; Lotito, K. J.; Fu, G. C.; Peters, J. C. *Science* **2012**, *338*, 647–651.

(38) Yang, F.; Koeller, J.; Ackermann, L. *Angew. Chem., Int. Ed.* **2016**, *55*, 4759–4762.

(39) Ratani, T. S.; Bachman, S.; Fu, G. C.; Peters, J. C. *J. Am. Chem. Soc.* **2015**, *137*, 13902–13907.

(40) Tan, Y.; Munoz-Molina, J. M.; Fu, G. C.; Peters, J. C. *Chem. Sci.* **2014**, *5*, 2831–2835.

(41) Johnson, M. W.; Hannoun, K. I.; Tan, Y.; Fu, G. C.; Peters, J. C. *Chem. Sci.* **2016**, *7*, 4091–4100.

(42) Kainz, Q. M.; Matier, C. D.; Bartoszewicz, A.; Zultanski, S. L.; Peters, J. C.; Fu, G. C. *Science* **2016**, *351*, 681–684.

(43) Ye, Y.; Sanford, M. S. *J. Am. Chem. Soc.* **2012**, *134*, 9034–9037.

(44) Yoo, W.; Tsukamoto, T.; Kobayashi, S. *Org. Lett.* **2015**, *17*, 3640–3642.

(45) Komiya, S.; Albright, T. A.; Hoffmann, R.; Kochi, J. K. *J. Am. Chem. Soc.* **1977**, *99*, 8440–8447.

(46) Han, R.; Hillhouse, G. L. *J. Am. Chem. Soc.* **1997**, *119*, 8135–8136.

(47) Lau, W.; Huffman, J. C.; Kochi, J. K. *Organometallics* **1982**, *1*, 155–169.

(48) Koo, K.; Hillhouse, G. L. *Organometallics* **1995**, *14*, 4421–4423.

(49) Terrett, J. A.; Cuthbertson, J. D.; Shurtleff, V. W.; MacMillan, D. W. C. *Nature* **2015**, *524*, 330–334.

(50) Tasker, S. Z.; Jamison, T. F. *J. Am. Chem. Soc.* **2015**, *137*, 9531–9534.

(51) Carrow, B. P.; Hartwig, J. F. *J. Am. Chem. Soc.* **2011**, *133*, 2116–2119.

(52) Amatore, C.; Grimaud, L.; Le Duc, G.; Jutand, A. *Angew. Chem., Int. Ed.* **2014**, *53*, 6982–6985.

(53) Casado, A. L.; Espinet, P. *J. Am. Chem. Soc.* **1998**, *120*, 8978–8985.

(54) Zuo, Z.; Ahneman, D. T.; Chu, L.; Terrett, J. A.; Doyle, A. G.; MacMillan, D. W. C. *Science* **2014**, *345*, 437–440.

(55) Tellis, J. C.; Primer, D. N.; Molander, G. A. *Science* **2014**, *345*, 433–436.

(56) Chu, L.; Lipshultz, J. M.; MacMillan, D. W. C. *Angew. Chem., Int. Ed.* **2015**, *54*, 7929–7933.

(57) Le, C. C.; MacMillan, D. W. C. *J. Am. Chem. Soc.* **2015**, *137*, 11938–11941.

(58) Noble, A.; McCarver, S. J.; MacMillan, D. W. C. *J. Am. Chem. Soc.* **2015**, *137*, 624–627.

(59) Luo, J.; Zhang, J. *ACS Catal.* **2016**, *6*, 873–877.

(60) El Khatib, M.; Serafim, R. A. M.; Molander, G. A. *Angew. Chem., Int. Ed.* **2016**, *55*, 254–258.

(61) Ryu, D.; Primer, D. N.; Tellis, J. C.; Molander, G. A. *Chem. – Eur. J.* **2016**, *22*, 120–123.

(62) Primer, D. N.; Karakaya, I.; Tellis, J. C.; Molander, G. A. *J. Am. Chem. Soc.* **2015**, *137*, 2195–2198.

(63) Karakaya, I.; Primer, D. N.; Molander, G. A. *Org. Lett.* **2015**, *17*, 3294–3297.

(64) Amani, J.; Sodagar, E.; Molander, G. A. *Org. Lett.* **2016**, *18*, 732–735.

(65) Yamashita, Y.; Tellis, J. C.; Molander, G. A. *Proc. Natl. Acad. Sci.* **2015**, *112*, 12026–12029.

(66) Jouffroy, M.; Primer, D. N.; Molander, G. A. *J. Am. Chem. Soc.* **2016**, *138*, 475–478.

(67) Jouffroy, M.; Kelly, C. B.; Molander, G. A. *Org. Lett.* **2016**, *18*, 876–879.

(68) Patel, N. R.; Kelly, C. B.; Jouffroy, M.; Molander, G. A. *Org. Lett.* **2016**, *18*, 764–767.

(69) Jouffroy, M.; Davies, G. H. M.; Molander, G. A. *Org. Lett.* **2016**, 10.1021/acs.orglett.6b00466.

(70) Leveque, C.; Chenneberg, L.; Corce, V.; Goddard, J.; Ollivier, C.; Fensterbank, L. *Org. Chem. Front.* **2016**, 10.1039/c6qo00014b.

(71) Joe, C. L.; Doyle, A. G. *Angew. Chem., Int. Ed.* **2016**, *55*, 4040–4043.

(72) Xuan, J.; Zeng, T.; Feng, Z.; Deng, Q.; Chen, J.; Lu, L.; Xiao, W.; Alper, H. *Angew. Chem., Int. Ed.* **2015**, *54*, 1625–1628.

(73) Gutierrez, O.; Tellis, J. C.; Primer, D. N.; Molander, G. A.; Kozlowski, M. C. *J. Am. Chem. Soc.* **2015**, *137*, 4896–4899.

(74) Oderinde, M. S.; Varela-Alvarez, A.; Aquila, B.; Robbins, D. W.; Johannes, J. W. *J. Org. Chem.* **2015**, *80*, 7642–7651.

(75) Zuo, Z.; Cong, H.; Li, W.; Choi, J.; Fu, G. C.; MacMillan, D. W. C. *J. Am. Chem. Soc.* **2016**, *138*, 1832–1835.

(76) Lang, S. B.; O'Nele, K. M.; Tunge, J. A. *J. Am. Chem. Soc.* **2014**, *136*, 13606–13609.

(77) Lang, S. B.; O'Nele, K. M.; Douglas, J. T.; Tunge, J. A. *Chem. – Eur. J.* **2015**, *21*, 18589–18593.

(78) Cheng, W.; Shang, R.; Yu, H.; Fu, Y. *Chem. – Eur. J.* **2015**, *21*, 13191–13195.

(79) Xuan, J.; Zeng, T.; Chen, J.; Lu, L.; Xiao, W. *Chem. – Eur. J.* **2015**, *21*, 4962–4965.

(80) Oderinde, M. S.; Frenette, M.; Robbins, D. W.; Aquila, B.; Johannes, J. W. *J. Am. Chem. Soc.* **2016**, *138*, 1760–1763.

(81) This includes cases where the role of the photoredox catalyst are unclear (ref 83, 84).

(82) Zhang, G.; Liu, C.; Yi, H.; Meng, Q.; Bian, C.; Chen, H.; Jian, J.; Wu, L.; Lei, A. *J. Am. Chem. Soc.* **2015**, *137*, 9273–9280.

(83) Sagadevan, A.; Ragupathi, A.; Lin, C.; Hwu, J. R.; Hwang, K. C. *Green Chem.* **2015**, *17*, 1113–1119.

(84) Osawa, M.; Nagai, H.; Akita, M. *Dalton Trans.* **2007**, 827–829.

(85) Inagaki, A.; Edure, S.; Yatsuda, S.; Akita, M. *Chem. Commun.* **2005**, 5468–5470.

(86) Choi, S.; Chatterjee, T.; Choi, W. J.; You, Y.; Cho, E. J. *ACS Catal.* **2015**, *5*, 4796–4802.

(87) Yoo, W.; Tsukamoto, T.; Kobayashi, S. *Angew. Chem., Int. Ed.* **2015**, *54*, 6587–6590.

(88) Fabry, D. C.; Zoller, J.; Raja, S.; Rueping, M. *Angew. Chem., Int. Ed.* **2014**, *53*, 10228–10231.

(89) Fabry, D. C.; Ronge, M. A.; Zoller, J.; Rueping, M. *Angew. Chem., Int. Ed.* **2015**, *54*, 2801–2805.

(90) Zoller, J.; Fabry, D. C.; Ronge, M. A.; Rueping, M. *Angew. Chem., Int. Ed.* **2014**, *53*, 13264–13268.

(91) Xu, N.; Li, P.; Xie, Z.; Wang, L. *Chem. – Eur. J.* **2016**, *22*, 2236–2242.

(92) Zhou, C.; Li, P.; Zhu, X.; Wang, L. *Org. Lett.* **2015**, *17*, 6198–6201.

(93) Zhong, J.; Wu, C.; Meng, Q.; Gao, X.; Lei, T.; Tung, C.; Wu, L. *Adv. Synth. Catal.* **2014**, *356*, 2846–2852.

(94) Magnuson, R. H.; Meirowitz, R.; Zulu, S. J.; Giering, W. P. *Organometallics* **1983**, *2*, 460–462.

(95) This is in contrast to 2-electron transmetallations and oxidative additions which have been shown to occur with both retentive and invertive stereospecificity depending on the conditions employed.

(96) Many reported transformations occur with concomitant release of a gaseous byproduct, complicating analysis of the energetics due to entropic factors.

(97) Dalton, D. M.; Ellis, S. R.; Nichols, E. M.; Mathies, R. A.; Toste, F. D.; Bergman, R. G.; Raymond, K. N. *J. Am. Chem. Soc.* **2015**, *137*, 10128–10131.

(98) Kaphan, D. M.; Levin, M. D.; Bergman, R. G.; Raymond, K. N.; Toste, F. D. *Science* **2015**, *350*, 1235–1238.

Chapter 2.

Visible light-mediated gold-catalysed carbon(sp^2)-carbon(sp) cross-coupling

2.1 Introduction

For over a decade, homogeneous gold catalysis has been investigated because it provides access to novel modes of reactivity and enables rapid generation of complex molecular architectures.[1-6] However, in contrast to other low-valent late transition metal catalysts, the majority of gold(I) complexes are unreactive towards the oxidative addition of aryl and vinyl halides and pseudohalides.[7-11] Consequently, most gold-catalysed cross-coupling reactions have required sacrificial oxidants to access the +3 oxidation state.[12-23] For example, this reactivity platform has been exploited in a gold-catalysed oxidative coupling of organosilanes and 1,2-alkene functionalizations (Scheme 1A). As an alternative, visible light-mediated oxidative addition of aryldiazoniums has emerged as a method for the generation of the requisite gold(III) intermediates via photoredox catalysis, thereby obviating the need for sacrificial oxidants.[24-27] These gold(III) intermediates have been intercepted by a variety of nucleophiles in dual catalytic photoredox–gold reactions (Scheme 1B).

Although aryldiazoniums and photoredox catalysts provide an efficient method to generate gold(III) intermediates, several challenges must be addressed in order to facilitate carbon– carbon cross-coupling via these species. First, aryldiazonium salts are highly electrophilic and reactive towards many classes of nucleophilic coupling partners. Aryldiazoniums are generally decomposed under Kumada and Negishi coupling conditions and do not tolerate ligand additives and stoichiometric bases employed in the majority of Suzuki, Sonogashira and Hiyama coupling reactions.[28] Second, as visible light-mediated oxidative addition of aryldiazoniums is proposed to proceed through radical intermediates, nucleophilic coupling partners that can participate in single electron transfer, such as organotin and organotrifluoroborates compounds, are problematic.[29-30] Inspired by the oxidative coupling of organosilanes, we envisioned that the gold(III) complexes generated via photoredox catalysis might undergo transmetalation with organosilanes, generating an intermediate poised for carbon–carbon bond formation through reductive elimination.[31-41]

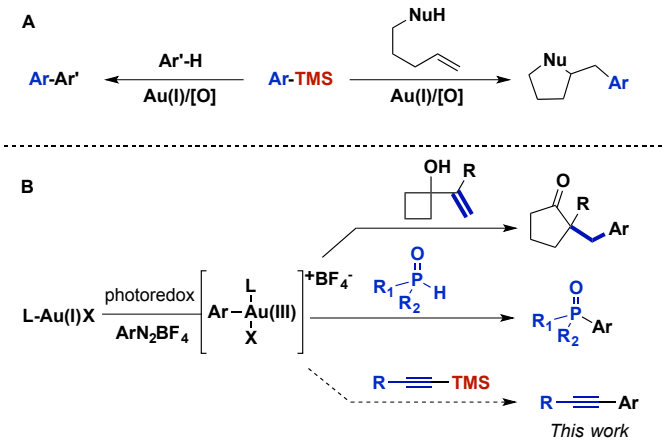

Scheme 2.1 Photoredox catalyst and visible light-mediated Au^{I}/Au^{III} catalysis

2.2 Results and discussions

While aryldiazonium tetrafluoroborates have been shown to react with halo-, azido-, allyl- and thiotrimethylsilanes, their reactions with alkynyltrimethylsilanes has not been previously reported.[42-44] Additionally, previous reports of organosilane transmetallation with gold lead us to hypothesize that the transmetallation of alkynyltrimethylsilanes to gold(III) intermediates might result in productive cross-coupling. On the basis of this hypothesis, we examined the combined gold/photoredox coupling of 1 equivalent of aryldiazonium salt **1a** and 1 equivalent of alkynyltrimethylsilane **2**.

Table 2.1 Optimization of reaction conditions

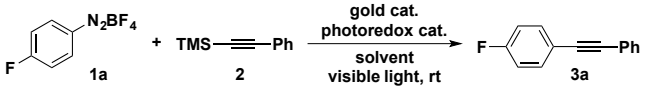

Entry	Gold cat.	Photoredox cat.	Solvent	Yield[a]
1	Ph_3PAuCl	$Ru(bpy)_3(PF_6)_2$	CH_3CN	70
2	Ph_3PAuCl	$Ru(bpy)_3(PF_6)_2$	Acetone	39
3	Ph_3PAuCl	$Ru(bpy)_3(PF_6)_2$	CH_3NO_2	15
4	Ph_3PAuCl	$Ru(bpy)_3(PF_6)_2$	DMF	10
5	Ph_3PAuCl	$Ru(bpy)_3(PF_6)_2$	MeOH	18
6	Ph_3PAuCl	$Ru(bpy)_3(PF_6)_2$	EtOH	4
7	Ph_3PAuCl	$Ir(ppy)_3$	CH_3CN	21
8	Ph_3PAuCl	$Ir(ppy)_2(dtbbpy)PF_6$	CH_3CN	45
9	$(p\text{-MeOPh})_3PAuCl$	$Ru(bpy)_3(PF_6)_2$	CH_3CN	73
10	$(p\text{-}CF_3Ph)_3PAuCl$	$Ru(bpy)_3(PF_6)_2$	CH_3CN	43
11	$(p\text{-tol})_3PAuCl$	$Ru(bpy)_3(PF_6)_2$	CH_3CN	72
12	$(o\text{-tol})_3PAuCl$	$Ru(bpy)_3(PF_6)_2$	CH_3CN	17
13	Cy_3PAuCl	$Ru(bpy)_3(PF_6)_2$	CH_3CN	48
14	Ph_3PAuCl	-	CH_3CN	0
15	Ph_3PAuCl	$Ru(bpy)_3(PF_6)_2$	CH_3CN	0[b]

Reaction conditions: aryldiazonium tetrafluoroborate **1a** (0.2 mmol, 1 equiv.), 1-trimethylsily-2-phenylacetylene **2** (0.2 mmol, 1 equiv.), gold catalyst (5 mol%), photoredox catalyst (1 mol%), solvent (2 mL), N_2 atmosphere, visible light, R.T. for 6 h. [a] GC yields. [b] The reaction was run in the drak.

Evaluation of reaction conditions showed that the combination of Ar_3PAuCl and $Ru(bpy)_3(PF_6)_2$, in acetonitrile gave the highest yield of aryl alkyne **3a** (Table 1). Changing either the solvent or the photoredox catalyst proved detrimental to the yield of the desired product. With respect to the ligands on the gold catalyst, both electronic and steric factors impacted the efficiency of the cross-coupling. For example, electron-deficient triarylphosphine ligands resulted in significantly lower yield of **3a** (Table 1, entry 10). The sterics of the ligand showed an even more dramatic effect on reaction yield. The reaction conducted with $(p\text{-tol})_3PAuCl$ provided 72% yield of the desired product, while the much more hindered $(o\text{-tol})_3PAuCl$-catalysed reaction only provided

17% yield of **3a** (Table 1, entry 11 and 12). The yield of product was lower when tricyclohexylphosphinegold(I) chloride was used as catalyst instead of triphenylphoshinegold(I) chloride (Table 1, entry 13). Gold(I) complexes of dialkylbiarylphosphine were also examined, but all showed less than 5% yield due to the combined effect of dialkyl groups and the steric effect of biaryl groups. Finally, no coupling product was observed in the absence of the ruthenium catalyst (entry 14) or when the reaction was conducted in the dark (entry 15).

Table 2.2 Scope of aryldiazonium tetrafluoroborates

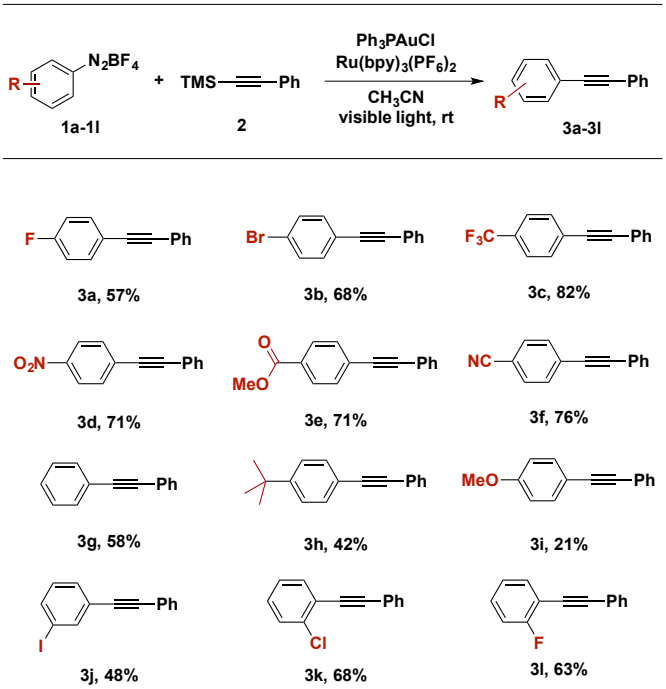

Reaction conditions: **1a-1l** (0.24 mmol, 1.2 equiv.), **2** (0.2 mmol, 1.0 equiv.), Ph_3PAuCl (10 mol%), $Ru(bpy)_3(PF_6)_2$ (2 mol%), acetonitrile (2 mL), N_2 atmosphere, visible light, R.T. for 3 h. Isolated yields.

With an optimized catalyst system in hand, the scope with respect to the aryldiazonium coupling partner was examined (Table 2). The yields of alkynylation reactions of electron-poor aryldiazonium salts were generally higher than those of reactions with electron-rich aryldiazonium coupling partners. It should be noted that the intrinsic instability of *ortho*-substituted aryldiazonium salts limited their use in this transformation (Table 2, entry **3k** and **3l**). It is also noteworthy that all halogen substitutions on the aryldiazonium coupling partner were preserved during the coupling reaction. Bromo- and iodoaryldiazonium salts were readily coupled and leaving halides intact for use in further reactions (Table 2, **3b** and **3j**); this chemoselectivity is challenging under typical palladiumcatalysed Sonogashira coupling reactions. [45-50]

The difference in reactivity of electron-rich and -poor aryldiazoniums may be the result of competing reaction pathways. Oxidative addition is believed to proceed through

single electron reduction of aryldiazoniums and this process is preferred with electron-poor aryldiazonium salts.[24-27] On the other hand, the generation of aryl cations, through loss of dinitrogen, is facile with electron-rich aryldiazoniums. Correspondingly, we observed trace amount of desired product when benzenediazonium tetrafluoroborate was heated at 60 °C for 9 hours in the presence of 1-trimethylsilyl-2-(4-methoxy)phenylacetylene; however the same reactivity was not observed with 4-fluorophenyldiazonium salts on the same conditions.

Table 2.3 Scope of alkynyltrimethylsilanes

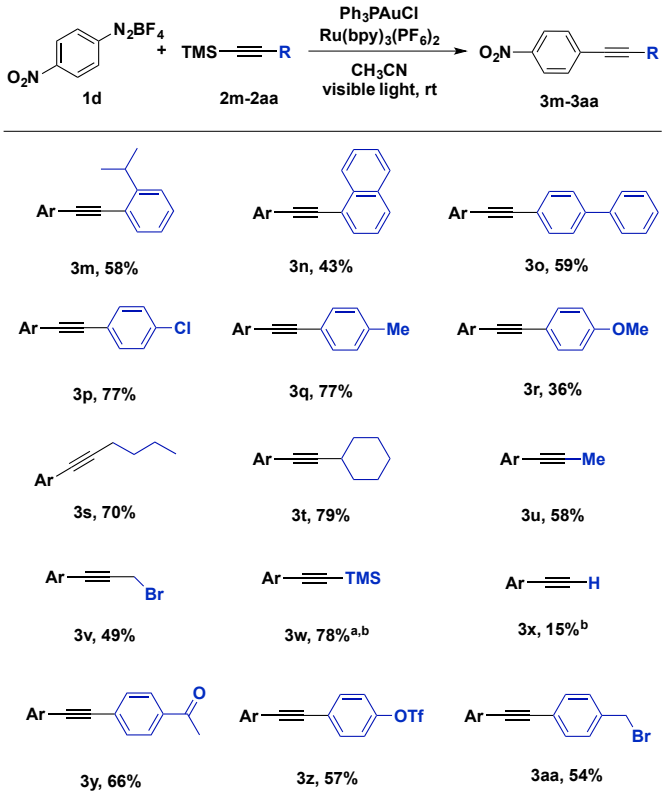

Reaction conditions: **1d** (0.24 mmol, 1.2 equiv.), **2m-2aa** (0.2 mmol, 1.0 equiv.), Ph_3PAuCl (10 mol%), $Ru(bpy)_3(PF_6)_2$ (2 mol%), acetonitrile (2 mL), N_2 atmosphere, visible light, R.T. for 3h. Isolated yields. Ar = p-nitrophenyl. [a] 5 equiv. of bis(trimethylsilyl)acetylene was used with 1 equiv. of 1d. [b] GC yields.

The scope of alkynyltrimethylsilanes was also investigated (Table 3). Both aryl- and alkylethynyltrimethylsilanes were coupled with modest to high product yields. *o*-Isopropylphenyl, biphenylyl and naphthylalkynyltrimethylsilanes participated in the gold-catalysed coupling (Table 3, **3m**, **3n** and **3o**). Potentially sensitive benzylic and propargylic C–H and C–X bonds were well tolerated under the reaction conditions (Table 3, **3q**, **3aa** and **3s**–**3v**). Additionally, alkynyltrimethylsilane **3w** was prepared in 78% yield from the coupling of aryldiazonium salt **1d** and bis(trimethylsilyl) acetylene, providing a compliment to using trimethylsilylacetylene in a traditional Sonogashira coupling (Table 3, **3w**).

Another interesting feature of this reaction is the effect of the silyl group on yield (Table 4). When trimethylsilylacetylene was coupled with **1d** to generate terminal alkyne **3x**, the yield was 15% with none of the corresponding silylacetylene **3w** (Table 3). This observation suggests that, under the current base free reaction conditions, the silyl group plays a critical role in the coupling. To investigate this role, a set of reactions was performed by varying counteranions of aryldiazonium salts and silyl group identities of alkynylsilanes. The yield of coupling product was diminished as the steric hindrance of silyl group was increased (Table 4, entry 1 and entries 4–7). While both tetrafluoroborate and tosylate diazonium salts proved efficient coupling partners, the yield was diminished when hexafluorophosphate salts were used.[51] Moreover, when the corresponding terminal alkyne was used instead of alkynyltrimethylsilanes, only 3% of the coupling product was observed (Table 4, entry 8).[52] Taken together, these results suggests that transmetallation from the organosilane is critical for high efficiency of the current coupling reaction.

Table 2.4 Effect of counteranion and silyl group

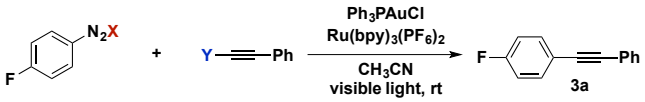

Entry	Counteranion(**X**)	Silyl group (**Y**)	Yield[a]
1	BF_4^-	TMS	70
2	TsO^-	TMS	68
3	PF_6^-	TMS	24
4	BF_4^-	TES	61
5	BF_4^-	TBDMS	10
6	BF_4^-	TIPS	10
7	BF_4^-	TBDPS	1
8	**BF_4^-**	**H**	**3**

Reaction conditions: Diazonium salt (0.2 mmol, 1 equiv.), phenylethynylsilane (0.2 mmol, 1 equiv.), Ph_3PAuCl (5 mol%), $Ru(bpy)_3(PF_6)_2$ (1 mol%), acetonitrile (2 mL), N_2 atmosphere, visible light, R.T. for 6 h. [a] GC yields.

Other organotrimethylsilanes were tested under the optimized reaction conditions. While the reactions of aryl and vinylsilanes were complicated by competing reactions,[53,54] the gold/photoredox-catalysed coupling of allenyltrimethylsilane **4** provided propargylic compound **5** as the sole coupling product (Scheme 2). The product from aryl–allenyl reductive elimination and the other aryl–propargylic coupling isomer were prepared independently (Scheme 2, **6** and **7**). We examined whether **6** was an intermediate that underwent isomerization to **5** facilitated by visible light and the photoredox catalyst. However, no isomerization was observed of **6** to either **5** or **7** under the reaction conditions. Therefore, the formation of **5** is best rationalized by transmetalation of **4** to the gold(III) intermediate, followed by 1,3-migration and aryl–propargyl reductive elimination.

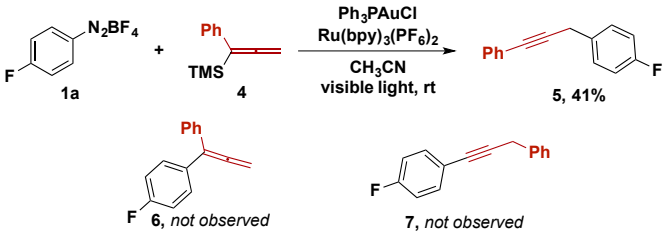

Scheme 2.2 Reaction with allenyltrimethylsilanes

2.3 Conclusions

In summary, we have demonstrated that trimethylsilylalkynes and aryldiazonium tetrafluoroborates can be coupled via dual photoredox and gold catalysis strategy. The reaction proceeds under mild conditions and shows excellent functional group tolerance, including aryl halides that may be reactive under traditional coupling conditions. This process compliments the Sonogashira coupling, especially when aryl–alkynyl coupling is required under non-basic conditions and may present an advantage when TMS-alkynes are available rather than corresponding terminal alkynes.

2.4 References and Notes

(1) Hashimi, A. S. K. *Acc. Chem. Res.* **2014**, *47*, 864.

(2) Obradors, C.; Echavarren, A. M. *Chem. Commun*. **2014**, *50*, 16.

(3) Garayalde, D.; Nevado, C. *ACS Catal.* **2012**, *2*, 1462.

(4) Rudolph, M.; Hashmi, A. S. K. *Chem. Soc. Rev.* **2012**, *41*, 2448.

(5) Liu, L. P.; Hammond, G. B. *Chem. Soc. Rev.* **2012**, *41*, 3129.

(6) Shapiro, N. D.; Toste, F. D. *Synlett* **2010**, *5*, 675.

(7) Lauterbach, T.; Livendahl, M.; Rosellón, A.; Espinet, P.; Echavarren, A. M. *Org. Lett.* **2010**, *12*, 3006.

(8) Levin, M. D.; Toste, F. D. *Angew. Chem. Int. Ed.* **2014**, *53*, 6211.

(9) Winston, M. S.; Wolf, W. J.; Toste, F. D. *J. Am. Chem. Soc.* **2014**, *136*, 7777.

(10) Guenther, J.; Mallet-Ladeira, S.; Estevez, L.; Miqueu, K.; Amgoune, A.; Bourissou, D. *J. Am. Chem. Soc.* **2014**, *136*, 1778.

(11) Joost, M.; Zeineddine, A.; Estevez, L.; Mallet−Ladeira, S.; Miqueu, K.; Amgoune, A.; Bourissou, D. *J. Am. Chem. Soc.* **2014**, *136*, 14654.

(12) Kar, A.; Mangu, N.; Kaiser, H. M.; Beller, M.; Tse, M. K. *Chem. Commun.* **2008**, 386.

(13) Zhang, G. Peng, Y.; Cui, L.; Zhang, L. *Angew. Chem. Int. Ed.* **2009**, *48*, 3112.

(14) Melhado, A. D.; Brenzovich, W. E.; Lackner, A. D.; Toste, F. D. *J. Am. Chem. Soc.* **2010**, *132*, 8885.

(15) Brenzovich, W. E.; Benitez, D.; Lackner, A. D.; Shunatona, H. P.; Tkatchouk, E.; Goddard, W. A.; Toste, F. D. *Angew. Chem., Int. Ed.* **2010**, *49*, 5519.

(16) Brenzovich, W. E.; Brazeau, J. F.; Toste, F. D. *Org. Lett.* **2010**, *12*, 4728.

(17) Zhang, G.; Cui, L.; Wang, Y.; Zhang, L. *J. Am. Chem. Soc.* **2010**, *132*, 1474.

(18) de Haro, T.; Nevado, C. *J. Am. Chem. Soc.* **2010**, *132*, 1512.

(19) Brand, J. P.; Charpentier, J.; Waser, J. *Angew. Chem. Int. Ed.* **2009**, *48*, 9346.

(20) Brand, J. P.; Waser, J. *Angew. Chem. Int. Ed.* **2010**, *49*, 7304.

(21) Hopkinson, M. N.; Tessier, A.; Salisbury, A.; Giuffredi, G. T.; Combettes, L. E. ; Gee, A. D.; Gouverneur, V. *Chem. − Eur. J.* **2010**, *16*, 4739.

(22) Ball, L. T.; Lloyd-Jones, G. C.; Russell, C. A. *Org. Lett.* **2010**, *12*, 4724.

(23) Ball, L. T.; Lloyd-Jones, G. C.; Russell, C. A. *Science* **2012**, *337*, 1644.

(24) Sahoo, B.; Hopkinson, M. N.; Glorius, F. *J. Am. Chem. Soc.* **2013**, *135*, 5505.

(25) Hopkinson, M. N.; Sahoo, B.; Glorius, F. *Adv. Synth. Catal.* **2014**, *356*, 2794.

(26) Shu, X. Z.; Zhang, M.; He, Y.; Frei, H.; Toste, F. D. *J. Am. Chem. Soc.* **2014**, *136*, 5844.

(27) He, Y.; Wu H.; Toste, F. D. *Chem. Sci.* **2015**, *6*, 1194.

(28) Roglans, A.; Pla-Quintana, A.; Moreno-Manas, M. *Chem. Rev.* **2006**, *106*, 4622.

(29) Tellis, J. C.; Primer, D. N.; Molander, G. A. *Science* **2014**, *345*, 433.

(30) Primer, D. N.; Karakaya, I.; Tellis, J. C.; Molander, G. A. *J. Am. Chem. Soc.* **2015**, *137*, 2195.

(31) Wolf, W. J.; Winston, M. S.; Toste, F. D. *Nat. Chem.* **2013**, *6*, 159.

(32) Lermontov, S. A.; Rakov, I. M.; Zefirov, N. S.; Stang, P. J. *Tet. Lett.* **1996**, *37*, 4051.

(33) Kabalka, G. W.; Wang, L.; Pagni, R. M. *Tetrahedron* **2001**, *57*, 8017.

(34) Kang, S.; Ryu, H.; Hong, Y. *J. Chem. Soc. Perkin Trans. 1* **2001**, *7*, 736.

(35) Yang, C.; Nolan, S. P. *Organometallics* **2002**, *21*, 1020.

(36) Hwang, L. K.; Na, Y.; Lee, J.; Do, Y.; Chang, S. *Angew. Chem. Int. Ed.* **2005**, *44*, 6166.

(37) Sommer, W. J.; Weck, M. *Adv. Synth. Catal.* **2006**, *348*, 2101.

(38) Sakai, N.; Komatsu, R.; Uchida, N.; Ikeda, R.; Konakahara, T. *Org. Lett.* **2010**, *12*, 1300.

(39) Nishihara, Y.; Noyori, S.; Okamoto, T.; Suetsugu, M.; Iwasaki, M. *Chem. Lett.* **2011**, *40*, 972.

(40) Nishihara, Y.; Ogawa, D.; Noyori, S.; Iwasaki, M. *Chem. Lett.* **2012**, *41*, 1503.

(41) Peng, L.; Xu, F.; Suzuma, Y.; Orita, A.; Otera, J. *J. Org. Chem.* **2013**, *78*, 12802.

(42) Keumi, T.; Umeda, T.; Inoue, Y.; Kitajima, H.; *Bull. Chem. Soc. Jpn.* **1989**, *62*, 89.

(43) Mayr, H.; Grimm, K. *J. Org. Chem.* **1992**, *57*, 1057.

(44) Prakash, G. K. S.; Hoole, D.; Ha, D. S.; Wilkinson, J.; Olah, G. A. *ARKIVOC*, **2002**, *13*, 50.

(45) Darses, S.; Michaud, G.; Genet, J. *Eur. J. Org. Chem.* **1999**, 1875.

(46) Fabrizi, G.; Goggiamani, A.; Sferrazza, A.; Cacchi, S. *Angew. Chem. Int. Ed.* **2010**, *49*, 4067.

(47) Panda, B.; Sarkar, T. K. *Chem. Commun.* **2010**, *46*, 3131.

(48) Wu, X.; Neumann, H.; Beller, M. *Chem. Commun.* **2011**, *47*, 7959.

(49) Barbero, M.; Cadamuro, S.; Dughera, S. *Eur. J. Org. Chem.* **2014**, 598.

(50) Cai, R.; Lu, M.; Aguilera, E. Y.; Xi, Y.; Akhmedov, N. G.; Petersen, J. L.; Chen, H.; Shi, X. *Angew. Chem. Int. Ed.* **2015**, *54*, 8772.

(51) After the completion of coupling reaction with tetrafluoroborate salts, stoichiometric amounts of trimethylsilyl fluoride were observed by ^{1}H NMR.

(52) To examine the robustness of this reaction towards terminal alkynes, 1 equiv. of phenylacetylene and 1 equiv. of phenylethynyltrimethylsilane were reacted with 1 equiv. **1a** Surprisingly, less than 5% of **3a** was detected.

(53) When (*Z*)-styryltrimethylsilane was used the corresponding *Z*-product was obtained from gold-catalysed cross coupling and *E*-product was obtained from uncatalysed addition of the aryldiazonium to the vinylsilane (see: Benkeser, A.; Bennet, E. W.; Hickner R. A. *J. Am. Chem. Soc.* **1957**, *79*, 6253.) After consumption of the starting material, photoredox promoted isomerization of *E*-stilbene to *Z*-stilbene occurred.

(54) In the case aryltrimethylsilanes, further optimization is required due to the formation of significant amounts of competing homo-coupling reactions.

2.5 Supporting information

2.5.1 General consideration

Unless otherwise noted, reagents were purchased from commercial suppliers and used without further purification. All magnetic stir bars were washed with freshly prepared aqua regia prior to use to minimize the potential for trace metal contamination. Column chromatography was performed using Sorbent Technology silica gel, (60 Å, 30-63 μm). Thin-layer chromatography analysis was performed using Merck silica gel 60 F254 TLC plates, and visualized by iodine, *p*-anisaldehyde, ceric ammonium molybdate, vanillin or UV lamp. All NMR spectra were recorded with Bruker AV-300, AVB-400, AVQ-400, AV-500, DRX-500 and AV-600 spectrometers. ^{1}H and ^{13}C chemical shifts were reported in ppm downfield of tetramethylsilane and referenced to residual solvent peak ($CHCl_3$; δH = 7.26 and δC = 77.00, CH_3CN; δH = 1.94 and δC = 1.32, 118.26, acetone; δH = 2.05 and δC = 29.84, 206.26, DMSO; δH = 2.50 and δC = 39.52). ^{19}F chemical shifts were reported in ppm upfield of $CFCl_3$ and referenced to internal standard (C_6F_6; δH = −164.9). Multiplicities were reported using the following abbreviations: s = singlet, d = doublet, t = triplet, q = quartet, m = multiplet. Gas chromatography was conducted on an

HP 6850A Series GC System on a Chiraldex 225 β-dex column with a flame ionization detector. (*E*)-Stilbene was used as an internal standard. Mass spectral data were obtained from the Autospec Premier magnetic sector mass spectrometer (EI) at the Micro-Mass/Analytical Facility operated by the College of Chemistry, University of California, Berkeley.

The gold-catalyzed carbon-carbon cross coupling were run in 2 dram (17 mm x 60 mm) vials (not dried) fitted with a screw cap and stirring was carried out using a 10 mm magnetic stir bar. All reactions were carried out under air unless otherwise noted. Acetonitrile, diethyl ether, tetrahydrofuran, dimethyl formamide, and triethylamine were purified by passage through an activated alumina column under argon. A household lamp with a 23 W fluorescent light bulb and a 17 W white LED was used for the light source of reactions. **Caution:** Appropriate safety precautions should be taken due to the explosive nature of diazonium salts, including the use of a blast shield.

2.5.2 Preparation of aryldiazonium salts

General procedure for aryldiazonium tetrafluoroborate preparation[1]

The aniline (10 mmol) was dissolved in a mixture of 50% (V/V) fluoroboric acid (3.5 mL) and water (3.5 mL). After cooling to 0 °C, an aqueous solution of sodium nitrite (700 mg, 10.1 mmol, in 1.5 mL H_2O) was added in 0.25 mL portions. The mixture was stirred for 30 min and the thick precipitate was collected by filtration and dissolved in minimal amount of acetone. The diazonium tetrafluoroborate was then precipitated by the addition of Et_2O. The product was dried under high vacuum for several hours.

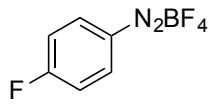

p-Fluorobenzenediazonium tetrafluoroborate, **1a**

White solid (1.36 g, 65%), ^{1}H NMR (400 MHz, CD_3CN) δ 8.62 – 8.59 (m, 2H), 7.68 – 7.64 (m, 2H). In accordance with previously reported spectra[2]

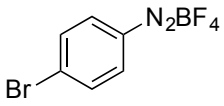

p-Bromobenzenediazonium tetrafluoroborate, **1b**

Pale pink solid (2.11 g, 78%), ^{1}H NMR (400 MHz, CD_3CN) δ 8.37 (d, J = 8.8 Hz, 2H), 8.10 (d, J = 8.9 Hz, 2H). In accordance with previously reported spectra.[3]

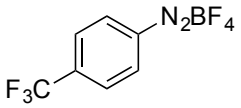

p-Trifluoromethylbenzenediazonium tetrafluoroborate, **1c**

White solid (1.66 g, 64%), ^{1}H NMR (400 MHz, CD_3CN) δ 8.71 (d, J = 8.6 Hz, 2H), 8.23 (d, J = 8.6 Hz, 2H). In accordance with previously reported spectra.[4]

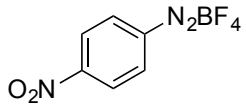

p-Nitrobenzenediazonium tetrafluoroborate, **1d**

White solid (1.73 g, 73%), ^{1}H NMR (400 MHz, CD_3CN) δ 8.77 (d, J = 9.0 Hz, 2H), 8.63 (d, J = 9.0 Hz, 2H). In accordance with previously reported spectra.[3]

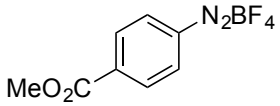

p-Methoxycarbonylbenzenediazonium tetrafluoroborate, **1e**

White solid (1.46 g, 58%), ^{1}H NMR (400 MHz, CD_3CN) δ 8.61 (d, J = 8.6 Hz, 2H), 8.41 (d, J = 8.6 Hz, 2H), 3.97 (s, 3H). In accordance with previously reported spectra.[2]

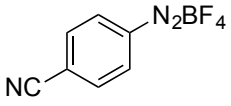

p-Cyanobenzenediazonium tetrafluoroborate, **1f**

White solid (1.83 g, 85%), ^{1}H NMR (400 MHz, CD_3CN) δ 8.64 (d, J = 9.0 Hz, 1H), 8.23 (d, J = 9.0 Hz, 1H). In accordance with previously reported spectra.[5]

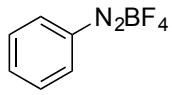

Benzenediazonium tetrafluoroborate, **1g**

White solid (1.37 g, 71%), ^{1}H NMR (400 MHz, CD_3CN) δ 8.50 (d, J = 8.2 Hz, 2H), 8.25 (t, J = 7.6 Hz, 1H), 7.92 (t, J = 7.5 Hz, 2H). In accordance with previously reported spectra.[3]

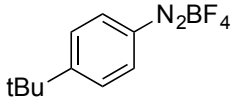

p-tert-Butylbenzenediazonium tetrafluoroborate, **1h**

White solid (0.915 g, 37%), ^{1}H NMR (400 MHz, CD_3CN) δ 8.42 (d, J = 9.1 Hz, 2H), 7.97 (d, J = 9.0 Hz, 2H), 1.38 (s, 1H). In accordance with previously reported spectra.[3]

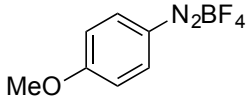

p-Methoxybenzenediazonium tetrafluoroborate, **1i**

Beige solid (1.59 g, 72%), ^{1}H NMR (400 MHz, CD_3CN) δ 8.43 (d, J = 9.4 Hz, 2H), 7.35 (d, J = 9.4 Hz, 2H), 4.05 (s, 3H). In accordance with previously reported spectra.[2]

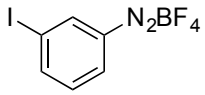

m-Iodobenzenediazonium tetrafluoroborate, **1j**

Beige solid (1.34 g, 42%), ^{1}H NMR (400 MHz, CD_3CN) δ 8.77 (s, 1H), 8.62 – 8.41 (m, 2H), 7.68 – 7.64 (m, 1H).

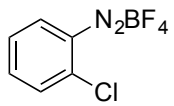

o-Chlorobenzenediazonium tetrafluoroborate, **1k**

White solid (1.72 g, 76%), ^{1}H NMR (400 MHz, CD_3CN) δ 8.70 – 8.50 (m, 1H), 8.33 – 8.16 (m, 1H), 8.02 – 8.00 (m, 1H), 7.90 – 7.86 (m, 1H).

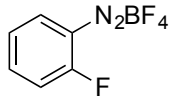

o-Fluorobenzenediazonium tetrafluoroborate, **1l**

White solid (1.81 g, 87%), ^{1}H NMR (400 MHz, CD_3CN) δ 8.54 – 8.50 (m, 1H), 8.37 – 8.31 (m, 1H), 7.79 – 7.73 (m, 2H).

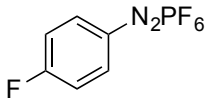

Proecdure for *p*-fluorobenzenediazonium hexafluorophosphate preparation[6]

p-Fluoroaniline (35.0 mmol) was dissolved in a mixture of 12N aqueous HCl solution (9.5 mL) and water (65 mL). After cooling to 0 °C, an aqueous solution of sodium nitrite (2.9 g, 42.0 mmol, in 7.5 mL H_2O) was added in 1.5 mL portions. 65% aqueous HPF_6 (7.4 mL, 13.4 g, 60 mmol) solution was added in one portion with vigorous stirring. The mixture was stirred for 30 min and the precipitate was collected by filtration. The precipitate was dissolved in acetone and then recrystallized by the addition of diethyl ether. Again, the precipitate was dissolved in methanol and recrystallized by the addition of diethyl ether. Colorless solid (5.77 g, 62%), ^{1}H NMR (400 MHz, CD_3CN) δ 8.59 – 8.54 (m, 2H), 7.71 – 7.61 (m, 2H).

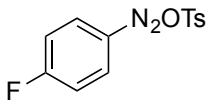

Procedure for p-fluorobenzenediazonium tosylate preparation[7]

p-Fluoroaniline (10.0 mmol) was dissolved in a mixture of 50% (V/V) glacial acetic acid (50 mL) and water (50 mL). *p*-Toluenesulfonic acid dihydrate (11.0 mmol) was added to the solution. After cooling to 0 °C, *tert*-butylnitrite (19.5 mmol) was added dropwise to the solution. The mixture was stirred for 30 min and stirred at 23 °C for another 30 min. Diethyl ether (500 mL) was poured into the solution and the precipitate was collected by filtration. The precipitate was dissolved in a minimal amount of methanol and then precipitated by the addition of diethyl ether. The product was dried under high vacuum for several hours. Colorless solid (2.64 g, 90%), ^{1}H NMR (400 MHz, DMSO-d_6) δ 8.86 –

8.78 (m, 2H), 7.91 – 7.87 (m, 2H), 7.47 (d, J = 8.0 Hz, 2H), 7.11 (d, J = 8.0 Hz, 2H), 2.28 (s, 3H).

2.5.3 Preparation of alkynylsilanes

General procedure for phenylethynylsilanes preparation[8]

Phenylacetylene (20.4 mmol) was dissolved in THF (60 mL). After cooling to –78 °C, *n*-BuLi (2.5M in hexanes, 8.3 mL, 20.8 mmol) was added dropwise to the solution. The mixture was stirred for 2 h at –78 °C. The silylchloride (20.0 mmol) dissolved in THF (10 mL) was added dropwise. The mixture was stirred 6 h at 23 °C. A saturated solution of aqueous ammonium chloride (100 mL) was added and the mixture was extracted with dichloromethane (2 × 100 mL). The collected organic layer was washed with a mixture of 50% (V/V) brine (100 mL) and water (100 mL), then dried over $MgSO_4$, filtered and concentrated under reduced pressure. The product was purified by flash column chromatography.

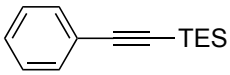

(Phenylethynyl)triethylsilane. Colorless liquid (2.96 g, 68%), ^{1}H NMR (400 MHz, $CDCl_3$) δ 7.53 – 7.49 (m, 2H), 7.33 – 7.32 (m, 3H), 1.10 (t, J = 7.9 Hz, 9H), 0.72 (q, J = 7.9 Hz, 6H), ^{13}C NMR (101 MHz, $CDCl_3$) δ 131.86, 128.18, 127.98 123.16, 106.20, 91.36, 7.34, 4.27. In accordance with previously reported spectra.[9]

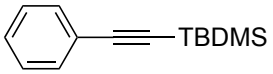

(Phenylethynyl)-*tert*-butyldimethylsilane. Colorless liquid (2.75 g, 64%), ^{1}H NMR (400 MHz, $CDCl_3$) δ 7.54 – 7.51 (m, 2H), 7.35 – 7.33 (m, 3H), 1.07 (s, 9H), 0.25 (s, 6H), ^{13}C NMR (101 MHz, $CDCl_3$) δ 131.97, 128.40, 128.16, 123.24, 105.78, 92.36, 26.15, 16.72, -4.58. In accordance with previously reported spectra.[10]

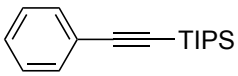

(Phenylethynyl)triisopropylsilane. Colorless liquid (4.09 g, 79%), ^{1}H NMR (400 MHz, $CDCl_3$) δ 7.56 – 7.54 (m, 2H), 7.38 – 7.31 (m, 3H), 1.22 (s, 21H), ^{13}C NMR (101 MHz, $CDCl_3$) δ 132.01, 128.25, 128.14, 123.57, 107.15, 90.36, 18.67, 11.34. In accordance with previously reported spectra.[11]

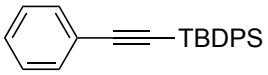

(Phenylethynyl)-*tert*-butyldiphenylsilane. Colorless liquid (2.89 g, 42%), ^{1}H NMR (400 MHz, $CDCl_3$) δ 8.03 – 8.00 (m, 4H), 7.76 – 7.69 (m, 2H), 7.54 – 7.50 (m, 6H), 7.47 – 7.42 (m, 3H), 1.30 (s, 9H), ^{13}C NMR (101 MHz, $CDCl_3$) δ 135.58, 133.27, 132.11, 129.50, 128.81, 128.26, 127.71, 122.96, 109.14, 89.29, 27.11, 18.71, m/z HRMS (EI) found 340.1646 $C_{24}H_{24}Si$ requires 340.1647.

General Procedure for alkynyltrimethylsilane[12]

Iodobenzene (4.0 mmol, 1 equiv.), $Pd(PPh_3)_2Cl_2$ (84 mg, 0.120 mmol, 3 mol%), CuI (46 mg, 0.242 mmol, 6 mol%) and triethylamine (1.63 g, 16.1 mmol, 4 equiv.) were dissolved in DMF (6.8 mL). Trimethylsilylacetylene (0.39 g, 4.00 mmol, 1 equiv.) was added to the mixture. After heating to 60°C, the mixture was stirred for 1 h. The mixture was diluted with a mixture of 50% (V/V) ethyl acetate (50 mL) and water (50 mL). The organic layer was collected and washed with water (3 × 50 mL) and brine (50 mL). The organic layer was dried over MgSO4, filtered and concentrated under reduced pressure. The residue was purified by flash chromatography on silica gel.

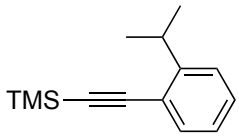

((*o*-Isopropylphenyl)ethynyl)trimethylsilane, **2m**

Yellow liquid (726 mg, 84%), ^{1}H NMR (500 MHz, $CDCl_3$) δ 7.44 (d, J = 7.7 Hz, 1H), 7.32 – 7.23 (m, 2H), 7.13 – 7.10 (m, 1H), 3.46 (hept, J = 6.9 Hz, 1H), 1.27 (d, J = 6.9 Hz, 6H), 0.27 (s, 9H), ^{13}C NMR (126 MHz, $CDCl_3$) δ 150.91, 132.55, 128.79, 125.36, 124.79, 121.87, 103.95, 97.98, 31.50, 22.87, -0.02. In accordance with previously reported spectra.[13]

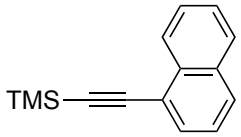

((1-Naphthyl)ethynyl)trimethylsilane, **2n**

Yellow liquid (731 mg, 81%), ^{1}H NMR (400 MHz, $CDCl_3$) δ 8.37 – 8.34 (m, 1H), 7.89 – 7.79 (m, 2H), 7.72 (dd, *J* = 7.2, 1.2 Hz, 1H), 7.59 (ddd, *J* = 8.3, 6.9, 1.4 Hz, 1H), 7.52 (ddd, *J* = 8.1, 6.8, 1.3 Hz, 1H), 7.42 (dd, *J* = 8.3, 7.1 Hz, 1H), 0.35 (s, 9H), ^{13}C NMR (101 MHz, $CDCl_3$) δ 133.37, 133.05, 130.78, 128.95, 128.23, 126.80, 126.36, 126.17, 125.09, 120.71, 103.03, 99.41, 0.11. In accordance with previously reported spectra.[12]

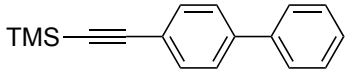

([1,1'-Biphenyl]-4-ylethynyl)trimethylsilane, **2o**

White solid (755 mg, 75%), ^{1}H NMR (400 MHz, $CDCl_3$) δ 7.65 – 7.53 (m, 6H), 7.48 – 7.44 (m, 2H), 7.41 – 7.34 (m, 1H), 0.31 (s, 9H), ^{13}C NMR (101 MHz, $CDCl_3$) δ 141.15, 140.28, 132.37, 128.81, 127.62, 126.99, 126.83, 122.02, 105.00, 94.83, 0.00. In accordance with previously reported spectra.[14]

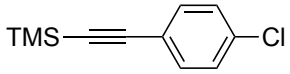

((*p*-Chlorophenyl)ethynyl)trimethylsilane, **2p**

White solid (690 mg, 83%), ^{1}H NMR (400 MHz, $CDCl_3$) δ 7.38 (d, *J* = 8.5 Hz, 2H), 7.27 (d, *J* = 8.5 Hz, 2H), 0.24 (s, 9H), ^{13}C NMR (101 MHz, $CDCl_3$) δ 134.47, 133.16, 128.52, 121.59, 103.79, 95.32, -0.12. In accordance with previously reported spectra.[15]

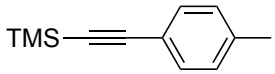

((*p*-Tolyl)ethynyl)trimethylsilane, **2q**

Yellow liquid (653 mg, 87%), ^{1}H NMR (400 MHz, $CDCl_3$) δ 7.36 (d, *J* = 8.1 Hz, 2H), 7.10 (d, *J* = 7.8 Hz, 2H), 2.34 (s, 3H), 0.25 (s, 9H), ^{13}C NMR (101 MHz, $CDCl_3$) δ

138.58, 131.83, 128.92, 120.01, 105.33, 93.20, 21.49, 0.02. In accordance with previously reported spetra.[16]

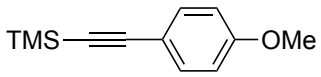

((*p*-Methoxyphenyl)ethynyl)trimethylsilane, **2r**

Yellow liquid (591 mg, 72%), ^{1}H NMR (400 MHz, $CDCl_3$) δ 7.40 (d, *J* = 8.6 Hz, 2H), 6.82 (d, *J* = 8.6 Hz, 2H), 3.80 (s, 3H), 0.24 (s, 9H), ^{13}C NMR (101 MHz, $CDCl_3$) δ 159.68, 133.44, 115.20, 113.76, 105.15, 92.39, 55.24, 0.05. In accordance with previously reported spectra.[12]

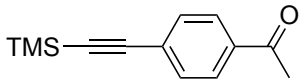

((*p*-Acetylphenyl)ethynyl)trimethylsilane, **2y**

Pale yellow liquid (646 mg, 75%), ^{1}H NMR (400 MHz, $CDCl_3$) δ 7.88 (d, *J* = 8.3 Hz, 2H), 7.53 (d, *J* = 8.3 Hz, 2H), 2.59 (s, 3H), 0.26 (s, 9H), ^{13}C NMR (101 MHz, $CDCl_3$) δ 197.25, 136.38, 132.04, 128.08, 127.94, 103.99, 98.08, 26.58, -0.19. In accordance with previously reported spectra.[17]

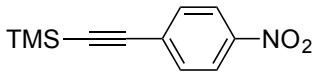

((*p*-Nitroxyphenyl)ethynyl)trimethylsilane, **3w**

Light yellow solid (500 mg, 57%), ^{1}H NMR (400 MHz, $CDCl_3$) δ 8.17 (d, *J* = 8.9 Hz, 2H), 7.60 (d, *J* = 8.9 Hz, 2H), 0.27 (s, 9H), ^{13}C NMR (101 MHz, $CDCl_3$) δ 147.10, 132.67, 129.95, 123.47, 102.66, 100.61, -0.31. In accordance with previously reported spectra.[12]

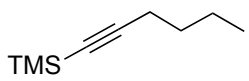

Procedure for 1-trimethylsilyl-1-hexyne preparation, **2s**[8]

1-Hexyne (20.4 mmol) was dissolved in THF (60 mL). After cooling to –78 °C, *n*-BuLi (2.5M in hexanes, 8.3 mL, 20.8 mmol) was added dropwise to the solution. The mixture

was stirred for 2 h at –78 °C. The trimethylsilylchloride (20.0 mmol) dissolved in THF (10 mL) was added dropwise. The mixture was stirred 3 h at 23 °C. A saturated solution of aqueous ammonium chloride (100 mL) was added and the mixture was extracted with dichloromethane (2 × 100 mL). The collected organic layer was washed with a mixture of 50% (V/V) brine (100 mL) and water (100 mL), then dried over $MgSO_4$, filtered and concentrated under reduced pressure. The residue was purified by flash chromatography on silica gel. Colorless liquid (1.14 g, 37%), ^{1}H NMR (400 MHz, $CDCl_3$) δ 2.19 (t, J = 7.1 Hz, 2H), 1.52 – 1.33 (m, 4H), 0.89 (t, J = 7.3 Hz, 3H), 0.12 (s, 9H), ^{13}C NMR (101 MHz, $CDCl_3$) δ 107.56, 84.11, 30.75, 21.90, 19.53, 13.58, 0.14. In accordance with previously reported spectra.[18]

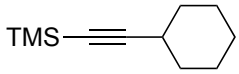

Procedure for (cyclohexylethynyl)trimethylsilane preparation, **2t**[19]

To a solution of ethynylcyclohexane (1.66 mL, 12.8 mmol) in THF (54 mL, 0.24 M) under N_2 at –78 ºC was added *n*-BuLi (2.5 M solution in hexanes, 5.6 mL, 14.0 mmol). The mixture was stirred for 30 min and then the cooling bath had been removed. The mixture was stirred for extra 30 min. The mixture was stirred for 17 h after the addition of trimethylsilylchloride (1.77 mL, 14.0 mmol). The mixture was diluted with Et_2O (50 mL) and H_2O (50 mL) and the layers were separated. After the aqueous layer had been extracted again with Et_2O (3 × 50 mL), the combined extracts were dried with $MgSO_4$ and concentrated. The residue was purified by flash chromatography on silica gel. Colorless liquid (1.43 g, 62%), ^{1}H NMR (400 MHz, $CDCl_3$) δ 2.45 – 2.29 (m, 1H), 1.89 – 1.62 (m, 4H), 1.53 – 1.39 (m, 3H), 1.36 – 1.19 (m, 3H), 0.14 (s, 9H), ^{13}C NMR (101 MHz, $CDCl_3$) δ 111.83, 83.66, 32.63, 30.00, 25.86, 24.81, 0.28. In accordance with previously reported spectra.[20]

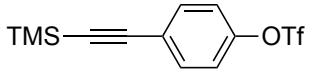

Procedure for 4-((trimethylsilyl)ethynyl)phenyl trifluoromethanesulfonate preparation, 2z[21]

A 20 mL vial was charged with 4-((trimethylsilyl)ethynyl)phenol[38] (500 mg, 2.62 mmol, 1.0 equiv.) and DCM (3 mL). the resulting solution was cooled to 0 ^{o}C, and pyridine (0.38g, 4.8 mmol, 2.0 equiv.) was added dropwise via syringe. A solution of trifilic anhydride (812 mg, 2.88 mmol, 1.1 equiv.) in DCM (1 mL) was added dropwise via syringe, and the vial was allowed to warm to 23 ^{o}C. After stirring for 1 h, the reaction mixture was diluted with Et_2O (20 mL), washed with 1 M HCl (20 mL), sat. $NaHCO_3$ (20 mL), H_2O (20 mL) and brine (20 mL). the organic layer was dried with $MgSO_4$ and concentrated in vacuo and purified via flash chromatography. Yellow liquid (543 mg, 64%), ^{1}H NMR (500 MHz, $CDCl_3$) δ 7.53 (d, J = 8.8 Hz, 2H), 7.21 (d, J = 8.8 Hz, 2H), 0.25 (s, 9H), ^{13}C NMR (101 MHz, $CDCl_3$) δ 149.04, 133.76, 123.85, 121.33, 118.71 (q, J = 322 Hz), 102.77, 96.62, -0.28. In accordance with previously reported spectra.[21]

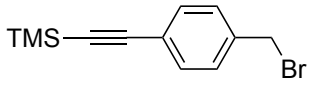

Procedure for ((4-(bromomethyl)phenyl)ethynyl)trimethylsilane preparation, 2aa[22]

To a solution of ((*p*-Tolyl)ethynyl)trimethylsilane, **2q** (900 mg, 4.78 mmol, 1.0 equiv.) in CCl_4 (7.5 mL), NBS (1.19 g, 6.70 mmol, 1.4 equiv.) and benzoyl peroxide (25 mg) were added. Then, reaction mixture was refluxed under nitrogen. After 3h, iced water (5 mL) was added to the reaction mixture, and the precipitate was removed by filtration. After the organic layer was separated, the solvent was evaporated under reduced pressure. The residue was then diluted with Et2O (10 mL) and the ethereal layer was washed with water and dried over $MgSO_4$. After filtration, the solvent was evaporated the resulting oliy product was purified by column chromatography. Yellow liquid (484 mg, 38%), ^{1}H NMR (500 MHz, $CDCl_3$) δ 7.43 (d, J = 8.1 Hz, 2H), 7.32 (d, J = 8.0 Hz, 2H), 4.46 (s, 2H), 0.25 (s, 9H), ^{13}C NMR (101 MHz, $CDCl_3$) δ 137.91, 132.20, 128.83, 123.15, 104.43, 95.14, 32.80, -0.10. In accordance with previously reported spectra.[22]

2.5.4 Preparation of gold catalyst and photoredox catalysts

Procedure for triphenylphosphinegold(I) chloride preparation[23]

Gold(III) chloride (5.11 mmol) was dissolved in ethanol (70 mL). 12N aqueous HCl solution was added dropwise with stirring until the solution became yellow and homogeneous. A solution of triphenylphosphine (7.24 mmol) in ethanol (100 mL) was added to the gold solution. The mixture immediately became colorless and a white precipitate appeared. The mixture was stirred for 2 min and the precipitate was collected by filtration, washed with diethyl ether (3 × 30 mL) and dried in vaccuo. The solid was dissolved in dichloromethane (20 mL) and was crystallized using hexane (120 mL) at –25 °C. Colorless solid (1.93 g, 75%), ^{1}H NMR (400 MHz, $CDCl_3$) δ 7.59 – 7.42 (m, 18H), ^{13}C NMR (101 MHz, $CDCl_3$) δ 134.19, 134.05, 131.98, 131.95, 129.27, 129.15.

Procedure for Tris(2,2'-bipyridine)ruthenium(II) hexafluorophosphate preparation[24]

Ruthenium(III) chloride (2.60 mmol) and 2,2'-bipyridine (16.0 mmol) were dissolved in ethanol (100 mL). The reaction mixture was heated to reflux for 12 h under nitrogen atmosphere. After cooling to 23 °C, potassium hexafluorophosphate (10 mmol) was added to the mixture and the precipitate was collected by filtration. The red solid was washed with water and then washed through the fritted funnel with acetone to remove excess ruthenium salts. The acetone eluent was diluted with diethyl ether to precipitate the ruthenium complex. The red precipitate was filtered and dried overnight in vaccuo. Red solid (1.82 g, 82%), ^{1}H NMR (300 MHz, DMSO-d_6) δ 8.84 (dd, J = 8.2, 1.4 Hz, 6H), 8.17 (ddd, J = 8.2, 7.2, 1.4 Hz, 6H), 7.73 (dd, J = 5.8, 1.4 Hz, 6H), 7.53 (ddd, J = 7.2, 5.8, 1.4 Hz, 6H), ^{13}C NMR (101 MHz, DMSO) δ 156.38, 151.05, 137.77, 127.74, 124.32.

Procedure for (4,4'-di-*tert*-butyl-2,2'-bipyridine)bis(2-(2-pyridinyl)phenyl)Iridium(III) hexa fluorophosphate preparation [25]

A mixture of 2-ethoxyethanol (30 mL) and water (10 mL) was placed in a flask containing $IrCl_3 \cdot 3H_2O$ (388 mg, 1.3 mmol) and 2-phenylpyridine (760 mg, 4.9 mmol). The mixture was heated under reflux for 24 h. After the mixture was cooled to 23 °C, the yellow precipitate was collected by filtration. The precipitate was washed with absolute ethanol (60 mL) and acetone (60 mL) and dissolved in dichoromethane (75 mL) and filtered. The filtrate was collected and solvent was removed in vaccuo to give the crude

$[Ir(ppy)_2Cl]_2$ which was used for the next step without further purification. Green solid (415 mg, 60%)

A mixture of 4,4′-di-tert-butyl-2,2′-dipyridyl (118 mg, 0.44 mmol) and $[Ir(ppy)_2Cl]_2$ (214 mg, 0.2 mmol) in 1,2-ethanediol (10 mL) under nitrogen was heated to 150 °C and stirred for 15 h. After the mixture was cooled to 23 °C, water (150 mL) was added. A solution was extracted with diethyl ether (3 × 50 mL). The aqueous layer was heated to 70 °C and NH_4PF_6 (1.00 g) in water (10 mL) was added to the aqueous solution. After the mixture was cooled to 5 °C, the yellow precipitate was collected by filtration, dried in vaccuo and recrystallized by vapor diffusion with acetonitrile and diethyl ether. Yellow solid (293 mg, 73%), ^{1}H NMR (400 MHz, Acetone-d_6) δ 8.88 (d, J = 2.0 Hz, 2H), 8.23 (dd, J = 8.2, 1.3 Hz, 2H), 8.01 – 7.86 (m, 6H), 7.79 (dt, J = 5.8, 1.1 Hz, 2H), 7.70 (dd, J = 5.9, 2.0 Hz, 2H), 7.13 (ddd, J = 7.3, 5.8, 1.4 Hz, 2H), 7.03 (td, J = 7.5, 1.2 Hz, 2H), 6.91 (td, J = 7.4, 1.4 Hz, 2H), 6.34 (dd, J = 7.6, 1.2 Hz, 2H), 2.84 (d, J = 13.4 Hz, 2H), 1.41 (s, 18H).

2.5.5 General procedure for gold-catalyzed aryl-akynyl cross coupling

Aryldiazonium tetrafluoroborate (0.24 mmol, 1.2 equiv.), alkynyltrimethylsilane (0.2 mmol, 1 equiv.) and triphenylphosphinegold(I) chloride (10 mg, 0.02 mmol, 10 mol%) were placed in a vial equipped with a stir bar. To the vial kept at –78°C was added the solution of tris(2,2'-bipyridine)ruthenium(II) hexafluorophosphate (3.3 mg, 0.004 mmol, 2 mol%) in acetonitrile (2 mL). The vial was evacuated and refilled with nitrogen three times. The mixture was slowly warmed up to 23 °C and stirred for 3 h under a household lamp with a 23 W fluorescent light bulb. After the completion of reaction, diethyl ether (20 mL) was added and filtered through a Celite plug. The filtrate was dried in vaccuo and purified by flash column chromatography to give the desired product.

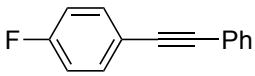

1-(*p*-Fluorophenyl)-2-phenylacetylene, **3a**

White solid (22.5 mg, 57%), ^{1}H NMR (500 MHz, $CDCl_3$) δ 7.54 – 7.50 (m, 4H), 7.37 – 7.33 (m, 3H), 7.07 – 7.03 (m, 2H), ^{13}C NMR (101 MHz, $CDCl_3$) δ 163.71, 161.23, 133.49, 133.41, 131.53, 128.35, 128.31, 123.06, 119.33, 115.73, 115.51, 89.01, 88.26, ^{19}F NMR (376 MHz, $CDCl_3$) δ -114.2, m/z HRMS (EI) found 196.0690 $C_{14}H_9F$ requires 196.0688. In accordance with previously reported spectra.[9]

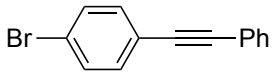

1-(*p*-Bromoophenyl)-2-phenylacetylene, **3b**

White solid (34.7 mg 68%), ^{1}H NMR (400 MHz, $CDCl_3$) δ 7.56 – 7.53 (m, 2H), 7.50 – 7.48 (m, 2H), 7.42 – 7.35 (m, 5H), ^{13}C NMR (101 MHz, $CDCl_3$) δ 132.98, 131.57, 131.55, 128.47, 128.36, 122.85, 122.43, 122.18, 90.47, 88.28, m/z HRMS (EI) found 255.9888 $C_{14}H_9Br$ requires 255.9888. In accordance with previously reported spectra.[26]

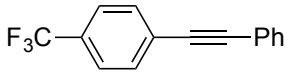

1-(*p*-Trifluoromethylphenyl)-2-phenylacetylene, **3c**

White solid (40.4 mg, 82%), ^{1}H NMR (400 MHz, $CDCl_3$) δ 7.65 – 7.56 (m, 6H), 7.39 – 7.38 (m, 3H), ^{13}C NMR (101 MHz, $CDCl_3$) δ 132.49, 131.78, 131.73, 131.48, 130.36, 130.04, 129.72, 129.39, 129.25, 128.81, 128.51, 128.43, 128.00, 127.11, 126.78, 125.31, 125.27, 125.23, 125.20, 124.62, 122.59, 122.55, 119.88, 91.74, 87.95, ^{19}F NMR (376 MHz, $CDCl_3$) δ -65.9, m/z HRMS (EI) found 246.0659 $C_{15}H_9F_3$ requires 246.0656. In accordance with previously reported spectra.[11]

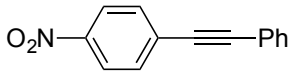

1-(*p*-Nitrophenyl)-2-phenylacetylene, **3d**

Yellow solid (31.7 mg, 71%), ^{1}H NMR (400 MHz, $CDCl_3$) δ 8.24 – 8.20 (m, 2H), 7.68 – 7.65 (m, 2H), 7.58 – 7.55 (m, 2H), 7.41 – 7.38 (m, 3H), ^{13}C NMR (101 MHz, $CDCl_3$) δ 146.91, 132.23, 131.80, 130.22, 129.25, 128.51, 123.60, 122.04, 94.67, 87.52, m/z HRMS (EI) found 223.0635 $C_{14}H_9NO_2$ requires 223.0633. In accordance with previously reported spectra.[9]

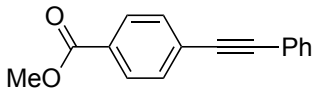

1-(*p*-Methoxycarbonylphenyl)-2-phenylacetylene, **3e**

White solid (33.5 mg, 71%), ^{1}H NMR (400 MHz, $CDCl_3$) δ 8.03 – 8.01 (m, 2H), 7.60 – 7.58 (m, 2H), 7.56 – 7.54 (m, 2H), 7.37 – 7.36 (m, 3H), 3.93 (s, 3H), ^{13}C NMR (101 MHz, $CDCl_3$) δ 166.51, 131.69, 131.46, 129.47, 129.40, 128.72, 128.39, 127.95, 122.64, 92.31, 88.58, 52.20, m/z HRMS (EI) found 236.0838 $C_{16}H_{12}O_2$ requires 236.0837. In accordance with previously reported spectra.[26]

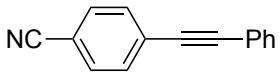

1-(*p*-Cyanophenyl)-2-phenylacetylene, **3f**

White solid (30.9 mg, 76%), ^{1}H NMR (400 MHz, $CDCl_3$) δ 7.65 – 7.60 (m, 4H), 7.56 – 7.54 (m, 2H), 7.39 – 7.37 (m, 3H), ^{13}C NMR (101 MHz, $CDCl_3$) δ 132.02, 131.99, 131.74, 129.08, 128.46, 128.20, 122.19, 118.47, 111.44, 93.75, 87.69, m/z HRMS (EI) found 203.0736 $C_{15}H_9N$ requires 203.0735. In accordance with previously reported spectra.[11]

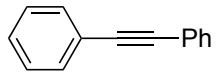

Diphenylacetylene, **3g**

White solid (20.5 mg, 58%), ^{1}H NMR (600 MHz, $CDCl_3$) δ 7.55 – 7.53 (m, 4H), 7.36 – 7.35 (m, 6H), ^{13}C NMR (101 MHz, $CDCl_3$) δ 131.58, 128.32, 128.23, 123.22, 89.34, m/z HRMS (EI) found 178.0780 $C_{14}H_{10}$ requires 178.0783. In accordance with previously reported spectra.[9]

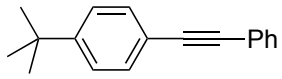

1-(*p-tert*-Butylphenyl)-2-phenylacetylene, **3h**

White solid (19.6 mg, 42%), ^{1}H NMR (400 MHz, $CDCl_3$) δ 7.56 – 7.51 (m, 2H), 7.48 (d, *J* = 8.3 Hz, 2H), 7.39 – 7.33 (m, 5H), 1.34 (s, 9H), ^{13}C NMR (101 MHz, $CDCl_3$) δ

151.48, 131.54, 131.30, 128.28, 128.04, 125.32, 123.47, 120.20, 89.51, 88.70, 34.76, 31.16, m/z HRMS (EI) found 234.1410 $C_{18}H_{18}$ requires 234.1409. In accordance with previously reported spectra.[27]

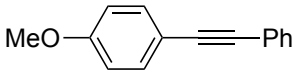

1-(*p*-Methoxyphenyl)-2-phenylacetylene, **3i**

Pale yellow solid (8.8 mg, 21%), ^{1}H NMR (400 MHz, $CDCl_3$) δ 7.51 – 7.46 (m, 4H), 7.35 – 7.20 (m, 3H), 6.89 – 6.87 (m, 2H), 3.83 (s, 3H), ^{13}C NMR (101 MHz, $CDCl_3$) δ ^{13}C NMR (101 MHz, $CDCl_3$) δ 159.59, 133.03, 132.49, 131.43, 128.43, 128.29, 127.91, 123.57, 115.36, 113.98, 89.34, 88.04, 55.30, m/z HRMS (EI) found 208.0889 $C_{15}H_{12}O$ requires 208.0888. In accordance with previously reported spectra.[28]

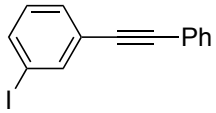

1-(*m*-Iodophenyl)-2-phenylacetylene, **3j**

White solid (29.0 mg, 48%), ^{1}H NMR (400 MHz, $CDCl_3$) δ 7.90 (t, J = 1.7 Hz, 1H), 7.67 (ddd, J = 8.0, 1.8, 1.1 Hz, 1H), 7.56 – 7.45 (m, 3H), 7.40 – 7.31 (m, 3H), 7.08 (t, J = 7.9 Hz, 1H), ^{13}C NMR (101 MHz, $CDCl_3$) δ 140.13, 137.20, 131.63, 130.68, 129.81, 128.58, 128.38, 125.36, 122.77, 93.67, 90.69, 87.61, m/z HRMS (EI) found 303.9752 $C_{14}H_9I$ requires 303.9749. In accordance with previously reported spectra.[29]

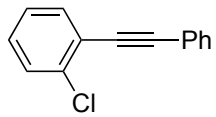

1-(*o*-Chlorophenyl)-2-phenylacetylene, **3k**

White solid (29.0 mg, 68%), ^{1}H NMR (400 MHz, $CDCl_3$) δ 7.62 – 7.55 (m, 3H), 7.46 – 7.42 (m, 1H), 7.39 – 7.34 (m, 3H), 7.30 – 7.22 (m, 2H), ^{13}C NMR (101 MHz, $CDCl_3$) δ ^{13}C NMR (101 MHz, $CDCl_3$) δ 135.92, 133.19, 131.72, 129.28, 129.21, 128.61, 128.35, 126.42, 123.22, 122.91, 94.52, 86.15, m/z HRMS (EI) found 212.0394 $C_{14}H_9Cl$ requires 212.0393. In accordance with previously reported spectra.[30]

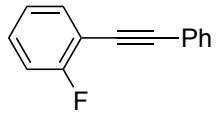

1-(*o*-Fluorophenyl)-2-phenylacetylene, **3l**

White solid (24.6 mg, 63%), ^{1}H NMR (400 MHz, $CDCl_3$) δ 7.58 – 7.51 (m, 3H), 7.37 – 7.29 (m, 4H), 7.15 – 7.09 (m, 2H), ^{13}C NMR (101 MHz, $CDCl_3$) δ 163.87, 161.37, 133.43, 131.69, 129.97, 129.89, 128.56, 128.34, 123.95, 123.91, 122.91, 115.61, 115.40, 112.01, 111.85, 94.41, 82.66, ^{19}F NMR (376 MHz, $CDCl_3$) δ -113.0, m/z HRMS (EI) found 196.0689 $C_{14}H_9F$ requires 196.0688. In accordance with previously reported spectra.[31]

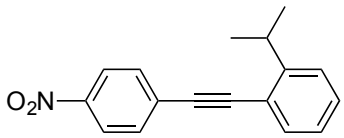

1-(*p*-Nitrophenyl)-2-(*o*-isopropylphenyl)acetylene, **3m**

Yellow solid (30.5 mg, 58%), ^{1}H NMR (400 MHz, $CDCl_3$) δ 8.23 (d, *J* = 8.9 Hz, 2H), 7.66 (d, *J* = 8.9 Hz, 2H), 7.56 – 7.48 (m, 1H), 7.40 – 7.31 (m, 2H), 7.24 – 7.16 (m, 1H), 3.51 (hept, *J* = 6.9 Hz, 1H), 1.33 (d, *J* = 6.9 Hz, 6H), ^{13}C NMR (101 MHz, $CDCl_3$) δ 150.91, 146.84, 132.61, 132.06, 130.54, 129.69, 125.73, 125.18, 123.64, 120.77, 93.74, 91.15, 31.80, 23.11, m/z HRMS (EI) found 265.1106 $C_{17}H_{15}NO_2$ requires 265.1103.

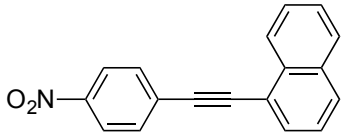

1-(*p*-Nitrophenyl)-2-(1-naphthyl)acetylene, **3n**

Yellow solid (23.4 mg, 43%), ^{1}H NMR (300 MHz, $CDCl_3$) δ 8.39 (d, *J* = 8.2 Hz, 1H), 8.28 (d, *J* = 8.5 Hz, 2H), 7.93 – 7.89 (m, 2H), 7.82 – 7.77 (m, 3H), 7.66 – 7.47 (m, 3H), ^{13}C NMR (101 MHz, $CDCl_3$) δ 147.00, 133.16, 133.10, 132.27, 131.12, 130.30, 129.88, 128.49, 127.16, 126.68, 125.82, 125.25, 123.71, 119.65, 92.94, 92.33. m/z HRMS (EI) found 273.0788 $C_{18}H_{11}NO_2$ requires 273.0790.

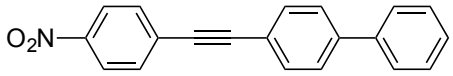

1-(*p*-Nitrophenyl)-2-(*p*-(1,1'-biphenyl)-yl)acetylene, **3o**

Yellow solid (35.4 mg, 59%), ^{1}H NMR (400 MHz, $CDCl_3$) δ 8.24 (d, *J* = 8.8 Hz, 2H), 7.69 (d, *J* = 8.8 Hz, 2H), 7.63 – 7.61 (m, 6H), 7.47 (t, *J* = 7.5 Hz, 2H), 7.40 – 7.38 (m, 1H), ^{13}C NMR (101 MHz, C_6D6) δ 146.92, 142.00, 140.02, 132.27, 132.22, 130.26, 128.91, 127.89, 127.17, 127.03, 123.64, 120.89, 94.69, 88.22, m/z HRMS (EI) found 299.0943 $C_{20}H_{13}NO_2$ requires 299.0946.

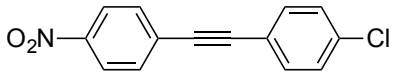

1-(*p*-Nitrophenyl)-2-(*p*-chlorophenyl)acetylene, **3p**

Pale yellow solid (39.8 mg, 77%), ^{1}H NMR (300 MHz, $CDCl_3$) δ 8.23 (d, *J* = 8.6 Hz, 2H), 7.66 (d, *J* = 8.6 Hz, 2H), 7.49 (d, *J* = 8.3 Hz, 2H), 7.37 (d, *J* = 8.3 Hz, 2H), ^{13}C NMR (101 MHz, $CDCl_3$) δ 147.11, 135.42, 133.02, 132.26, 129.84, 128.91, 123.65, 120.57, 93.40, 88.38, m/z HRMS (EI) found 257.0246 $C_{14}H_8NO_2Cl$ requires 257.0244.

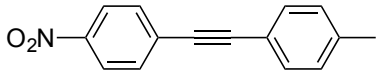

1-(*p*-Nitrophenyl)-2-*p*-tolylacetylene, **3q**

Yellow solid (36.4 mg, 77%), ^{1}H NMR (400 MHz, $CDCl_3$) δ 8.22 (d, *J* = 8.3 Hz, 2H), 7.65 (d, *J* = 8.3 Hz, 2H), 7.46 (d, *J* = 7.8 Hz, 2H), 7.20 (d, *J* = 7.7 Hz, 2H), 2.39 (s, 3H), ^{13}C NMR (101 MHz, $CDCl_3$) δ 146.83, 139.63, 132.13, 131.74, 130.51, 129.29, 123.60, 119.02, 95.09, 87.06, 21.59, m/z HRMS (EI) found 237.0792 $C_{15}H_{11}NO_2$ requires 237.0790. In accordance with previously reported spectra.[32]

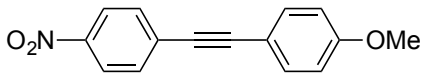

1-(*p*-Nitrophenyl)-2-(*p*-methoxyphenyl)acetylene, **3r**

Yellow (18.2 mg, 36%), ^{1}H NMR (300 MHz, $CDCl_3$) δ 8.21 (d, *J* = 8.5 Hz, 2H), 7.63 (d, *J* = 8.7 Hz, 2H), 7.50 (d, *J* = 8.8 Hz, 2H), 6.91 (d, *J* = 8.5 Hz, 2H), 3.85 (s, 3H), ^{13}C NMR (101 MHz, $CDCl_3$) δ 160.38, 146.64, 133.42, 131.96, 130.67, 123.60, 114.18, 114.08,

95.12, 86.61, 55.34, m/z HRMS (EI) found 253.0741 $C_{15}H_{11}NO_3$ requires 253.0739. In accordance with previously reported spectra.[33]

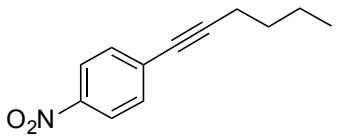

1-(*p*-Nitrophenyl)-1-hexyne, **3s**

Yellow oil (28.3 mg, 70%), ^{1}H NMR (300 MHz, $CDCl_3$) δ 8.15 (d, *J* = 8.6 Hz, 2H), 7.51 (d, *J* = 8.6 Hz, 2H), 2.45 (t, *J* = 7.0 Hz, 2H), 1.66 – 1.42 (m, 4H), 0.96 (t, *J* = 7.2 Hz, 3H), ^{13}C NMR (101 MHz, $CDCl_3$) δ 146.51, 132.19, 131.19, 123.43, 96.73, 79.25, 30.43, 22.00, 19.22, 13.57, m/z HRMS (EI) found 203.0947 $C_{12}H_{13}NO_2$ requires 203.0946. In accordance with previously reported spectra.[34]

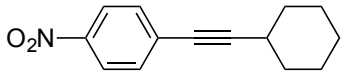

1-(*p*-Nitrophenyl)-2-cyclohexylacetylene, **3t**

Orange oil (36.4 mg, 79%), ^{1}H NMR (400 MHz, $CDCl_3$) δ 8.14 (d, J = 8.8 Hz, 2H), 7.51 (d, J = 8.8 Hz, 2H), 2.72 – 2.52 (m, 1H), 1.92 – 1.87 (m, 2H), 1.80 – 1.71 (m, 2H), 1.57 – 1.53 (m, 3H), 1.43 – 1.31 (m, 3H). ^{13}C NMR (101 MHz, $CDCl_3$) δ 146.46, 132.21, 131.25, 123.40, 100.63, 79.25, 32.31, 29.76, 25.76, 24.80, m/z HRMS (EI) found 229.1107 $C_{14}H_{15}NO_2$ requires 229.1103.

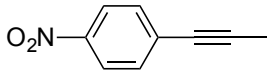

1-(*p*-Nitrophenyl)-1-propyne, **3u**

White solid (18.5 mg, 58%), ^{1}H NMR (400 MHz, $CDCl_3$) δ 8.15 (d, *J* = 8.9 Hz, 2H), 7.51 (d, *J* = 8.8 Hz, 2H), 2.10 (s, 3H), ^{13}C NMR (101 MHz, $CDCl_3$) δ 146.57, 132.17, 131.10, 123.47, 92.16, 78.43, 4.53, m/z HRMS (EI) found 161.0480 $C_9H_7NO_2$ requires 161.0477. In accordance with previously reported spectra.[35]

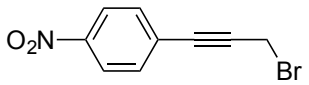

1-(*p*-Nitrophenyl)-3-bromo-1-propyne, **3v**

Pale yellow solid (23.5 mg, 49%), ^{1}H NMR (400 MHz, $CDCl_3$) δ 8.20 (d, *J* = 8.6 Hz, 2H), 7.59 (d, *J* = 8.6 Hz, 2H), 4.16 (s, 2H), ^{13}C NMR (101 MHz, $CDCl_3$) δ 147.43, 132.63, 128.92, 123.57, 89.29, 84.36, 14.02, m/z HRMS (EI) found 238.9581 $C_9H_6NO_2Br$ requires 238.9582. In accordance with previously reported spectra.[36]

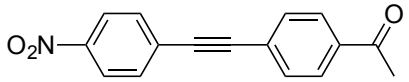

1-(*p*-Nitrophenyl)-2-(*p*-acetylphenyl)acetylene, **3y**

Pale yellow solid (35 mg, 66%), ^{1}H NMR (400 MHz, $CDCl_3$) δ 8.24 (d, *J* = 8.7 Hz, 2H), 7.98 (d, *J* = 8.3 Hz, 2H), 7.70 (d, *J* = 8.7 Hz, 2H), 7.65 (d, *J* = 8.3 Hz, 2H), 2.63 (s, 3H), ^{13}C NMR (101 MHz, $CDCl_3$) δ 197.13, 147.25, 136.91, 132.41, 131.93, 129.46, 128.32, 126.76, 123.65, 93.41, 90.29, 26.62, m/z HRMS (EI) found 265.0739 $C_{16}H_{11}NO_3$ requires 265.0739.

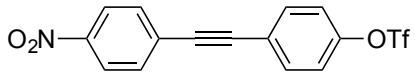

4-((4-nitrophenyl)ethynyl)phenyl trifluoromethanesulfonate, **3z**

Pale Yellow solid (42 mg, 57%), ^{1}H NMR (400 MHz, $CDCl_3$) δ 8.24 (d, *J* = 8.9 Hz, 2H), 7.68 (d, J = 8.9 Hz, 2H), 7.64 (d, J = 8.8 Hz, 2H), 7.31 (d, J = 8.8 Hz, 2H), ^{13}C NMR (101 MHz, $CDCl_3$) δ 149.51, 147.31, 133.70, 132.40, 129.34, 123.68, 122.77, 121.74, 118.66 (q, *J* = 322 Hz), 92.19, 89.10, m/z HRMS (EI) found 371.0075 $C_{15}H_8NO_5SF_3$ requires 371.0075.

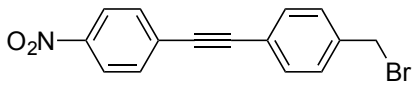

1-(*p*-Nitrophenyl)-2-(*p*-(bromomethyl)phenyl)acetylene, **3aa**

Yellow solid (34 mg, 54%), ^{1}H NMR (400 MHz, $CDCl_3$) δ 8.23 (d, *J* = 8.9 Hz, 2H), 7.67 (d, *J* = 8.9 Hz, 2H), 7.53 (d, *J* = 8.3 Hz, 2H), 7.41 (d, *J* = 8.2 Hz, 2H), 4.50 (s, 2H), ^{13}C NMR (101 MHz, $CDCl_3$) δ 147.04, 138.87, 132.29, 132.19, 129.96, 129.21, 123.63, 122.17, 94.03, 88.28, 32.65, m/z HRMS (EI) found 314.9895 $C_{15}H_{10}NO_2{}^{79}Br$ requires 314.9895.

2.5.6 Preparation of allene substrates and authentic products

Preparation of p-nitrophenylacetylene, 3x[37]

To a solution of ((*p*-nitrophenyl)ethynyl)trimethylsilane, **3w** (0.5 mmol) in diethyl ether (3 mL) was added methanol (3 mL) and aqueous sodium hydroxide solution (1.5 mL, 10 wt%). The mixture was stirred for 10 min at 23 °C and neutralized with 1 N HCl solution. The organic layer was separated, and the aqueous layer was extracted with diethyl ether (3 × 3 mL). The combined organic layers were washed with brine (10 mL) and water (10 mL), dried over $MgSO_4$, and concentrated. The residue was purified by flash chromatography on silica gel. Yellow Solid (68.1 mg, 93%), ^{1}H NMR (500 MHz, $CDCl_3$) δ 8.20 (d, *J* = 8.6 Hz, 2H), 7.64 (d, *J* = 8.6 Hz, 2H), 3.36 (s, 1H), ^{13}C NMR (101 MHz, $CDCl_3$) δ 147.49, 132.93, 128.87, 123.52, 82.30, 81.57. In accordance with previously reported spectra.[12]

Preparation of 1-phenyl-3-*p*-fluorophenyl-1-propyne, 5

p-Fluorobenzenediazonium tetrafluoroborate, **1a** (42.0 mg, 0.20 mmol, 1.0 eq.), 1-phenyl-1-trimethylsilylprop-1,2-diene, **4**[38] (38 mg, 0.20 mmol, 1.0 eq.) and triphenylphosphinegold(I) chloride (4.9 mg, 0.01 mmol, 5 mol%) were placed in a vial equipped with a stir bar. To the vial kept at –78°C was added the solution of tris(2,2'-bipyridine)ruthenium(II) hexafluorophosphate (1.7 mg, 0.002 mmol, 1 mol%) in acetonitrile (2 mL). The vial was evacuated and refilled with nitrogen three times. The mixture was slowly warmed up to 23 °C and stirred for 6 h under a household lamp with a 23 W fluorescent light bulb. After the completion of reaction, diethyl ether (20 mL) was added and filtered through a Celite plug. The filtrate was dried in vaccuo and purified by flash column chromatography to give the desired product. Pale orange solid (17.0 mg, 41%), ^{1}H NMR (400 MHz, $CDCl_3$) δ 7.44 (dd, J = 6.6, 2.9 Hz, 2H), 7.37 (dd, J = 8.1, 5.9 Hz, 2H), 7.33 – 7.28 (m, 3H), 7.03 (t, J = 8.7 Hz, 2H), 3.80 (s, 2H), ^{13}C NMR (101 MHz, $CDCl_3$) δ 161.73 (d, J = 244.6 Hz), 132.38 (d, J = 2.9 Hz), 131.61, 129.37 (d, J = 8.0 Hz), 128.25, 127.91, 123.50, 115.30 (d, J = 21.5 Hz), 87.25, 82.82, 25.00, ^{19}F NMR (376 MHz, $CDCl_3$) δ -119.7, m/z HRMS (EI) found 209.0768 $C_{15}H_{10}F$ requires 209.0767.

Preparation of 1-phenyl-1-*p*-fluorophenylprop-1,2-diene, **6**[39]

To a solution of 1-phenyl-1-propyne (116 mg, 1.00 mmol) in THF (7.7 mL) at –78 °C under N_2 was added *n*-BuLi (2.5 M in hexanes, 0.46 mL, 1.14 mmol). After stirring at –78 °C for 1 h, a solution of dry $ZnBr_2$ (450 mg, 2.00 mmol) in THF (10.0 mL) was added. After stirring 10 min, the reaction mixture was slowly warmed to 23 °C. $Pd(PPh_3)_4$ (39 mg, 5 mol %) and *p*-fluoroiodobenzene (77 μL, 0.67 mmol) were subsequently added at 23 °C with stirring. After stirring 1 h, the mixture was quenched with saturated NH_4Cl, extracted with diethyl ether, dried over $MgSO_4$ and concentrated. The residue was purified by flash column chromatography to give the desired product. White solid (132 mg, 93%), ^{1}H NMR (400 MHz, $CDCl_3$) δ 7.41 – 7.27 (m, 7H), 7.04 (t, J = 8.7 Hz, 2H), 5.27 (s, 2H), ^{13}C NMR (101 MHz, CDCl3) δ 209.68, 162.06 (d, J = 246.4 Hz), 136.08, 132.15 (d, J = 3.3 Hz), 129.98 (d, J = 8.0 Hz), 128.45, 128.26, 127.32, 115.29 (d, J = 21.5 Hz), 108.29, 78.20, ^{19}F NMR (376 MHz, $CDCl_3$) δ -118.4, m/z HRMS (EI) found 209.0769 $C_{15}H_{10}F$ requires 209.0767.

Preparation of 1-*p*-fluorophenyl-3-phenyl-1-propyne, **7**[38]

Preparation of LDA solution: To a solution of diisopropylamine (0.30 mL, 2 mmol) in THF (1 mL) at -78 ºC and under N_2 was added *n*-BuLi (2.5 M in hexanes, 0.80 mL, 2 mmol) and the mixture was stirred for 30 min at this temperature.

To a solution of 1-phenyl-1-propyne (116 mg, 1.00 mmol) in THF (7.7 mL) at –78 °C under N_2 was added the prepared LDA solution. The reaction mixture was slowly warmed to 23 °C and stirred for 1 h. To the mixture, a solution of dry ZnBr2 (450 mg, 2 mmol) in THF (10 mL) was added. After stirring at 23 °C for 25 min, $Pd(PPh_3)_4$ (39 mg, 5 mol %) and *p*-fluoroiodobenzene (77 μL, 0.67 mmol) were added. After stirring 1 h, the mixture was quenched with saturated NH_4Cl, extracted with diethyl ether, dried over $MgSO_4$ and concentrated. The residue was purified by flash column chromatography to give the desired product. Orange solid (141 mg, 99%), ^{1}H NMR (400 MHz, $CDCl_3$) 7.48 – 7.39 (m, 4H), 7.35 (t, J = 7.4 Hz, 2H), 7.30 – 7.22 (m, 1H), 7.00 (t, J = 8.7 Hz, 2H), 3.82 (s, 2H), ^{13}C NMR (101 MHz, $CDCl_3$) δ 162.15 (d, J = 248.6 Hz), 136.57, 133.38 (d, J = 8.2 Hz), 128.51, 127.88, 126.63, 119.67 (d, J = 3.4 Hz), 115.39 (d, J = 22.0 Hz),

87.16, 81.52, 25.60, ^{19}F NMR (376 MHz, $CDCl_3$) δ -115.0, m/z HRMS (EI) found 209.0768 $C_{15}H_{10}F$ requires 209.0767.

2.5.7 References

(1) Nelson, H. M.; Reisberg, S. H.; Shunatona, H. P.; Patel, J. S.; Toste, F. D. *Angew. Chem. Int. Ed.* **2014**, *53*, 5600.

(2) Blank, O.; Ullrich, D.; Kirschstein, M.; Heinrich, M. R. *J. Org. Chem.* **2007**, *72*, 9609.

(3) Piao, Y.; Meany, B.; Powell, L. R.; Valley, N.; Kwon, H.; Schatz, G. C.; Wang, Y. *Nat. Chem.* **2013**, *5*, 840.

(4) Dirk, S. M.; Pylypenko, S.; Howell, S. W.; Fulghum, J. E.; Wheeler, D. R. *Langmuir* **2005**, *21*, 10899.

(5) Prechter, A.; Heinrich, M. R. *Synthesis* **2011**, *10*, 1515.

(6) Rutherford, K. G.; Redmond, W. *Org. Synth.* **1963**, *43*, 12.

(7) Tang, Z. Y.; Zhang, Y.; Wang, T.; Wang, W. *Synlett.* **2010**, *5*, 804.

(8) Chen, C. C.; Waser, J. *Org. Lett.* **2015**, *17*, 736.

(9) Carril, M.; Correa, A.; Bolm, C. *Angew. Chem. Int. Ed.* **2008**, *47*, 4862.

(10) Uhl, W.; Kovert, D.; Zemke, S.; Hepp, A. *Organometallics* **2011**, *30*, 4736.

(11) Truong, T.; Daugulis, O. *Org. Lett.* **2011**, *13*, 4172.

(12) Ueda, H.; Yamaguchi, M.; Kameya, H.; Sugimoto, K.; Tokuyama, H. *Org. Lett.* **2014**, *16*, 4948.

(13) Tobisu, M.; Nakai, H.; Chatani, N. *J. Org. Chem.* **2009**, *74*, 5471.

(14) Pena, M. A.; Sestelo, J. P.; Sarandeses, L. A. *Synthesis* **2005**, *3*, 485.

(15) Cai, M.; Sha, J.; Xu, Q. *Tetrahedron* **2007**, *63*, 4642.

(16) Rawashdeh, A. M.; Elder, I. A.; Yang, J.; Dass, A. ; Sotiriou-Leventis, C.; Leventis, N. *Chem. Mater.* **2004**, *16*, 1493.

(17) Fabrizi, G.; Goggiamani, A.; Sferrazza, A.; Cacchi, S. *Angew. Chem. Int. Ed.* **2010**, *49*, 4067.

(18) Gager, O.; Buendia, J.; Cahiez, G. *Angew. Chem. Int. Ed.* **2010**, *49*, 1278.

(19) Huestis, M. P.; Chan, L.; Stuart, D. R.; Fagnou, K. *Angew. Chem. Int. Ed.* **2011**, *50*, 1338.

(20) Zhang, H.; Fu, X.; Chen, J.; Wang, E.; Liu, Y.; Li, Y. *J. Org. Chem.* **2009**, *74*, 9351.

(21) Greszler, S. N.; Reichard, H. A.; Micalizio, G. C. *J. Am. Chem. Soc.* **2012**, *134*, 2766.

(22) Kawamura, H.; Takeyama, Y.; Yamamoto, M.; Kurihara, H.; Morino, K.; Yashima, E. *Chirality* **2011**, *23*, E35.

(23) Braunstein, P.; Lehner, H.; Matt, D. *Inorg. Synth.* **1990**, *27*, 218.

(24) Ischay, M. A.; Lu, Z.; Yoon, T. P. *J. Am. Chem. Soc.* **2010**, *132*, 8572.

(25) (a) Sprouse, S.; King, K. A.; Spellane, P. J.; Watts, R. J. *J. Am. Chem. Soc.* **1984**, *106*, 6647. (b) Ru, J.; Guan, L.; Tang, X.; Dou, W.; Yao, X.; Chen, W.; Liu, Y.; Zhang, G.; Liu, W.; Meng, Y.; Wang, C. *Inorg. Chem.* **2014**, *53*, 11498. (c) Slinker, J. D.; Gorodetsky, A. A.; Lowry, M. S.; Wang, J.; Parker, S.; Rohl, R.; Bernhard, S.; Malliaras, G. G. *J. Am. Chem. Soc.* **2004**, *126*, 2763.

(26) Fabrizi, G.; Goggiamani, A.; Sferrazza, A.; Cacchi, S. *Angew. Chem. Int. Ed.* **2010**, *49*, 4067.

(27) Moon, J.; Jeong, M.; Nam, H.; Ju, J.; Moon, J. H.; Jung, H. M.; Lee, S. *Org. Lett.* **2008**, *10*, 945.

(28) Park, S. B.; Alper, H. *Chem. Commun.* **2004**, 1306.

(29) Orita, A.; Taniguchi, H.; Otera, J. *Chem. − Asian J.* **2006**, *1*, 430.

(30) Novak, Z.; Nemes, P.; Kotschy, A. *Org. Lett.* **2004**, *6*, 4917.

(31) Xu, C.; Xu, M.; Jia, Y.; Li, C. *Org. Lett.* **2011**, *13*, 1556.

(32) Gholap, A. R.; Venkatesan, K.; Pasricha, R.; Daniel, T.; Lahoti, R. J.; Srinivasan, K. V. *J. Org. Chem.* **2005**, *70*, 4869.

(33) Rao, M. L. N.; Jadhav, D. N.; Dasgupta, P. *Org. Lett.* **2010**, *12*, 2048.

(34) Liang, B.; Dai, M.; Chen, J.; Yang, Z. *J. Org. Chem.* **2005**, *70*, 391.

(35) Weerasooriya, U.; Gilbert, J. C. *J. Org. Chem.* **1982**, *47*, 1837.

(36) Maji, M.; Mallick, D.; Mondal, S.; Anoop, A.; Bag, S. S.; Basak, A.; Jemmis, E. D.

Org. Lett. **2011**, *13*, 888.

(37) Feng, Y.; Xie, C.; Qiao, W.; Xu, H. *Org. Lett.* **2013**, *15*, 936.

(38) Williams, D. R.; Shah, A. A. *Chem. Commun*. **2010**, *46*, 4297.

(39) Ma, S.; He, Q.; Zhang, X. *J. Org. Chem.* **2005**, *70*, 3336.

2.5.8 NMR Spectra

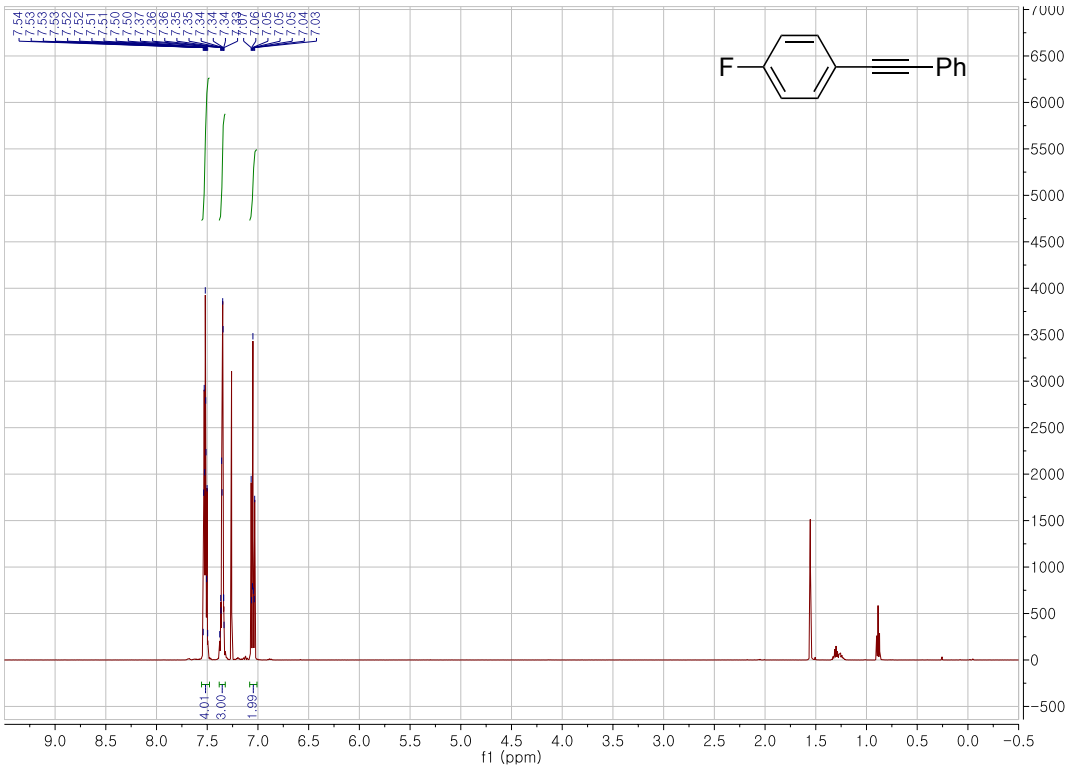

Figure 2.1 ^{1}H NMR Spectrum of **3a**

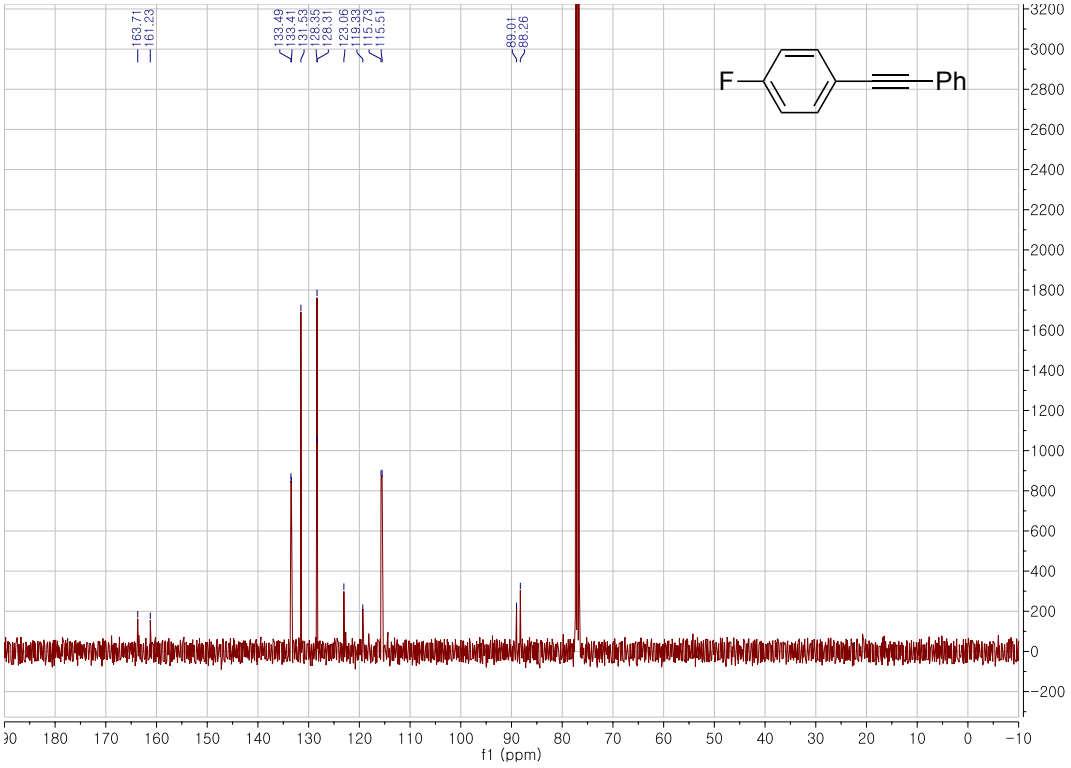

Figure 2.2 ^{13}C NMR Spectrum of **3a**

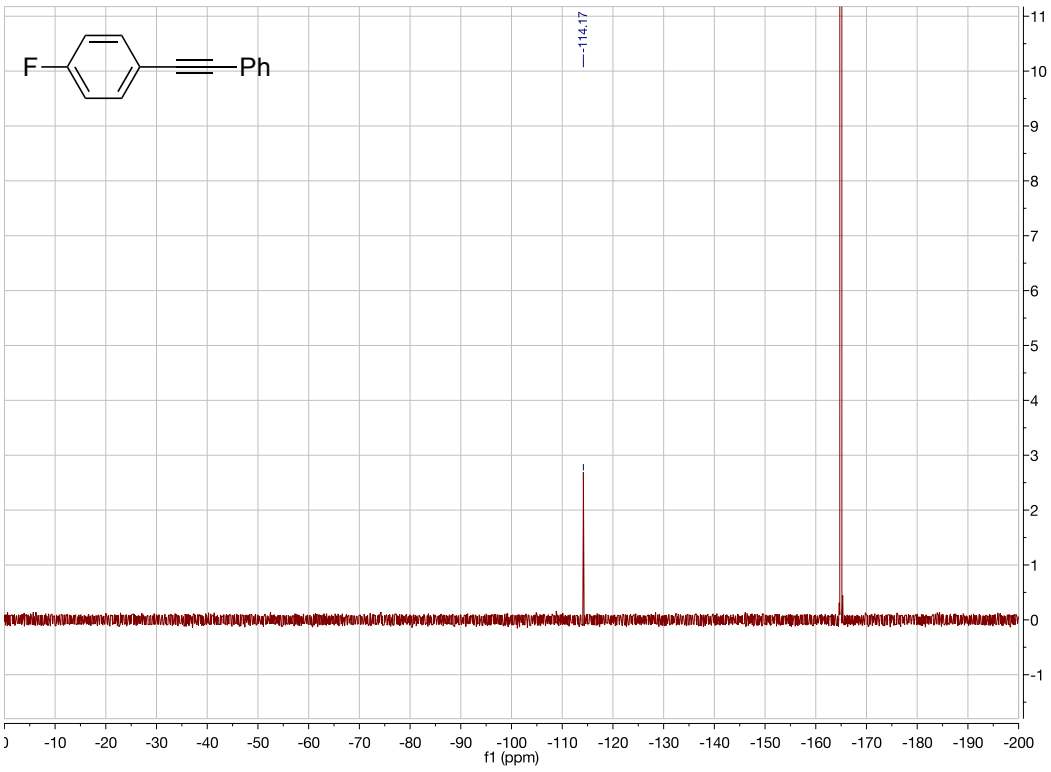

Figure 2.3 ^{19}F NMR Spectrum of **3a**

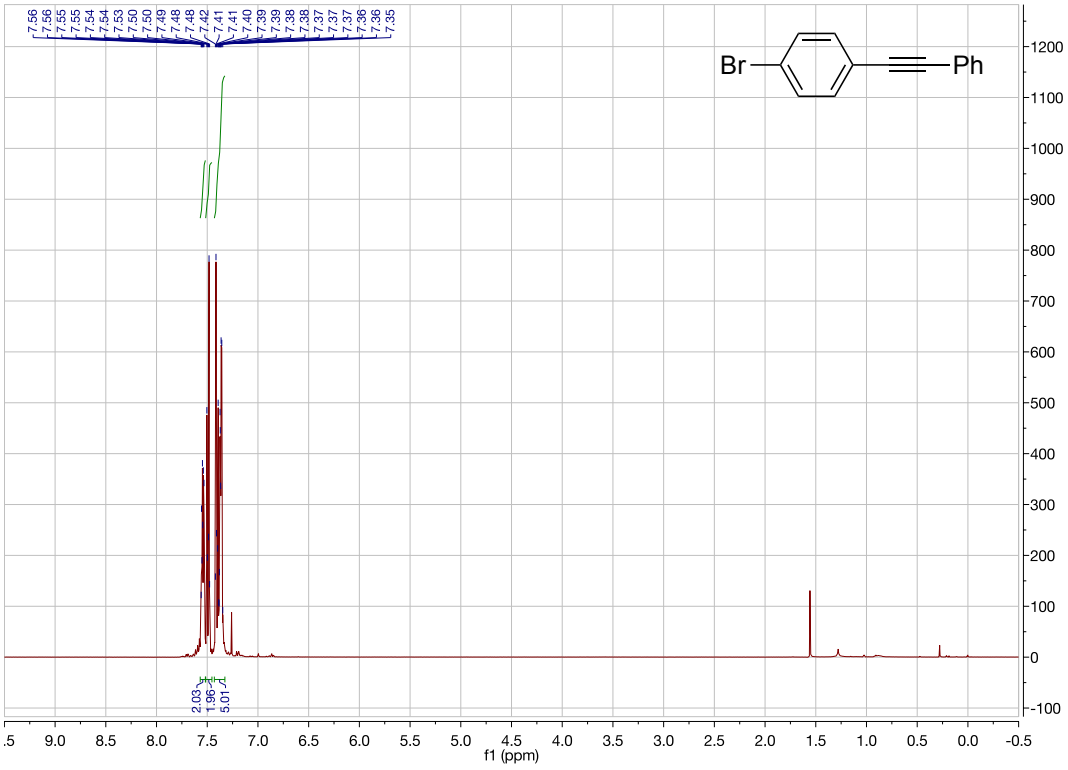

Figure 2.4 ^{1}H NMR Spectrum of **3b**

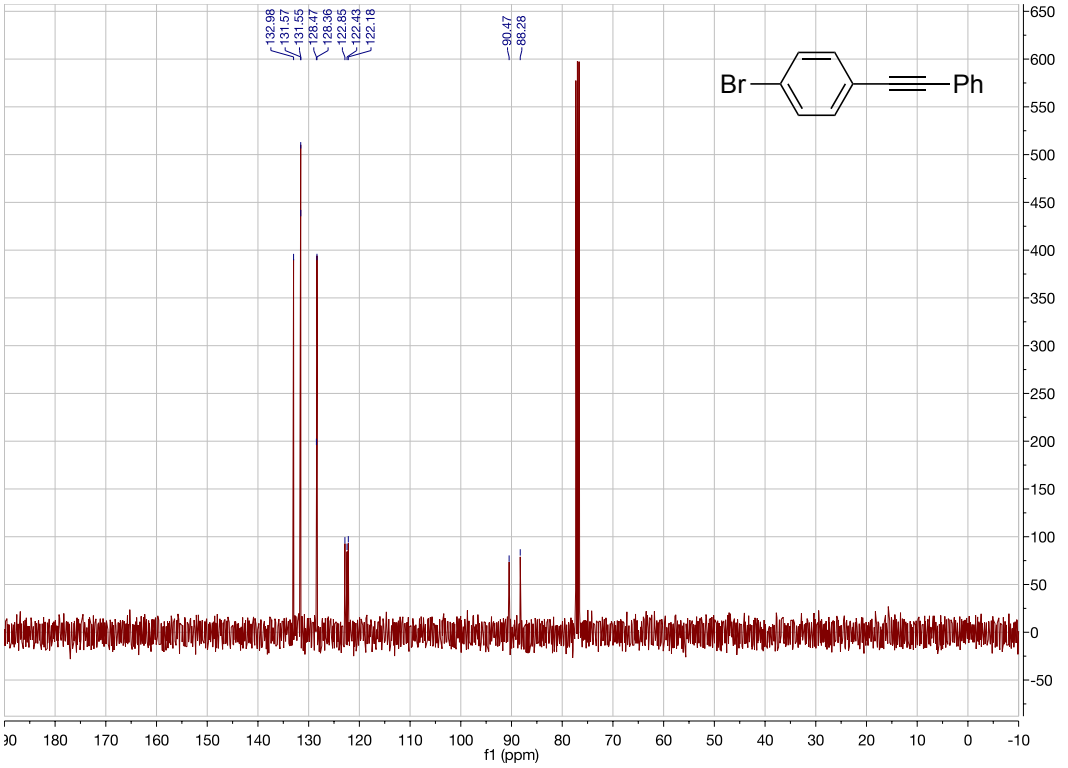

Figure 2.5 ^{13}C NMR Spectrum of **3b**

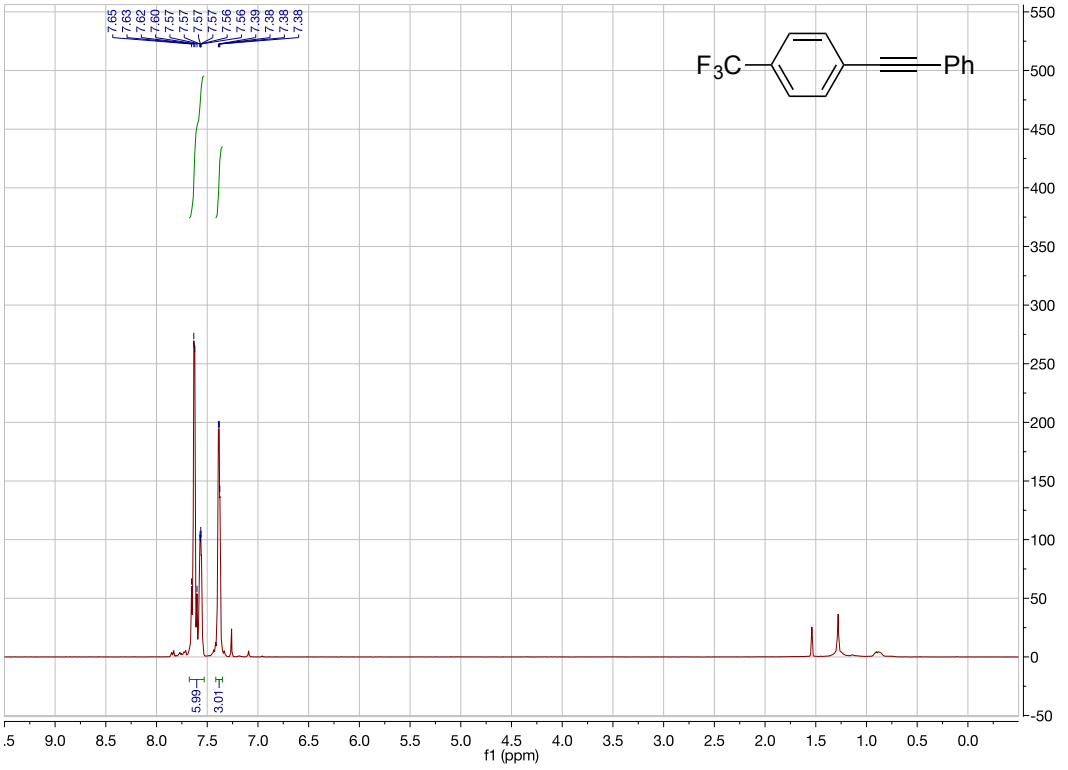

Figure 2.6 ^{1}H NMR Spectrum of **3c**

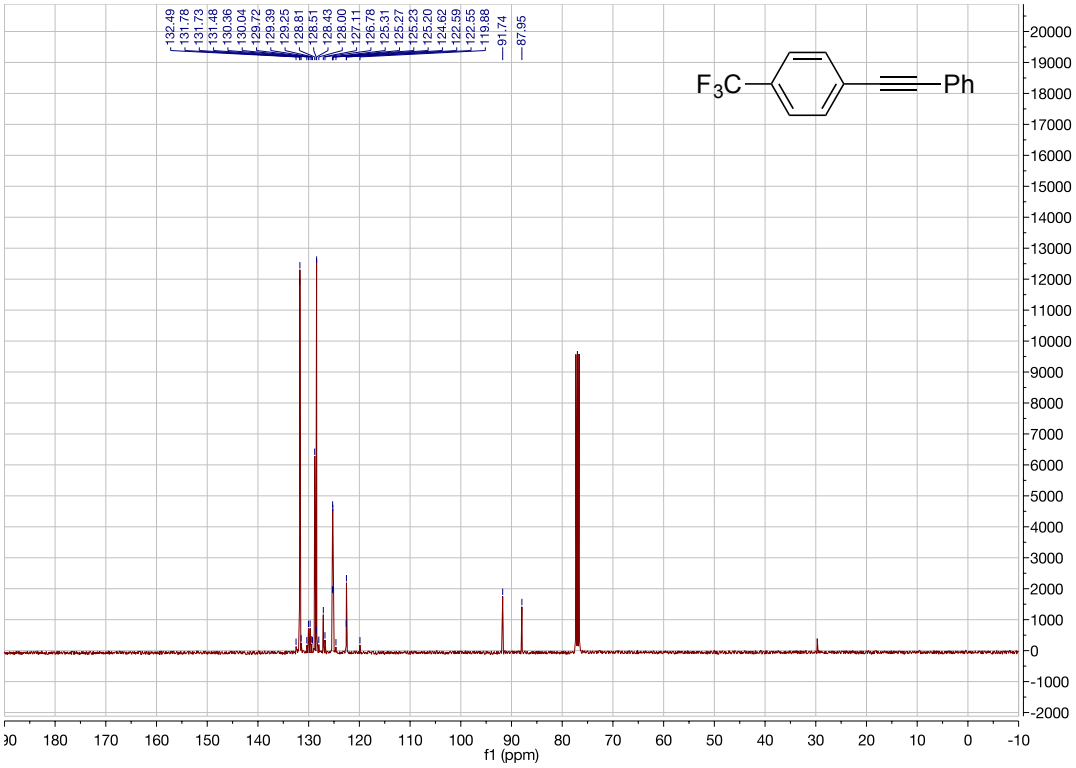

Figure 2.7 ^{13}C NMR Spectrum of **3c**

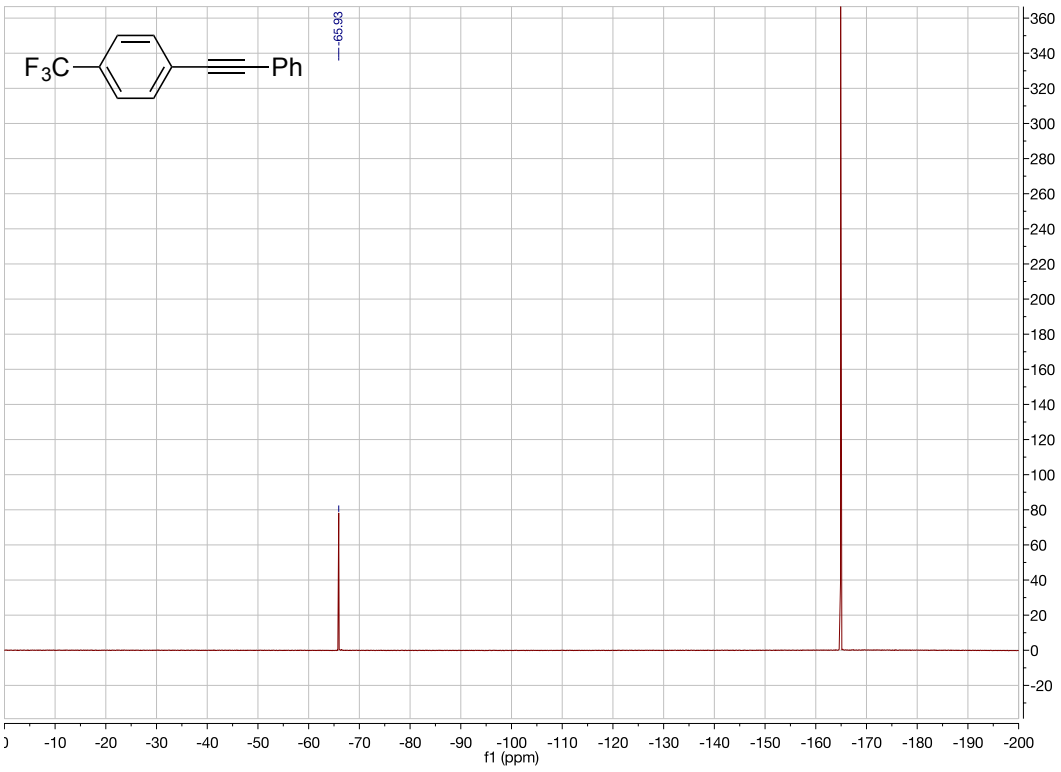

Figure 2.8 ^{19}F NMR Spectrum of **3c**

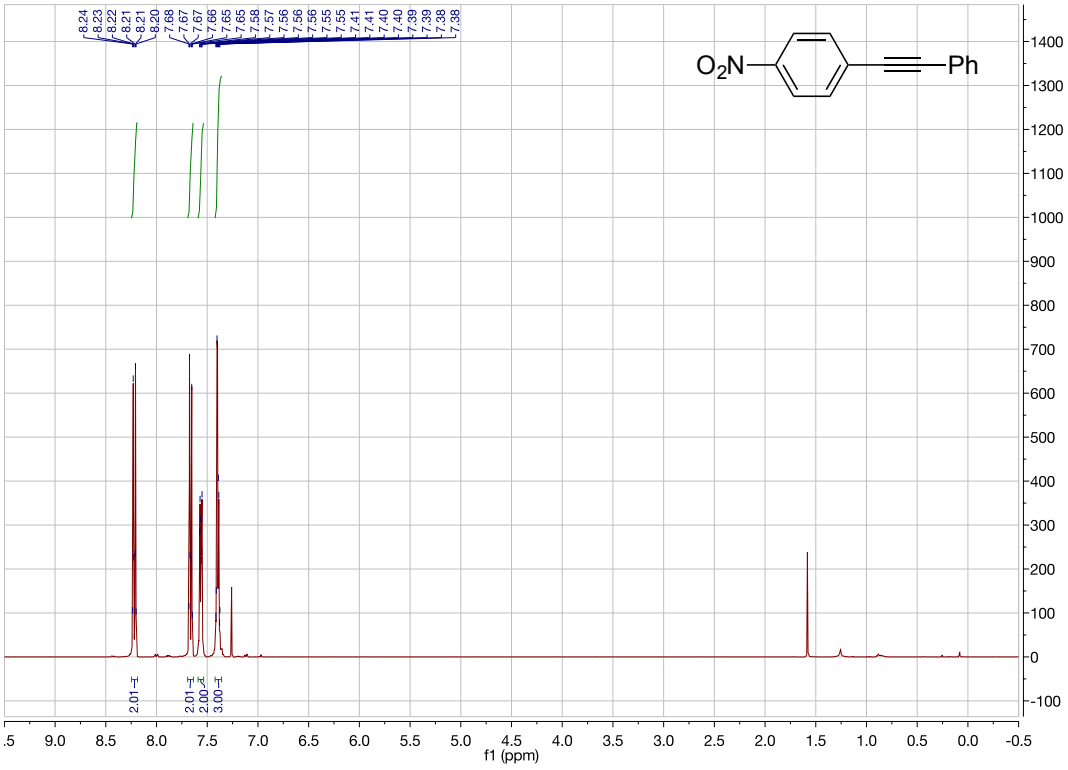

Figure 2.9 ^{1}H NMR Spectrum of **3d**

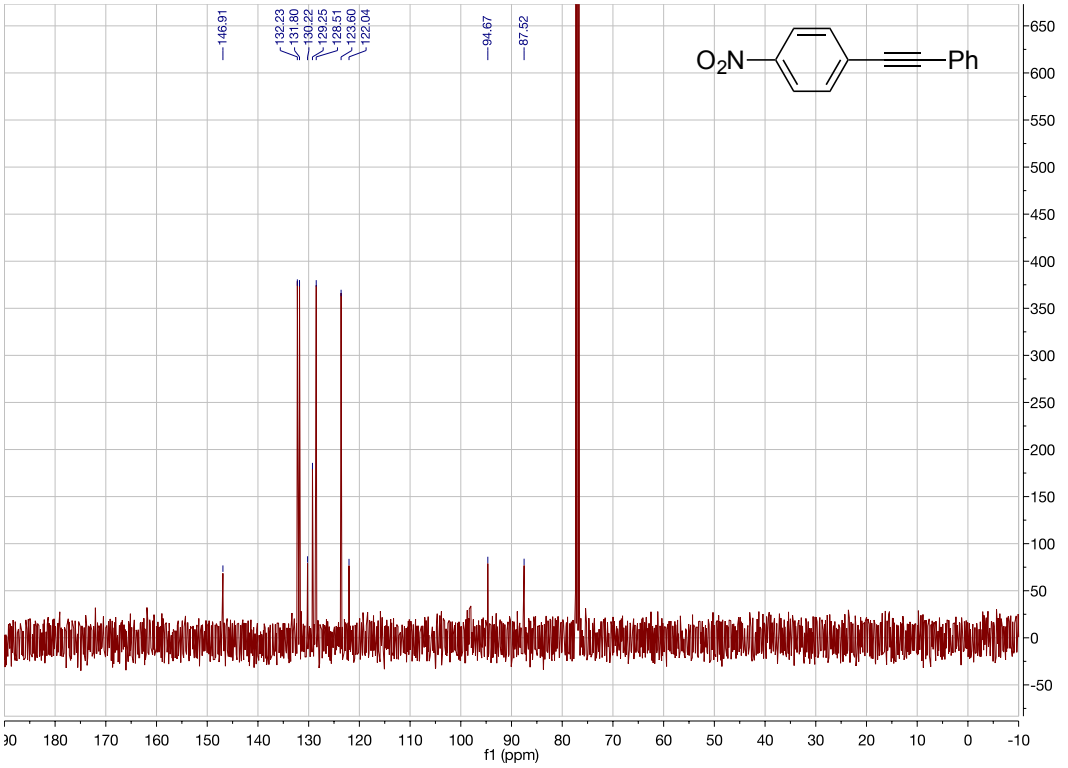

Figure 2.10 ^{13}C NMR Spectrum of **3d**

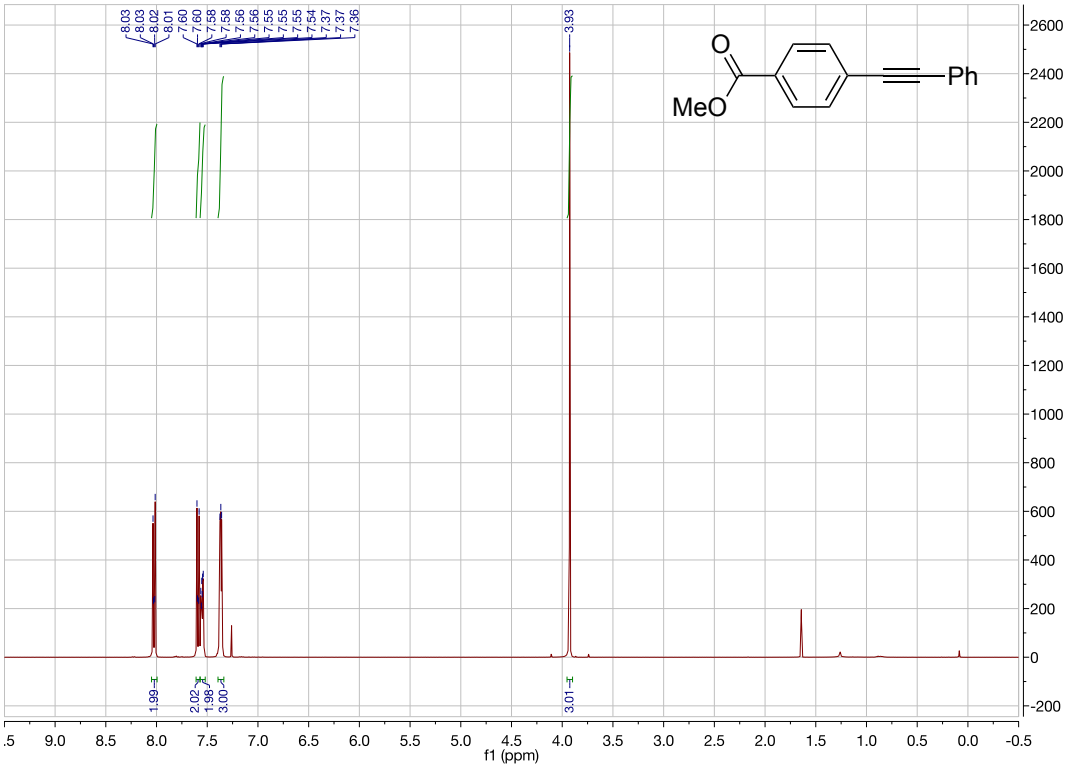

Figure 2.11 ^{1}H NMR Spectrum of **3e**

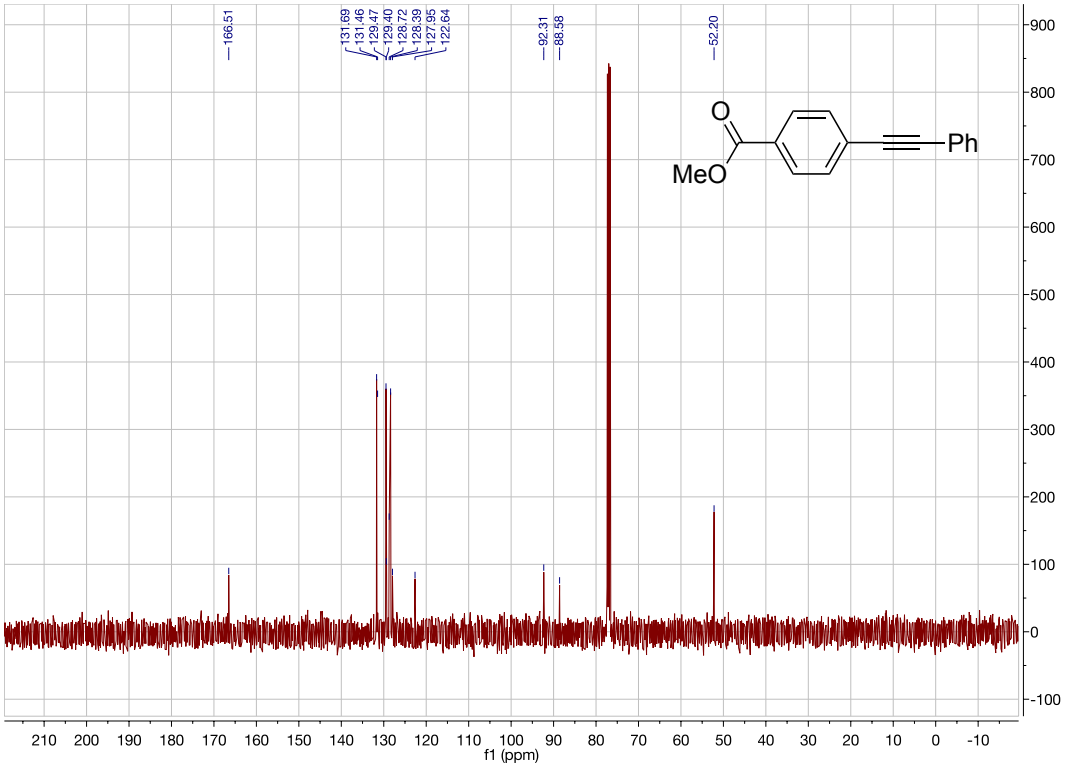

Figure 2.12 ^{13}C NMR Spectrum of **3e**

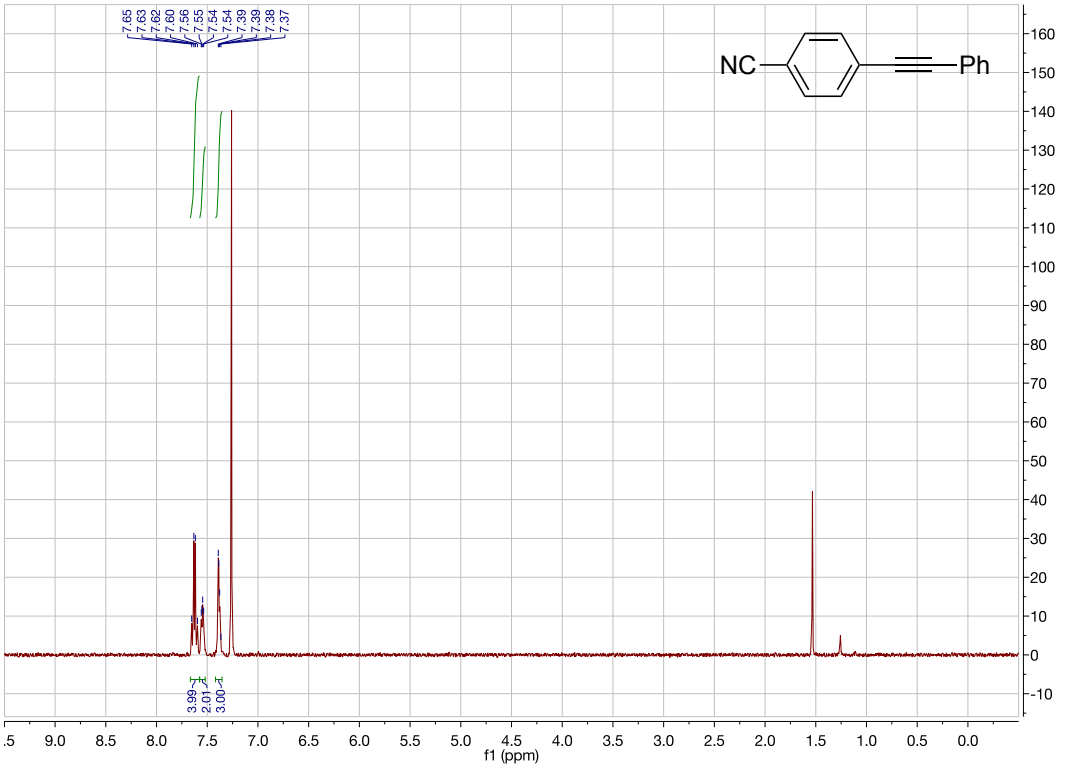

Figure 2.13 ^{1}H NMR Spectrum of **3f**

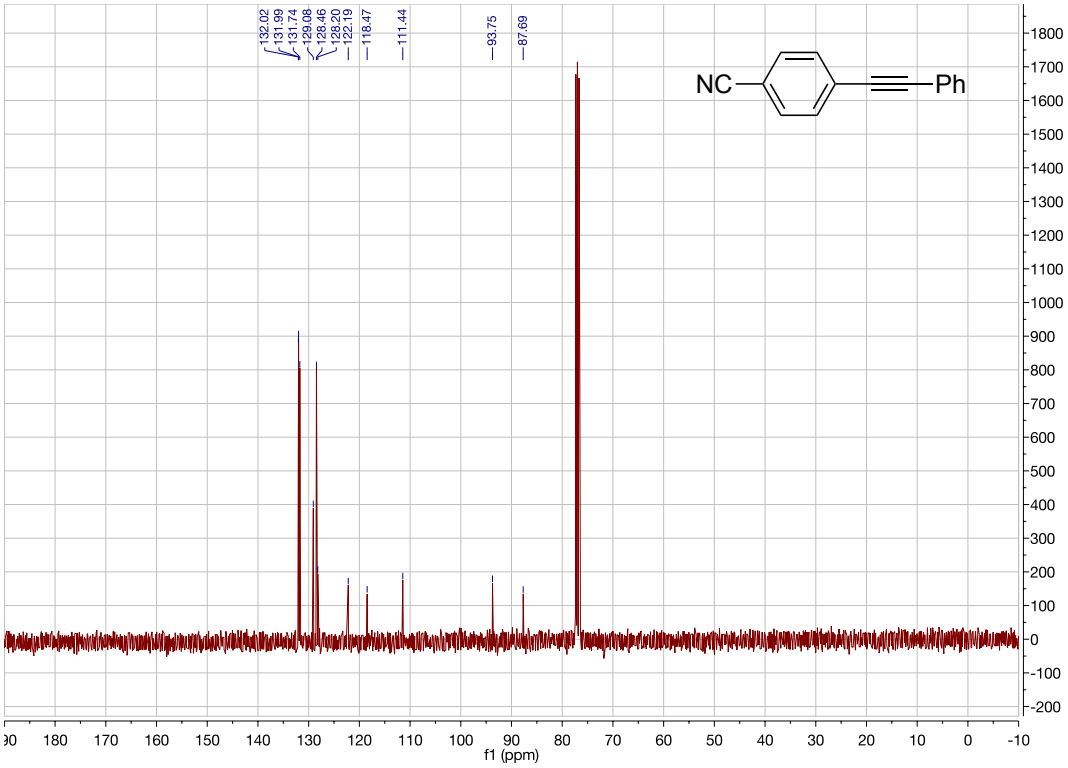

Figure 2.14 ^{13}C NMR Spectrum of **3f**

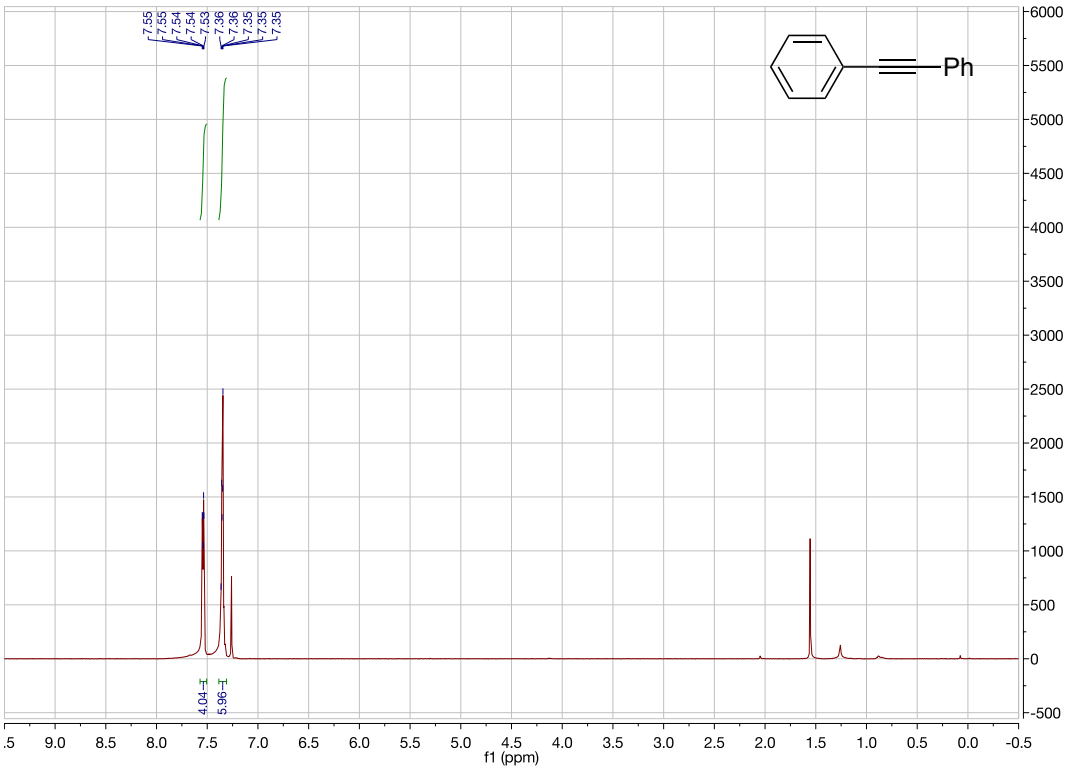

Figure 2.15 ^{1}H NMR Spectrum of **3g**

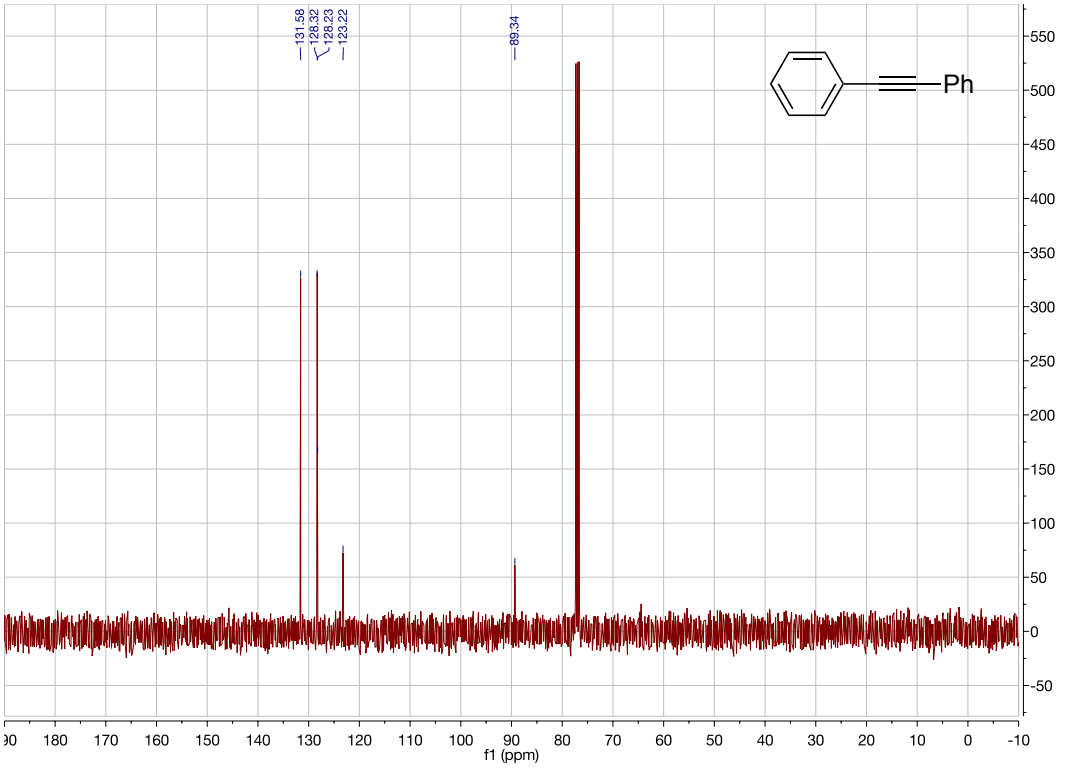

Figure 2.16 ^{13}C NMR Spectrum of **3g**

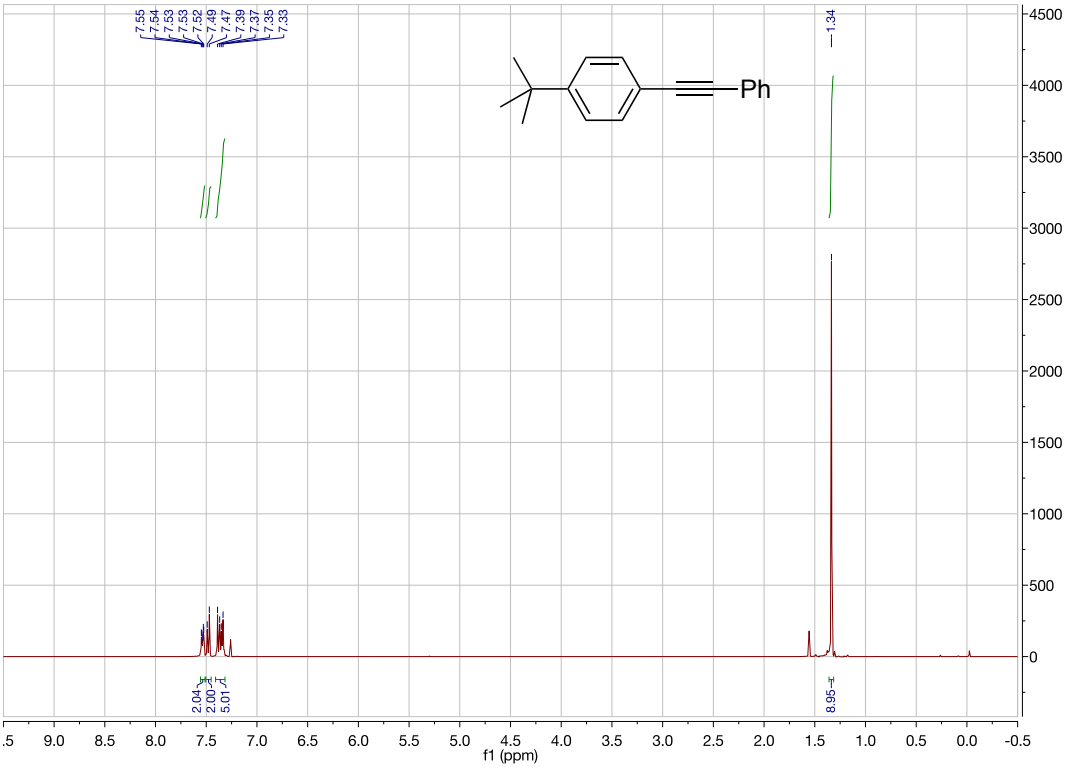

Figure 2.17 ^{1}H NMR Spectrum of **3h**

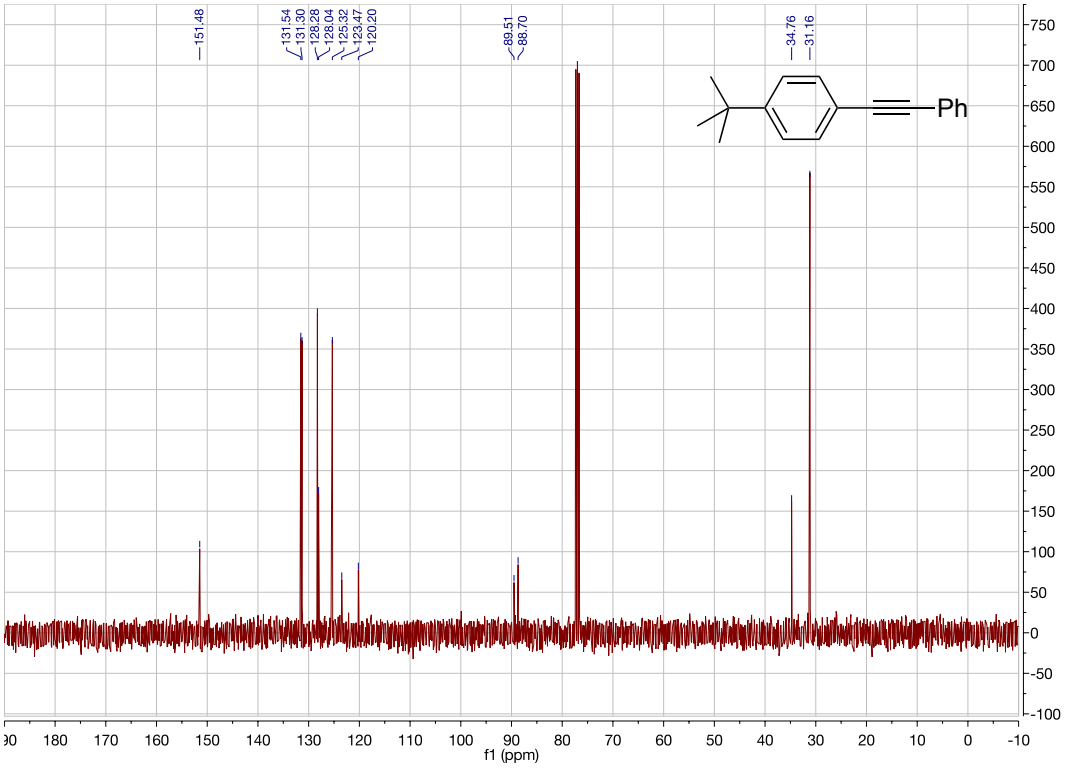

Figure 2.18 ^{13}C NMR Spectrum of **3h**

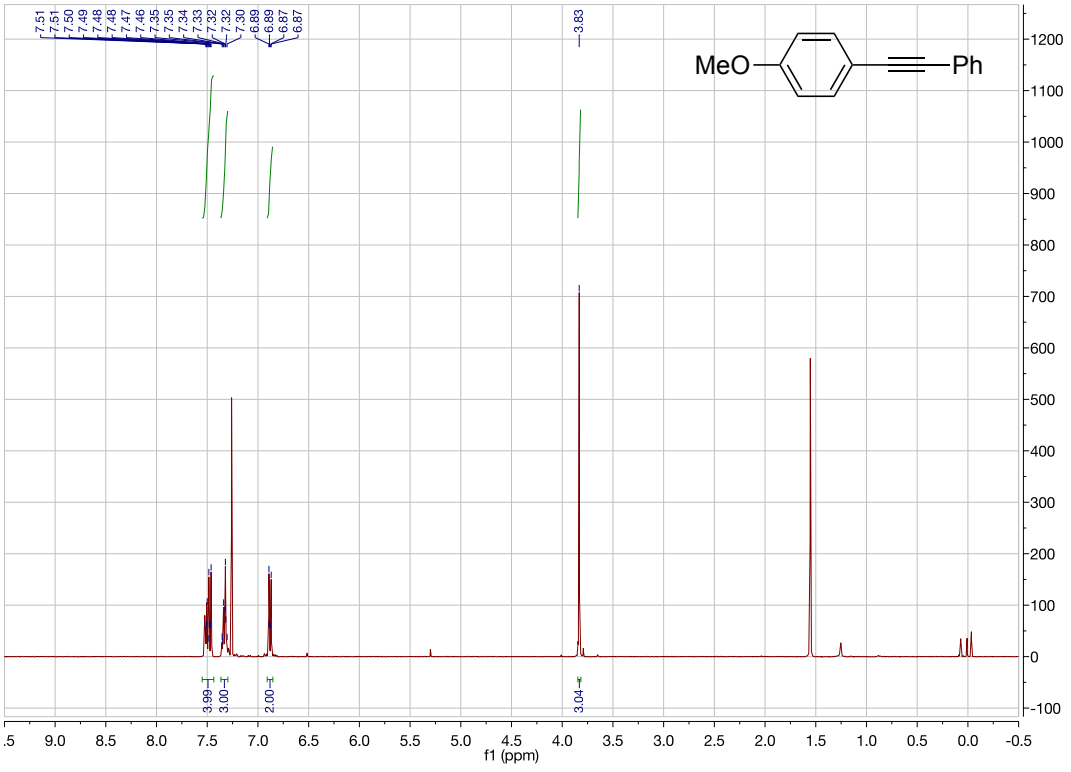

Figure 2.19 ^{1}H NMR Spectrum of **3i**

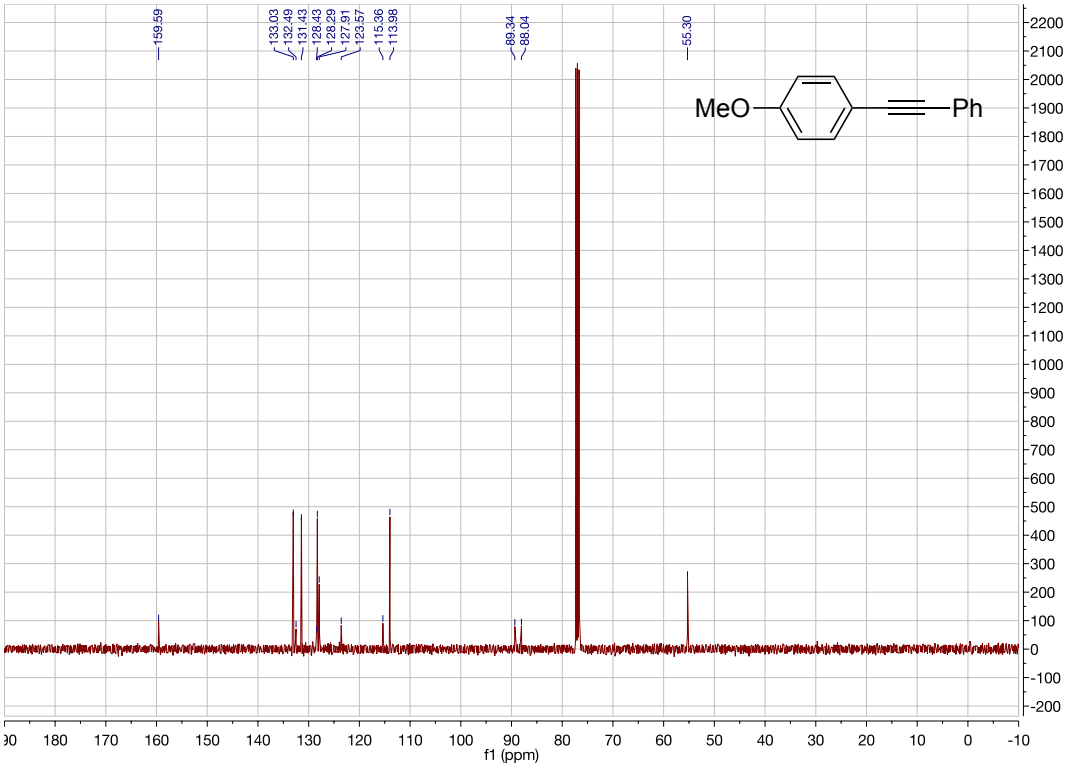

Figure 2.20 ^{13}C NMR Spectrum of **3i**

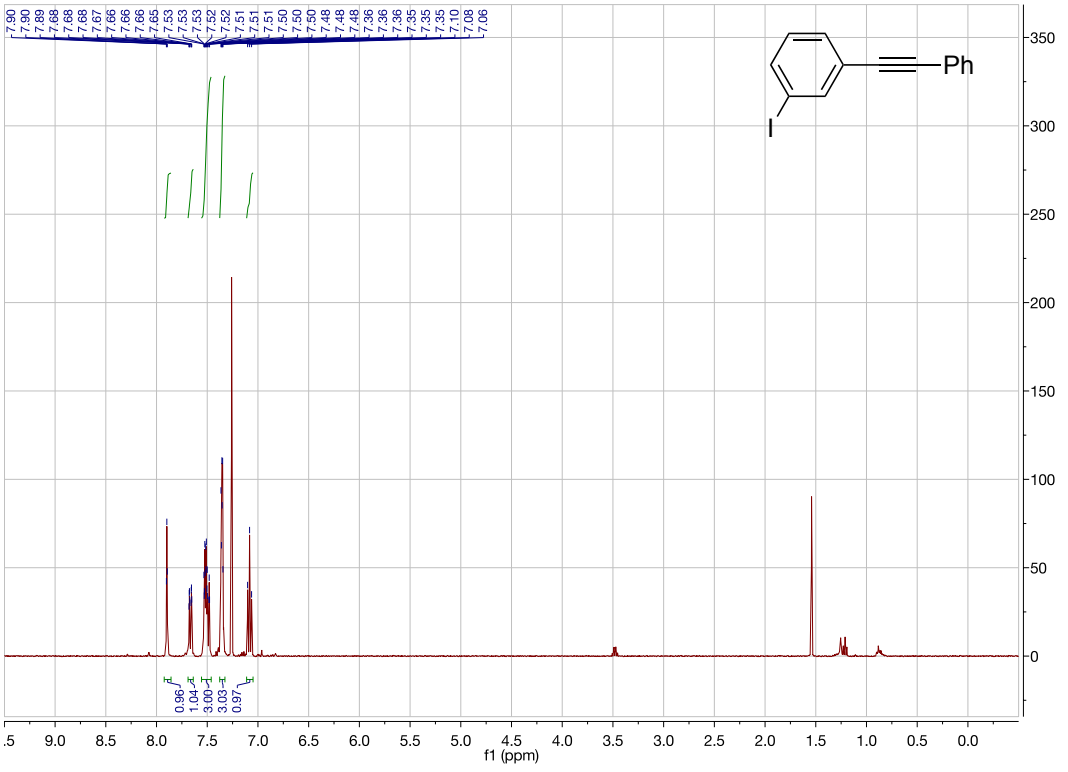

Figure 2.21 ^{1}H NMR Spectrum of **3j**

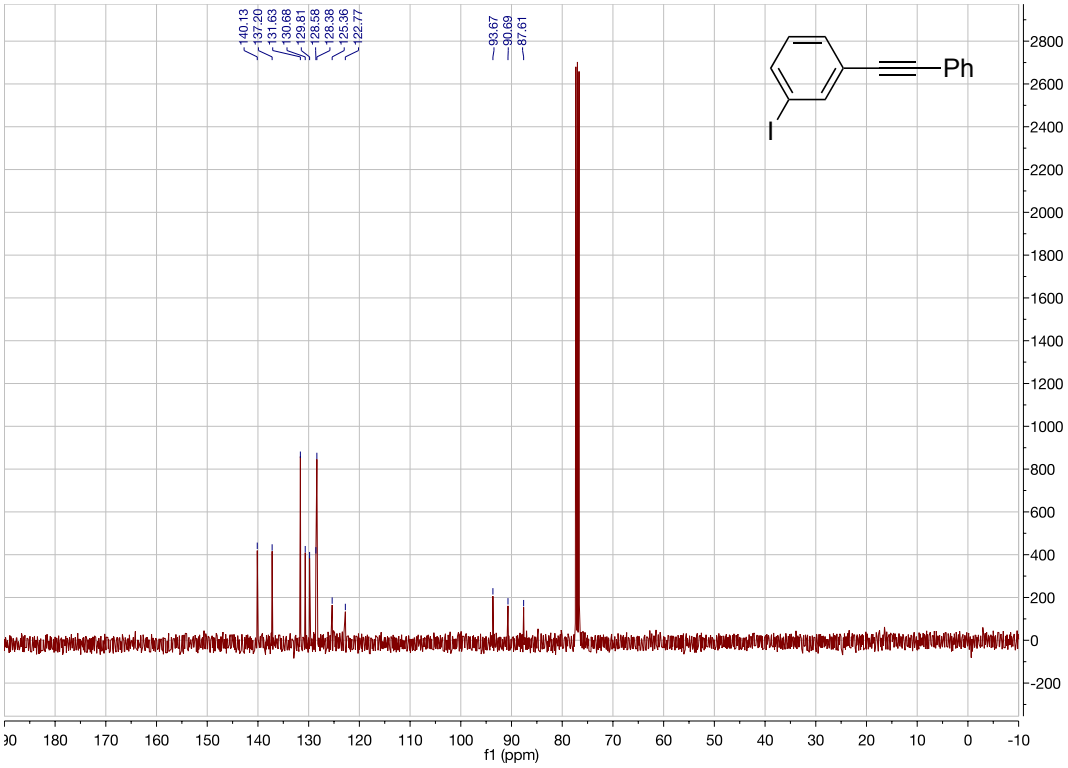

Figure 2.22 ^{13}C NMR Spectrum of **3j**

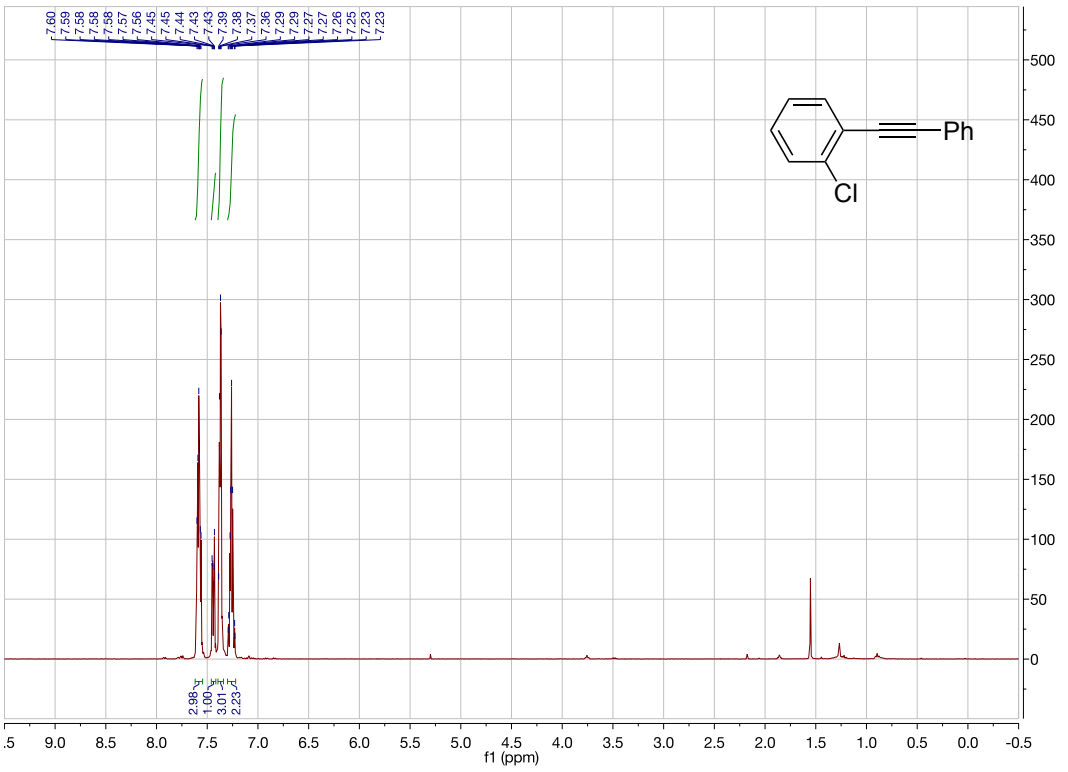

Figure 2.23 ^{1}H NMR Spectrum of **3k**

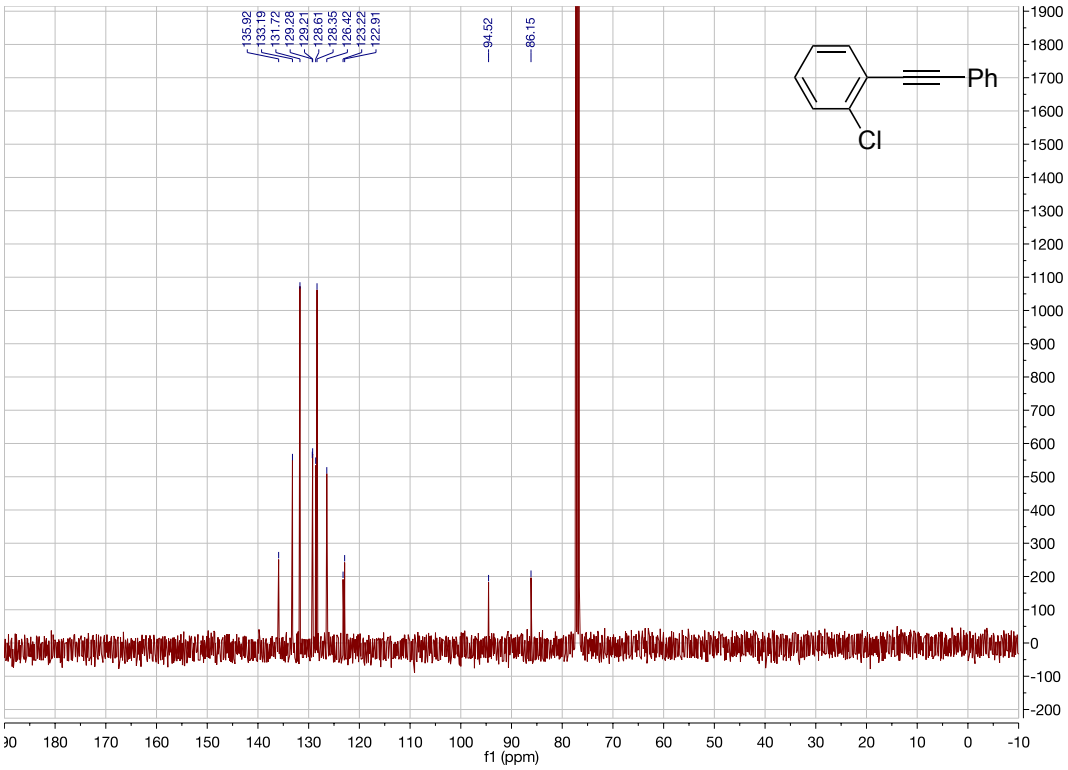

Figure 2.24 ^{13}C NMR Spectrum of **3k**

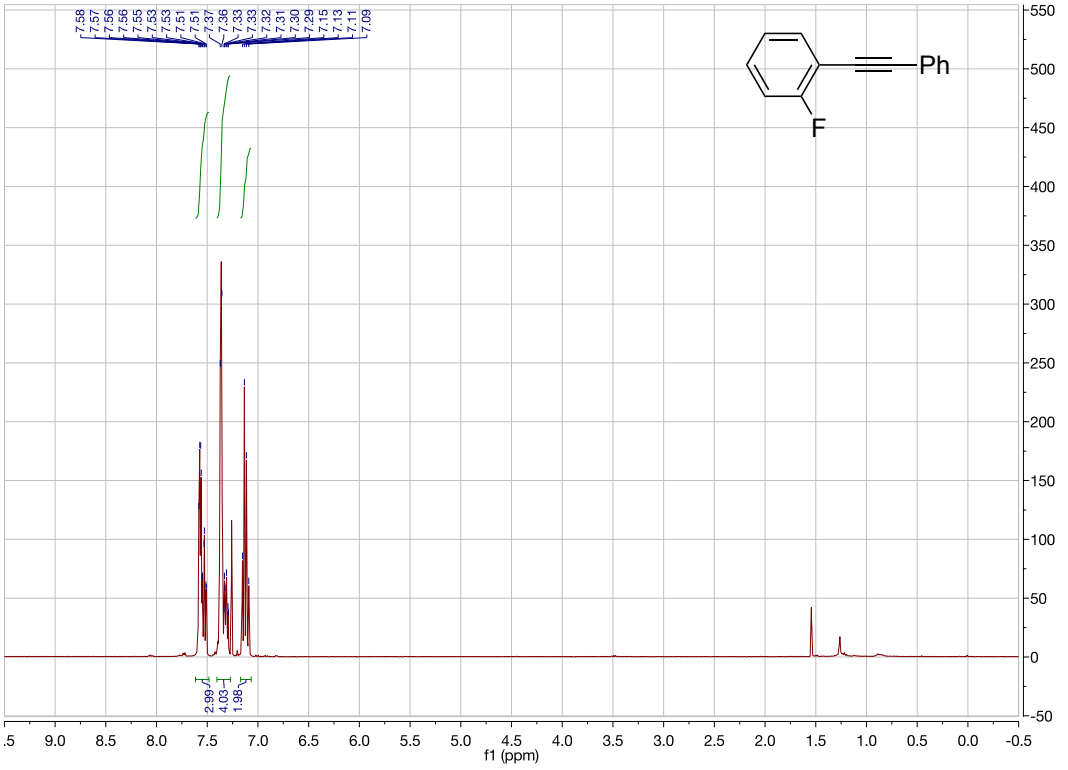

Figure 2.25 ^{1}H NMR Spectrum of **3l**

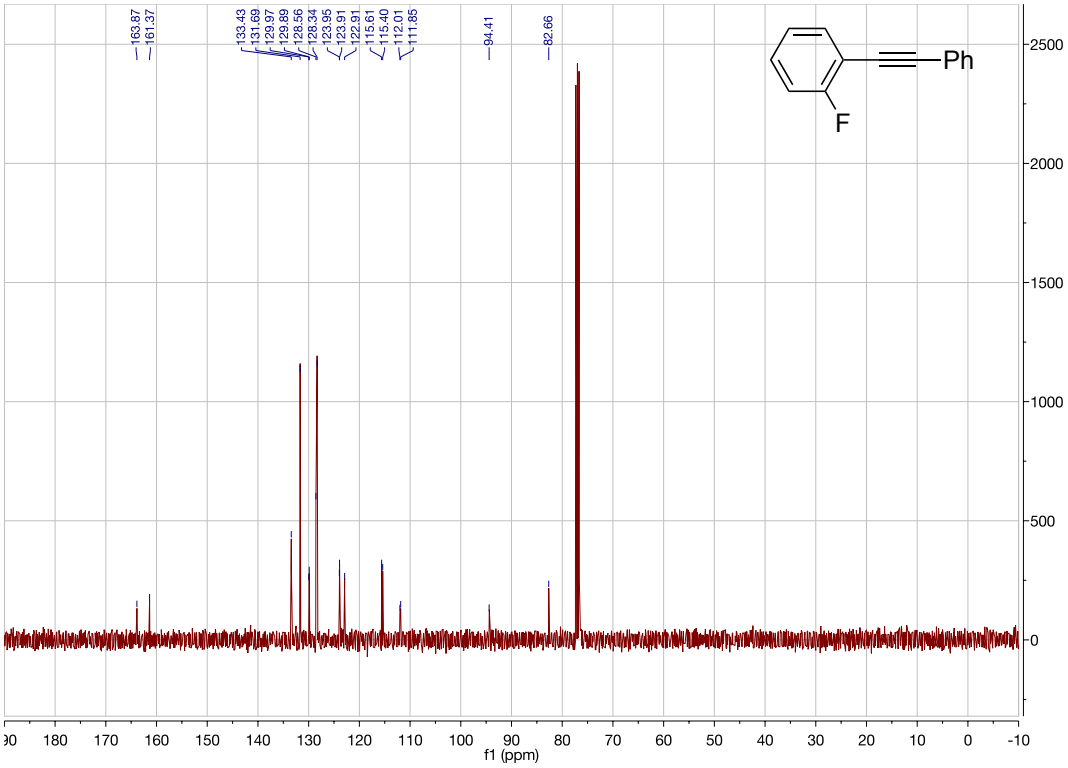

Figure 2.26 ^{13}C NMR Spectrum of **3l**

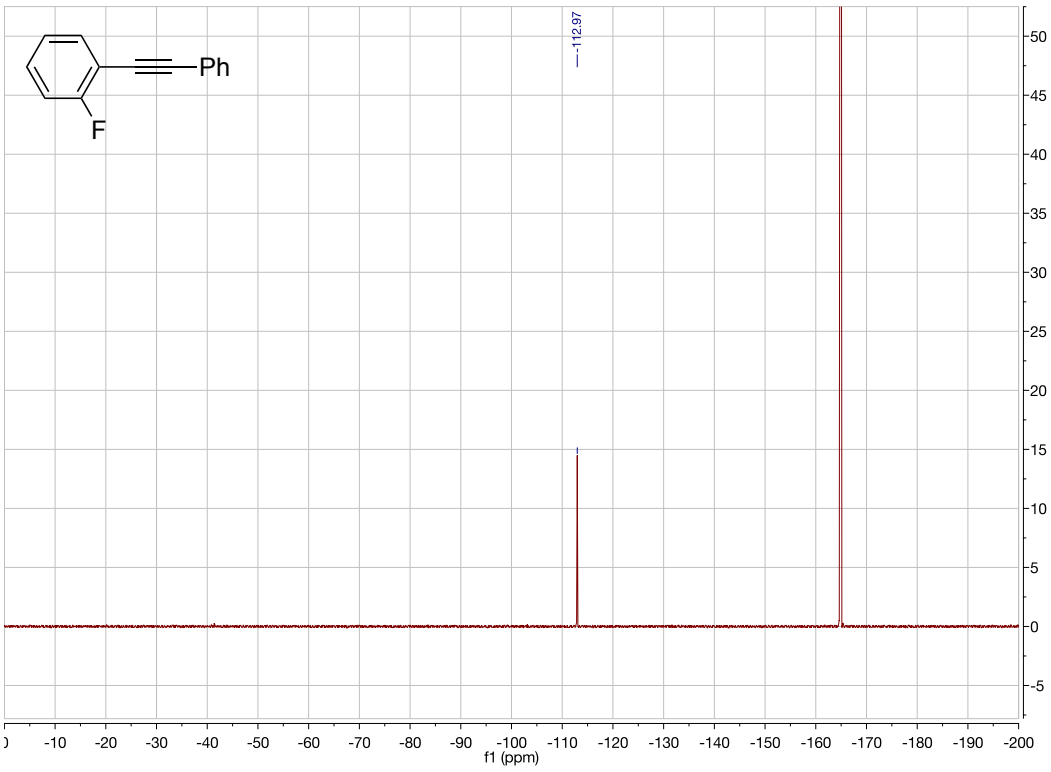

Figure 2.27 ^{19}F NMR Spectrum of **3l**

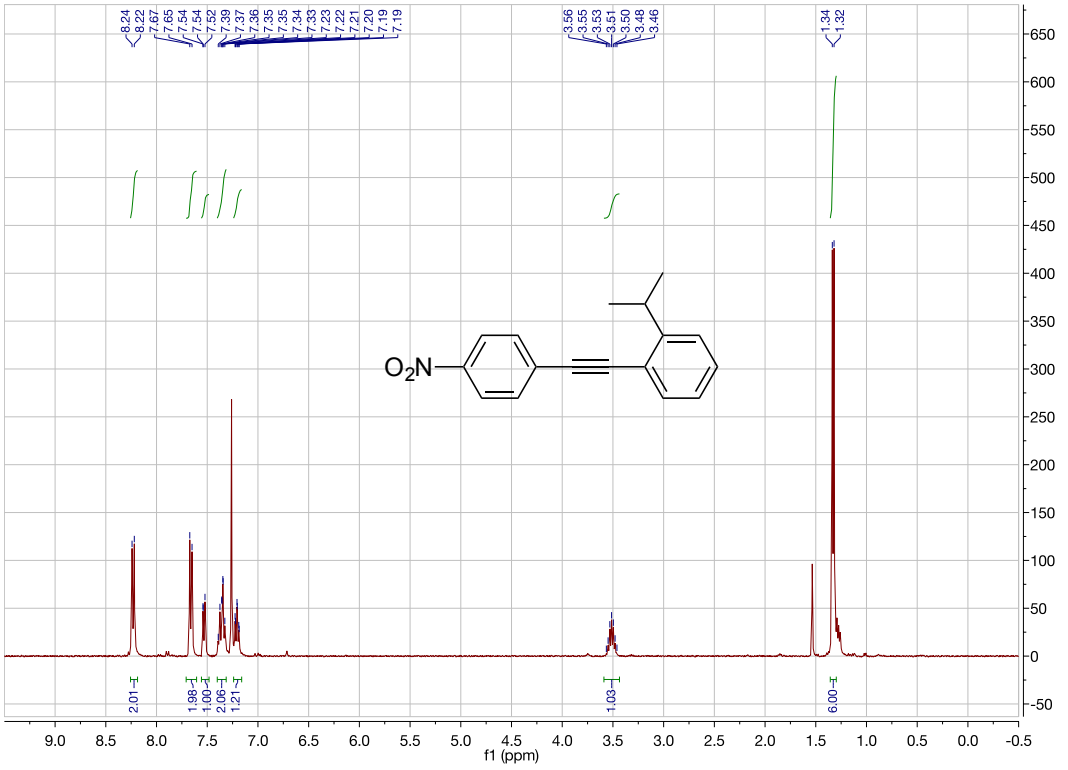

Figure 2.28 ^{1}H NMR Spectrum of **3m**

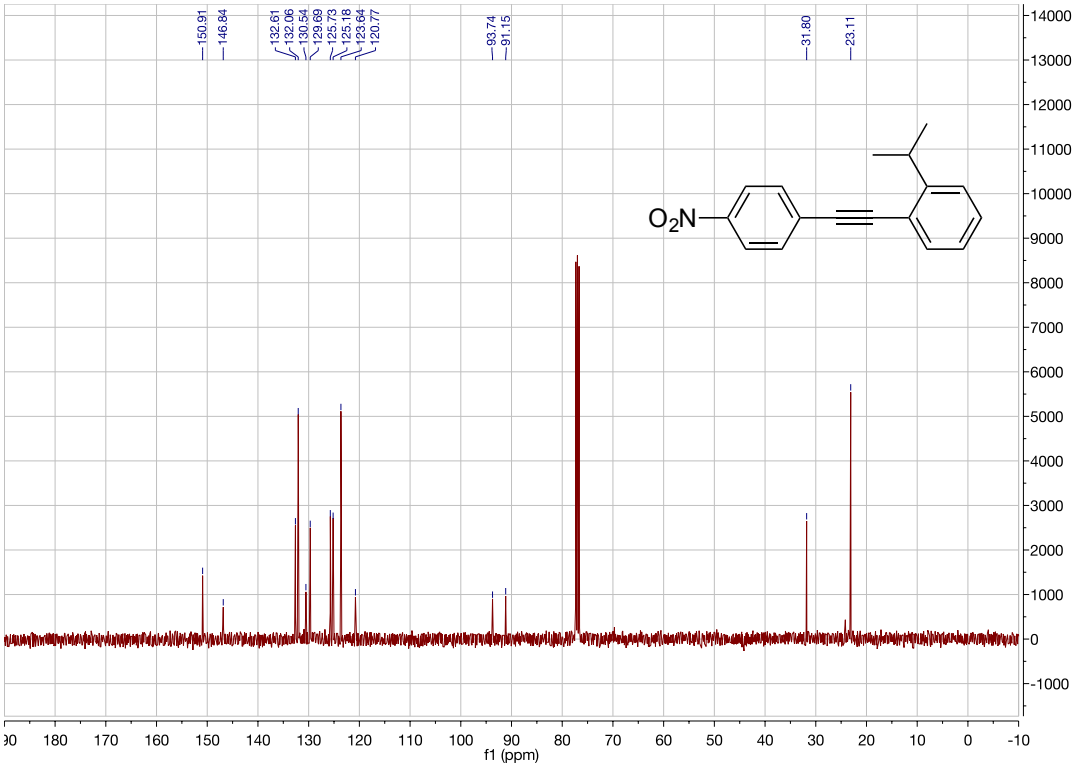

Figure 2.29 ^{13}C NMR Spectrum of **3m**

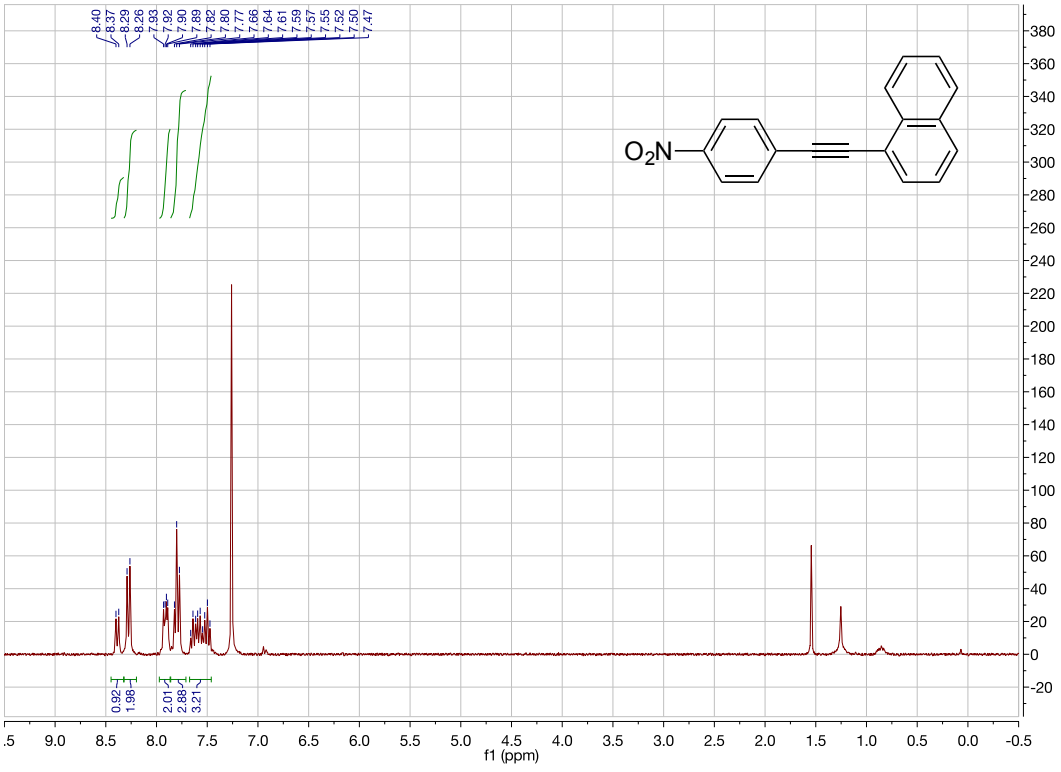

Figure 2.30 ^{1}H NMR Spectrum of **3n**

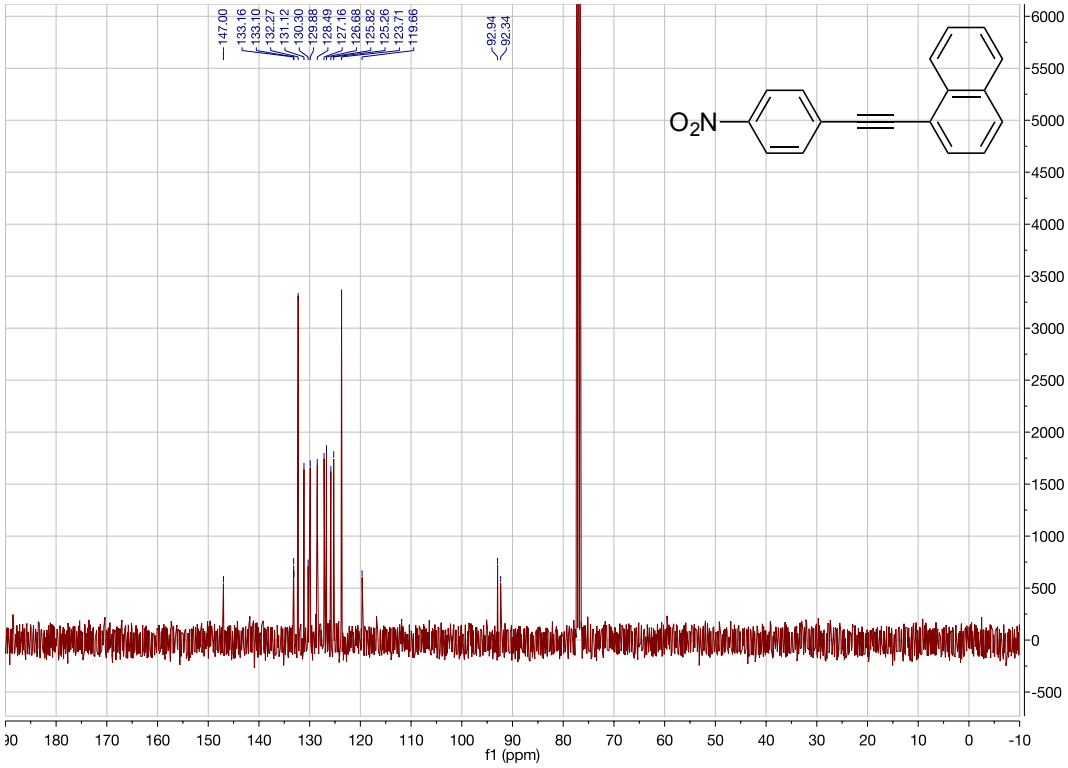

Figure 2.31 ^{13}C NMR Spectrum of **3n**

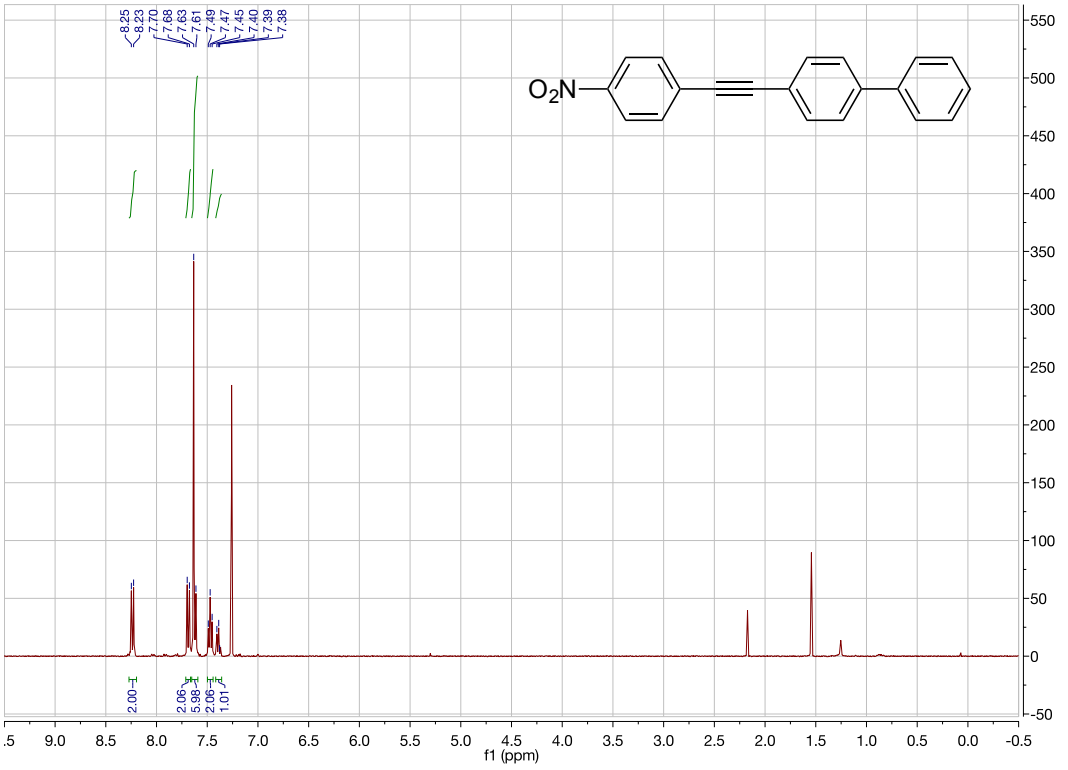

Figure 2.32 ^{1}H NMR Spectrum of **3o**

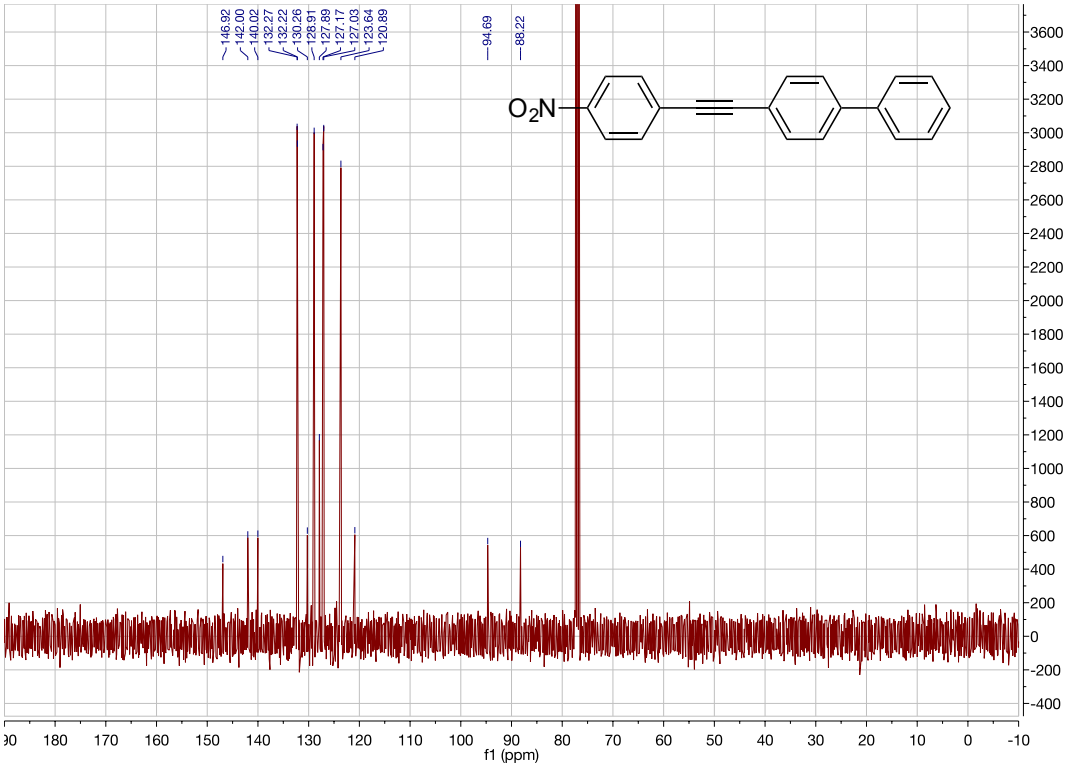

Figure 2.33 ^{13}C NMR Spectrum of **3o**

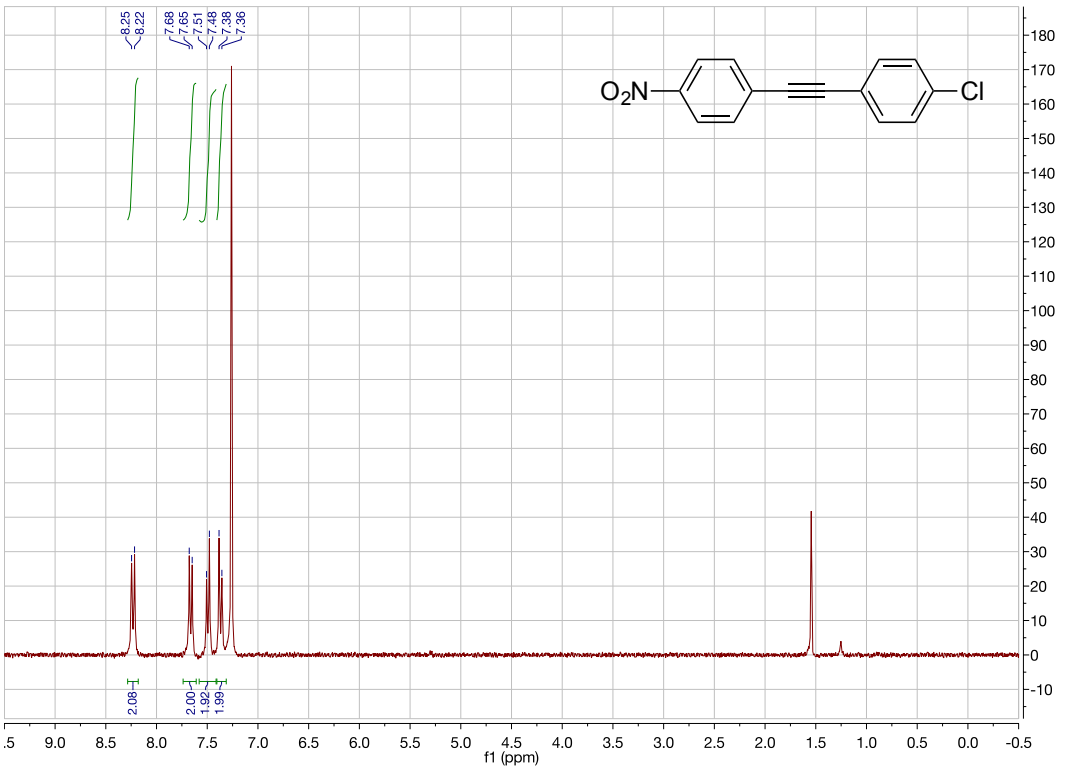

Figure 2.34 ^{1}H NMR Spectrum of **3p**

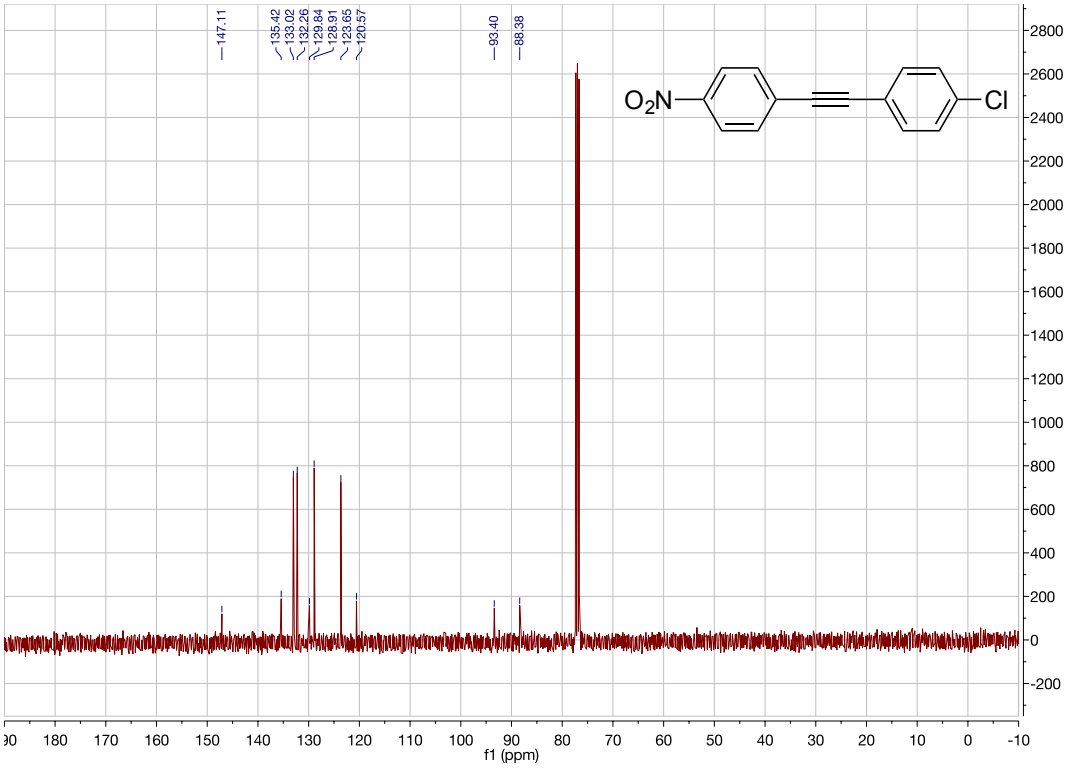

Figure 2.35 ^{13}C NMR Spectrum of **3p**

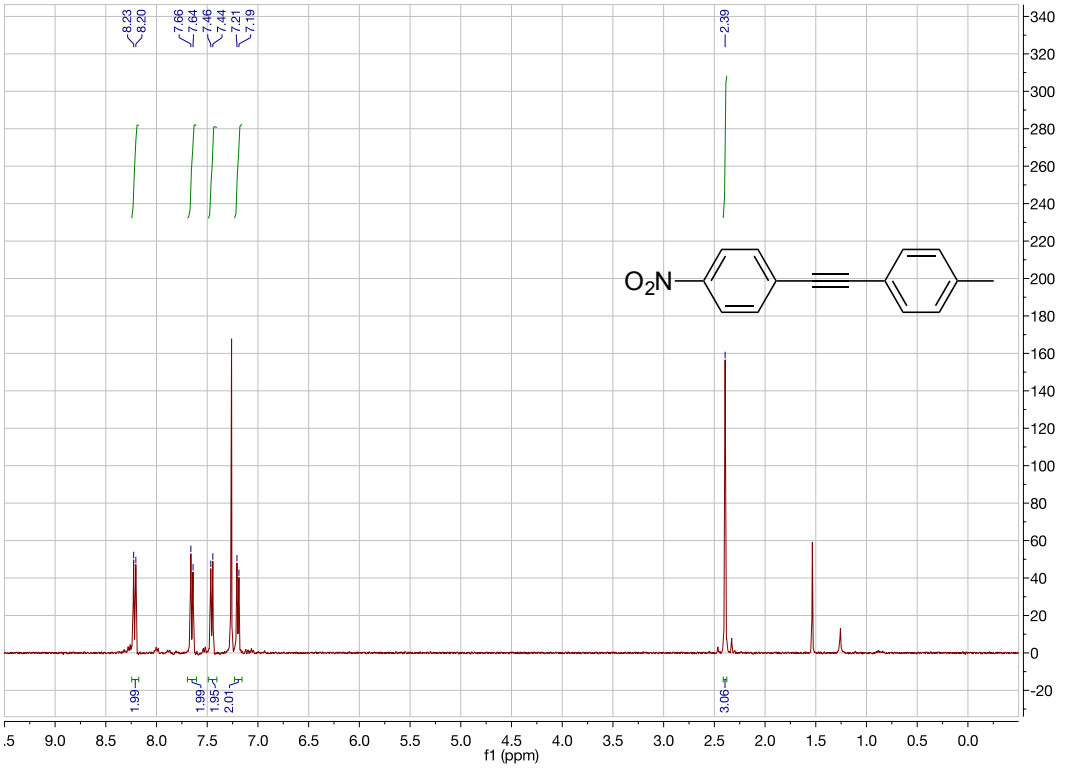

Figure 2.36 ^{1}H NMR Spectrum of **3q**

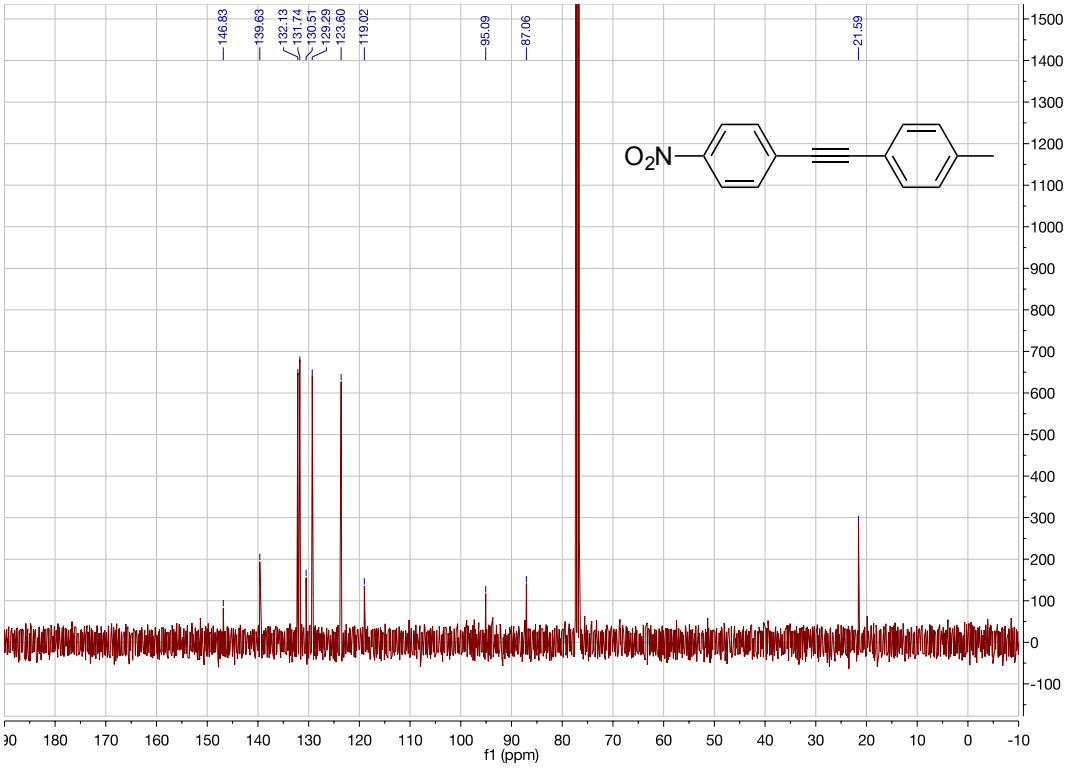

Figure 2.37 ^{13}C NMR Spectrum of **3q**

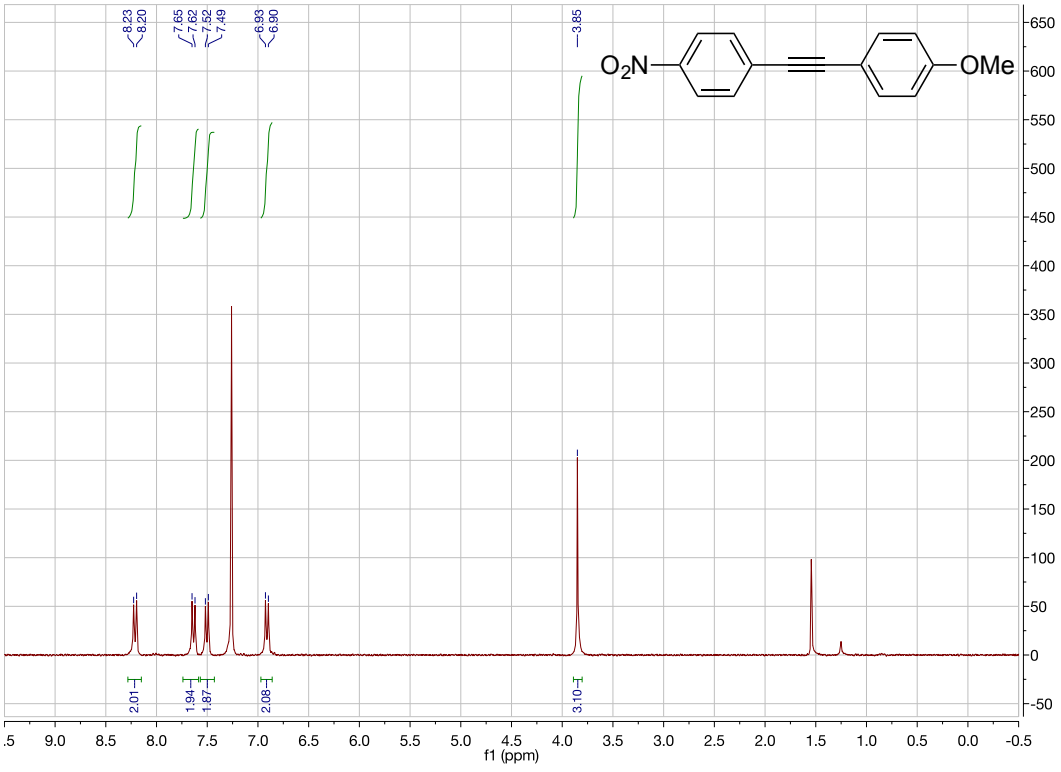

Figure 2.38 ^{1}H NMR Spectrum of **3r**

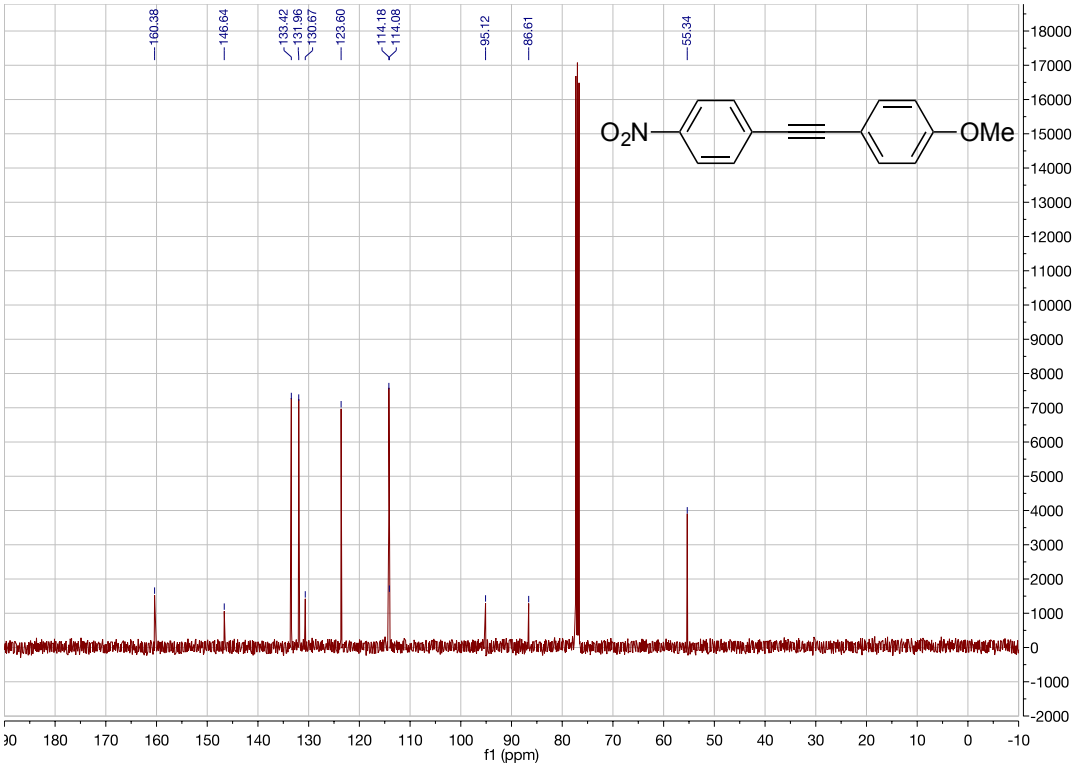

Figure 2.39 ^{13}C NMR Spectrum of **3r**

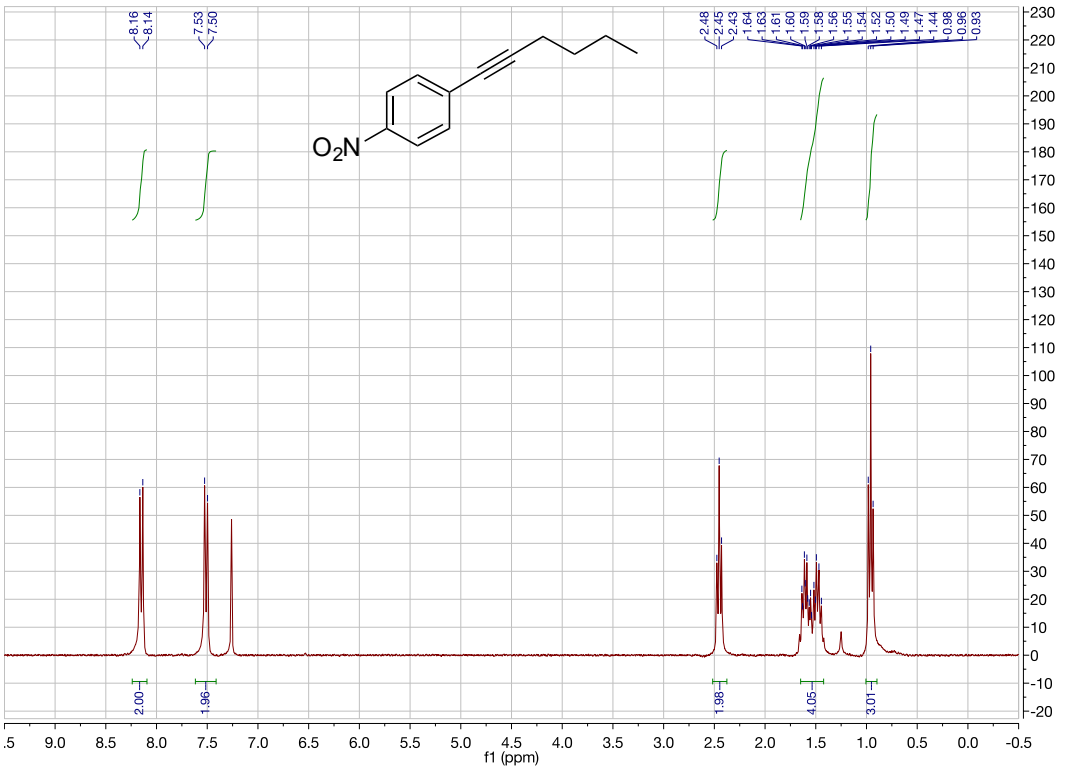

Figure 2.40 ^{1}H NMR Spectrum of **3s**

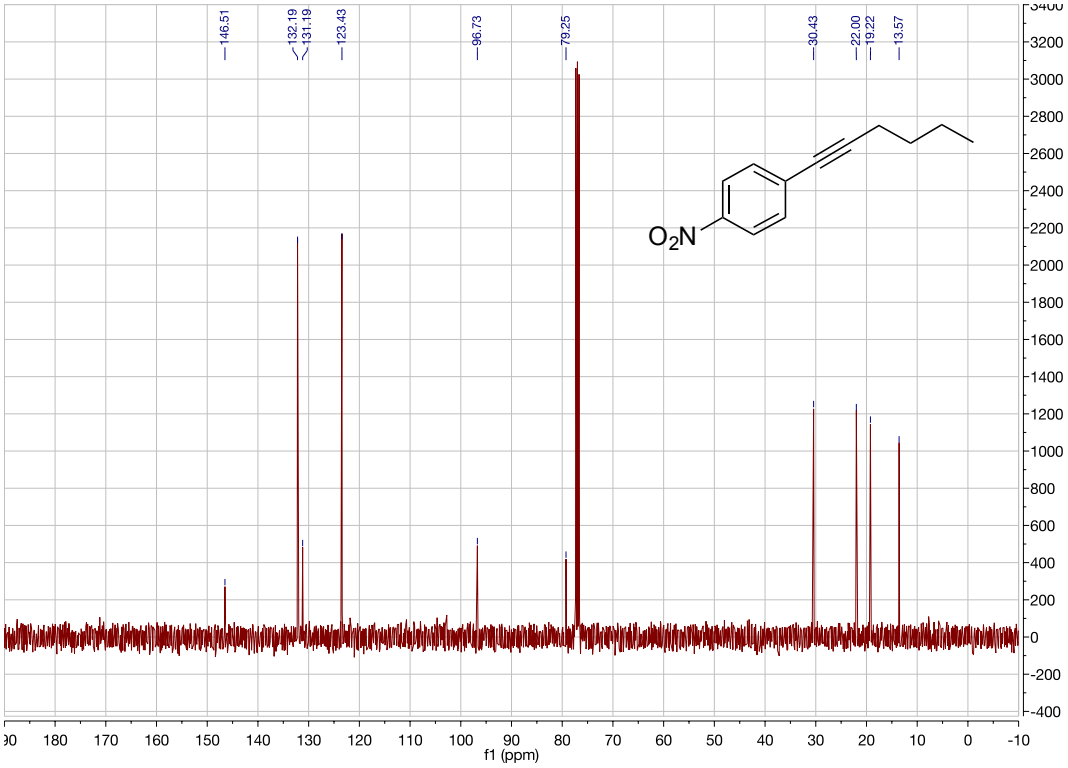

Figure 2.41 ^{13}C NMR Spectrum of **3s**

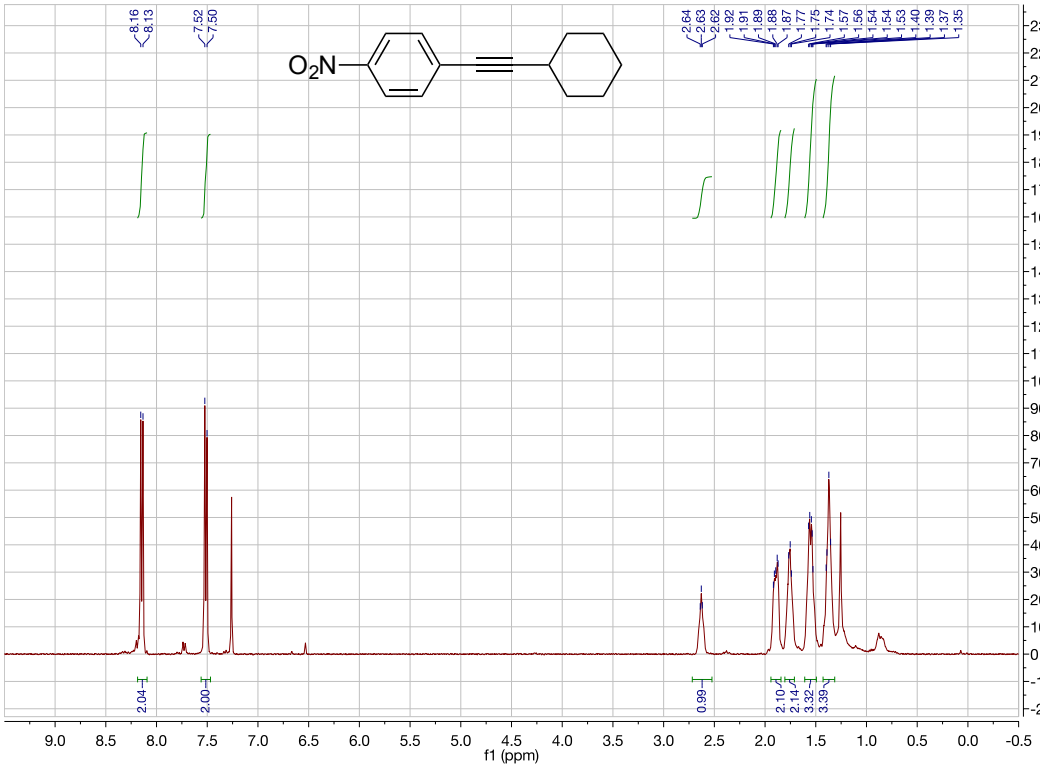

Figure 2.42 ^{1}H NMR Spectrum of **3t**

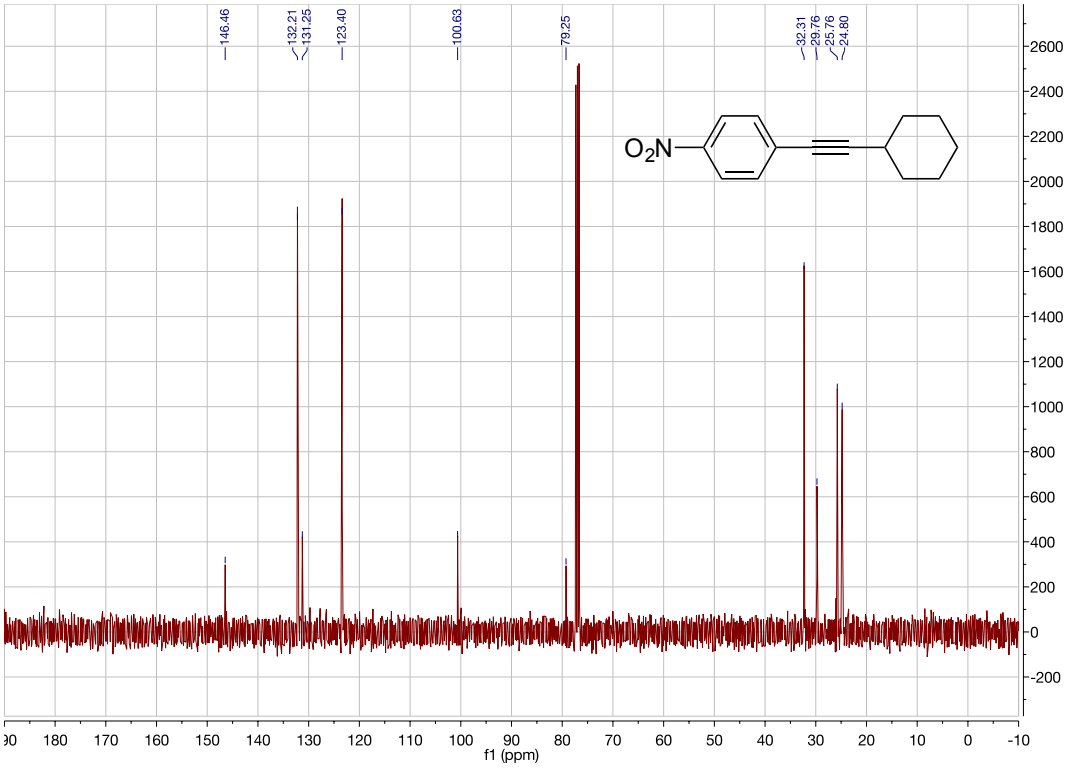

Figure 2.43 ^{13}C NMR Spectrum of **3t**

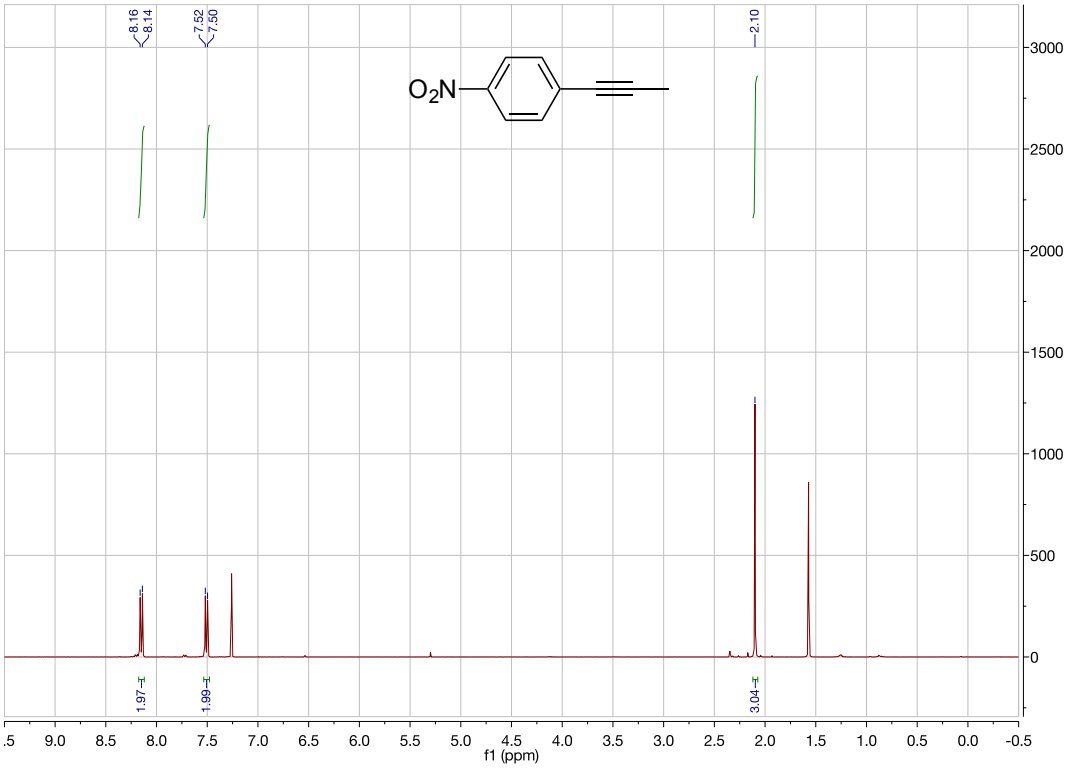

Figure 2.44 ^{1}H NMR Spectrum of **3u**

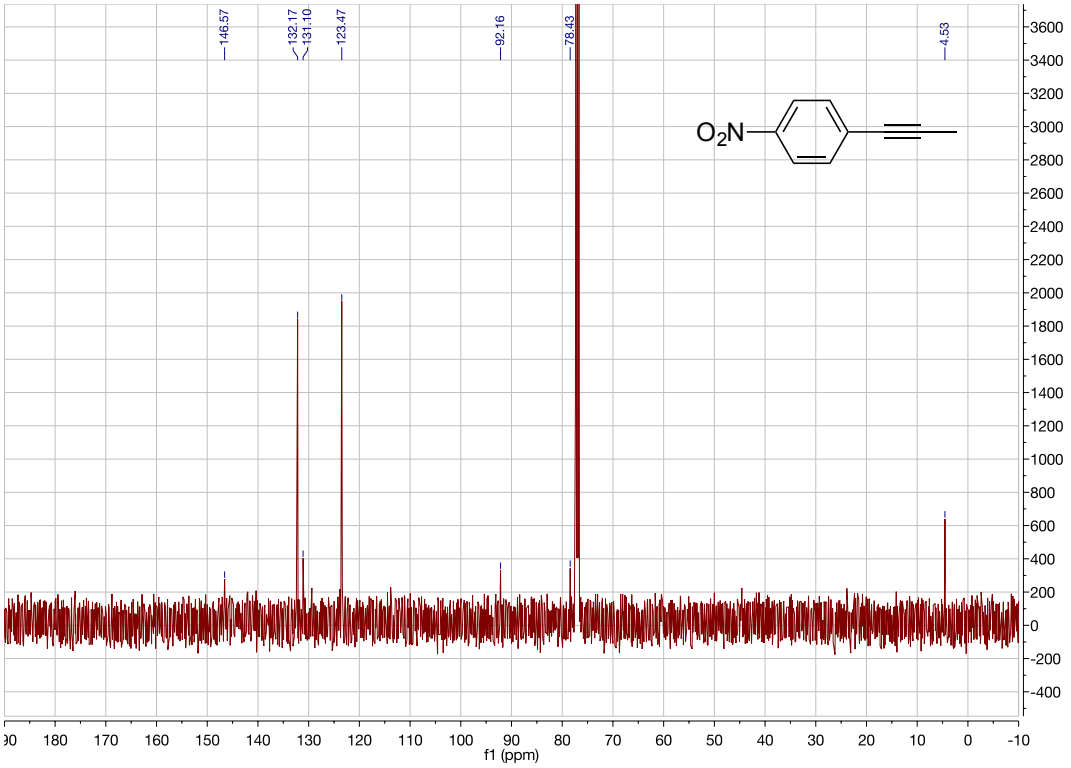

Figure 2.45 ^{13}C NMR Spectrum of **3u**

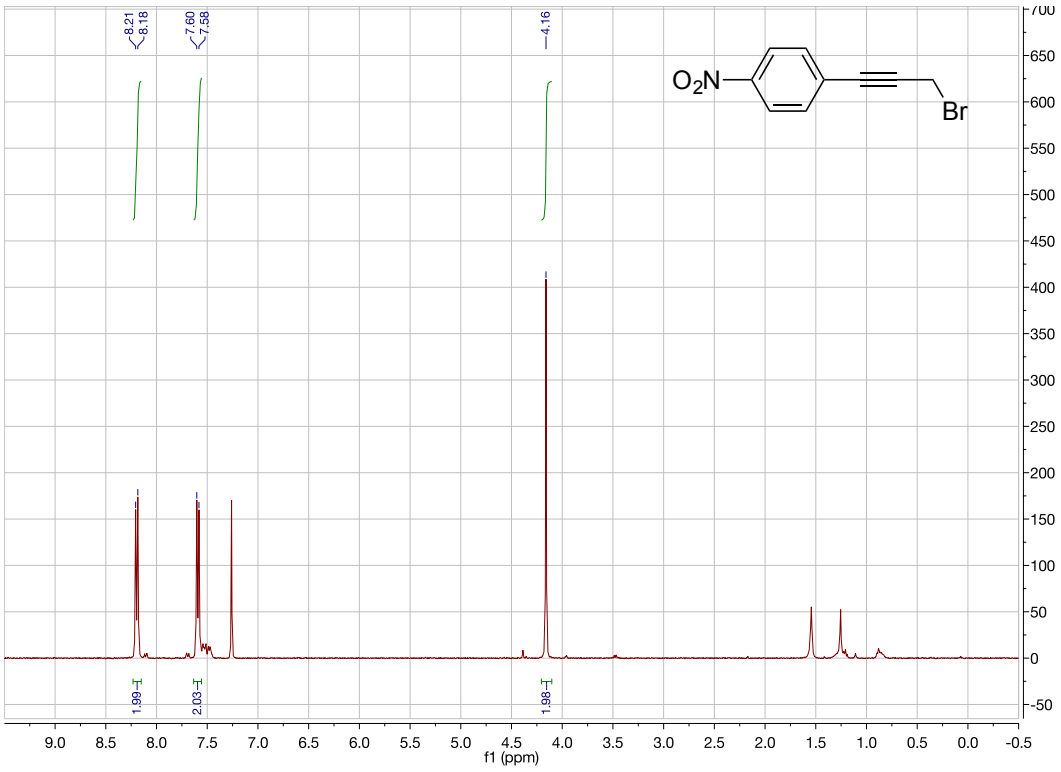

Figure 2.46 ^{1}H NMR Spectrum of **3v**

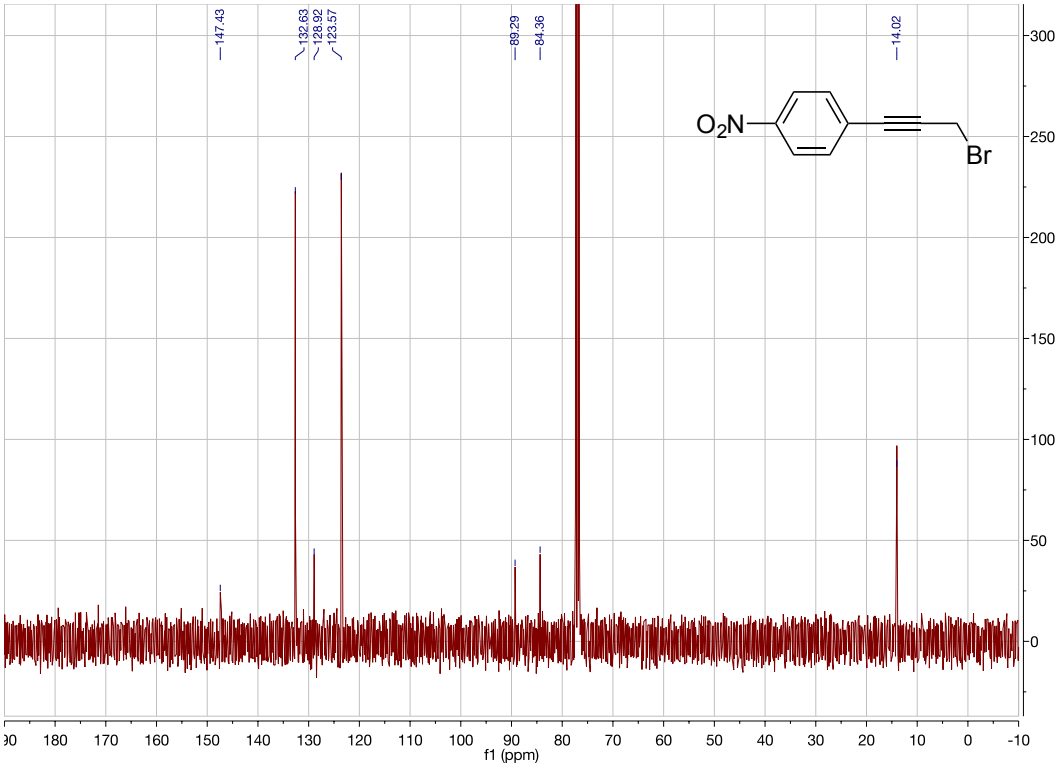

Figure 2.47 ^{13}C NMR Spectrum of **3v**

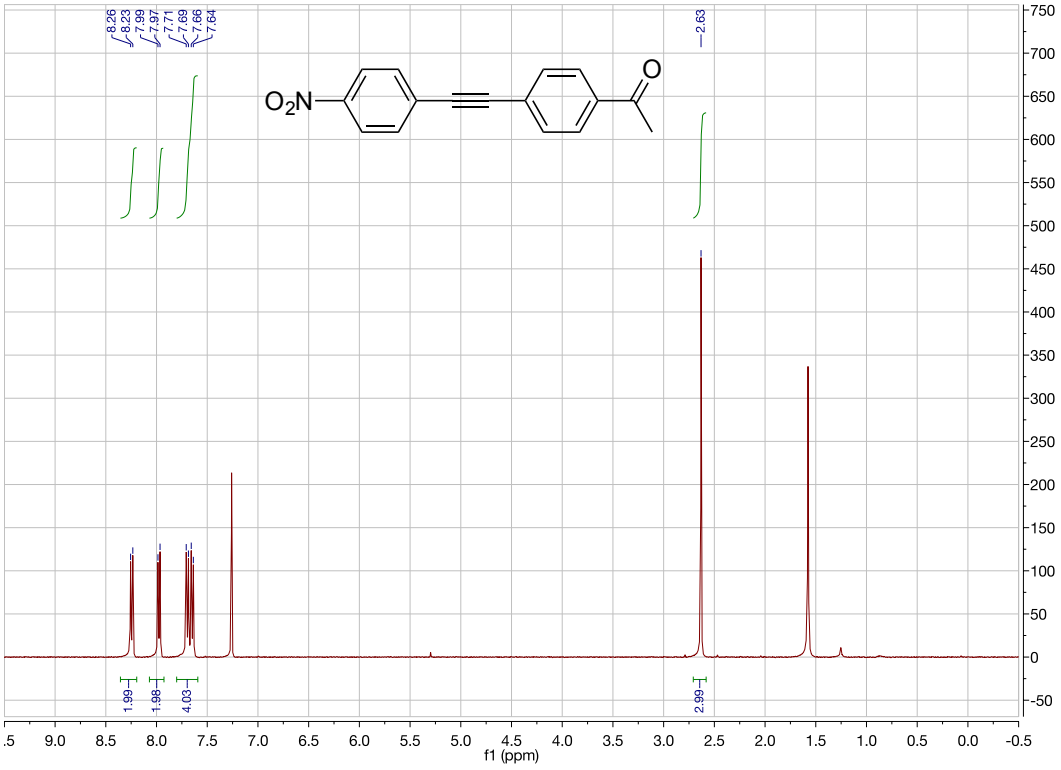

Figure 2.48 ^{1}H NMR Spectrum of **3y**

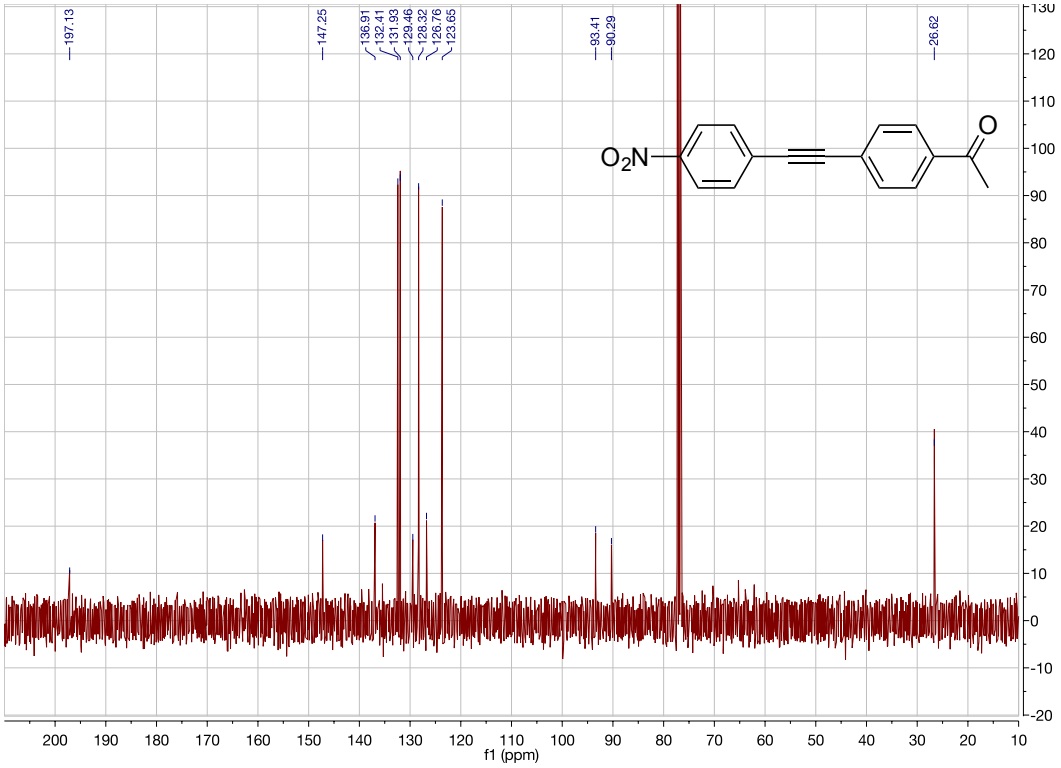

Figure 2.49 ^{13}C NMR Spectrum of **3y**

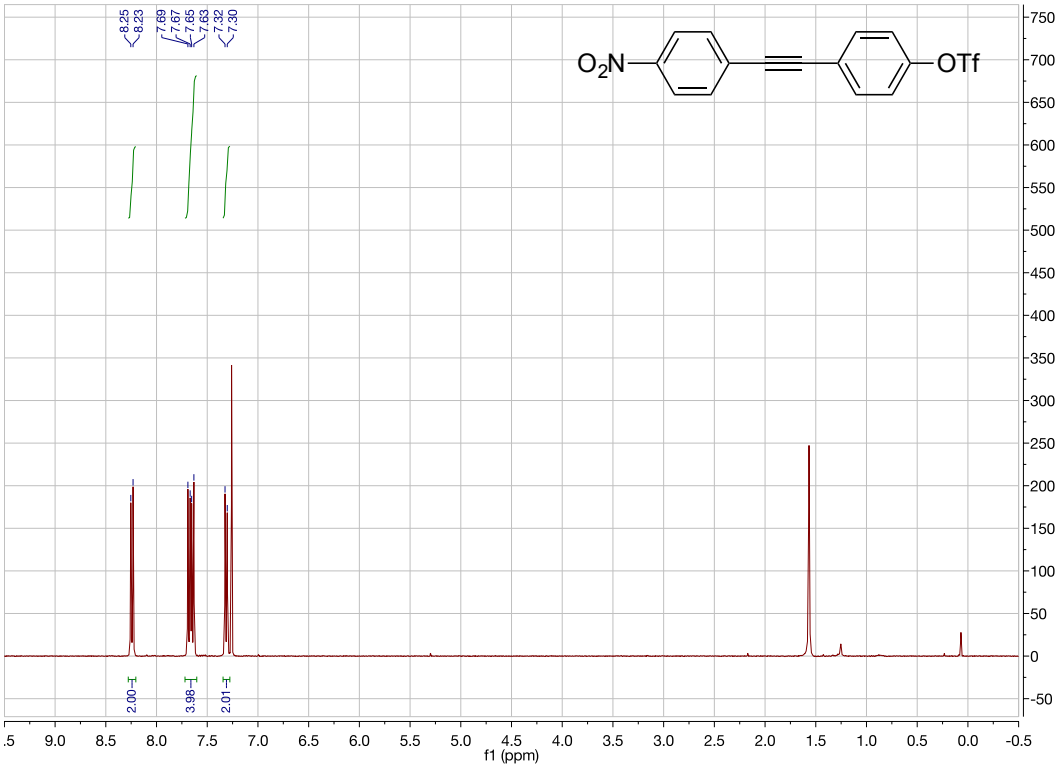

Figure 2.50 ^{1}H NMR Spectrum of **3z**

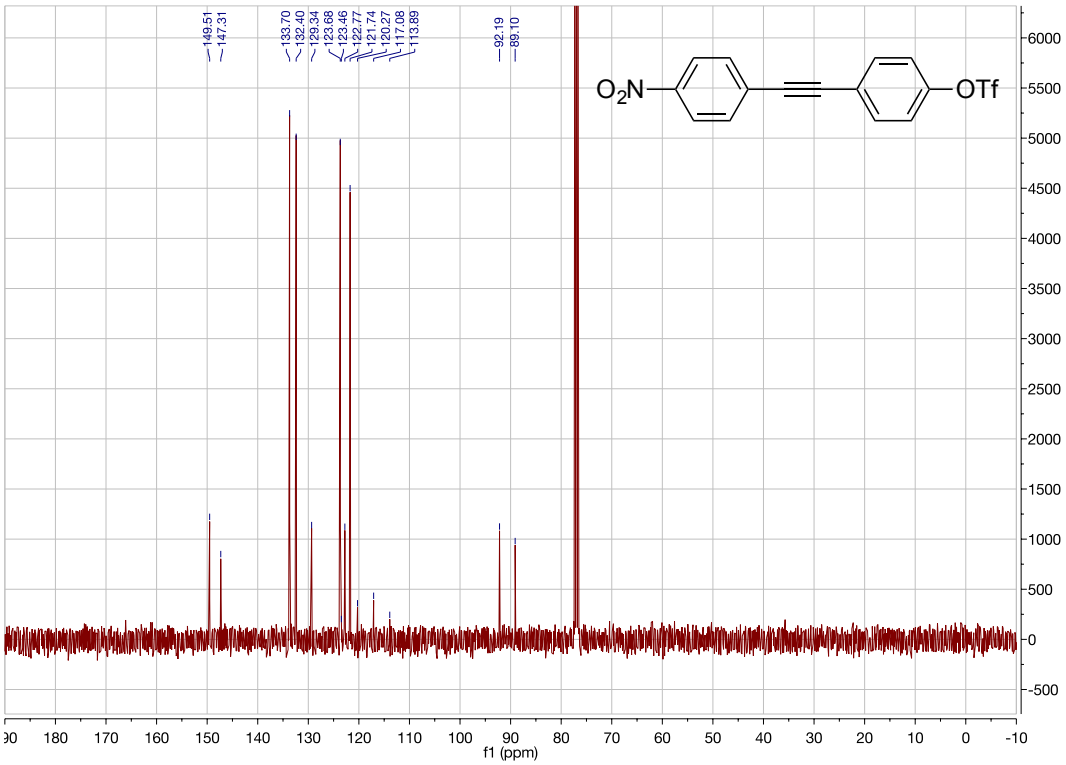

Figure 2.51 ^{13}C NMR Spectrum of **3z**

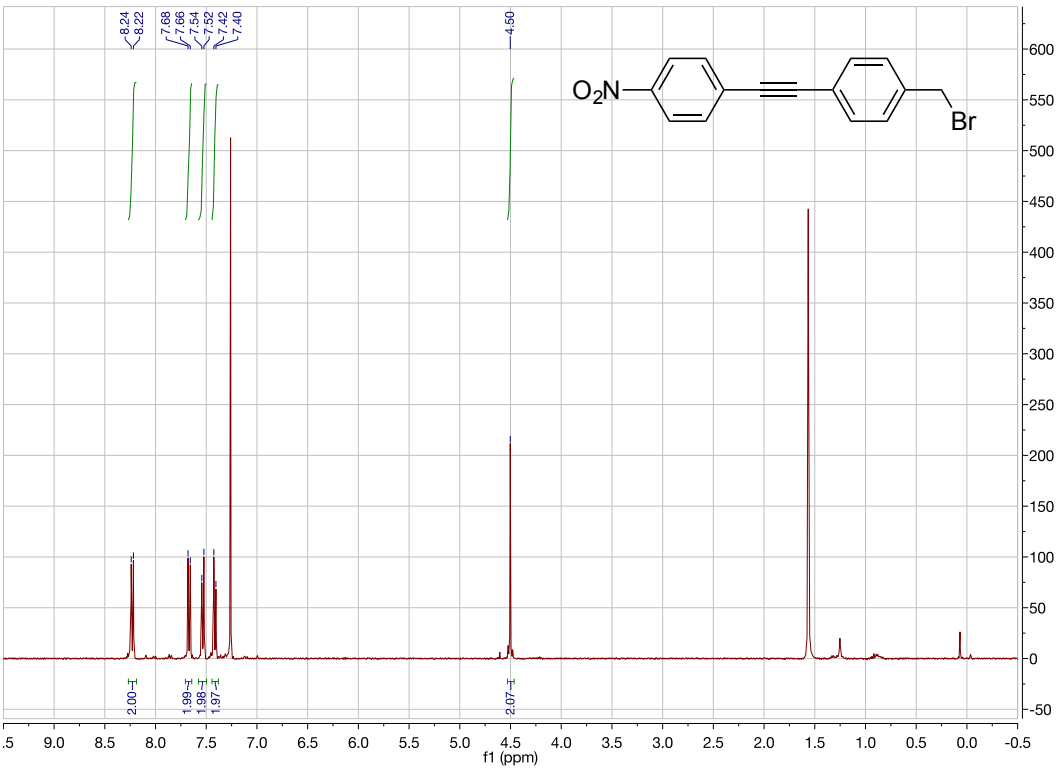

Figure 2.52 ^{1}H NMR Spectrum of **3aa**

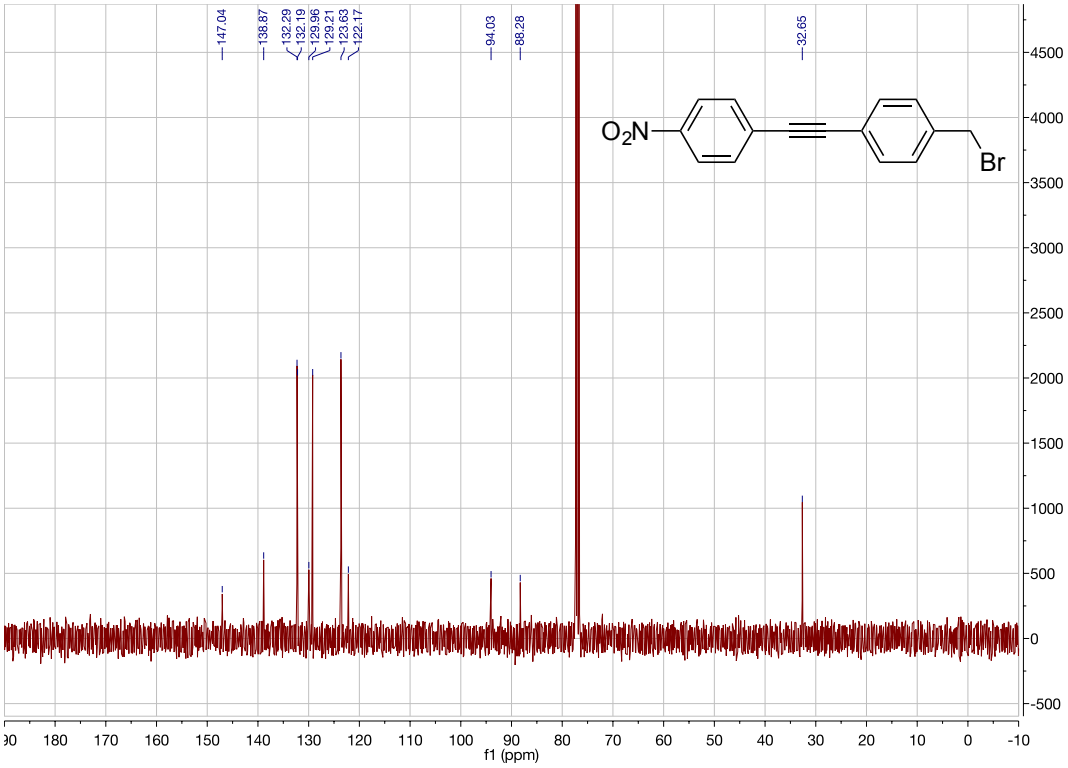

Figure 2.53 ^{13}C NMR Spectrum of **3aa**

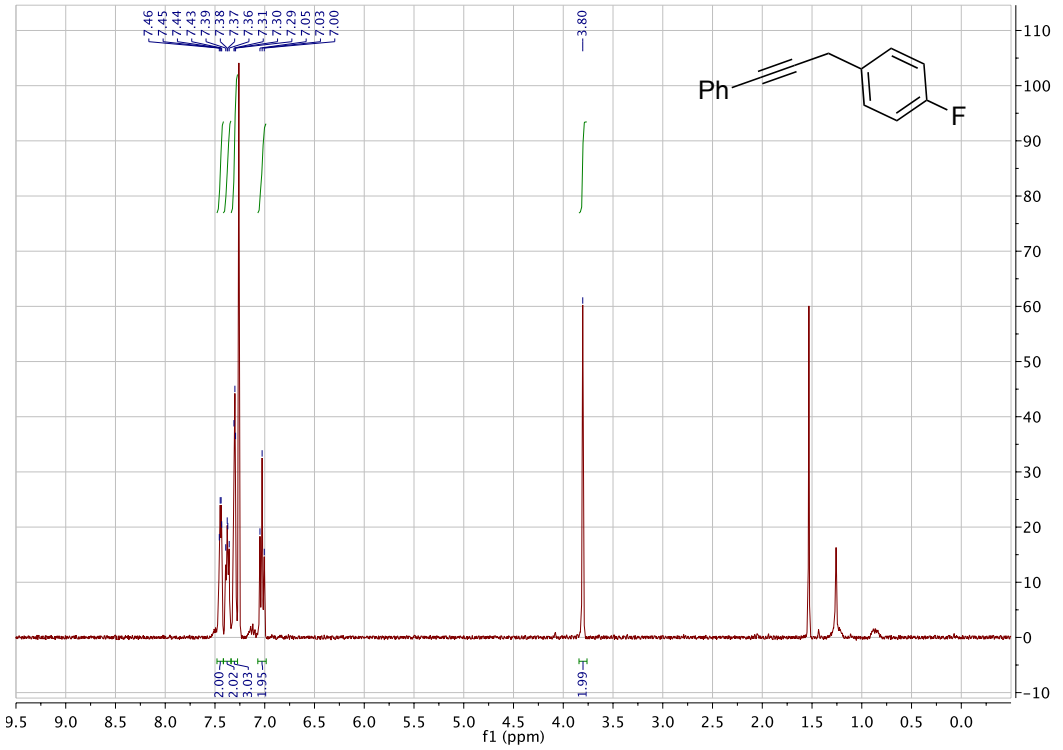

Figure 2.54 ^{1}H NMR Spectrum of **5**

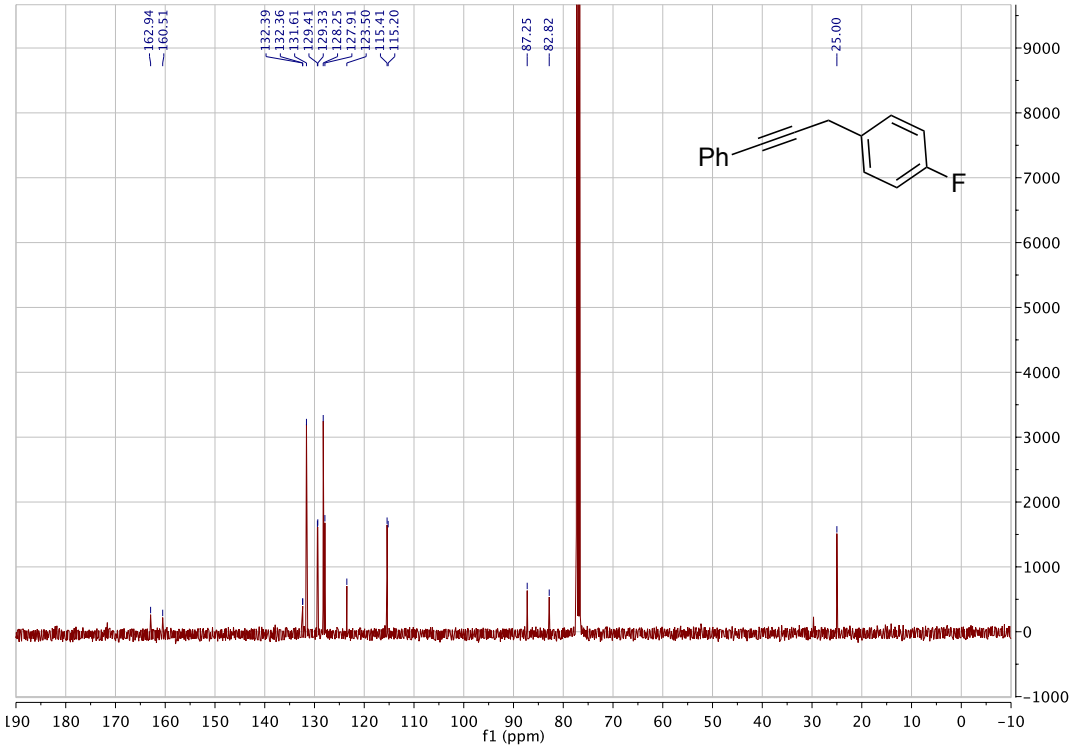

Figure 2.55 ^{13}C NMR Spectrum of **5**

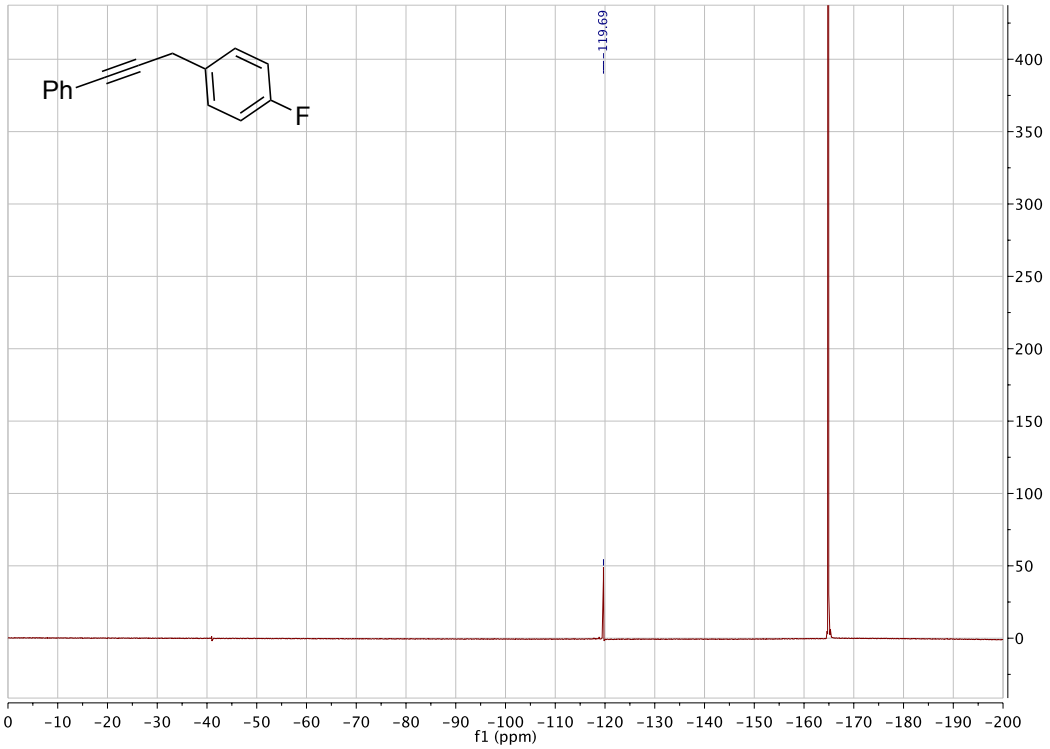

Figure 2.56 ^{19}F NMR Spectrum of **5**

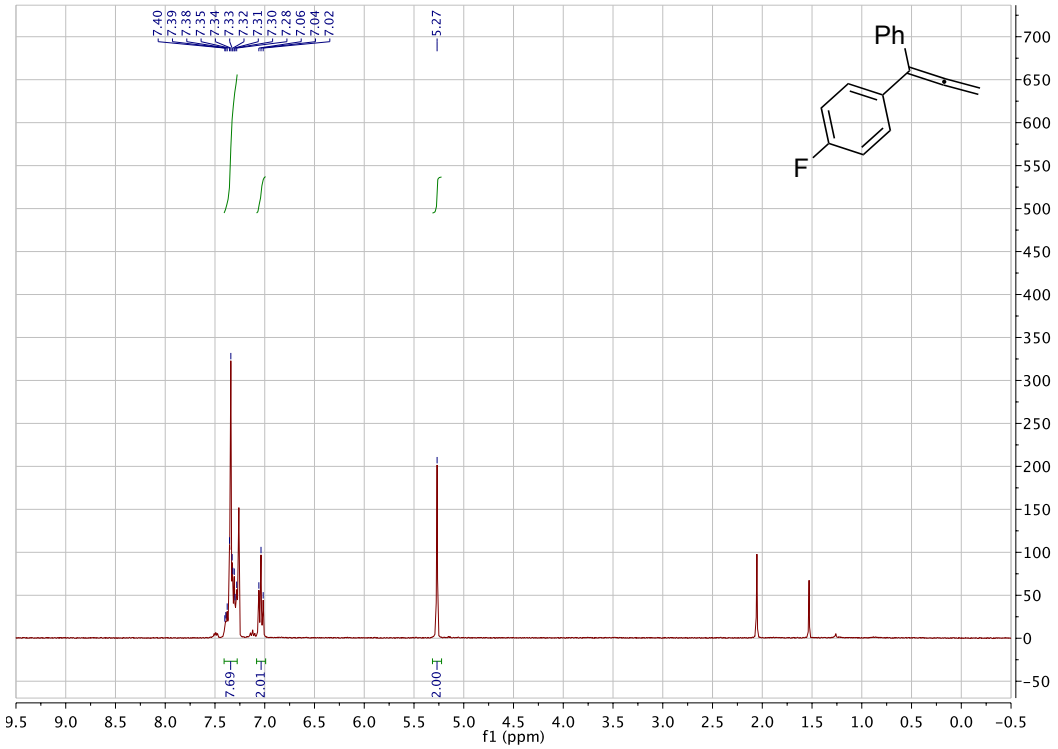

Figure 2.57 ^{1}H NMR Spectrum of **6**

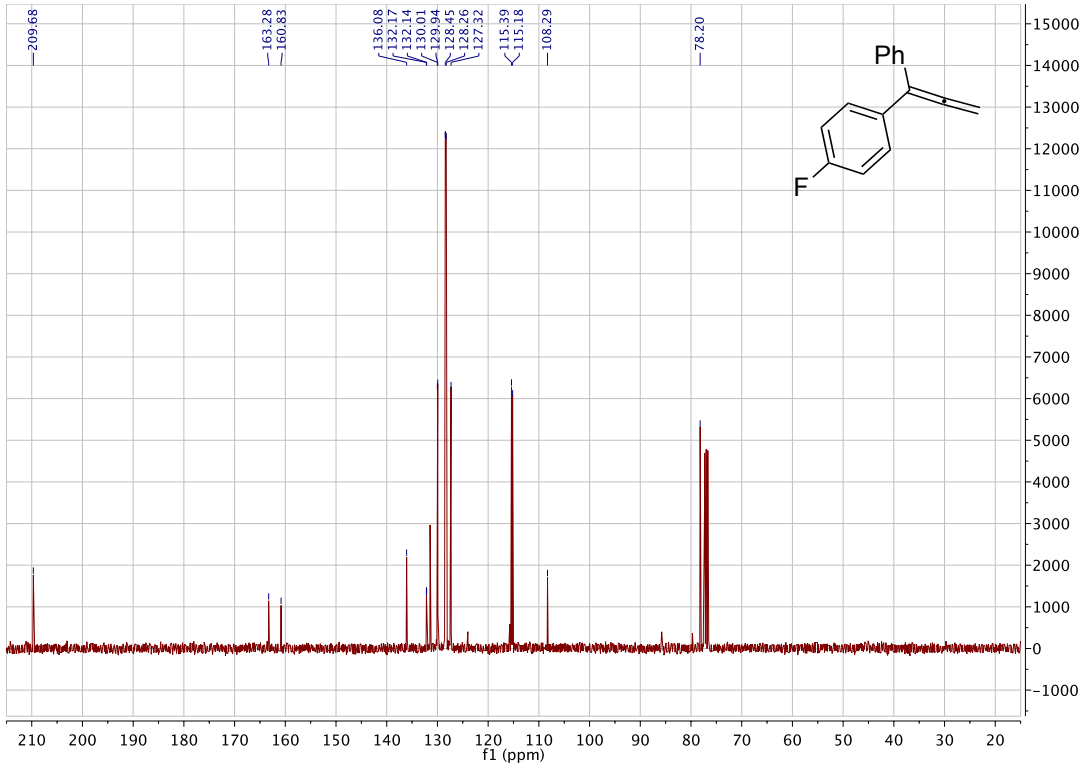

Figure 2.58 ^{13}C NMR Spectrum of **6**

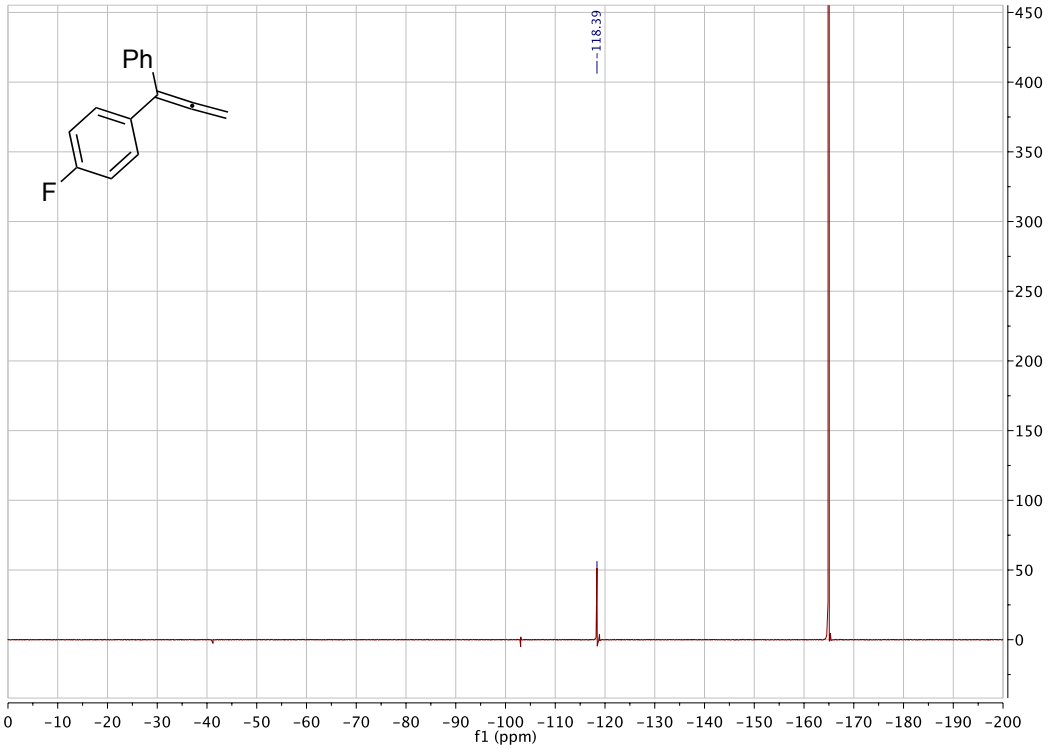

Figure 2.59 ^{19}F NMR Spectrum of **6**

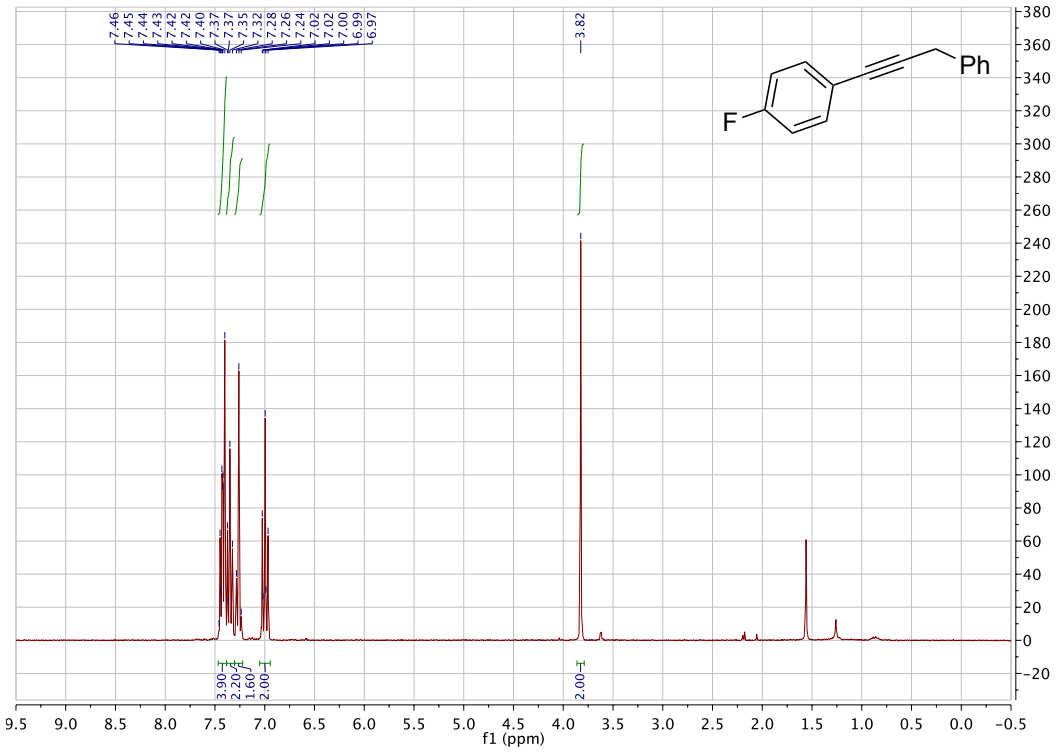

Figure 2.60 ^{1}H NMR Spectrum of **7**

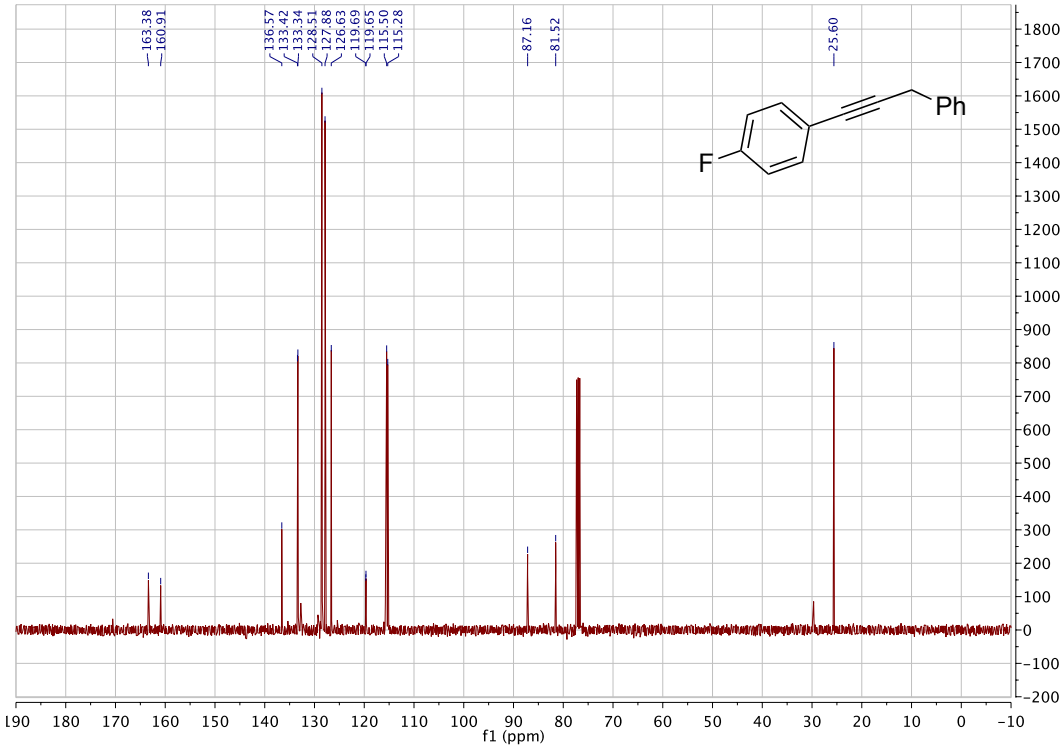

Figure 2.61 ^{13}C NMR Spectrum of **7**

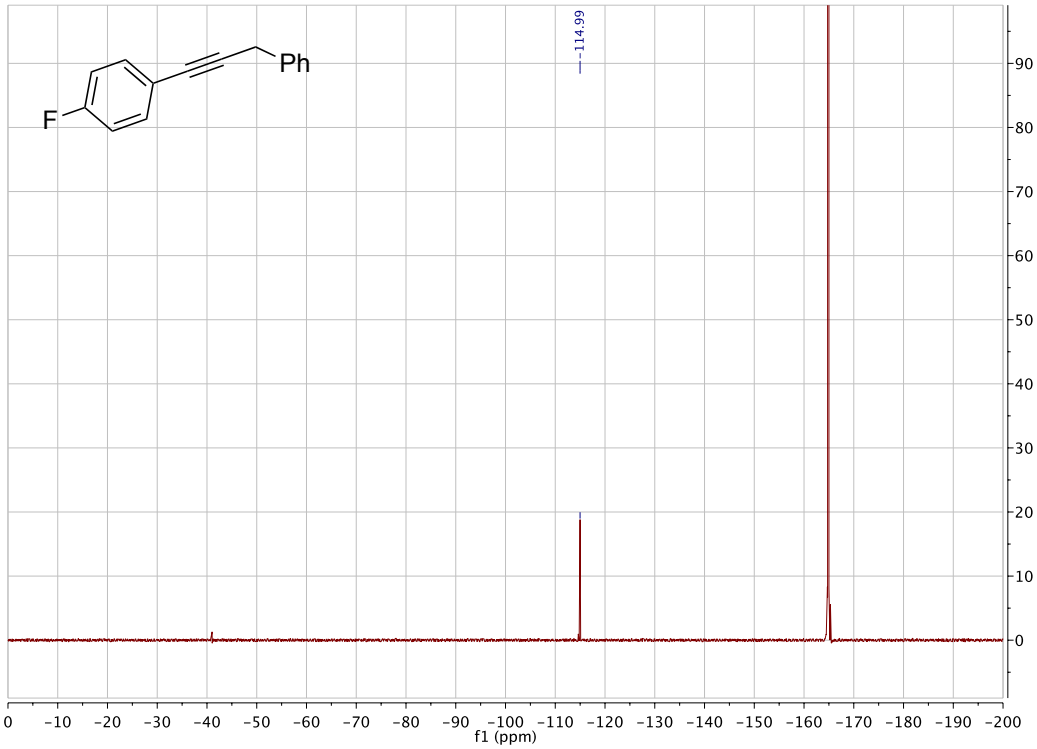

Figure 2.62 ^{19}F NMR Spectrum of **7**

Chapter 3.

The Mechanism of Photoredox-Catalyzed C−C and C−N Bond Formation by Arylation of IPrAu(I)−CF_3 and IPrAu(I)−Succinimide

3.1 Introduction

The merger of photoredox catalysis and transition metal catalysis has enabled novel modes of reactivity via organic radical intermediates and odd-electron transition metal intermediates.[1] While this synergistic combination has been incredibly successful in upgrading the arsenal of synthetic chemists,[2] current mechanistic understanding of key bond-forming events remains limited. Transition metal catalysts and intermediates are subject to various visible light-induced reactions such as charge-transfer, electron-transfer, and energy-transfer that can complicate mechanistic analysis. For example, in the case of nickel/photoredox dual catalysis, the Doyle group proposed photolysis of aryl nickel(III) chloride intermediates and metal to ligand charge transfer (MLCT) of aryl nickel(II) halide intermediates as elementary steps.[3] These light-induced processes, combined with the potential for odd electron intermediates and the instability of high-valent transition metal complexes can make the details of the bond-forming step often difficult to ascertain.

A number of possibilities exist for the mechanism of bond formation in combined photoredox-transition metal catalysis, including a traditional reductive elimination,[4] radical substitution[5,6] or radical recombination (Scheme 1A).[7] For example, copper/photoredox dual catalysis has been used by the MacMillan group to facilitate the formation of C–N bonds. These reaction are proposed to proceed via reductive elimination from a copper(III) intermediate (Scheme 1B).[8] On the other hand, under the photoinduced Ullmann C–N coupling conditions reported by the Fu and Peters groups, the prevailing explanation for C–N bond-forming step is radical substitution reaction between copper(II) intermediates and carbon-centered radical intermediates (Scheme 1C).[9] In this latter case, EPR and radical clock experiments are consistent with copper(II) and aryl radical species; however the formation of a copper(III) intermediate has yet to be directly observed or excluded from a light induced transformation. These mechanistic considerations are challenging to address due to the short lifetimes of radical and postulated high-valent copper(III) intermediates, especially under metallaphotoredox catalysis conditions.

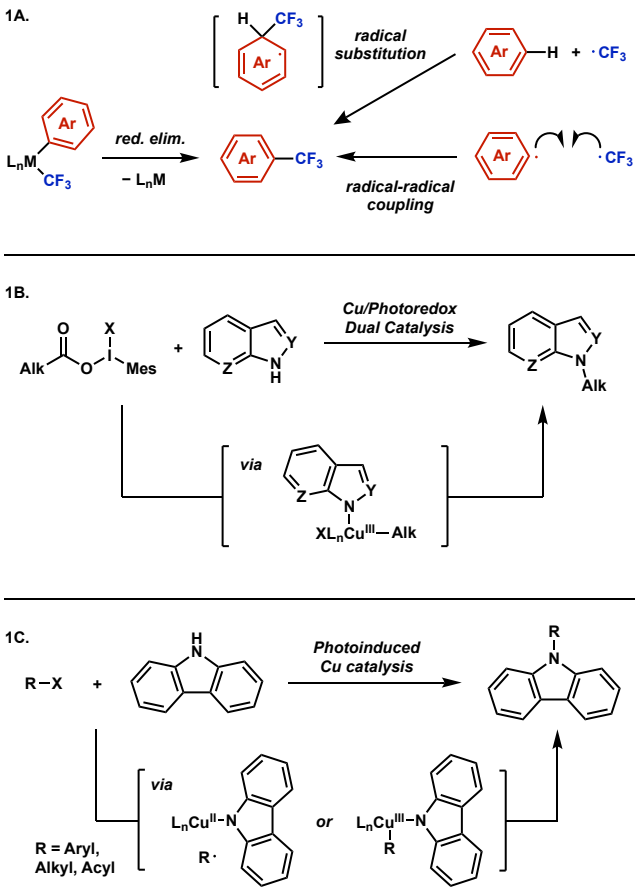

Scheme 3.1 Potential bond-forming steps of metallaphotoredox catalysis(1A) Copper(III) intermediates proposed for photochemical C−N coupling reactions(1B and 1C)

Recent studies from our group demonstrated that reductive elimination of trifluoromethylgold(III) complexes is a viable strategy to forge C–CF_3 bonds.[10] Therefore, inspired by Kochi's seminal mechanistic studies on the use of gold(I/III) as a mechanistic probe for gaining insight into carbon-carbon bond formation from copper(III),[11] we hypothesized that diamagnetic gold(III) complexes might allow for a direct observation of the gold(III) analog to the copper(III) complexes proposed as intermediates in metallaphotoredox cross-coupling catalysis. Moreover, trapping of these intermediates, presumably as less reactive and detectable d^8-square planar complexes, would allow for examination of the viability of the bond formation event. Ultimately, on the basis of our understanding of the intermediates, we hoped to elucidate the bond-forming step of gold-mediated photoreodox catalysis and eventually, to provide mechanistic insight to related heretofore uncharacterized metallaphotoredox processes.

Finally, we realized if mechanistic evidence supported the reductive elimination as the bond-forming step, we could also take advantage of these findings to examine other unprecedented reductive elimination reaction at gold(III). For example, we were especially intrigued by C(sp^2)–N coupling reactions due to the ambiguity over the copper(III) intermediates in the copper-catalyzed C(sp^2)–amide coupling reactions and

the dearth of examples of C–N reductive elimination from gold(III) complexes. Although copper(III)-mediated C(sp^2)–N reductive elimination is evidenced by stoichiometric reactions of well-defined aryl-copper(III) complexes,[12] and the formation of free aryl radical intermediates during the copper-catalyzed C(sp^2)–amide coupling reaction are not plausible,[13] the formation of copper(III) intermediates during the catalytic reactions remain inconclusive.[14] In this study, we provide mechanistic support for the formation of high-valent gold intermediates during photoredox-catalyzed gold-mediated C(sp^2)–CF_3 and C(sp^2)–N coupling reactions.

3.2 Results and Discussion

We decided to investigate the reaction mechanism of photoredox-catalyzed gold-mediated C(sp^2)−CF_3 coupling reaction as a consequence of the following consideration. All three proposed bond-forming scenarios (Scheme 1A) are plausible with a trifluoromethyl group, and as a result, the accessible reaction mechanism is not biased. Also, if transition metal trifluoromethyl complexes are involved, undesired side reactions such as hydrogen atom transfer and β-hydride elimination from the resulting trifluoromethylgold(III) intermediates could be largely ignored.

With this in mind, we sought conditions for the photoredox induced coupling of trifluoromethylgold(I) complex **1** with 4-nitrophenyl diazonium tetrafluoroborate. The desired C(sp^2)–CF_3 coupling product was obtained in 60% yield using nitromethane as a solvent, one equivalent of **1**, and 1.5 equivalents of 4-nitrophenyl diazonium tetrafluoroborate (Table 1, entry 1). Control experiments support that this transformation is enabled by photoredox catalysis (Table 1, entry 2 and 3). The analogous iodonium electrophile was not as efficient as the diazonium (Table 1, entry 4) and significantly less of the desired product was formed when the $Ru(bpy)_3(PF_6)_2$ was replaced by other photoredox catalysts (Table 1, entries 5–9). The exclusion of air and water from the reaction media was critical for efficient reaction (Table 1, entry 10 and 11).

Table 3.1 Control experiment[a,b]

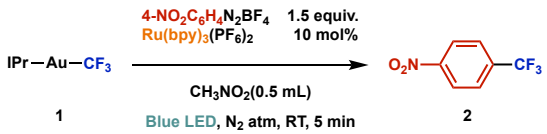

Entry	Variation from the reaction condition	Yield[c,d]
1	None	60%
2	No catalyst	< 1%
3	Dark and 40 °C instead of Blue LED and RT	< 1%
4	ArI(Mes)OTf instead of ArN_2BF_4	22%
5	$Ir(ppy)_2(dtbbpy)PF_6$ instead of $Ru(bpy)_3(PF_6)_2$	11%
6	$Ir\{dF(CF_3)ppy\}_2(dtbbpy)PF_6$ instead of $Ru(bpy)_3(PF_6)_2$	18%
7	$Ru(bpz)_3(PF_6)_2$ instead of $Ru(bpy)_3(PF_6)_2$	19%

8	$Cu(dap)_2Cl$ instead of $Ru(bpy)_3(PF_6)_2$	< 1%
9	Mes-$AcrBF_4$ instead of $Ru(bpy)_3(PF_6)_2$	7%
10	Under air instead of three freeze-pump-thaw cycles	24%
11	CH_3NO_2:H_2O = 96:4(v/v) instead of CH_3NO_2	< 1%[e]

[a] Reactions run at 8 μmol scale. [b] The temperature increases up to 40 °C [c] ^{19}F NMR yield by using $PhOCF_3$ as an internal standard. [d] *in triplicate* [e] 9% of $IPrAuCF_3$ and 55% of $Au^{III}CF_3$ were observed.

When water was present in the reaction mixture, instead of the desired product, another CF_3 containing species was observed by ^{19}F NMR (55% yield in Table 1, entry 11). We postulated that this trifluoromethyl-containing species might be the four-coordinate gold(III) intermediate with one of the coordination sites occupied by water, thereby inhibiting reductive elimination (Scheme 2). This hypothesis led us to evaluate other coordinating aprotic polar solvents. In the event, replacing nitromethane with acetonitrile provided the analogous CF_3 containing gold(III) acetonitrile complex. In this case, other CF_3 containing species such as the starting gold(I) complex, the coupling product, and any other side products were not detected using ^{19}F NMR (Figure 1).

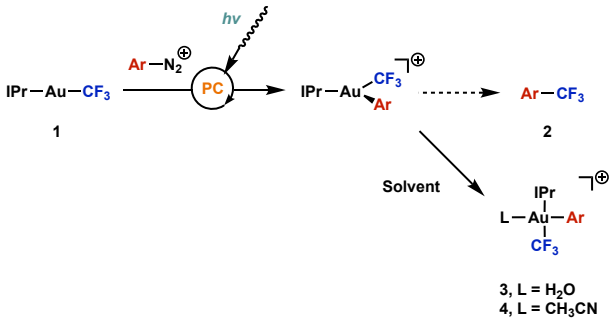

Scheme 3.2 Intercepted gold(III)-CF_3 intermediates, Ar = 4-nitrophenyl

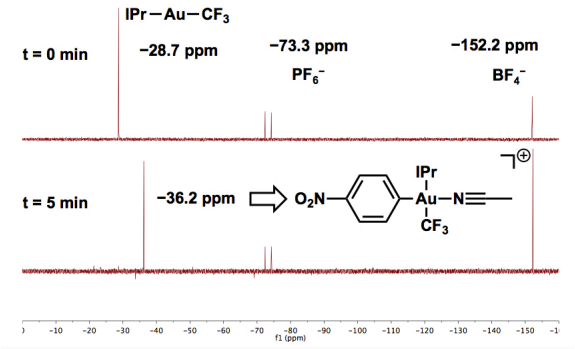

Figure 3.1 ^{19}F NMR spectra of gold-mediated $C(sp^2)$–CF_3 coupling reaction, solvent = CH_3CN.

This new species, **4**, was analyzed by HRMS, ^{13}C NMR, and ^{1}H NOESY (see supporting information). Two new quartets in the ^{13}C NMR spectrum with $^{3}J_{C\text{-}F}$ values of

25 Hz and 4.6 Hz respectively support that the IPr, CF_3, and 4-nitrophenyl are all bound on the same gold atom but in a different stereochemical relationship. ^{1}H NOE between IPr and 4-nitrophenyl supports that they are *cis* to each other and therefore, we predicted the CF_3 group would be *trans* to the IPr ligand. After the acetonitrile-bound gold(III) intermediate was characterized by NMR studies, the gold(III) aquo complex was crystallized as the tetrafluoroborate salt. The structure was analyzed by single-crystal X-ray diffraction and further supported the aforementioned spectroscopic characterizations (Figure 2).[15]

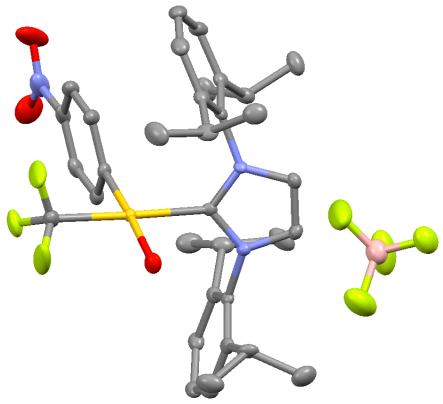

Figure 3.2 Crystal structure of **3**-BF_4. Thermal ellipsoid plot is drawn at 50% probability. Hydrogen atoms and solvents are omitted for clarity.

Based on this evidence for the formation of a gold(III) complex as an intermediate, we sought to unravel the mechanism of photoredox-catalyzed oxidative addition. In order to gain a deeper insight into the role of the visible light in this transformation, the emission spectrum of the light source, Kessil® H150, was compared with the absorption spectra of all chemical compounds in the reaction mixture. Although there are a few examples in which gold complexes initiate radical reactions as photosensitizers,[16] we observed that the radiated visible light was exclusively absorbed by the ruthenium photoredox catalysts in our system (Figure 3). This conclusion is further supported by the previously performed control experiment (Table 1, entry 2).

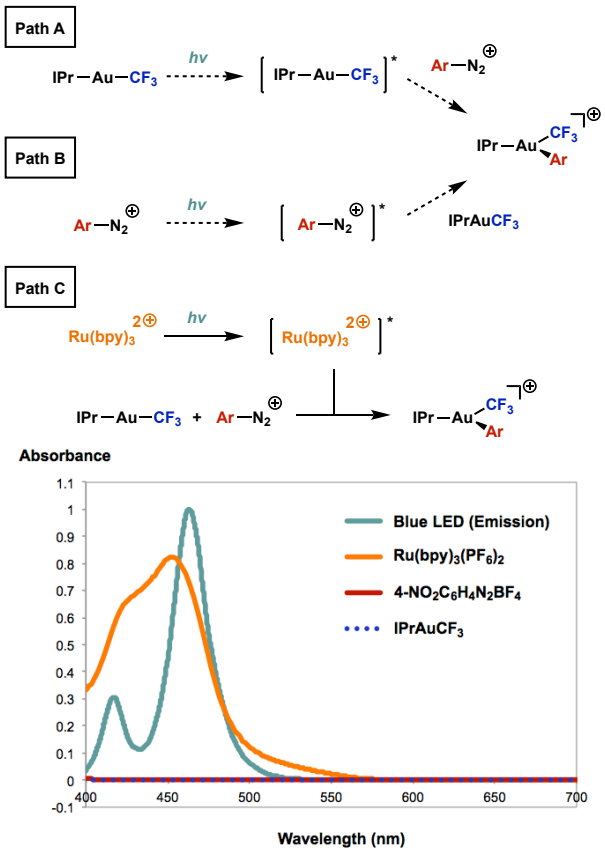

Figure 3.3 (Top) Three possible modes of sensitization with visible light. Path A and B were ruled out. (Bottom) UV-Vis absorption spectra of all chemicals (concentration = 0.05 mM in CH_3NO_2) and emission spectrum of the light source, Kessil® H150.

To explore the elementary step following the excitation of the photoredox catalyst, a photoluminescence quenching experiment was performed. The Stern-Volmer relationship supports the hypothesis that only the aryldiazonium salt reacts with the excited photoredox catalyst (Figure 4, see supporting information). An electron-transfer process is supported by the evolution of nitrogen gas upon radiation of visible light in the absence of gold complexes.[17]

The generation of odd-electron intermediates from photoluminescence quenching suggests that oxidative addition could proceed through a gold(II) intermediate. Two distinct gold(II) intermediates were considered; a neutral or a cationic gold(II) species (Figure 5). The cationic pathway would presumably result from oxidation of the gold complexes by the photoredox catalysts. To clarify whether the Ru(III) intermediate is capable of oxidizing $IPrAuCF_3$, the cyclic voltammogram of both $Ru(bpy)_3(PF_6)_2$ and $IPrAuCF_3$ was measured and showed that the redox potential of Ru(II)/Ru(III) is not adequate to oxidize $IPrAuCF_3$ to the corresponding cationic gold(II) intermediate (Figure 5, see supporting information). As a result, we envision that the free aryl radical reacts directly with **1** to generate a neutral (trifluoromethyl)arylgold(II) intermediate.

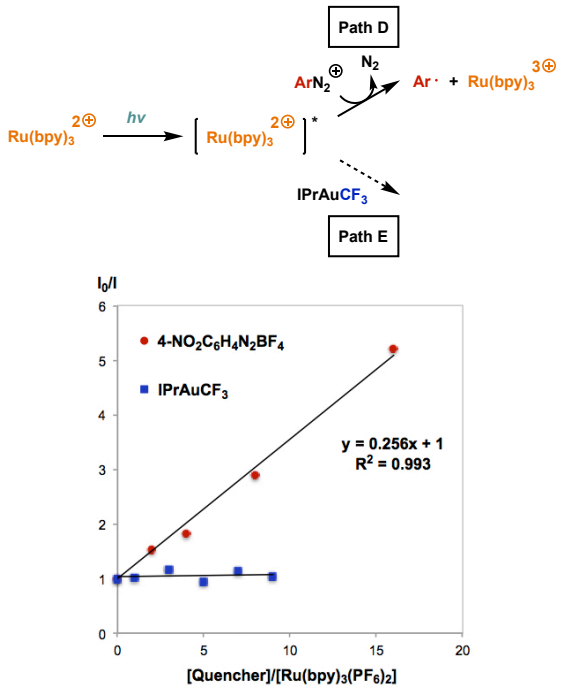

Figure 3.4 (Top) Two possible modes of photoluminescence quenching. Path E was ruled out. (Bottom) Stern-Volmer relationship. $[Ru(bpy)_3(PF_6)_2] = 0.05$ mM in CH_3NO_2.

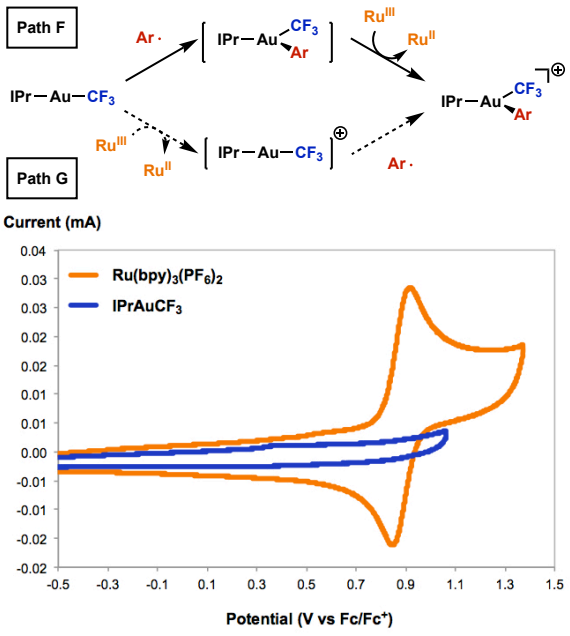

Figure 3.5 (Top) Two possible reaction mechanisms of oxidative addition. (Bottom) Cyclic voltammogram of $Ru(bpy)_3(PF_6)_2$ and $IPrAuCF_3$, scan rate = 100 mV/s.

With the implication of the neutral gold(II) intermediate and the direct observation of a trifluoromethylgold(III) species, we sought to ascertain the oxidant

responsible for the single electron oxidation from the gold(II) to gold(III). To this end, the quantum yield of oxidative addition was mearsured.[18] By radiating 3.3 mol% of photons over 20 minutes in a fluorometer at room temperature, the nitromethane-ligated trifluoromethylgold(III) complex was observed in 22% yield, but the reductive elimination product was not detected (Figure 6, see supporting information). The quantum yield of 6.6 implies that the oxidative addition involves a chain process; the gold(II) intermediate is mainly oxidized by aryldiazonium. Furthermore, in sharp contrast to the CH_3CN and H_2O-bound gold(III) complexes, the CH_3NO_2-bound gold(III) complex readily undergoes quantitative reductive elimination upon heating up to 40 ^oC (Figure 6). This observation suggests that the activation barrier of reductive elimination might be overcome by heat from the light source.[19]

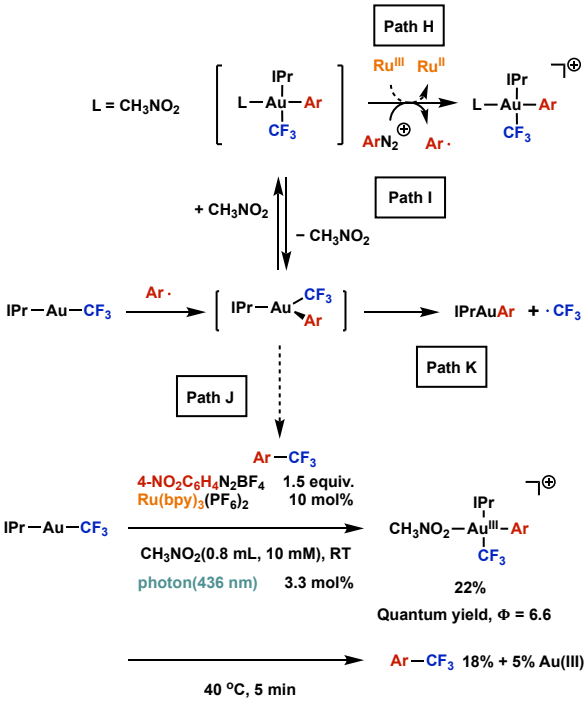

Figure 3.6 (Top) Revised reaction mechanism of oxidative addition. The major operating pathway is path I. Path J was not observed. (Bottom) Quantum yield and reductive elimination of CH_3NO_2-bound gold(III) intermediate. Yields are reported *in triplicate*.

Table 3.2 Electronic effect on aryldiazonium[a,b]

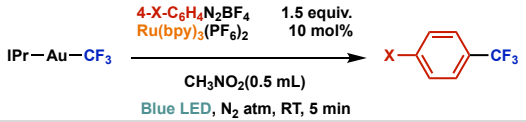

Entry	X	Yield[c,d]
1	NO_2	60%
2	CO_2Me	48%
3	Ac	43%

4	Br	46%
5	Cl	52%
6	F	44%
7	H	19%
8	Me	17%
9	*tert*-Bu	16%
10	OMe	15%

[a] Reactions run at 8 μmol scale. [b] The temperature increases up to 40 °C
[c] ^{19}F NMR yield by using $PhOCF_3$ as an internal standard. [d] *in triplicate*

During quantum yield measurements, we also uncovered a chain terminating event. The presence of unreacted $IPrAuCF_3$ and 4-nitrophenyl diazonium salts indicates that the chain propagation is interrupted. According to a previous report on gold(II) intermediates,[8] we proposed the release of trifluoromethyl radical from the gold(II) intermediate as the chain terminating event (Figure 6, Path K). Additionally, given that this process competes with oxidation of the gold(II) intermediate, the electronic properties of aryldiazonium are expected to influence the yield of the reaction. As we hypothesized, a decrease in product yield was observed as the σ_{para} of substituents inverts from positive values (Table 2, entries 1–6) to negative values (Table 2, entries 8–10). Moreover, to support the release of trifluoromethyl radical, we attempted to intercept the trifluoromethyl radical with radical traps. Addition of 70 equivalents of benzene to the optimized reaction condition produced trifluoromethylbenzene as a major product (Scheme 3, see supporting information).[20]

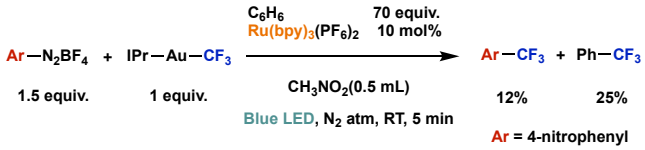

Scheme 3.3 Radical trapping experiment

Having gained evidence for the stepwise formation of a gold(III) intermediate as relevant to the C–C bond formation in the photoredox-catalyzed gold-mediated $C(sp^2)$–CF_3 coupling reaction, we sought to apply these mechanistic insight to examine the possibility that a similar pathway is involved in previously unknown photoredox driven $C(sp^2)$–N bond formation.

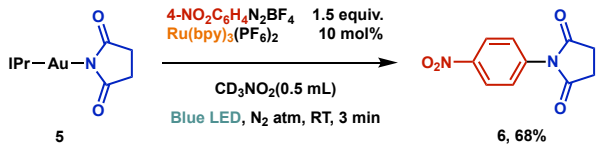

Scheme 3.4 Photoredox-catalyzed gold-mediated $C(sp^2)$–succinimide coupling reaction [a-d]

[a] Reactions run at 8 μmol scale. [b] The temperature increases up to 35 °C [c] ^{1}H NMR yield by using residual CHD_2NO_2 as an internal standard. [d] *in triplicate*

In the event, the product (**6**) of the photoredox-catalyzed gold-mediated C(sp^2)–N coupling reaction was obtained in 68% yield from gold(I)-succinimide (**5**) by only slight modification of the reaction conditions previously employed for trifluoromethylation (Scheme 4). It is notable that other gold-amides did not undergo the C-N bond-forming reaction with the same efficiency; rather, competitive protodeauration (formation of an N-H bond) was observed. Notably, the relative stability of the *N*-centered radical species that would be generated by Au-N bond scission appears to be irrelevant to the efficiency of the gold-mediated C(sp^2)–N coupling reactions. On the basis of additional experiments (see supporting information), we propose that the nature of the amide ligand is important for suppressing uncatalyzed reactions of the gold(I)-amide, such as direct oxidation by the photoredox catalyst or reaction with electrophilic diazonium salt. This hypothesis is consistent with our previous observations that gold(I)amides show increased nucleophilicity.[21]

To further explore the possibility that high-valent gold(III) intermediates are involved in the C(sp^2)–N coupling reaction, experiments to intercept the potential gold(III) imide intermediate were untaken (Scheme 5). These experiments resulted in the successful isolation and characterization of a gold(III) aquo succinimide complex (Figure 7). The isolation of this gold(III) species from a photoredox catalyzed process is consistent with the hypothesis that the photoredox-catalyzed gold-mediated C(sp^2)–succinimide coupling reaction proceeds by a mechanism closely related to that established for the photoredox-catalyzed gold-mediated C(sp^2)–CF_3 coupling reaction; namely oxidative addition followed by gold(III)-centered C(sp^2)–N reductive elimination.

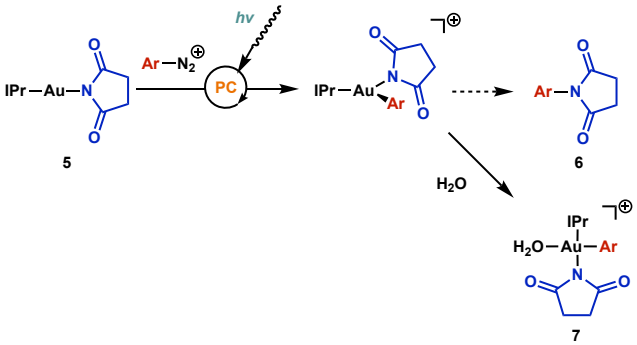

Scheme 3.5 Intercepted gold(III)-succinimide intermediate, Ar = 4-nitrophenyl

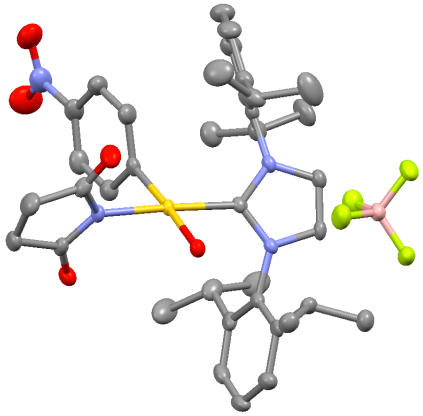

Figure 3.7 Crystal structure of **7**-BF_4. Thermal ellipsoid plot is drawn at 50% probability. Hydrogen atoms and solvents are omitted for clarity.

3.3 Conclusion

In summary, the unique characteristics of gold have simplified the mechanistic understanding of metallaphotoredox-catalyzed trifluoromethylation. This reaction was to be initiated by visible light and photoredox catalysis. Evidence was gained in support of a mechanistic scenario involving addition of the aryl radical to trifluoromethylgold(I) complex to generate a gold(II) species that undergoes a single electron oxidation to access the gold(III) intermediate. This oxidation likely occurs by reaction of the gold(II) species with the aryldiazonium salt, thereby generating an aryl radical. This chain mechanism is consistent with the measured quantum yield (6.6) for the process. After radical chain oxidative addition, the gold(III) intermediate, which was isolable in coordinating solvents, is converted to the desired product via reductive elimination (Figure 8). We propose that the reductive elimination, which regenerates gold(I), is the bond-forming step of photoredox-catalyzed gold-mediated $C(sp^2)$–CF_3 and $C(sp^2)$–N coupling reactions. To the best of our knowledge, the analogous copper(III) intermediates in copper/photoredox dual catalytic trifluoromethylation and amination reactions have not been isolated or characterized. Thus, the use of gold, as another member of group 11, may provide useful insight into the mechanism of these metallaphotoredox catalyzed transformations.

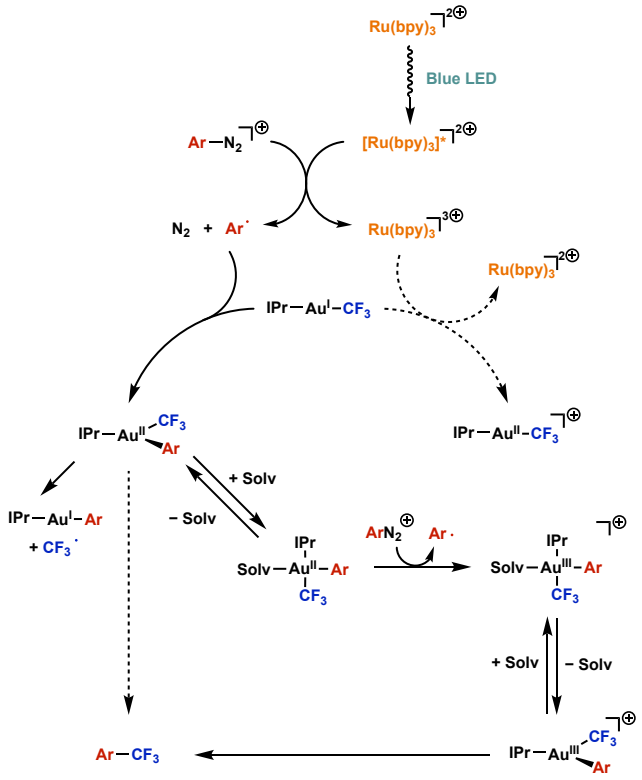

Figure 3.8 Summary of proposed reaction mechanism, Solv = CH_3NO_2

3.4 References and Notes

(1) For reviews of metallaphotoredox catalysis, see:

(a) Twilton, J.; Le, C.; Zhang, P.; Shaw, M. H.; Evans, R. W.; MacMillan, D. W. C. The merger of transition metal and photocatalysis. *Nat. Rev. Chem.* **2017**, *1*, 52.

(b) Levin, M. D.; Kim, S.; Toste, F. D. Photoredox Catalysis Unlocks Single-Electron Elementary Steps in Transition Metal Catalyzed Cross-Coupling. *ACS Cent. Sci.* **2016**, *2*, 293−301.

(c) Skubi, K. L.; Blum, T. R.; Yoon, T. P. Dual Catalysis Strategies in Photochemical Synthesis. *Chem. Rev.* **2016**, *116*, 10035−10074.

(d) Hopkinson, M. N.; Sahoo, B.; Li, J.-L.; Glorius, F. Dual Catalysis Sees the Light: Combining Photoredox with Organo-, Acid, and Transition-Metal Catalysis. *Chem. Eur. J.* **2014**, *20*, 3874−3886.

(e) Prier, C. K.; Rankic, D. A.; MacMillan, D. W. C. Visible Light Photoredox Catalysis with Transition Metal Complexes: Applications in Organic Synthesis. *Chem. Rev.* **2013**, *113*, 5322−5363.

(2) For seminal reports, see:

(a) Tellis, J. C.; Primer, D. N.; Molander, G. A. Single-electron transmetalation in organoboron cross-coupling by photoredox/nickel dual catalysis. *Science* **2014**, *345*, 433−436.

(b) Zuo, Z.; Ahneman, D. T.; Chu, L.; Terrett, J. A.; Doyle, A. G.; MacMillan, D. W. C. Merging photoredox with nickel catalysis: Coupling of α-carboxyl sp^3-carbons with aryl halides. *Science* **2014**, *345*, 437−440.

(c) Tasker, S. Z.; Jamison, T. F. Highly Regioselective Indoline Synthesis under Nickel/Photoredox Dual Catalysis. *J. Am. Chem. Soc.* **2015**, *137*, 9531−9534.

(d) Terrett, J. A.; Cuthbertson, J. D.; Shurtleff, V. W.; MacMillan, D. W. C. Switching on elusive organometallic mechanisms with photoredox catalysis. *Nature* **2015**, *524*, 330−334.

(e) Kalyani, D.; McMurtrey, K. B.; Neufeldt, S. R.; Sanford, M. S. Room-Temperature C–H Arylation: Merger of Pd-Catalyzed C–H Functionalization and Visible-Light Photocatalysis. *J. Am. Chem. Soc.* **2011**, *133*, 18566−18569.

(f) Ye, Y.; Sanford, M. S. Merging Visible-Light Photocatalysis and Transition-Metal Catalysis in the Copper-Catalyzed Trifluoromethylation of Boronic Acids with CF_3I. *J. Am. Chem. Soc.* **2012**, *134*, 9034−9037.

(3) (a) Shields, B. J.; Doyle, A. G. Direct $C(sp^3)$–H Cross Coupling Enabled by Catalytic Generation of Chlorine Radicals. *J. Am. Chem. Soc.* **2016**, *138*, 12719−12722.

(b) Shields, B. J.; Kudisch, B.; Scholes, G. D.; Doyle, A. G. Long-Lived Charge-Transfer States of Nickel(II) Aryl Halide Complexes Facilitate Bimolecular Photoinduced Electron Transfer. *J. Am. Chem. Soc.* **2018**, *140*, 3035−3039.

(4) Hartwig, J. F. Carbon−Heteroatom Bond-Forming Reductive Eliminations of Amines, Ethers, and Sulfides. *Acc. Chem. Res.* **1998**, *31*, 852−860.

(5) For perfluorinated alkyl radicals: see

(a) Bravo, A.; Bjørsvik, H.-R.; Fontana, F.; Liguori, L.; Mele, A.; Minisci, F. New Methods of Free-Radical Perfluoroalkylation of Aromatics and Alkenes. Absolute Rate Constants and Partial Rate Factors for the Homolytic Aromatic Substitution by n-Perfluorobutyl Radical. *J. Org. Chem.* **1997**, *62*, 7128−7136.

(b) Studer, A. A "Renaissance" in Radical Trifluoromethylation. *Angew. Chem., Int. Ed.* **2012**, *51*, 8950−8958.

(6) For N-centered radicals, see:

(a) Kärkäs, M. D. Photochemical Generation of Nitrogen-Centered Amidyl, Hydrazonyl, and Imidyl Radicals: Methodology Developments and Catalytic Applications. *ACS Catal.* **2017**, *7*, 4999–5022.

(b) Zard, S. Z. Recent progress in the generation and use of nitrogen-centred radicals. *Chem. Soc. Rev.* **2008**, *37*, 1603–1618.

(c) Xiong, T.; Zhang, Q. New amination strategies based on nitrogen-centered radical chemistry. *Chem. Soc. Rev.* **2016**, *45*, 3069–3087.

(7) In the recent example of copper/photoredox dual catalytic aryl trifluoromethylation, both CF_3 radical and carbon(sp^2)-centered radicals were proposed as viable intermediates. Le, C.; Chen, T. Q.; Liang, T.; Zhang, P.; MacMillan, D. W. C. A radical approach to the copper oxidative addition problem: Trifluoromethylation of bromoarenes. *Science* **2018**, *360*, 1010–1014.

(8) Liang, Y.; Zhang, X.; MacMillan, D. W. C. Decarboxylative sp^3 C–N coupling via dual copper and photoredox catalysis. *Nature* **2018**, *559*, 83−88.

(9) (a) Creutz, S. E.; Lotito, K. J.; Fu, G. C.; Peters, J. C. Photoinduced Ullmann C–N Coupling: Demonstrating the Viability of a Radical Pathway. *Science* **2012**, *338,* 647−651.

(b) Bissember, A. C.; Lundgren, R. J.; Creutz, S. E.; Peters, J. C.; Fu, G. C. Transition-Metal-Catalyzed Alkylations of Amines with Alkyl Halides: Photoinduced, Copper-Catalyzed Couplings of Carbazoles. *Angew. Chem. Int. Ed.* **2013**, *52*, 5129–5133.

(c) Ziegler, D. T.; Choi, J.; Muñoz-Molina, J. M.; Bissember, A. C.; Peters, J. C.; Fu, G. C. A Versatile Approach to Ullmann C–N Couplings at Room Temperature: New Families of Nucleophiles and Electrophiles for Photoinduced, Copper-Catalyzed Processes. *J. Am. Chem. Soc.* **2013**, *135*, 13107–13112.

(d) Do, H.; Bachman, S.; Bissember, A. C.; Peters, J. C.; Fu, G. C. Photoinduced, Copper-Catalyzed Alkylation of Amides with Unactivated Secondary Alkyl Halides at Room Temperature. *J. Am. Chem. Soc.* **2014**, *136*, 2162−2167.

(e) Kainz, Q. M.; Matier, C. D.; Bartoszewicz, A.; Zultanski, S. L.; Peters, J. C.; Fu, G. C. Asymmetric copper-catalyzed C-N cross-couplings induced by visible light. *Science* **2016,** *351*, 681−684.

(10) (a) Winston, M. S.; Wolf, W. J.; Toste, F. D. Photoinitiated Oxidative Addition of CF3I to Gold(I) and Facile Aryl-CF3 Reductive Elimination. *J. Am. Chem. Soc.* **2014**, *136*, 7777−7782.

(b) Winston, M. S.; Wolf, W. J.; Toste, F. D. Halide-Dependent Mechanisms of Reductive Elimination from Gold(III). *J. Am. Chem. Soc.* **2015**, *137*, 7921−7928.

(c) Levin, M. D.; Chen, T. Q.; Neubig, M. E.; Hong, C. M.; Theulier, C. A.; Kobylianskii, I. J.; Janabi, M.; O'Neil, J. P.; Toste, F. D. A catalytic fluoride-rebound mechanism for $C(sp^3)$-CF_3 bond formation. *Science* **2017**, *356*, 1272−1276.

(11) (a) Tamaki, A.; Kochi, J. K. Catalytic mechanism involving oxidative addition in the coupling of alkylgold(I) with alkyl halides. *J. Organomet. Chem.* **1972**, *40*, C81−C84.

(b) Tamaki, A.; Magennis, S. A.; Kochi, J. K. Rearrangement and decomposition of trialkylgold(III) complexes. *J. Am. Chem. Soc.* **1973**, *95*, 6487–6488.

(c) Tamaki, A.; Magennis, S. A.; Kochi, J. K. Catalysis by gold. Alkyl isomerization, cis-trans rearrangement, and reductive elimination of alkylgold(III) complexes. *J. Am. Chem. Soc.* **1974**, *96*, 6140–6148.

(d) Komiya, S.; Kochi, J. K. Electrophilic cleavage of organogold complexes with acids. The mechanism of the reductive elimination of dialkyl(aniono)gold(III) species. *J. Am. Chem. Soc.*, **1976**, *98*, 7599–7607.

(e) Komiya, S.; Albright, T. A.; Hoffmann, R.; Kochi, J. K. The stability of organogold compounds. Hydrolytic, thermal, and oxidative cleavages of dimethylaurate(I) and tetramethylaurate(III). *J. Am. Chem. Soc.* **1977**, *99*, 8440–8447.

(12) (a) Huffman, L. M.; Stahl, S. S. Carbon−Nitrogen Bond Formation Involving Well-Defined Aryl−Copper(III) Complexes. *J. Am. Chem. Soc.* **2008**, *130* 9196–9197.

(b) King, A. E.; Huffman, L. M.; Casitas, A.; Costas, M. Ribas, X.; Stahl, S. S. Copper-Catalyzed Aerobic Oxidative Functionalization of an Arene C−H Bond: Evidence for an Aryl-Copper(III) Intermediate. *J. Am. Chem. Soc.* **2010**, *132*, 12068–12073.

(c) Casitas, A.; King, A. E.; Parella, T.; Costas, M.; Stahl, S. S.; Ribas, X. Direct observation of Cu^{I}/Cu^{III} redox steps relevant to Ullmann-type coupling reactions. *Chem. Sci.* **2010**, *1*, 326–330.

(13) Tye, J. W.; Weng, Z.; Johns, A. M.; Incarvito, C. D.; Hartwig, J. F. Copper Complexes of Anionic Nitrogen Ligands in the Amidation and Imidation of Aryl Halides. *J. Am. Chem. Soc.* **2008**, *130*, 9971–9983.

(14) Strieter, E. R.; Bhayana, B.; Buchwald, S. L. Mechanistic Studies on the Copper-Catalyzed N-Arylation of Amides. *J. Am. Chem. Soc.* **2009**, *131*, 78–88.

(15) Gold(III) salts have been isolated but they are irrelevant to catalytically active gold(III) intermediates. See:

(a) Tlahuext-Aca, A.; Hopkinson, M. N.; Daniliuc, C. G.; Glorius, F. Oxidative Addition to Gold(I) by Photoredox Catalysis: Straightforward Access to Diverse (C,N)-Cyclometalated Gold(III) Complexes. *Chem. Eur. J.* **2016**, *22*, 11587−11592.

(b) Huang, L.; Rominger, F.; Rudolph, M.; Hashmi, A. S. K. A general access to organogold(III) complexes by oxidative addition of diazonium salts. *Chem. Commun.* **2016**, *52*, 6435−6438.

(16) For gold complex photosensitizers, see:

(a) Xie, J.; Shi, S.; Zhang, T.; Mehrkens, N.; Rudolph, M.; Hashmi, A. S. K. A Highly Efficient Gold-Catalyzed Photoredox α-C(sp^3)−H Alkynylation of Tertiary Aliphatic Amines with Sunlight. *Angew. Chem., Int. Ed.* **2015**, *54*, 6046−6050.

(b) Xie, J.; Zhang, T.; Chen, F.; Mehrkens, N.; Rominger, F.; Rudolph, M.; Hashmi, A. S. K. Gold-Catalyzed Highly Selective Photoredox C(sp^2)−H Difluoroalkylation and Perfluoroalkylation of Hydrazones. *Angew. Chem., Int. Ed.* **2016**, *55*, 2934−2938.

(c) Huang, L.; Rudolph, M.; Rominger, F.; Hashmi, A. S. K. Photosensitizer-Free Visible-Light-Mediated Gold-Catalyzed 1,2-Difunctionalization of Alkynes. *Angew. Chem., Int. Ed.* **2016**, *55*, 4808−4813.

(17) Cano-Yelo, H.; Deronzier, A. Photocatalysis of the Pschorr reaction by tris-(2,2′-bipyridyl)ruthenium(II) in the phenanthrene series. *J. Chem. Soc., Perkin Trans. 2* **1984**, 1093−1098.

(18) Cismesia, M. A.; Yoon, T. P. Characterizing chain processes in visible light photoredox catalysis. *Chem. Sci.* **2015**, *6*, 5426−5434.

(19) Both thermal and photochemical reductive eliminations from NHC−Gold complexes are plausible. Ghidiu, M. J.; Pistner, A. J.; Yap, G. P. A.; Lutterman, D. A.; Rosenthal, J. Thermal versus Photochemical Reductive Elimination of Aryl Chlorides from NHC–Gold Complexes. *Organometallics* **2013**, *32*, 5026−5029.

(20) Nagib, D. A.; MacMillan, D. W. C. Trifluoromethylation of arenes and heteroarenes by means of photoredox catalysis. *Nature* **2011**, *480*, 224−228.

(21) Due to the repulsive interaction with d^{10} gold(I) metal, gold-bound nitrogen ligands become more nucleophilic. Johnson, M. W.; Shevick, S. L.; Toste, F. D.; Bergman, R. G. Preparation and reactivity of terminal gold(I) amides and phosphides. *Chem. Sci.* **201**3, *4*, 1023−1027.

3.5 Supporting information

3.5.1 General consideration

Unless stated otherwise, reagents were purchased from commercial suppliers and used without further purification. All reactions were performed in oven-dried glassware sealed with rubber septa under a nitrogen atmosphere. Dry tetrahydrofuran (THF), benzene (C_6H_6), and dichloromethane (DCM) were obtained by passing these previously degassed solvents through activated alumina columns. Dry acetonitrile and nitromethane were obtained by fractional distillation after stirring with 3 Å molecular sieves (20% m/v) for 24 hours under nitrogen atmosphere.[1] All magnetic stir bars were washed with freshly prepared aqua regia prior to use in order to minimize the potential for trace metal contamination. Reactions were monitored with ^{1}H NMR as well as ^{19}F NMR. ^{1}H NMR, ^{13}C NMR were taken with Bruker spectrometers operating at 300, 400, 500, 600, or 700 MHz for ^{1}H (75, 100, 125, 150, or 175 MHz for ^{13}C). ^{1}H and ^{13}C chemical shifts were reported in ppm downfield of tetramethylsilane and referenced to residual solvent peak. ^{19}F NMR was also taken with Bruker spectrometers operating at 376, 470, or 564 MHz and chemical shifts were reported in ppm upfield of $CFCl_3$ and referenced to trifluorotoluene(−63.70 ppm). Multiplicities were reported using the following abbreviations: s = singlet, d = doublet, t = triplet, q = quartet, hept = heptet, m = multiplet. Mass spectral data were obtained from the Autospec Premier magnetic sector mass spectrometer at the Micro-Mass/Analytical Facility operated by the College of Chemistry, University of California, Berkeley.

$Ru(bpy)_3(PF_6)_2$,[2] $Ir(ppy)_2(dtbbpy)PF_6$,[3] $Ir\{dF(CF_3)ppy\}_2(dtbbpy)PF_6$,[4] $Ru(bpz)_3(PF_6)_2$,[5] Mes-AcrBF_4,[6] aryldiazonium tetrafluoroborate salts,[7] 4-nitrophenyl(mesityl)iodonium triflate,[8] and N-(4-nitrophenyl)succinimide[9] were synthesized according to literature procedures. $Cu(dap)_2Cl$ was purchased from Sigma-Aldrich and used without further purification.

UV-Vis spectroscopic measurements were performed in dry nitromethane. Absorption spectra were recorded using a Varian Cary 50 spectrophotometer and samples for absorption measurements were prepared in 1 cm × 0.5 cm quartz cuvettes (1.4 mL volume, Starna).

3.5.2 Preparation of $IPrAuCF_3$, 1

Synthesis of IPrAuCl

To the suspension of $AuCl_3$ (1.515 g, 5.00 mmol) in methanol (15 mL) at 0 °C, minimal amount of aqueous solution of HCl (12 M) was added dropwise with vigorous stirring until the solution become homogeneous. The yellow homogenous solution was titrated with dimethyl sulfide at 0 °C with vigorous stirring. The addition was immediately halted when a visible red color from adding a drop of dimethyl sulfide stopped to appear. The reaction was slowly warmed to room temperature until the yellow color disappears. The resulting white suspension was diluted with excess amount of DCM and filtered through a filter paper to remove any residual solid impurities. The filtrate was slowly concentrated at 0 °C under 50 mbar until no further precipitation was observed. The precipitate was collected by filtration, washed with *n*-pentane, and dried in the dark under the atmospheric condition. DMSAuCl (1.267 g, 4.38 mmol, 88%) was obtained as a colorless solid and directly used for the synthesis of IPrAuCl by following a previously procedure reported by Nolan and co-workers.[10] IPrAuCl (2.359 g, 3.80 mmol, 87%) was obtained as a colorless solid.

^{1}H NMR (300 MHz, CD_2Cl_2) δ 7.56 (t, J = 7.8 Hz, 2H), 7.35 (d, J = 7.8 Hz, 4H), 7.23 (s, 2H), 2.56 (hept, J = 6.8 Hz, 4H), 1.33 (d, J = 6.9 Hz, 12H), 1.23 (d, J = 6.9 Hz, 12H) in accordance with a previously reported spectrum.

Synthesis of IPrAuMe

To the solution of IPrAuCl (1.24 g, 2.00 mmol) in THF (20 mL) at −78 °C, the 3.0 mL of MeMgBr solution (3.0 M in Et_2O, 9.0 mmol) was added dropwise. The reaction mixture was warmed to room temperature, stirred for 2 hours, and cooled to 0 °C. The reaction was quenched with a minimal amount of H_2O, diluted with DCM (50 mL), dried with

Na_2SO_4 and filtered through a filter paper. The solid residue was washed with DCM (2 × 50 mL). The organic phase was collected and the solvent was removed under vacuum. The residual solid was washed with excess *n*-pentane and recrystallized with DCM and *n*-pentane. IPrAuMe (1.00 g, 1.66 mmol, 83% yield) was obtained as a colorless solid.
^{1}H NMR (500 MHz, CD_2Cl_2) δ 7.53 (t, *J* = 7.8 Hz, 2H), 7.32 (d, *J* = 7.8 Hz, 4H), 7.11 (s, 2H), 2.63 (hept, *J* = 6.9 Hz, 4H), 1.34 (d, *J* = 6.9 Hz, 12H), 1.21 (d, *J* = 6.9 Hz, 12H), −0.30 (s, 3H) in accordance with a previously reported spectrum.[11]

Synthesis of $IPrAuCF_3$

To a 50 mL flame-dried schlenk flask, IPrAuMe (1.00g, 1.66 mmol) and DCM (20 mL) were added. The solution was degassed by three freeze-pump-thaw cycles and backfilled with 1 atm of CF_3I. The reaction mixture was radiated with sunlight for 5 minutes. The solvent was removed under vacuum and the residual solid was recrystallized with DCM and *n*-pentane. $IPrAuCF_3$ (977 mg, 1.49 mmol, 90% yield) was obtained as a colorless solid.
^{1}H NMR (400 MHz, CD_2Cl_2) δ 7.56 (t, *J* = 7.8 Hz, 2H), 7.35 (d, *J* = 7.8 Hz, 4H), 7.22 (s, 2H), 2.54 (hept, *J* = 6.8 Hz, 4H), 1.32 (d, *J* = 6.9 Hz, 12H), 1.23 (d, *J* = 6.9 Hz, 12H) in accordance with a previously reported spectrum.[12]

^{1}H NMR (700 MHz, CD_3CN) δ 7.57 (t, *J* = 7.8 Hz, 2H), 7.48 (s, 2H), 7.40 (d, *J* = 7.8 Hz, 4H), 2.54 (hept, *J* = 6.9 Hz, 4H), 1.29 (d, *J* = 6.9 Hz, 12H), 1.22 (d, *J* = 6.9 Hz, 12H).
^{13}C NMR (176 MHz, CD_3CN) δ 187.76 (q, *J* = 14.5 Hz), 163.42 (q, *J* = 344.1 Hz), 146.86, 134.86, 131.56, 125.05, 29.54, 24.56, 23.92.
^{19}F NMR (376 MHz, CD_3CN) −28.67 (s)

3.5.3 General procedure of photoredox-catalyzed gold-mediated trifluoromethylation

To an oven-dried NMR tube, $IPrAuCF_3$ (5.2 mg, 8.0 μmol), 4-nitrobenzenediazonium tetrafluoroborate (2.8 mg, 12.0 μmol), $Ru(bpy)_3(PF_6)_2$ (0.7 mg, 0.8 μmol) and dry nitromethane (0.5 mL) were added under a nitrogen atmosphere. The NMR tube was

sealed with a rubber septum, degassed three times via freeze-pump-thaw cycles, and backfilled with nitrogen. After then, the reaction mixture was radiated with Blue LEDs for 5 minutes.

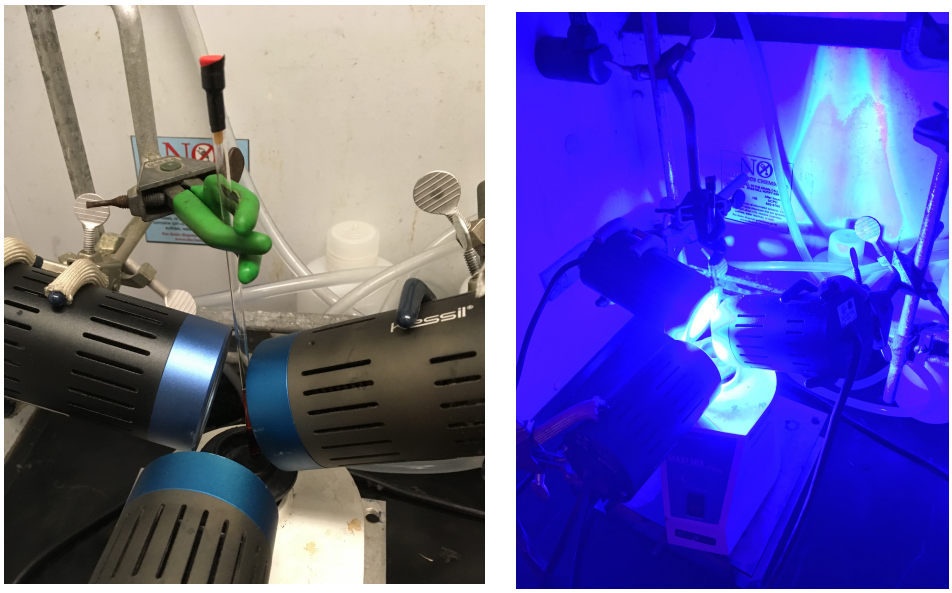

Figure 3.9 Photoreactor used in this study

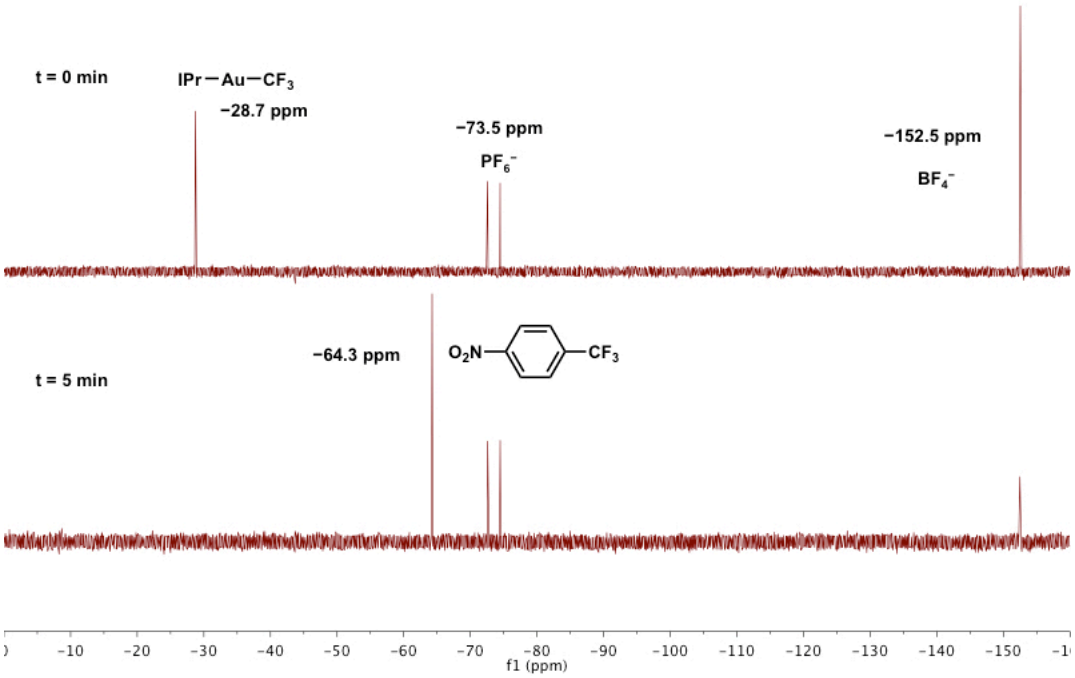

Figure 3.10 ^{19}F NMR spectra of reaction mixture, solvent = CH_3NO_2

3.5.4 Photoluminescence quenching experiment

Photoluminescence quenching experiment was performed in dry nitromethane. Samples were prepared in 1 cm × 0.5 cm quartz cuvettes (1.4 mL volume, Starna), purged for 1 minute with a continuous nitrogen flow, and luminescence spectra were recorded using a Photon Technology International QuantaMaster spectrofluorometer. Detailed experimental conditions are provided below.

Excitation wavelength = 452 nm, emission wavelength = 500−700 nm, slit width = 3 nm, step size = 1 nm, integration = 0.1 s

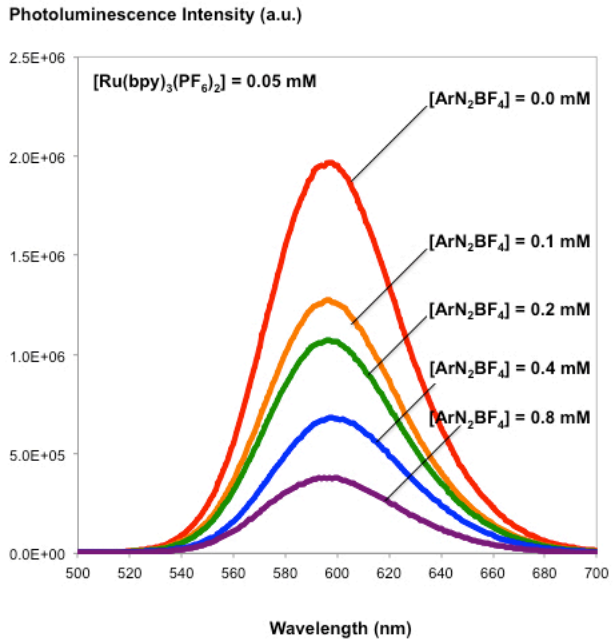

Figure 3.11 Photoluminescence quenching of $Ru(bpy)_3(PF_6)_2$ by varying concentration of ArN_2BF_4, Ar = 4-nitrophenyl

Photoluminescence intensities were measured at λ = 596 nm. Concentration of $Ru(bpy)_3(PF_6)_2$ was maintained as 0.05 mM. I_0 was recorded as an average of thee trials. Other intensities were recorded as the maximum value of three trials to minimize the effect of aerobic quenching.

$[ArN_2BF_4]$	0.0 mM	0.1 mM	0.2 mM	0.4 mM	0.8 mM
I	1964458	1276549	1075957	679006	377112
I_0/I	1	1.54	1.83	2.89	5.21

Table 3.3 Stern-Volmer experiment with ArN_2BF_4, Ar = 4-nitrophenyl. $K_{sv} = 5.11 \times 10^4\ M^{-1}$

$[IPrAuCF_3]$	0.0 mM	0.05 mM	0.15 mM	0.25 mM	0.35 mM	0.45 mM
I	2018494	1963639	1744430	2106027	1786658	1940486
I_0/I	1	1.03	1.16	0.96	1.13	1.04

Table 3.4 Stern-Volmer experiment with $IPrAuCF_3$

3.5.5 Cyclic Voltammogram of $IPrAuCF_3$ and $Ru(bpy)_3(PF_6)_2$

General Methods for Electrochemistry. Non-aqueous electrochemical experiments were conducted under Ar atmosphere in 0.1 M NBu_4PF_6 electrolyte in dry acetonitrile. Cyclic voltammetry experiments were performed using an Epsilon potentiostat from Bioanalytical Systems, Inc. The working electrode was a 3.0 mm diameter glassy carbon disk (from Bioanalytical Systems, Inc.) and was polished between every scan with 0.05-micron alumina powder on a felt pad. The counter electrode was a platinum wire. A silver wire in porous Vycor tip glass tube filled with 0.1 M NBu_4PF_6 in acetonitrile was used as a pseudo-reference electrode. At the conclusion of a series of experiments, the pseudo-reference potentials were referenced against ferrocene/ferrocenium as an external standard. All scans were compensated for internal resistance.

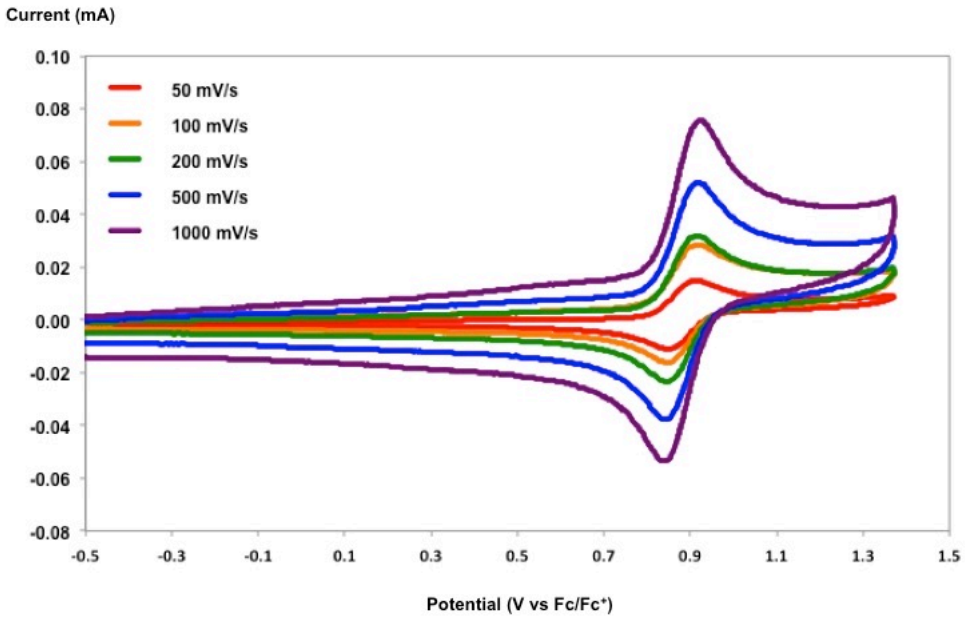

Figure 3.12 Cyclic voltammogram of $Ru(bpy)_3(PF_6)_2$ by varying the scan rate.

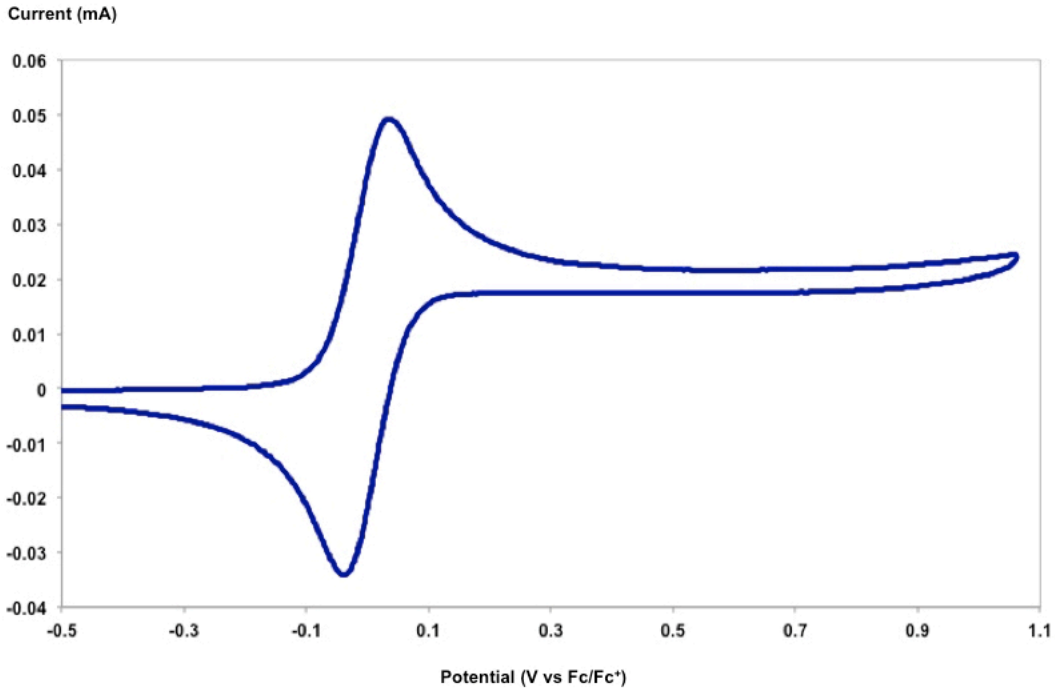

Figure 3.13 Cyclic voltammogram of ferrocene and $IPrAuCF_3$ mixture, scan rate = 100 mV/s.

3.5.6 *In situ* identification of acetonitrile-bound gold(III)−CF_3 complex, 4

To an oven-dried NMR tube, $IPrAuCF_3$ (5.2 mg, 8.0 μmol), 4-nitrophenyl diazonium tetrafluoroborate (2.8 mg, 12.0 μmol), $Ru(bpy)_3(PF_6)_2$ (0.7 mg, 0.8 μmol) and dry CD_3CN (0.5 mL) were added under a nitrogen atmosphere. The NMR tube was sealed with a rubber septum, degassed three times via freeze-pump-thaw cycles, and backfilled with nitrogen. After then, the reaction mixture was radiated with Blue LED for 5 minutes.

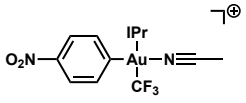

CH_3CN was used instead of CD_3CN.

m/z HRMS (ESI positive) found 817.2999 $C_{36}H_{43}O_2N_4AuF_3^+$ requires 817.2998.

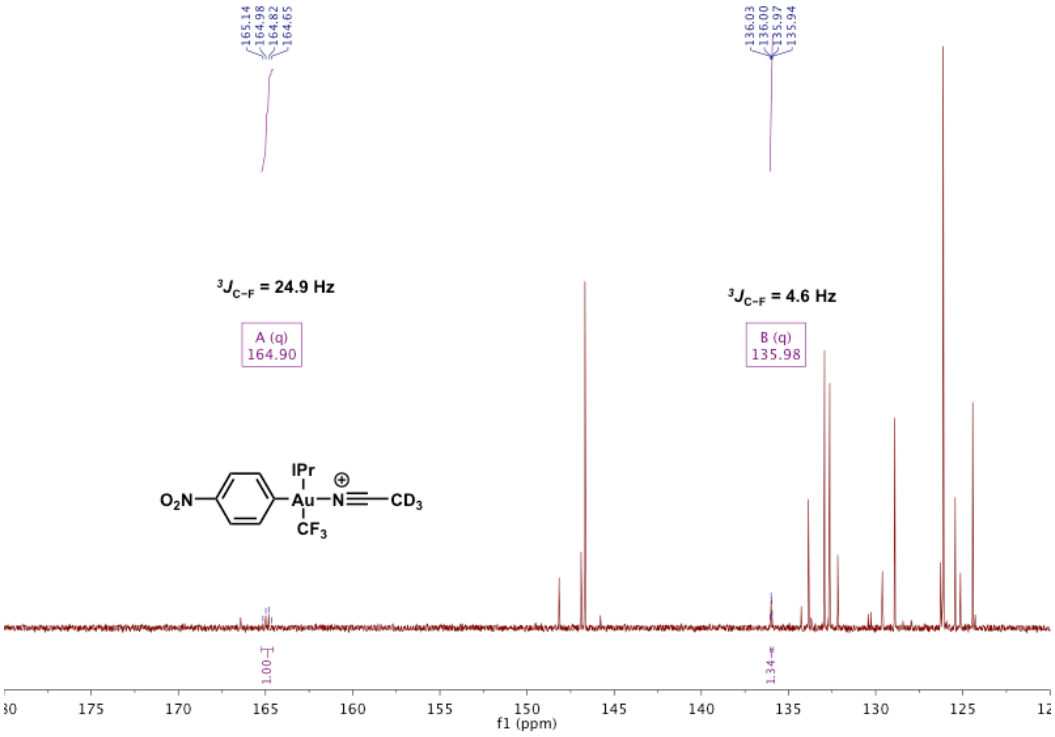

Figure 3.14 ^{13}C NMR spectrum of reaction mixture, solvent = CD_3CN.

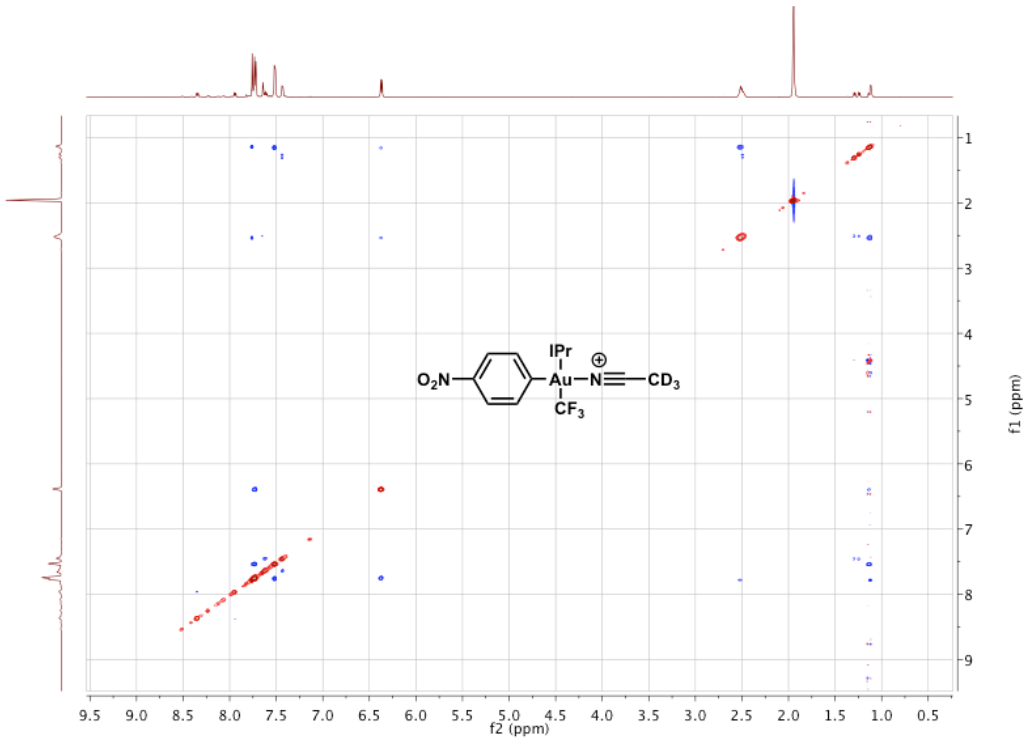

Figure 3.15 ^1H-^1H NOESY spectrum of reaction mixture, solvent = CD_3CN

3.5.7 H_2O-bound gold(III)−CF_3 complex, 3

To an oven-dried NMR tube, $IPrAuCF_3$ (5.2 mg, 8.0 μmol), 4-nitrobenzenediazonium tetrafluoroborate (2.8 mg, 12.0 μmol), $Ru(bpy)_3(PF_6)_2$ (0.7 mg, 0.8 μmol) and solvent mixture (CH_3NO_2:H_2O = 96:4 v/v, 0.5 mL) were added under a nitrogen atmosphere. The NMR tube was sealed with a rubber septum, degassed three times via freeze-pump-thaw cycles, and backfilled with nitrogen. After then, the reaction mixture was radiated with Blue LED for 5 minutes and the product yield was measured by using ^{19}F NMR. For quantitative analysis, the number of scan was set as 1 to avoid any error caused by relaxation time. The null signal appears at the center of single scan spectrum.

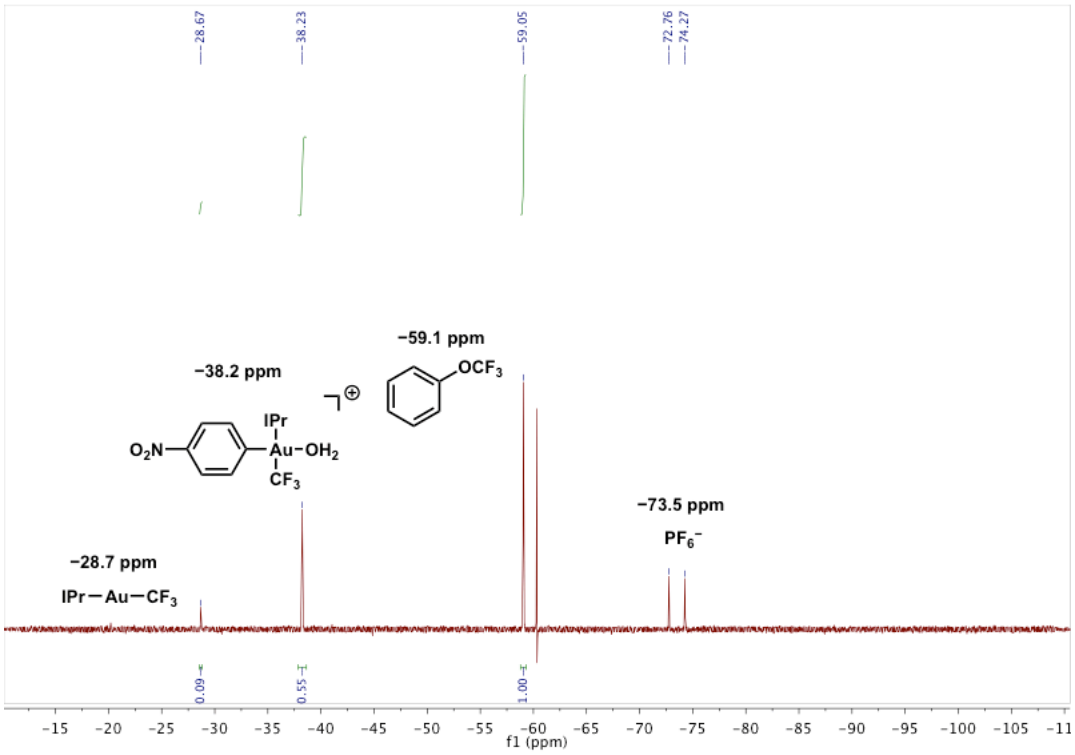

Figure 3.16 ^{19}F NMR spectrum of reaction mixture, solvent = mixture of CH_3NO_2 and H_2O (96:4 v/v)

Crystals of **3** suitable for X-ray diffraction were grown by sequential vapor diffusion of CH_2Cl_2 and layer diffusion of pentane to crude mixture at –20 ^oC. Pentane was layered onto the mixture after photoredox catalysts precipitated out by vapor diffusion of CH_2Cl_2.

3.5.8 Quantum yield measurement

Actinometry at 436 nm

The photon flux of Photon Technology International QuantaMaster spectrofluorometer was determined by following the procedure described in the literature.[13] Potassium ferrioxalate was recrystallized three times in the dark prior to use. To determine the photon flux of the spectrophotometer, 0.8 mL of the ferrioxalate solution was placed in 1 cm × 0.5 cm quartz cuvettes (1.4 mL volume, Starna) and irradiated for 120 seconds at λ = 436 nm with an emission slit width at 10.0 nm. 0.14 mL of the phenanthroline buffer solution was added to the cuvette. After 1 hour, the absorbance of solution was measured at λ = 510 nm by using Varian Cary 50 spectrophotometer. Background sample was prepared by adding 0.14 mL of the phenanthroline buffer solution to the non-irradiated ferrioxalate solution. Photon flux was calculated as described below. ΔA was obtained as an average of three trials.

$$photon\ flux = \frac{mol\ Fe^{2+}}{\Phi \cdot t \cdot f}, where\ mol\ Fe^{2+} = \frac{V \cdot \Delta A}{l \cdot \varepsilon}$$

V = 0.00094 L, the total volume of the solution after addition of phenanthroline buffer

ΔA = 0.3135, the absorbance at λ = 510 nm relative to non-irradiated solution

l = 1.0 cm, the path length of the cuvette

ε = 11,100 L mol^{-1} cm^{-1}, the molar absorptivity at 510 nm

Φ = 1.01, the quantum yield of the ferrioxalate actinometer solution at λ = 436 nm

t = 120 s, the duration of radiation

f = 1 – 10^{-A} = 0.9947, the fraction of light absorbed at λ = 436 nm, when A = 2.275(measured)

photon flux = 2.20 × 10^{-10} einstein/s

Reaction with monochromatic light at λ = 436 nm

To a 1 cm × 0.5 cm quartz cuvette (1.4 mL volume, Starna), $IPrAuCF_3$ (5.2 mg, 8.0 μmol), 4-nitrobenzenediazonium tetrafluoroborate (2.8 mg, 12.0 μmol), $Ru(bpy)_3(PF_6)_2$ (0.7 mg, 0.8 μmol) and dry nitromethane (0.8 mL) were added under a nitrogen

atmosphere. The cuvette was sealed with a cap equipped with septum, degassed for 1 minute via a continuous nitrogen flow, and then, radiated with monochromatic light at λ = 436 nm for 20 minutes. After 20 minutes, the stock solution of internal standard was added to the cuvette and the aliquot (0.5 mL) was taken in order to measure the yield by using ^{19}F NMR. For quantitative analysis, the number of scan was set as 1 to avoid any error caused by relaxation time. The null signal appears at the center of single scan spectrum.

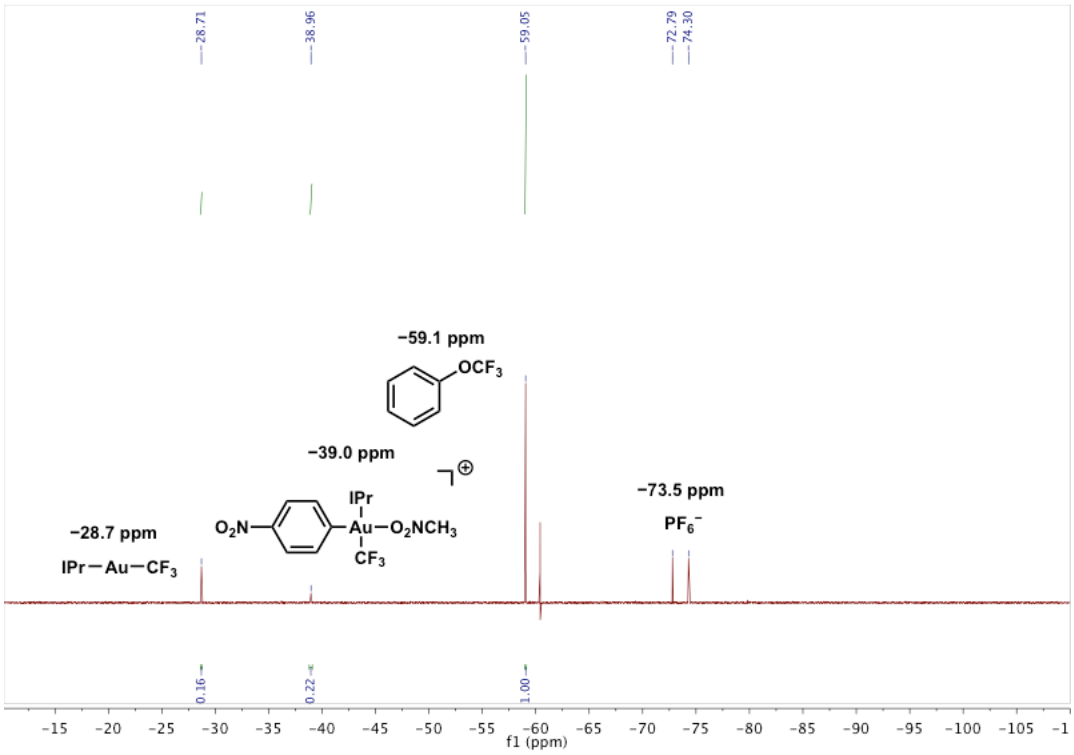

Figure 3.17 ^{19}F NMR spectrum of reaction mixture with monochromatic light at λ = 436 nm, solvent = CH_3NO_2

The overall number of photons radiated during 20 minutes was 0.264 μmol, (1200 × 2.20 × 10^{-10} mol), which corresponds to 3.3 mol%. Quantum yield of the photoredox-catalyzed oxidative arylation was calculated as 6.6. The quenching fraction, $Q = 1 - I/I_0 = 1 - (1 + K_{sv}[ArN_2BF_4])^{-1}$, was calculated as 0.99, where $K_{sv} = 5.11 \times 10^4\ M^{-1}$ and $[ArN_2BF_4]$ = 15 mM. The chain length of the photoredox-catalyzed oxidative arylation was obtained as 6.6. If Ru(III) is not responsible for the oxidation of Au(II) intermeidates

to Au(III) intermediates, the chain length must be the upper limit of the turnover number. The turnover number of 6.0 suggests that Ru(III) is almost not involved for the Au^{II}/Au^{III} redox event of the optimized reaction condition.

Thermal reductive elimination of CH_3NO_2-bound gold(III) complex

The aliquot (0.5 mL) used above in an oven-dried NMR tube was immersed in 40 ^oC oil bath for 5 minutes. The product yield was measured by using ^{19}F NMR. For quantitative analysis, the number of scan was set as 1 to avoid any error caused by relaxation time. Reductive elimination was not observed upon heating with H_2O-bound gold(III) complex as well as acetonitrile-bound gold(III) complex.

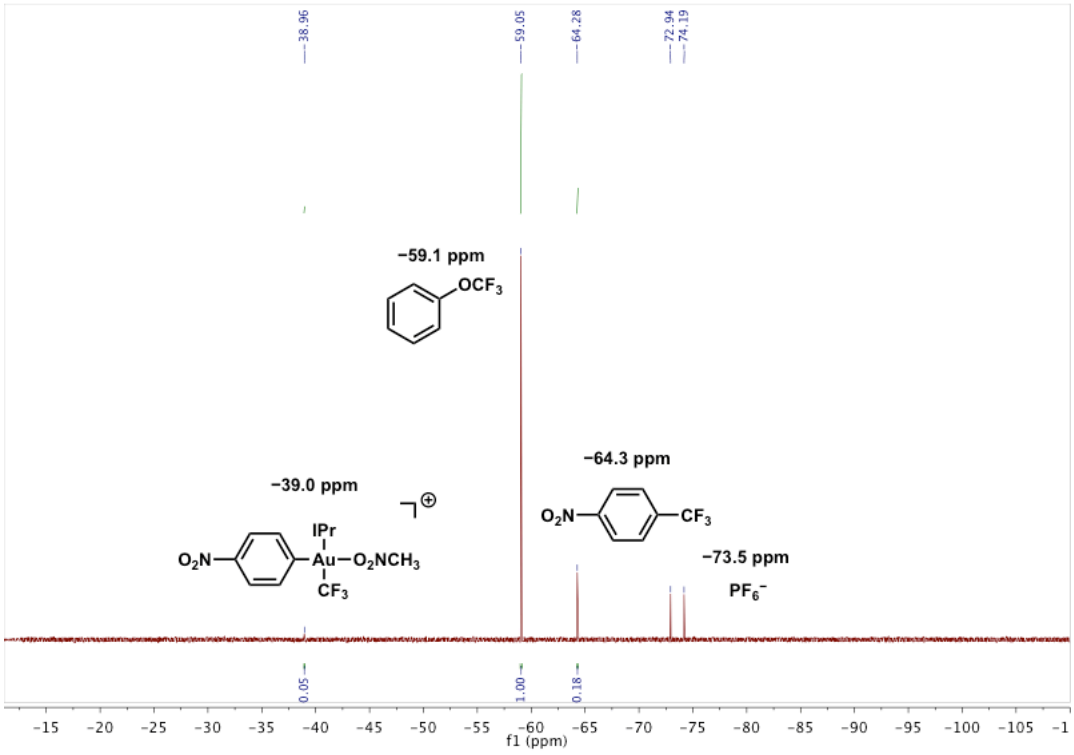

Figure 3.18 ^{19}F NMR spectrum of the aliquot shown above (Figure 3.17) after heating for 5 minutes at 40 ^oC, solvent = CH_3NO_2

3.5.9 Radical trapping experiment

To an oven-dried NMR tube, $IPrAuCF_3$ (5.2 mg, 8.0 μmol), 4-nitrobenzenediazonium tetrafluoroborate (2.8 mg, 12.0 μmol), $Ru(bpy)_3(PF_6)_2$ (0.7 mg, 0.8 μmol), C_6H_6 (44 mg, 560 μmol, 0.05 mL) and dry nitromethane (0.5 mL) under a nitrogen atmosphere. The NMR tube was sealed with a rubber septum, degassed were added three times via freeze-pump-thaw cycles, and backfilled with nitrogen. After then, the reaction mixture was radiated with Blue LED for 5 minutes. The product yield was measured by using ^{19}F NMR. For quantitative analysis, the number of scan was set as 1 to avoid any error caused by relaxation time. The null signal appears at the center of single scan spectrum.

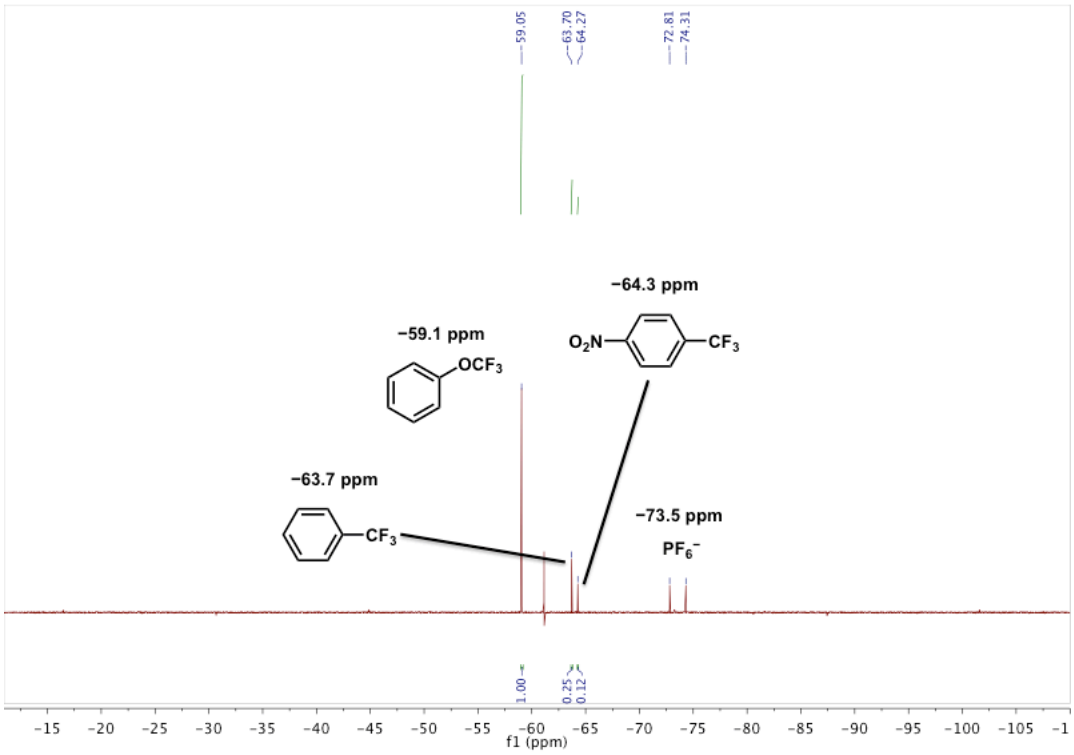

Figure 3.19 ^{19}F NMR spectrum of reaction mixture with 70 equivalents of benzene, solvent = CH_3NO_2

3.5.10 Photoredox-catalyzed gold-mediated C(sp^2)–N coupling reaction

General procedure of substrate preparation

To a solution of IPrAuCl(124 mg, 0.2 mmol, 1 equiv.) in CH_2Cl_2(2 mL) was added AgOTf(77 mg, 0.3 mmol, 1.5 equiv.). The mixture was sonicated for 5 minutes and filtered through a pad of Celite®. The Celite® pad was washed with CH_2Cl_2(2 mL). To the filtrate, was added the lithium amide salt (0.25 mmol, 1.25 equiv.). The mixture was sonicated for 10 minutes and filtered through a pad of basic alumina. The basic alumina pad was washed with CH_2Cl_2(5 mL). The filtrate was concentrated under reduced pressure and then, the product was precipitated out by adding pentane. The lithium salt was prepared as THF adduct by mixing equimolar lithium *tert*-butoxide and the amide, imide, or carbazole in THF. The lithium salt was dried under vacuum for overnight prior to use.

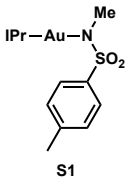

S1

The reaction was run at 0.1 mmol scale. **S1**(61 mg, 0.079 mmol, 79%) was isolated as a colorless solid.

^{1}H NMR (500 MHz, CD_2Cl_2) δ 7.60 (t, *J* = 7.8 Hz, 2H), 7.37 (d, *J* = 7.8 Hz, 4H), 7.24 (s, 2H), 7.14 (d, *J* = 8.1 Hz, 2H) 6.98 (d, *J* = 7.8 Hz, 2H), 2.56 (hept, *J* = 6.9 Hz, 4H), 2.35 (s, 3H), 2.33 (s, 3H), 1.32 (d, *J* = 6.9 Hz, 12H), 1.23 (d, *J* = 6.9 Hz, 12H).

^{13}C NMR (126 MHz, CD_2Cl_2) δ 175.29, 146.27, 140.72, 140.13, 130.86, 128.95, 127.09, 124.50, 123.65, 36.59, 29.20, 24.43, 24.16, 21.42.

Elem. Analysis found C 54.48 %, H 6.08 %, N 5.29 %, S 3.96% $C_{35}H_{46}AuN_3O_2S$ requires C 54.61 %, H 6.02 %, N 5.46 %, S 4.16%.

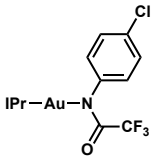

S2

S2(104 mg, 0.129 mmol, 64%) was isolated as a colorless solid.

^{1}H NMR (500 MHz, CD_2Cl_2) δ 7.56 (t, *J* = 7.8 Hz, 2H), 7.31 (d, *J* = 7.8 Hz, 4H), 7.27 (s, 2H), 6.94 (d, *J* = 8.7 Hz, 2H), 6.67 (d, *J* = 8.8 Hz, 2H), 2.49 (hept, *J* = 6.9 Hz, 4H), 1.20 (d, *J* = 6.9, 12H).

^{13}C NMR (176 MHz, CD_2Cl_2) δ 173.85, 146.12, 146.05, 134.42, 130.95, 128.51, 128.20, 127.02, 124.52, 123.81, 29.18, 24.35, 24.01. (low intensity $COCF_3$ resonance not detected)

^{19}F NMR (376 MHz, CD_2Cl_2) δ −72.28(s).

m/z HRMS (ESI positive) found 808.2577 $C_{35}H_{41}O_1N_3AuClF_3^+$ requires 808.2550.

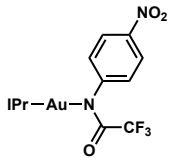

S3

S3(134 mg, 0.163 mmol, 82%) was isolated as a bright yellow solid.

^{1}H NMR (500 MHz, CD_2Cl_2) δ 7.82 (d, *J* = 9.1 Hz, 2H), 7.59 (t, *J* = 7.8 Hz, 2H), 7.33 (d, *J* = 7.8 Hz, 4H), 7.30 (s, 2H), 6.95 (d, *J* = 9.0 Hz, 2H), 2.50 (hept, *J* = 7.1 Hz, 4H), 1.21 (app. dd, *J* = 6.8, 2.4 Hz, 24H).

^{13}C NMR (126 MHz, CD_2Cl_2) δ 173.08, 154.33, 146.12, 143.33, 134.30, 131.04, 125.83, 124.58, 123.94, 123.92, 29.17, 24.33, 24.06. (low intensity $COCF_3$ resonance not detected)

^{19}F NMR (376 MHz, CD_2Cl_2) δ −72.41(s).

m/z HRMS (ESI positive) found 819.2820 $C_{35}H_{41}O_3N_4AuF_3^+$ requires 819.2791.

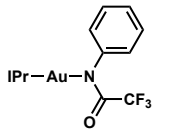

S4

S4(133 mg, 0.172 mmol, 86%) was isolated as a colorless solid.

^{1}H NMR (500 MHz, CD_2Cl_2) δ 7.54 (t, *J* = 7.8 Hz, 2H), 7.30 (d, *J* = 7.8 Hz, 4H), 7.26 (s, 2H), 6.97 (t, *J* = 7.7 Hz, 2H), 6.88 (t, *J* = 7.3 Hz, 1H), 6.68 (d, *J* = 7.8 Hz, 2H), 2.50 (hept, *J* = 7.3 Hz, 4H), 1.19 (app. dd, *J* = 6.9, 3.2 Hz, 24H).

^{13}C NMR (151 MHz, CD_2Cl_2) δ 174.27, 147.34, 146.13, 134.50, 130.92, 128.32, 125.76, 124.51, 123.78, 123.68, 29.19, 24.38, 23.97. (low intensity $COCF_3$ resonance not detected)

^{19}F NMR (376 MHz, CD_2Cl_2) δ −72.07(s).

m/z HRMS (ESI positive) found 774.2943 $C_{35}H_{42}O_1N_3AuF_3^+$ requires 774.2940.

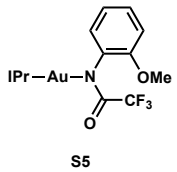

S5

S5(131 mg, 0.163 mmol, 82%) was isolated as a colorless sold.

^{1}H NMR (500 MHz, CD_2Cl_2) δ 7.49 (t, *J* = 7.8 Hz, 2H), 7.25 (d, *J* = 7.8 Hz, 4H), 7.22 (s, 2H), 6.94 (td, *J* = 8.6, 1.7 Hz, 1H), 6.66 (d, *J* = 8.2 Hz, 1H), 6.62 (td, *J* = 7.6, 0.8 Hz, 1H), 6.43 (dd, *J* = 7.5, 1.6 Hz, 1H), 3.44 (s, 3H), 2.45 (hept, *J* = 6.9 Hz, 4H), 1.18 (d, *J* = 7.3 Hz, 12H), 1.16 (d, *J* = 7.4 Hz, 12H).

^{13}C NMR (176 MHz, CD_2Cl_2) δ 174.25, 153.93, 146.10, 136.09, 134.43, 130.78, 127.33, 125.44, 124.36, 123.67, 120.62, 112.12, 56.00, 29.12, 24.27, 23.91. (low intensity $COCF_3$ resonance not detected)

^{19}F NMR (376 MHz, CD_2Cl_2) δ −72.29(s).

m/z HRMS (ESI positive) found 804.3065 $C_{36}H_{44}O_2N_3AuF_3^+$ requires 804.3046.

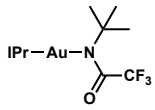

S6

The reaction was run at 0.1 mmol scale. AgOAc(4 equiv.) was used instead of AgOTf(1.5 equiv.) 10 equivalents of lithium salt were used. **S6**(38.2 mg, 0.051 mmol, 51%) was isolated as a colorless solid

^{1}H NMR (500 MHz, CD_2Cl_2) δ 7.50 (t, *J* = 7.8 Hz, 2H), 7.31 (d, *J* = 7.8 Hz, 4H), 7.26 (s, 2H), 2.56 (hept, *J* = 6.9 Hz, 4H), 1.31 (d, *J* = 6.9 Hz, 12H), 1.21 (d, *J* = 7.0 Hz, 12H), 0.92 (s, 9H).

^{13}C NMR (151 MHz, CD_2Cl_2) δ 176.60, 146.03, 134.79, 130.76, 56.94, 30.16, 29.20, 24.55, 23.93. (low intensity $COCF_3$ resonance not detected)

^{19}F NMR (376 MHz, CD_2Cl_2) δ −70.57(s).

m/z HRMS (ESI positive) found 754.3275 $C_{33}H_{46}O_1N_3AuF_3^+$ requires 754.3253.

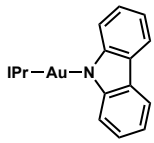

S7

The reaction was run at 0.1 mmol scale. The precipitate was washed with minimal amount of diethyl ether to remove residual carbazole. **S7**(54.1 mg, 0.072 mmol, 72%) was isolated as a colorless solid.

^{1}H NMR (500MHz, CD_2Cl_2) δ 7.87 (d, *J* = 7.7 Hz, 2H), 7.64 (t, *J* = 7.8 Hz, 2H), 7.43 (d, *J* = 7.9 Hz, 4H), 7.35 (s, 2H), 7.06 – 6.94 (m, 2H), 6.85 (t, *J* = 7.3 Hz, 2H), 6.71 (d, *J* = 8.1 Hz, 2H), 2.71 (hept, *J* = 7.1 Hz, 4H), 1.37 (d, *J* = 6.9 Hz, 12H), 1.28 (d, *J* = 6.9 Hz, 12H).

^{13}C NMR (151 MHz, CD_2Cl_2) δ 179.09, 149.78, 146.58, 134.76, 131.04, 124.65, 123.88, 123.78, 123.72, 119.48, 116.00, 113.85, 29.40, 24.58, 24.32.

m/z HRMS (ESI positive) found 774.3090 $C_{39}H_{44}N_3AuNa^+$ requires 774.3093.

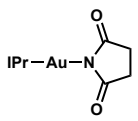

5

5(134.3 mg, 0.196 mmol, 98%) was isolated as a colorless solid.

^{1}H NMR (500MHz, CD_2Cl_2) δ 7.55 (t, *J* = 7.8 Hz, 2H), 7.34 (d, *J* = 7.8 Hz, 4H), 7.23 (s, 2H), 2.57 (hept, *J* = 6.9 Hz, 4H), 2.27 (s, 4H), 1.36 (d, *J* = 6.8 Hz, 12H), 1.23 (d, *J* = 6.9 Hz, 12H).

^{13}C NMR (176 MHz, CD_2Cl_2) δ 187.68, 176.99, 146.36, 134.50, 130.89, 124.52, 123.79, 31.75, 29.28, 24.50, 24.14.

m/z HRMS (ESI positive) found 684.2858 $C_{31}H_{41}O_2N_3Au^+$ requires 684.2859.

General procedure of photoredox-catalyzed gold-mediated C(sp^2)−N coupling reaction

To an oven-dried NMR tube, Au(I)-amide substrate(8.0 μmol), 4-nitrophenyl diazonium tetrafluoroborate (2.8 mg, 12.0 μmol), $Ru(bpy)_3(PF_6)_2$ (0.7 mg, 0.8 μmol) and dry nitromethane (0.5 mL) were added under a nitrogen atmosphere. The NMR tube was sealed with a rubber septum, degassed three times via freeze-pump-thaw cycles, and backfilled with nitrogen. After then, the reaction mixture was radiated with Blue LEDs for 3 minutes.

Summary of C(sp^2)−N coupling optimization

In the initial study, **S1** was tested in consideration of direct protonation by nitromethane, but N-H amide was observed as the only sulfonamide product. Gold(I) aryl trifluoroacetamides were studied to avoid any H-atom transfer while maintaining similar pKa with sulfonamide, and **S2**-**S5** provided C(sp^2)−N coupling product in low yield(20-30%).[14] We synthesized **S6** to suppress the release of N-centered radical from the neutral Au(II) intermediate, but no C(sp^2)−N coupling product was obtained with **S6**. This result implies that the reaction mechanism of C(sp^2)−N coupling is not identical with that of C(sp^2)−CF_3 coupling. We observed background reaction between **S7** and aryldiazonium salts and proposed that this process depends on the electronics of gold-bound nitrogen atom. By decreasing the electron density on gold-bound nitrogen atom with electron withdrawing groups, C(sp^2)−N coupling yield was optimized up to similar level of C(sp^2)−CF_3 coupling.

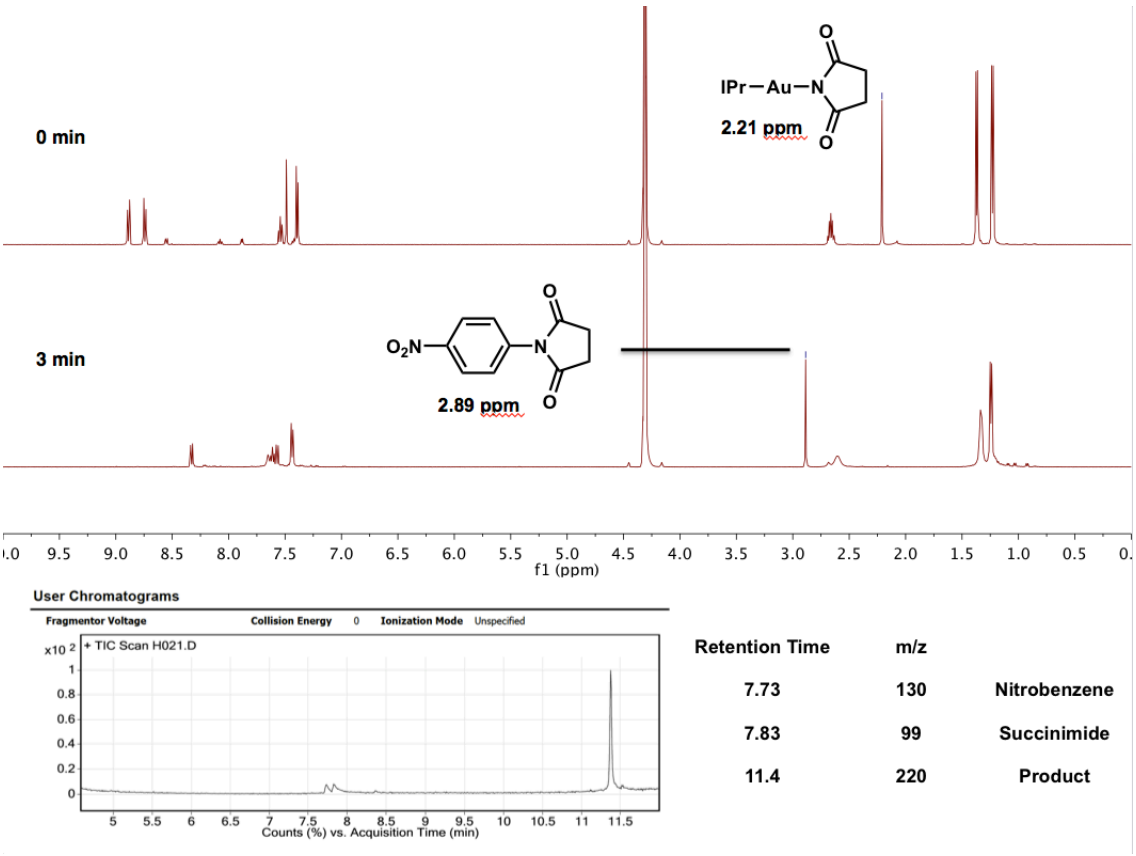

Figure 3.20 ^{1}H NMR spectra and GC-MS trace of C(sp^2)−N coupling reaction mixture, solvent = CD_3NO_2

3.5.11 H_2O-bound gold(III)−succinimide complex, 7

To an oven-dried NMR tube, **5** (5.5 mg, 8.0 μmol), 4-nitrobenzenediazonium tetrafluoroborate (2.8 mg, 12.0 μmol), $Ru(bpy)_3(PF_6)_2$ (0.7 mg, 0.8 μmol) and solvent mixture (CH_3CN:H_2O = 96:4 v/v, 0.5 mL) were added under a nitrogen atmosphere. The NMR tube was sealed with a rubber septum, degassed three times via freeze-pump-thaw cycles, and backfilled with nitrogen. After then, the reaction mixture was radiated with Blue LED for 3 minutes. Crystals of **7** suitable for X-ray diffraction were grown by sequential vapor diffusion of CH_2Cl_2 and layer diffusion of pentane to crude mixture at –20 ^{o}C. Pentane was layered onto the mixture after photoredox catalysts precipitated out by vapor diffusion of CH_2Cl_2.

3.5.12 References

(1) Williams, D. B. G.; Lawton, M. Drying of Organic Solvents: Quantitative Evaluation of the Efficiency of Several Desiccants. *J. Org. Chem.* **2010**, *75*, 8351−8354.

(2) Ischay, M. A.; Lu, Z.; Yoon, T. P. [2+2] Cycloadditions by Oxidative Visible Light Photocatalysis. *J. Am. Chem. Soc.* **2010**, *132*, 8572−8574.

(3) Slinker, J. D.; Gorodetsky, A. A.; Lowry, M. S.; Wang, J.; Parker, S.; Rohl, R.; Bernhard, S.; Malliaras, G. G. Efficient Yellow Electroluminescence from a Single Layer of a Cyclometalated Iridium Complex. *J. Am. Chem. Soc.* **2004**, *126*, 2763−2767.

(4) Lowry, M. S.; Goldsmith, J. I.; Slinker, J. D.; Rohl, R.; Pascal, R. A.; Malliaras, G. G.; Bernhard, S. Single-Layer Electroluminescent Devices and Photoinduced Hydrogen Production from an Ionic Iridium(III) Complex. *Chem. Mater.* **2005**, *17*, 5712−5719.

(5) Schultz, D. M.; Sawicki, J. W.; Yoon, T. P. An improved procedure for the preparation of $Ru(bpz)_3(PF_6)_2$ via a high-yielding synthesis of 2,2'-bipyrazine. *Beilstein J. Org. Chem.* **2015**, *11*, 61−65.

(6) (a) Kotani, H.; Ohkubo, K.; Fukuzumi, S. Photocatalytic Oxygenation of Anthracenes and Olefins with Dioxygen via Selective Radical Coupling Using 9-Mesityl-10-methylacridinium Ion as an Effective Electron-Transfer Photocatalyst. *J. Am. Chem. Soc*. **2004**, *126*, 15999−16006.

(b) Hamilton, D. S.; Nicewicz, D. A. Direct Catalytic Anti-Markovnikov Hydroetherification of Alkenols. *J. Am. Chem. Soc.* **2012**, *134*, 18577−18580.

(c) Wilger, D. J.; Gesmundoa, N. J.; Nicewicz, D. A. Catalytic hydrotrifluoromethylation of styrenes and unactivated aliphatic alkenes via an organic photoredox system. *Chem. Sci.* **2013**, *4*, 3160−3165.

(7) (a) Kim, S.; Rojas-Martin, J.; Toste, F. D. Visible light-mediated gold-catalysed carbon(sp^2)–carbon(sp) cross-coupling. *Chem. Sci.* **2016**, *7*, 85−88.

(b) Avila, C. M.; Patel, J. S.; Reddi, Y.; Saito, M.; Nelson, H. M.; Shunatona, H. P. Sigman, M. S.; Sunoj, R. B.; Toste, F. D. Enantioselective Heck–Matsuda Arylations through Chiral Anion Phase-Transfer of Aryl Diazonium Salts. *Angew. Chem. Int. Ed.* **2017**, *56*, 5806−5811.

(8) Phipps, R. J.; Gaunt, M. J. A Meta-Selective Copper-Catalyzed C–H Bond Arylation. *Science* **2009**, *323*, 1593−1597.

(9) Kobeissi, M.; Yazbeck, O.; Chreim, Y. A convenient one-pot synthesis of polysubstituted pyrroles from N-protected succinimides. *Tet. Lett.* **2014**, *55*, 2523−2526.

(10) Collado, A.; Gómez-Suárez, A.; Martin, A. R.; Slawina, A. M. Z.; Nolan, S. P. Straightforward synthesis of [Au(NHC)X] (NHC = N-heterocyclic carbene, X = Cl, Br, I) complexes. *Chem. Commun*. **2013**, *49*, 5541−5543.

(11) Mankad, N. P.; Toste, F. D. C(sp^3)–F reductive elimination from alkylgold(III) fluoride complexes. *Chem. Sci.* **2012**, *3*, 72−76.

(12) Blaya, M.; Bautista, D.; Gil-Rubio, J.; Vicente, J. Synthesis of Au(I) Trifluoromethyl Complexes. Oxidation to Au(III) and Reductive Elimination of Halotrifluoromethanes. *Organometallics* **2014**, *33*, 6358−6368.

(13) Cismesia, M. A.; Yoon, T. P. Characterizing chain processes in visible light photoredox catalysis. *Chem. Sci.* **2015**, *6*, 5426−5434.

(14) Augurusa, A.; Mehta, M.; Perez, M.; Zhu, J.; Stephan, D. W. Catalytic reduction of amides to amines by electrophilic phosphonium cations via FLP hydrosilylation. *Chem. Commun.* **2016**, *52*, 12195−12198.

3.5.13 NMR Spectra

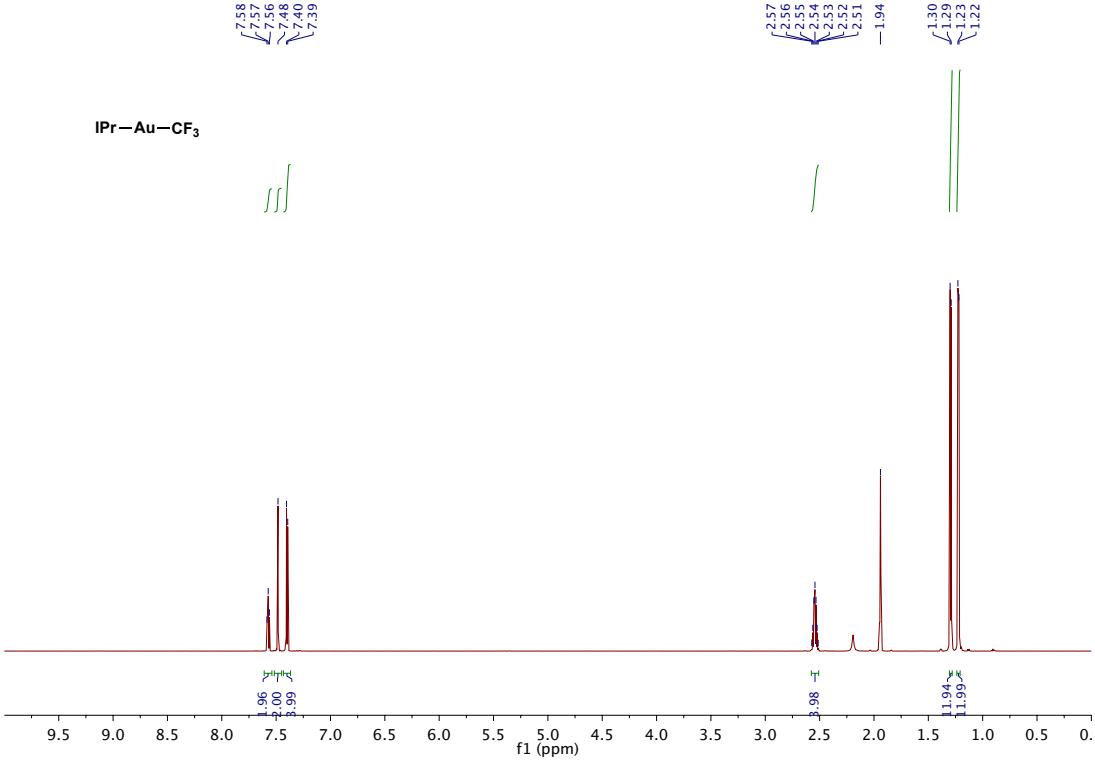

Figure 3.21 . ^{1}H NMR spectrum of **1**

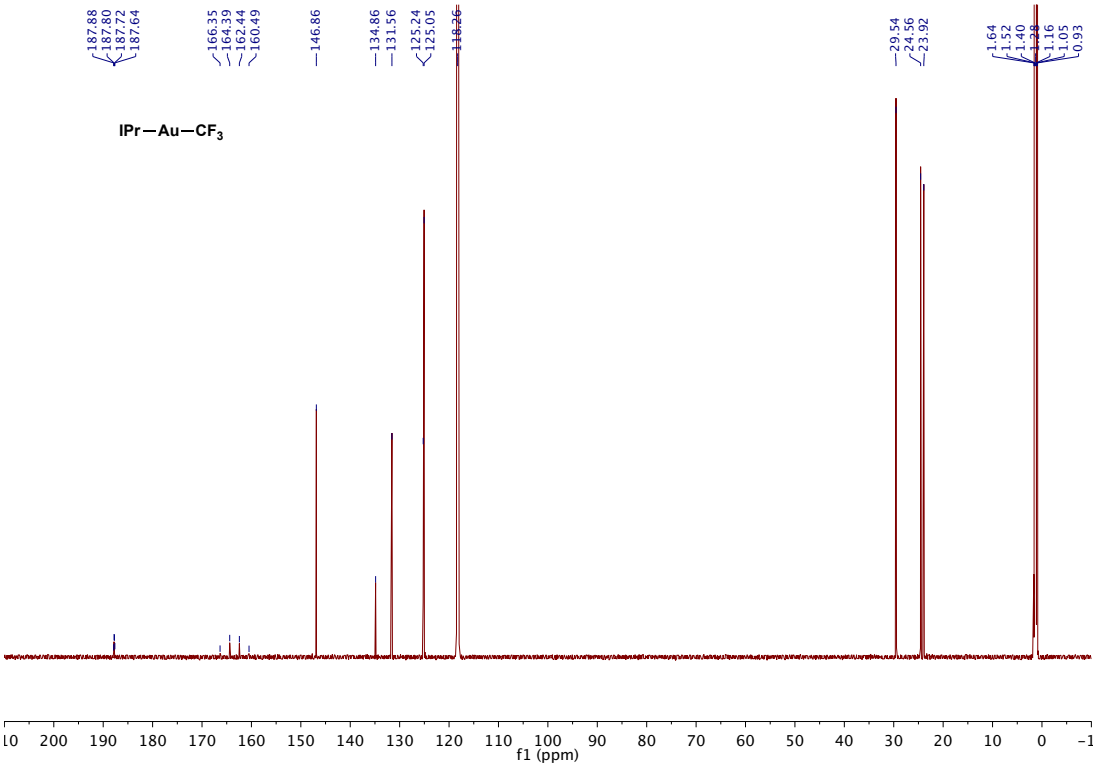

Figure 3.22 ^{13}C NMR spectrum of **1**

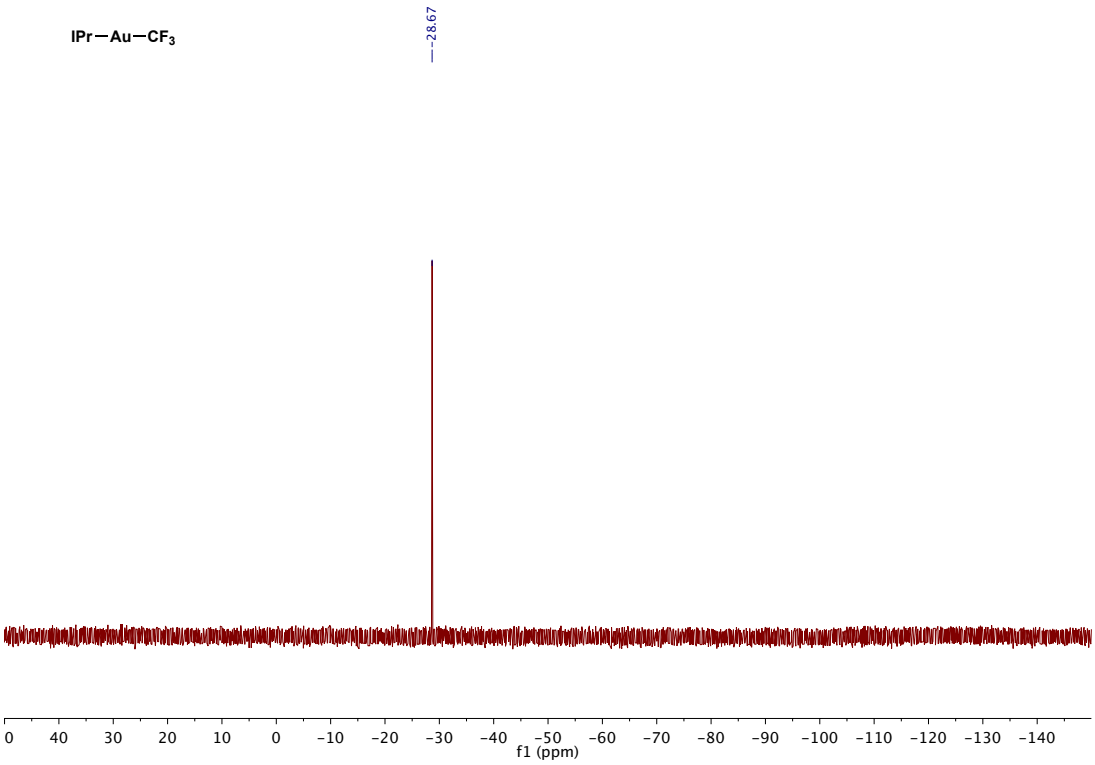

Figure 3.23 ^{19}F NMR spectrum of **1**

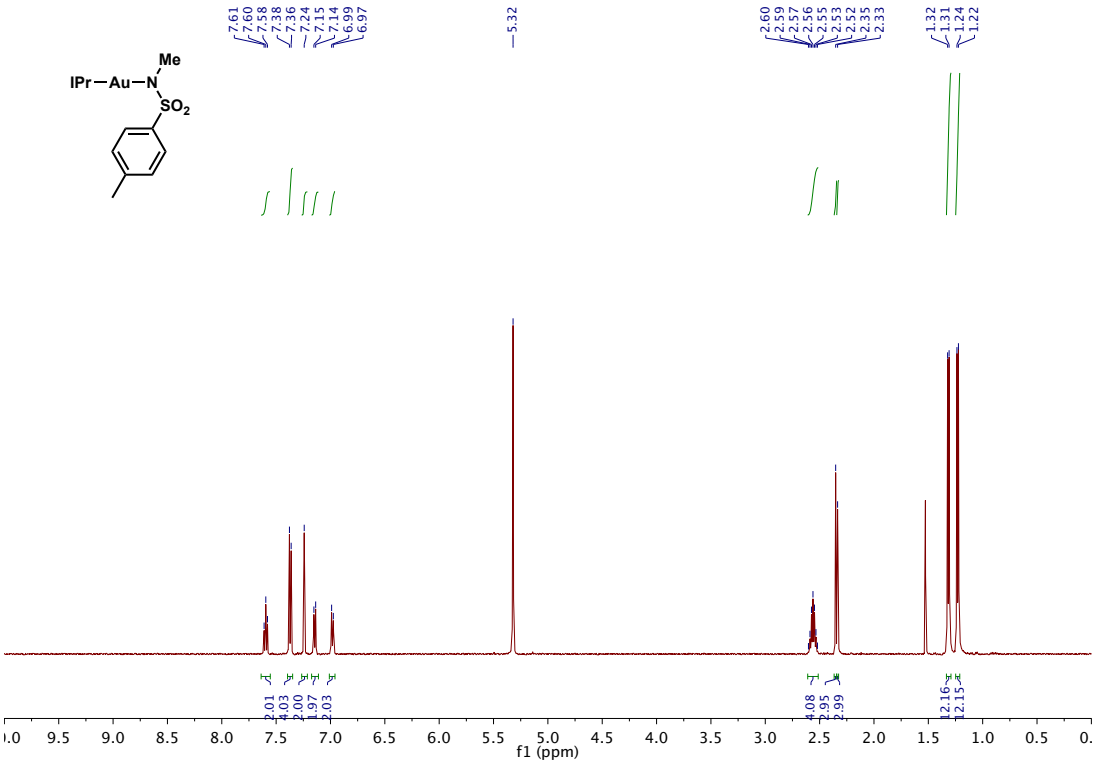

Figure 3.24 ^{1}H NMR spectrum of **S1**

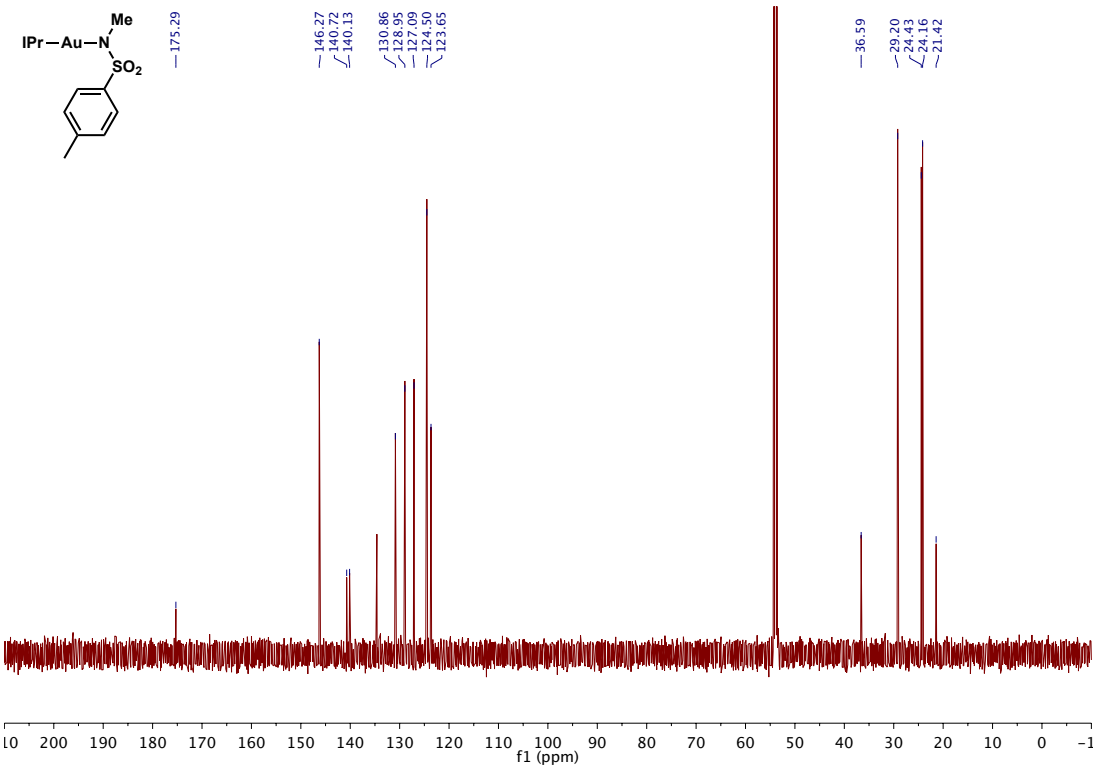

Figure 3.25 ^{13}C NMR spectrum of **S1**

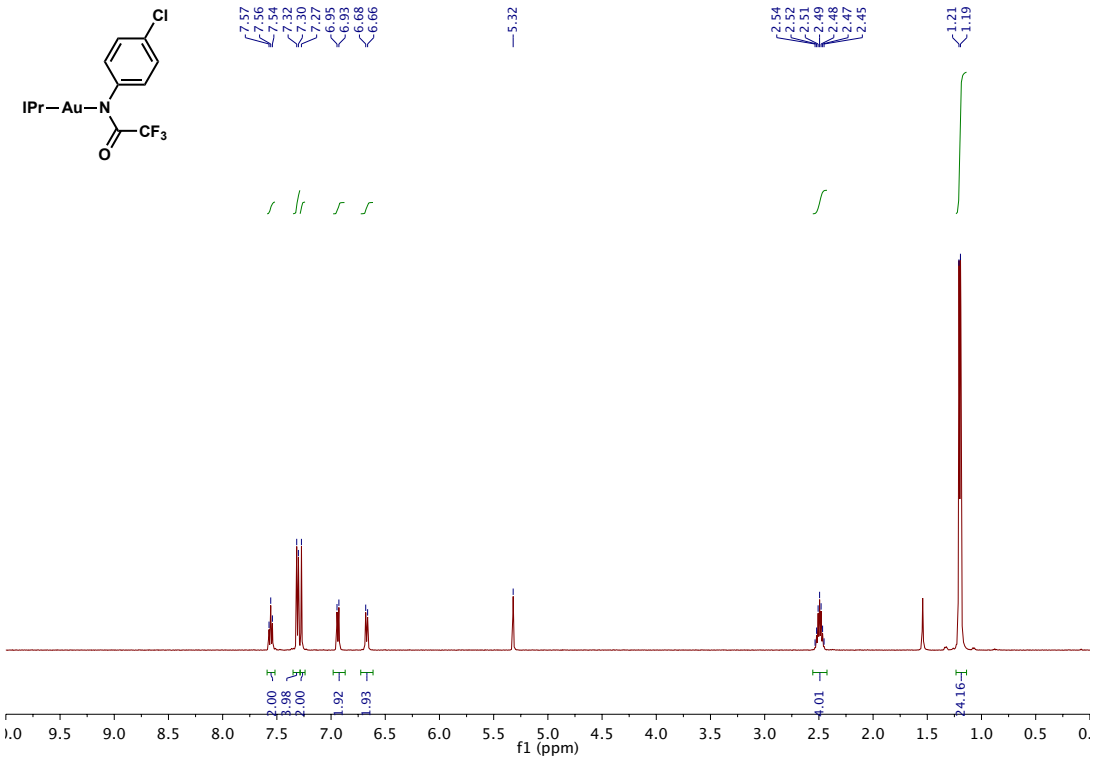

Figure 3.26 ^{1}H NMR spectrum of **S2**

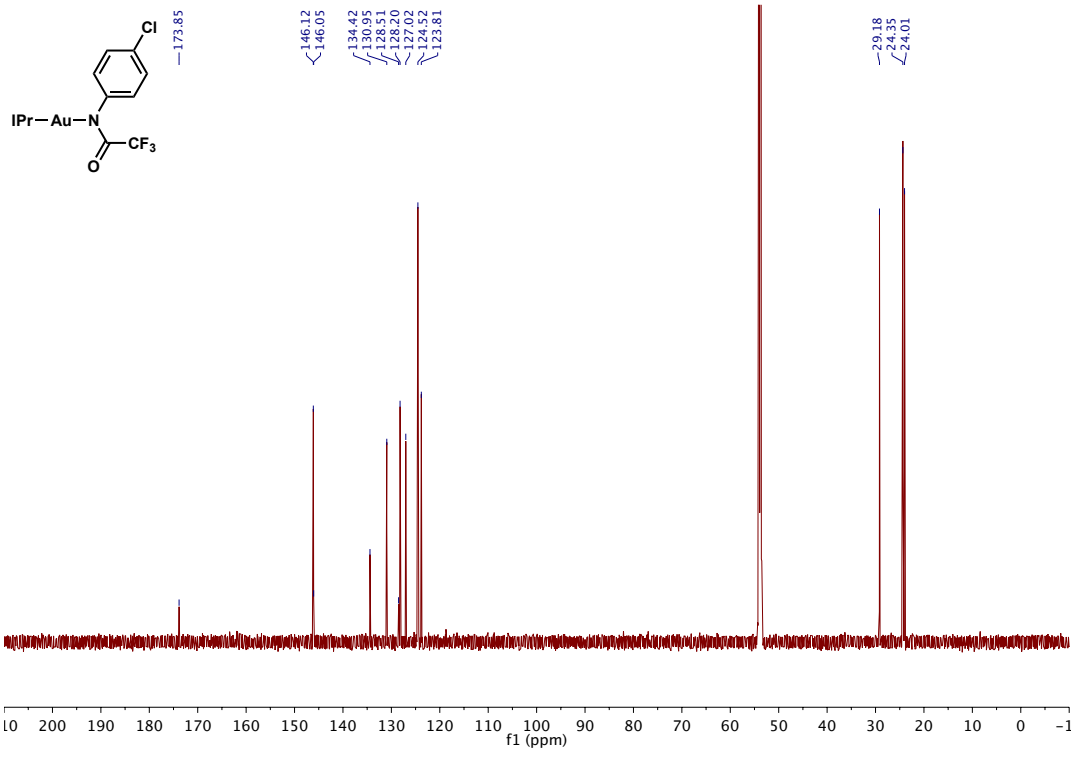

Figure 3.27 ^{13}C NMR spectrum of **S2**

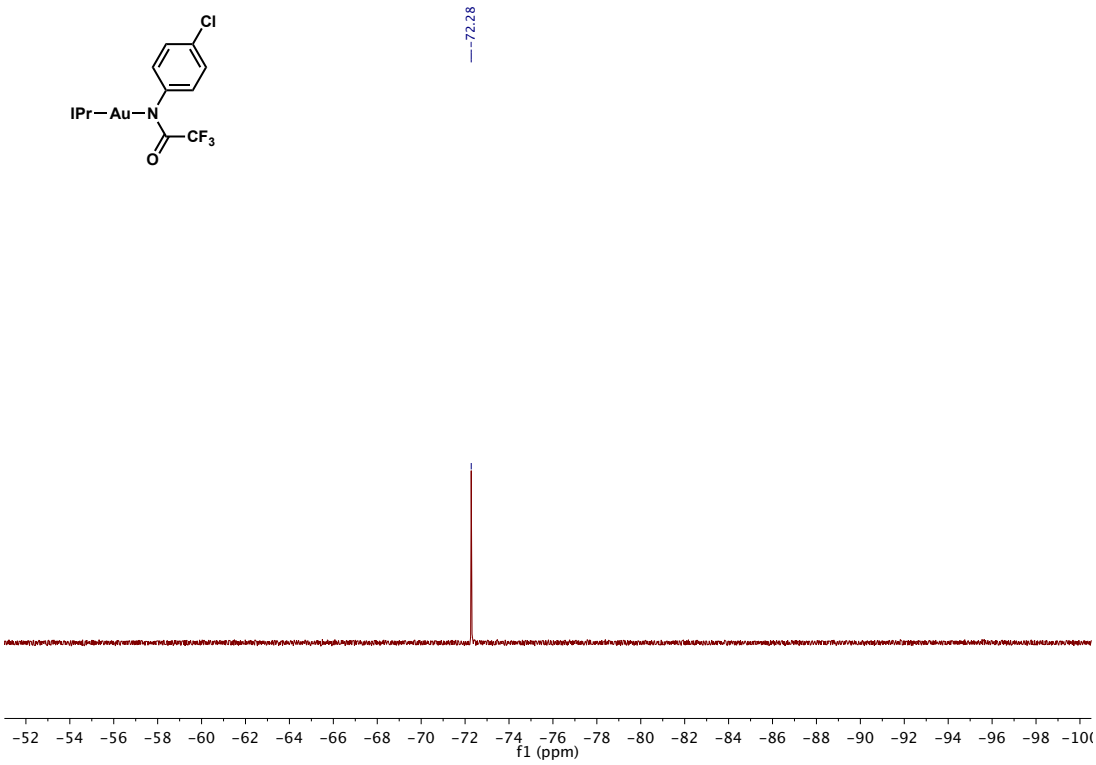

Figure 3.28 ^{19}F NMR spectrum of **S2**

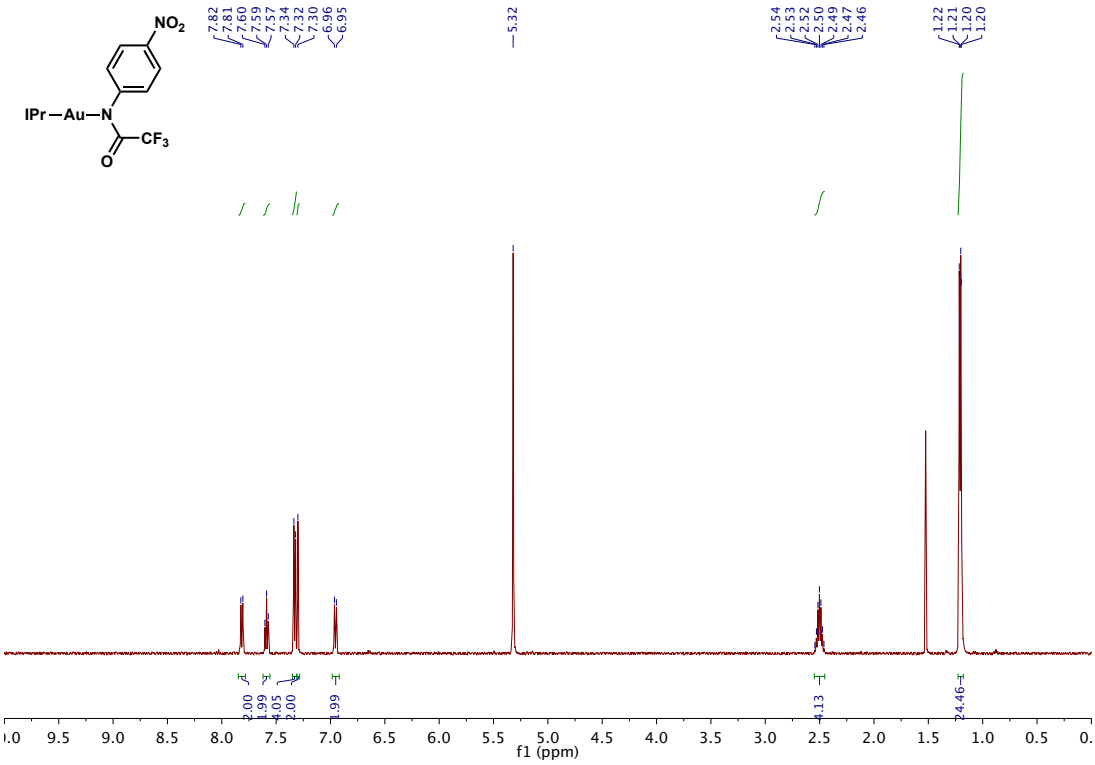

Figure 3.29 ^{1}H NMR spectrum of **S3**

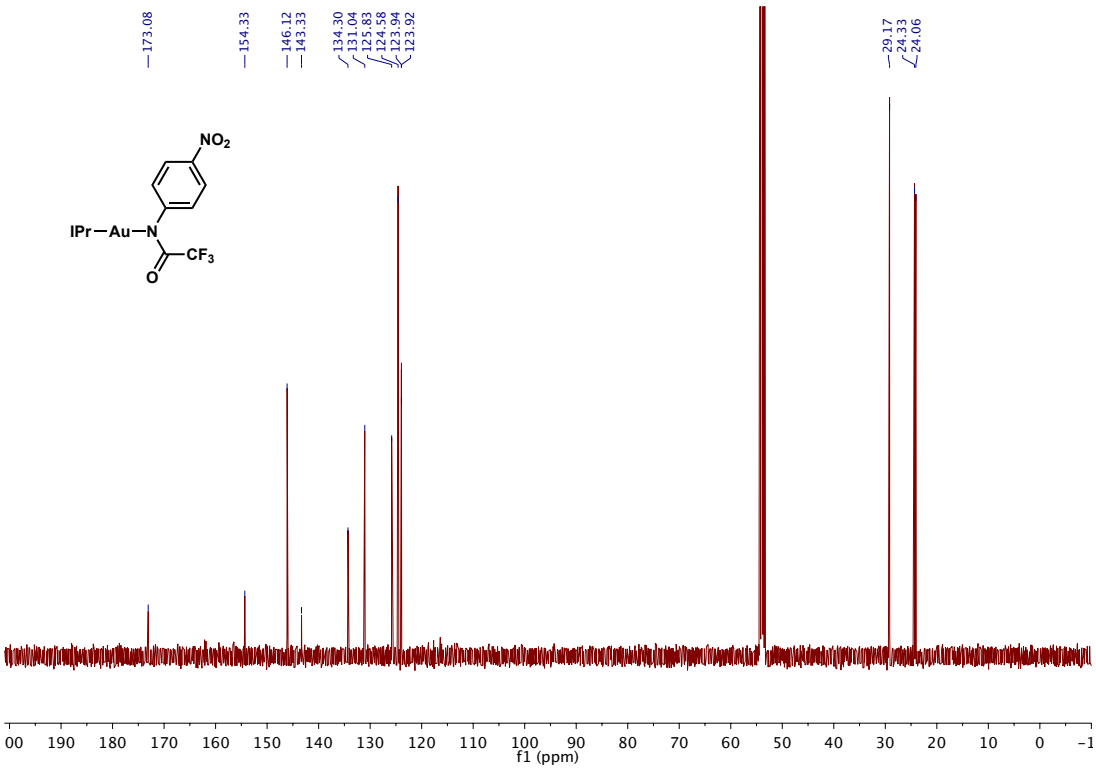

Figure 3.30 ^{13}C NMR spectrum of **S3**

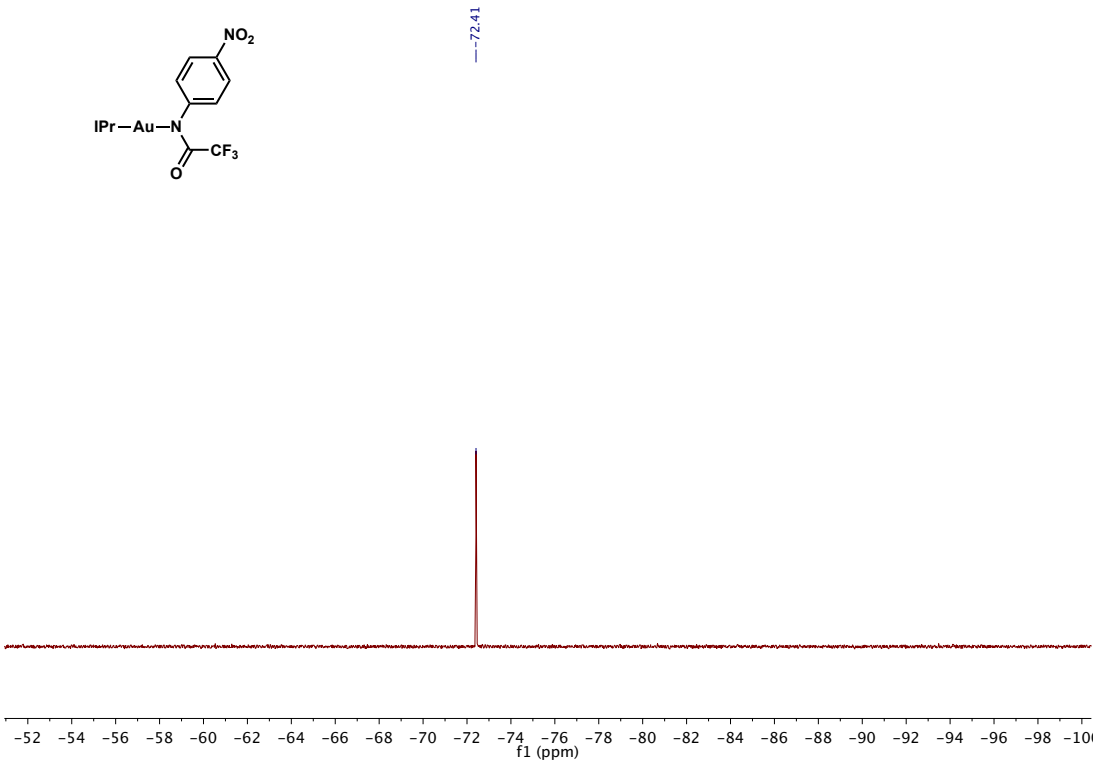

Figure 3.31 ^{19}F NMR spectrum of **S3**

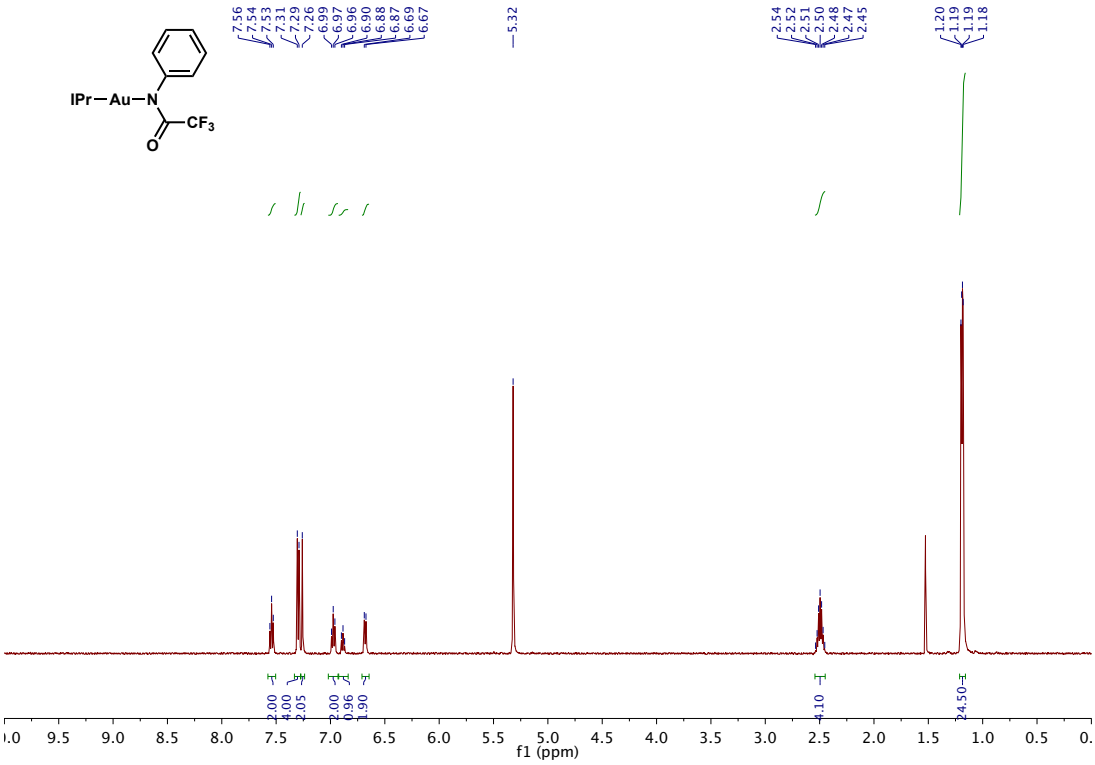

Figure 3.32 ^{1}H NMR spectrum of **S4**

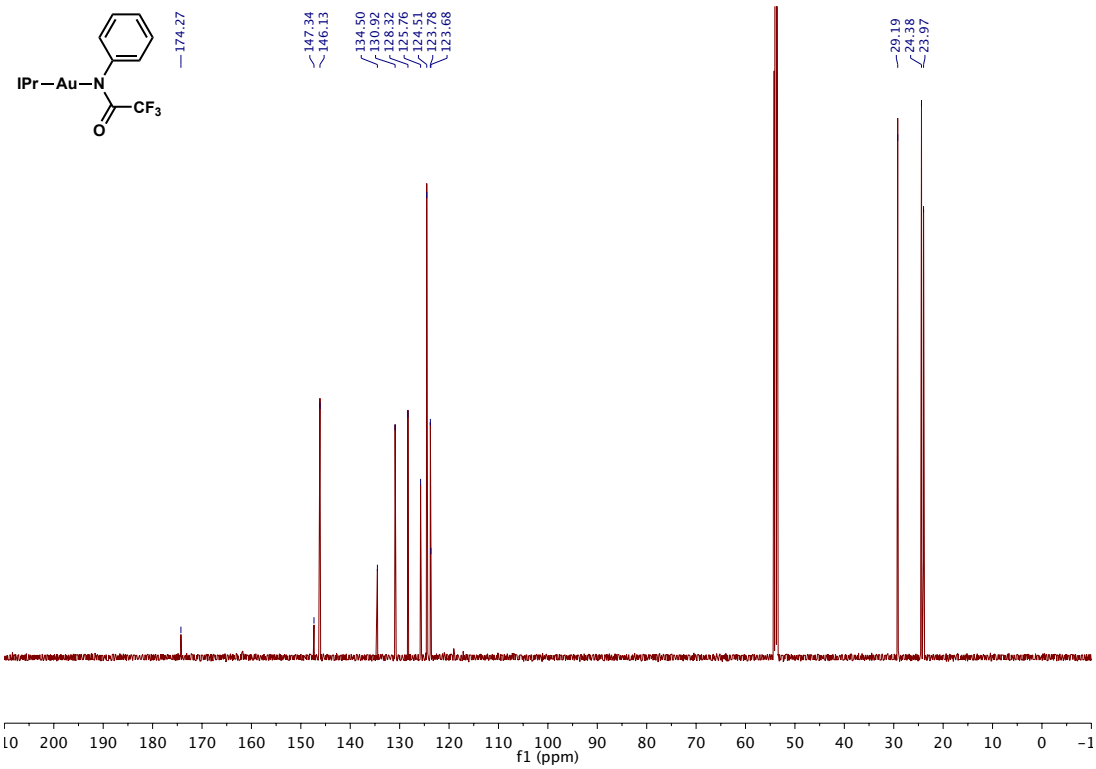

Figure 3.33 ^{13}C NMR spectrum of **S4**

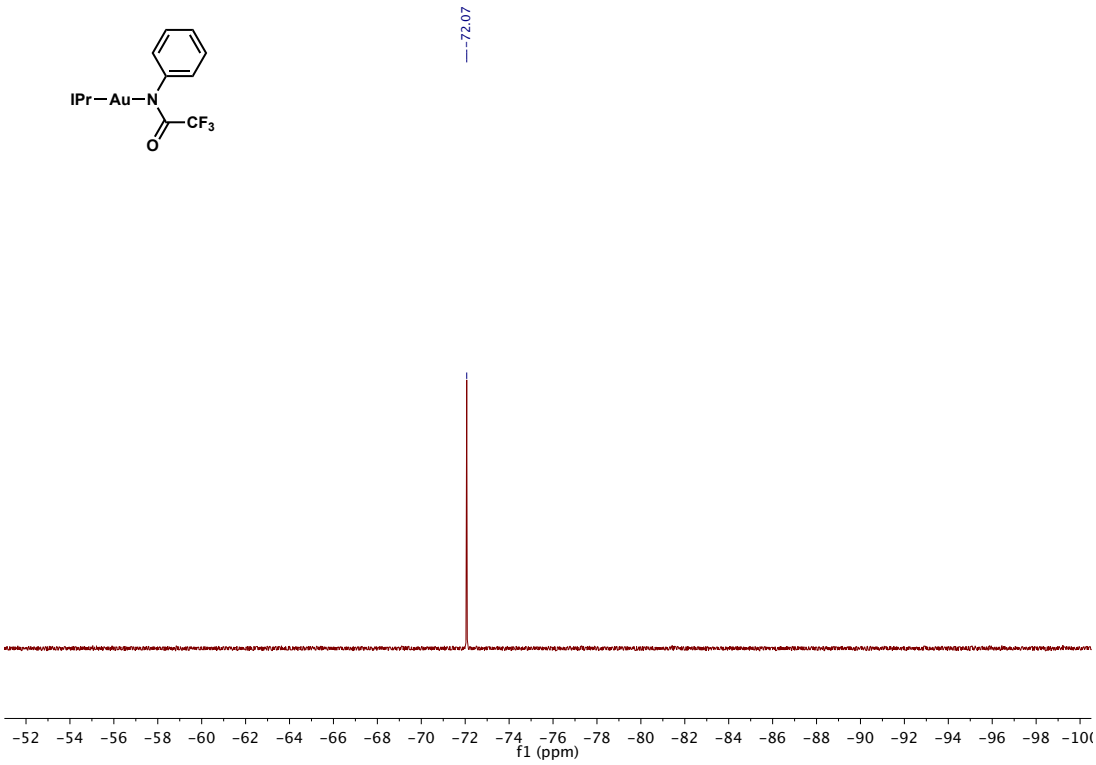

Figure 3.34 ^{19}F NMR spectrum of **S4**

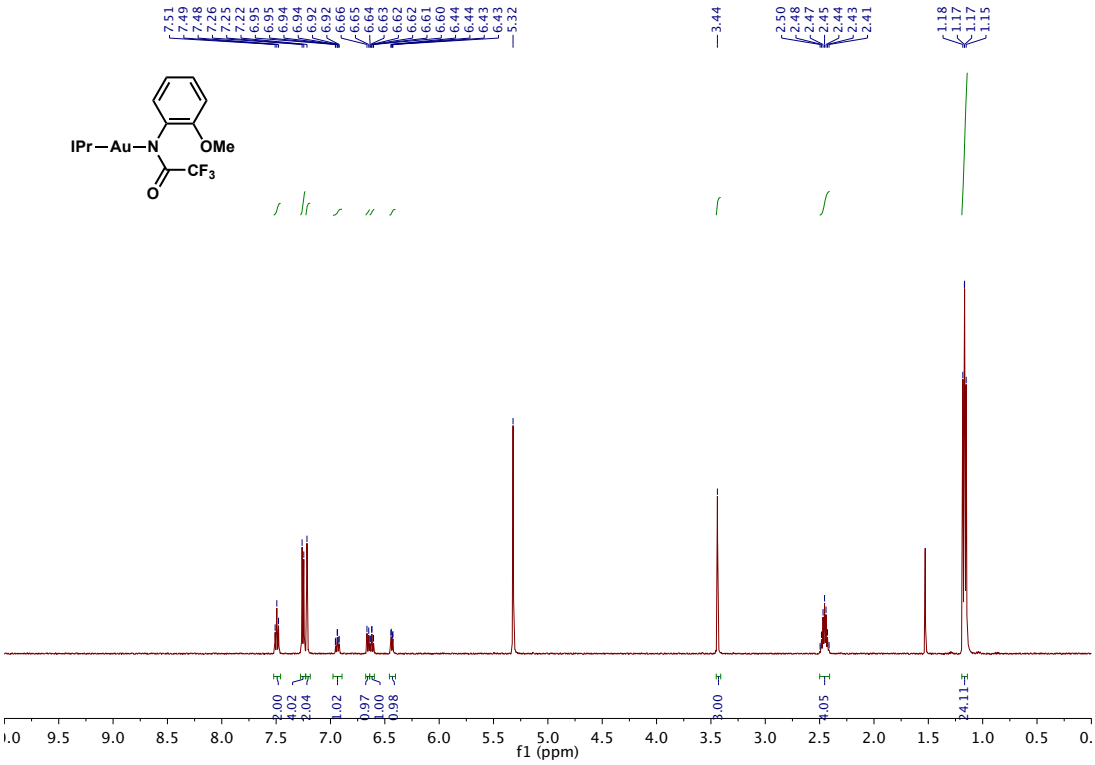

Figure 3.35 ^{1}H NMR spectrum of **S5**

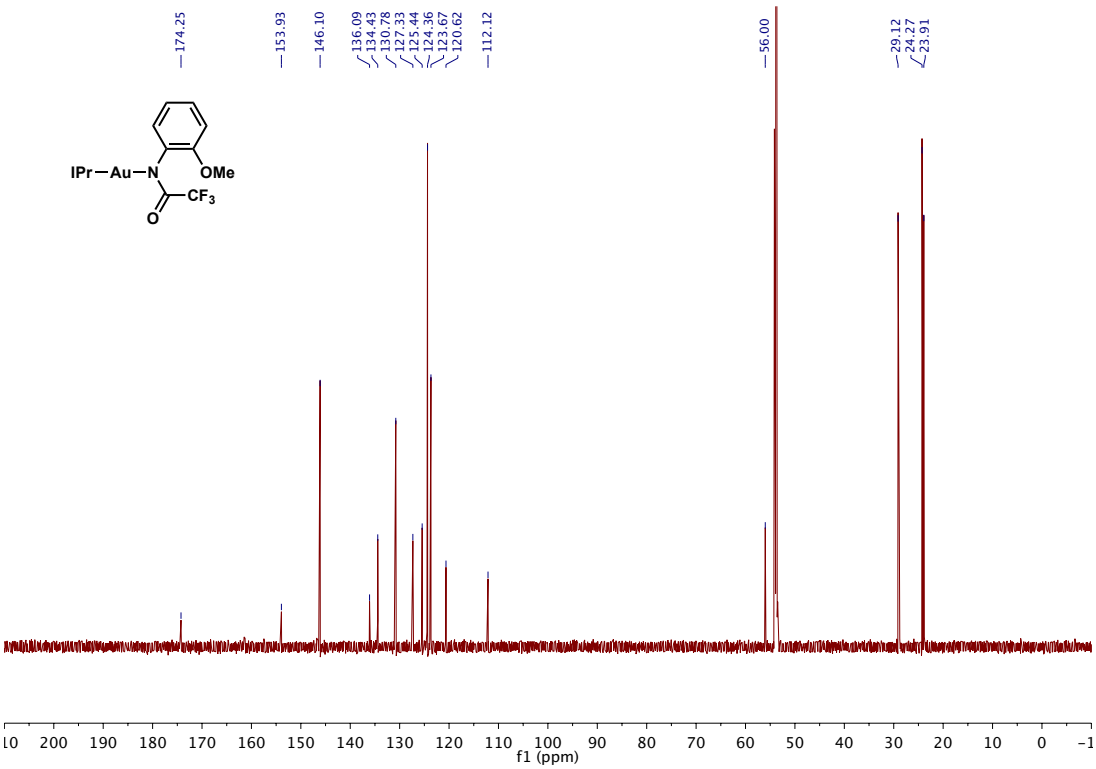

Figure 3.36 ^{13}C NMR spectrum of **S5**

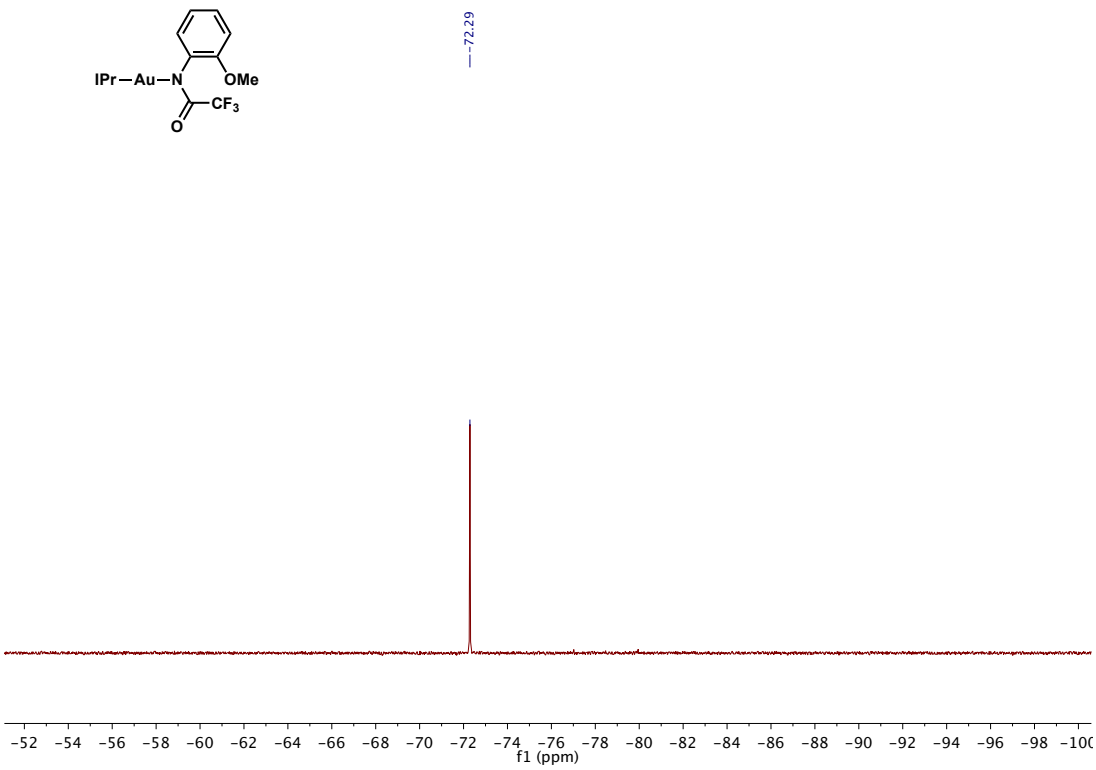

Figure 3.37 ^{19}F NMR spectrum of **S5**

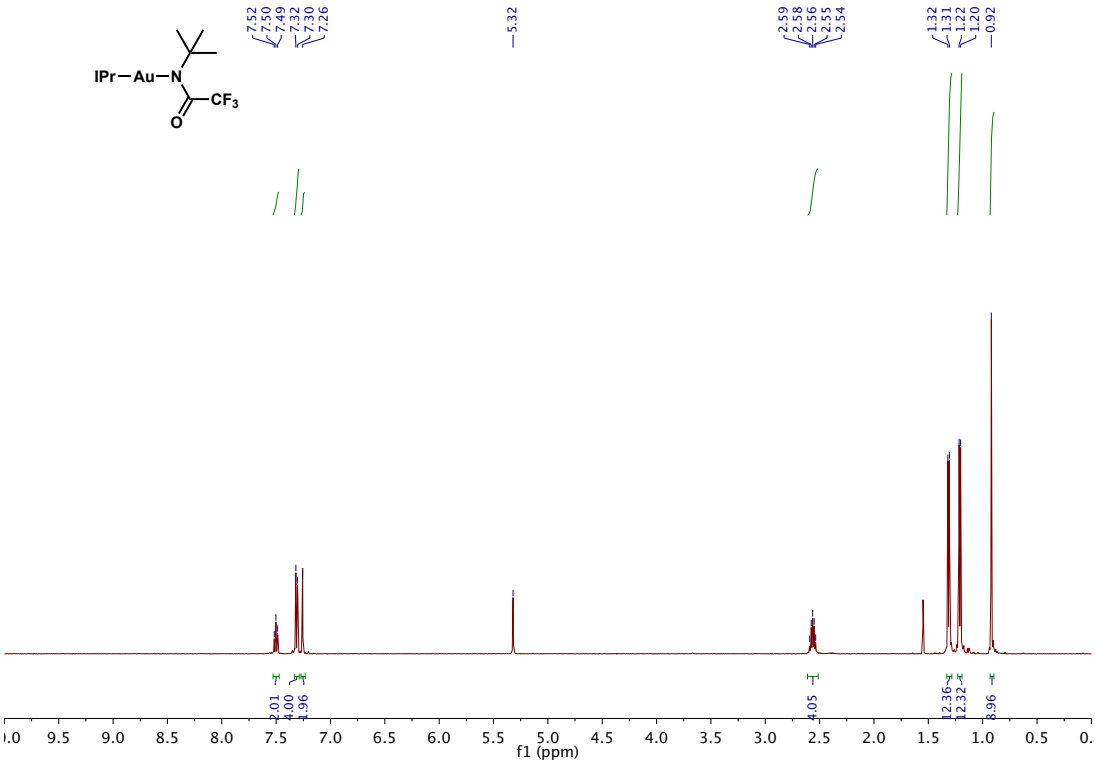

Figure 3.38 ^{1}H NMR spectrum of **S6**

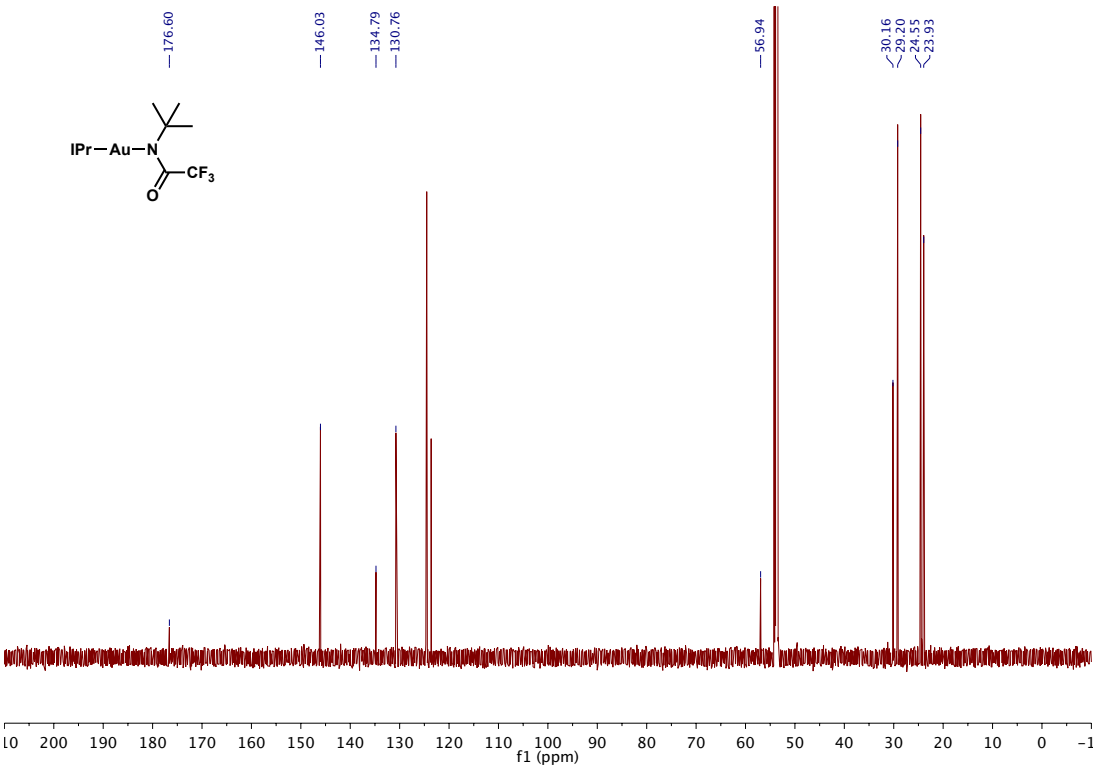

Figure 3.39 ^{13}C NMR spectrum of **S6**

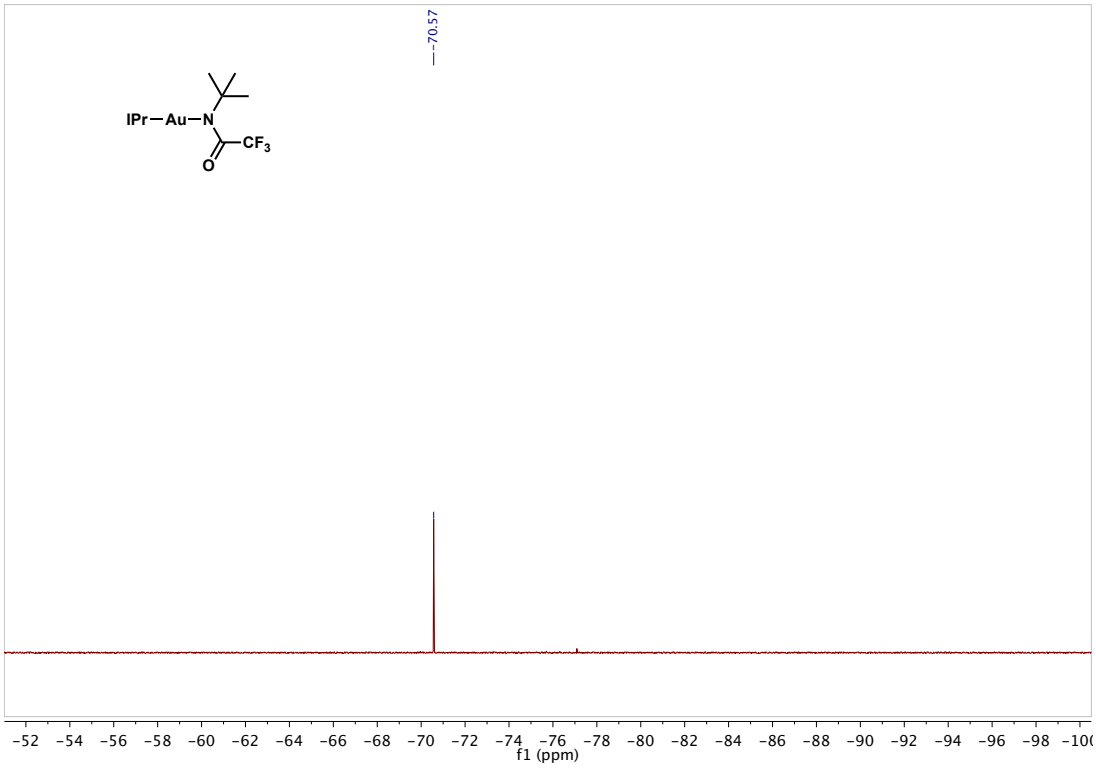

Figure 3.40 ^{19}F NMR spectrum of **S6**

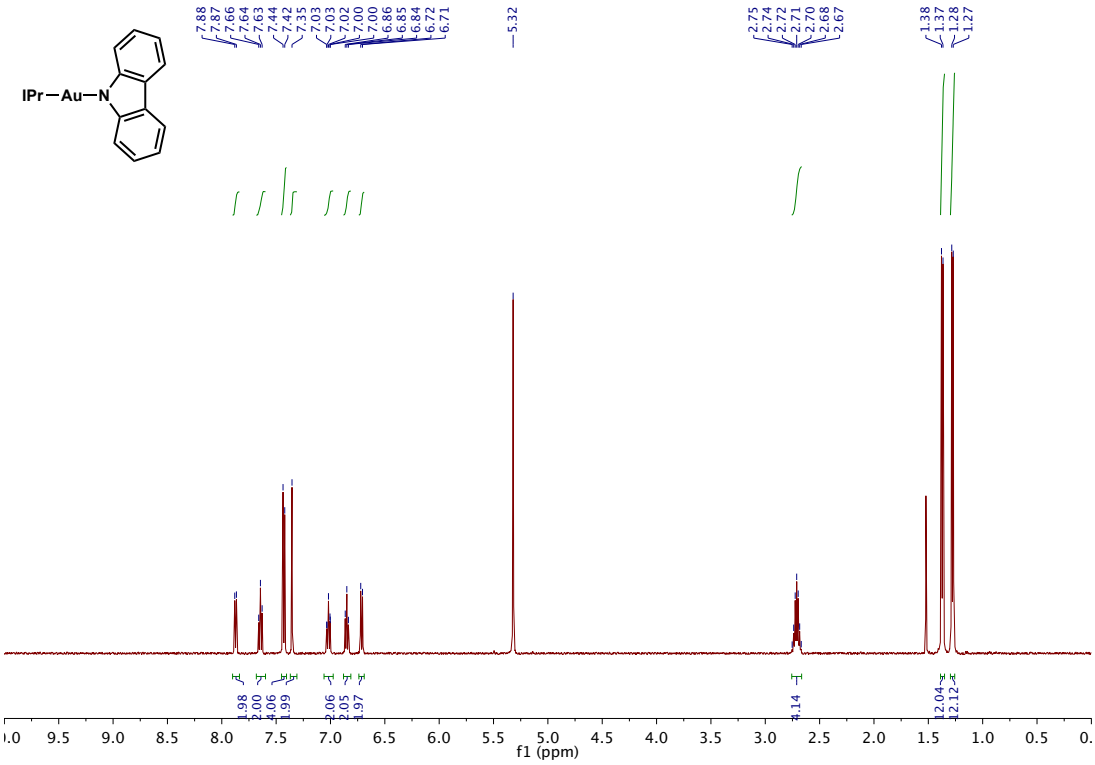

Figure 3.41 ^{1}H NMR spectrum of **S7**

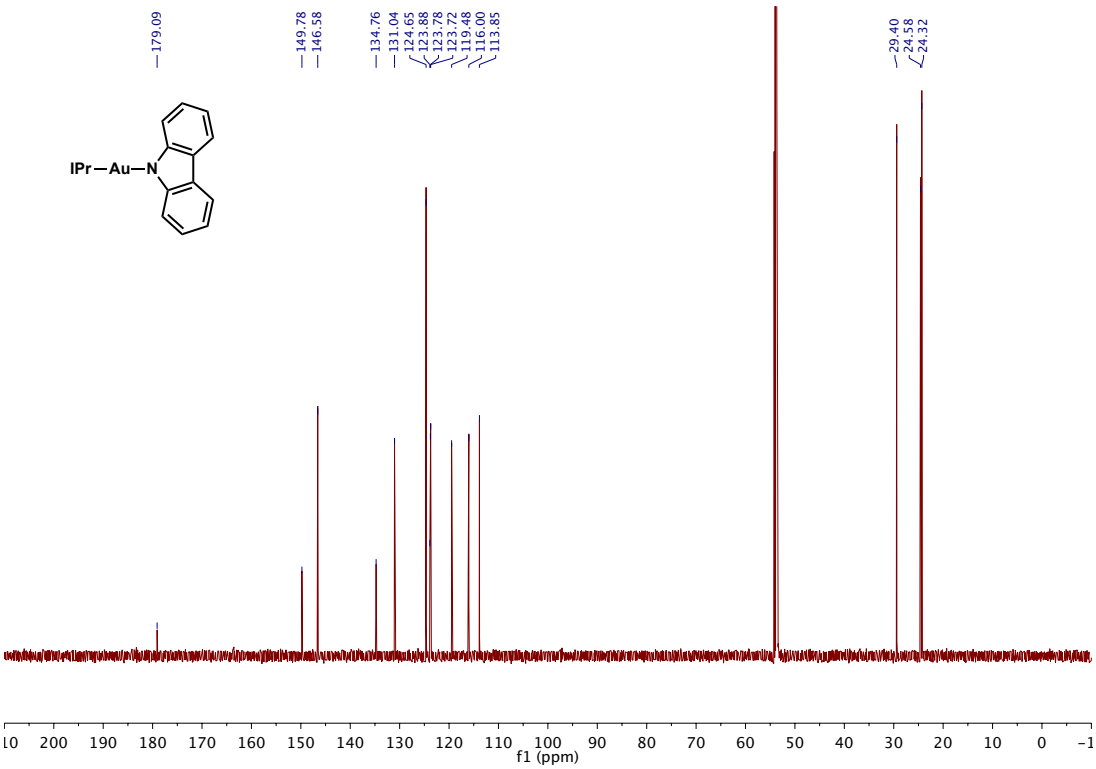

Figure 3.42 ^{13}C NMR spectrum of **S7**

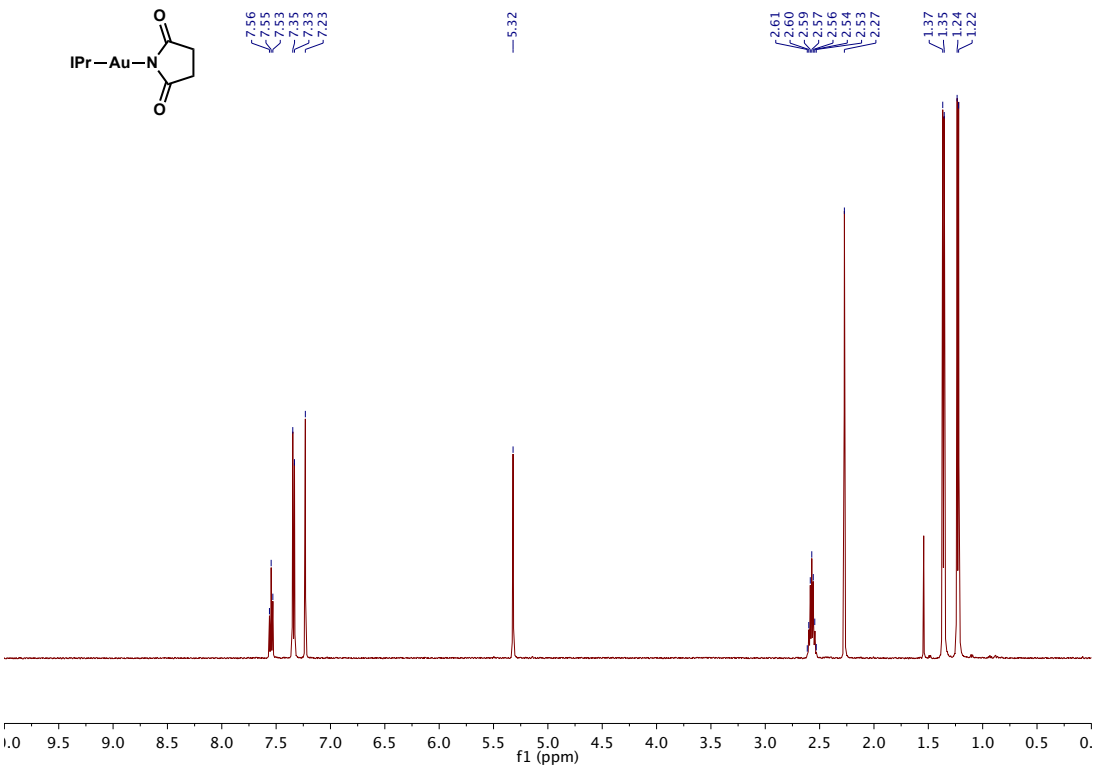

Figure 3.43 ^{1}H NMR spectrum of **5**

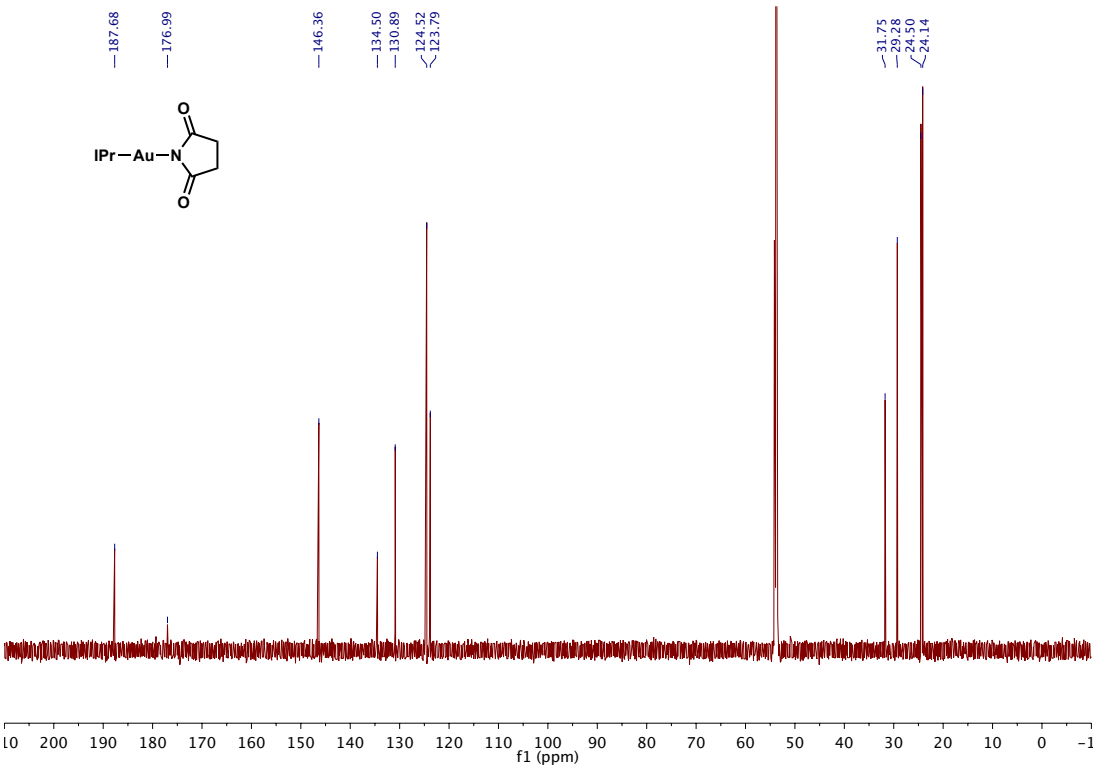

Figure 3.44 ^{13}C NMR spectrum of **5**

3.5.14 Crystallographic Data

Table 3.5 Crystal data and structure refinement for **3**-BF_4.

Identification code	ch_sk_0104
Empirical formula	$C_{35}H_{48}AuBCl_2F_7N_3O_5$
Formula weight	1002.44
Temperature	100(2) K
Wavelength	0.71073 Å
Crystal system	Orthorhombic
Space group	P 2_1 2_1 2_1
Unit cell dimensions	a = 10.0952(2) Å α = 90°.
	b = 13.0588(3) Å β = 90°.
	c = 31.2002(8) Å γ = 90°.
Volume	4113.1(6) $Å^3$
Z	4
Density	1.619 Mg/m^3
Absorption coefficient	3.781 mm^{-1}
F(000)	2000
Crystal size	0.08 × 0.04 × 0.02 mm^3
Theta range for data collection	3.188° to 26.3681°
Index ranges	−12<=h<=12,
	−16<=k<=16,
	−39<=l<=39
Reflections collected	61611
Independent reflections	8391 [R(int) = 0.0574]
Completeness to theta = 25.242°	99.7 %
Absorption correction	Semi-empirical from equivalents
Max. and min. transmission	1.000 and 0.6105
Refinement method	Full-matrix least-squares on F^2
Data / restraints / parameters	8391 / 10 / 525
Goodness-of-fit on F^2	1.030

Final R indices [I>2sigma(I)]	R1 = 0.0228, wR2 = 0.0484
R indices (all data)	R1 = 0.0245, wR2 = 0.0488
Absolute structure parameter	−0.008(3)
Extinction coefficient	n/a
Largest diff. peak and hole	1.001 and −0.799 e.Å^{-3}

Table 3.6 Atomic coordinates (Å x 10^4) and equivalent isotropic displacement parameters (Å^2 x 10^3) for **3**-BF_4. U(eq) is defined as one third of the trace of the orthogonalized U^{ij} tensor.

	x	y	z	U(eq)
C(1)	6276(5)	3921(3)	3734(2)	24(1)
C(2)	4222(6)	2795(3)	3366(1)	18(1)
C(3)	4383(6)	1843(3)	3564(2)	23(1)
C(4)	4448(5)	970(4)	3309(2)	30(1)
C(5)	4364(5)	1072(4)	2870(2)	28(1)
C(6)	4201(6)	2008(4)	2671(2)	25(1)
C(7)	4124(5)	2878(3)	2926(2)	20(1)
C(8)	2197(4)	4234(3)	3732(2)	13(1)
C(9)	175(5)	4193(4)	4033(2)	18(1)
C(10)	198(5)	4980(3)	3758(2)	17(1)
C(11)	1799(5)	5612(3)	3194(2)	14(1)
C(12)	1694(5)	5137(4)	2793(2)	18(1)
C(13)	1452(7)	3569(4)	2305(2)	34(1)
C(14)	1066(5)	4096(4)	2729(2)	24(1)
C(15)	-450(6)	4186(5)	2749(2)	35(1)
C(16)	2107(5)	5711(4)	2440(2)	22(1)
C(17)	2541(5)	6711(4)	2483(2)	24(1)
C(18)	2569(5)	7162(4)	2881(2)	22(1)
C(19)	2193(5)	6628(4)	3251(2)	18(1)
C(20)	3426(6)	7793(4)	3763(2)	36(1)
C(21)	2153(5)	7184(3)	3679(2)	23(1)
C(22)	925(6)	7883(4)	3696(2)	36(1)
C(23)	1734(5)	2733(4)	4195(2)	16(1)

C(24)	1278(5)	1868(4)	3979(2)	18(1)
C(25)	907(6)	1318(4)	3208(2)	30(1)
C(26)	365(5)	1914(4)	3595(2)	22(1)
C(27)	-1010(5)	1527(4)	3716(2)	30(1)
C(28)	1665(5)	909(4)	4145(2)	24(1)
C(29)	2444(5)	838(4)	4505(2)	26(1)
C(30)	2842(6)	1721(4)	4717(2)	25(1)
C(31)	2501(5)	2690(4)	4569(2)	19(1)
C(32)	4304(7)	3648(5)	4969(2)	37(1)
C(33)	2857(6)	3644(4)	4821(2)	24(1)
C(34)	1918(6)	3762(4)	5201(2)	31(1)
C(35)	7089(8)	8020(5)	3986(2)	54(2)
Au(1)	4240(1)	4085(1)	3714(1)	13(1)
B(1)	-564(8)	6642(6)	4864(2)	38(2)
Cl(1)	6928(2)	9260(1)	3786(1)	70(1)
Cl(2)	7113(2)	7109(1)	3564(1)	48(1)
F(1)	6889(3)	4800(3)	3830(2)	52(1)
F(2)	6866(3)	3581(3)	3377(1)	34(1)
F(3)	6645(4)	3263(3)	4047(1)	48(1)
F(4)	266(4)	5913(5)	5017(2)	95(2)
F(5)	125(5)	7544(3)	4788(2)	67(1)
F(6)	-1585(4)	6820(3)	5154(1)	45(1)
F(7)	-1109(4)	6338(4)	4489(2)	74(2)
N(1)	1440(4)	5002(3)	3571(1)	14(1)
N(2)	1409(4)	3728(3)	4014(1)	13(1)
N(3)	4465(5)	148(4)	2600(2)	38(1)
O(1)	4359(4)	5447(3)	4069(1)	23(1)
O(2)	4503(5)	259(3)	2210(2)	50(1)
O(1W)	6162(5)	5980(5)	4616(2)	53(1)
O(3)	4518(6)	-685(3)	2786(2)	64(2)
O(2W)	2788(5)	6128(4)	4680(2)	42(1)

Table 3.7 Bond lengths [Å] and angles [º] for **3**-BF_4.

C(1)-F(1)	1.338(6)	C(18)-C(19)	1.401(7)
C(1)-F(2)	1.339(6)	C(19)-C(21)	1.518(7)
C(1)-F(3)	1.354(7)	C(20)-C(21)	1.534(7)
C(1)-Au(1)	2.067(5)	C(21)-C(22)	1.541(7)
C(2)-C(7)	1.381(7)	C(23)-C(24)	1.394(7)
C(2)-C(3)	1.399(6)	C(23)-C(31)	1.402(7)
C(2)-Au(1)	2.003(4)	C(23)-N(2)	1.454(6)
C(3)-C(4)	1.392(7)	C(24)-C(28)	1.411(7)
C(4)-C(5)	1.377(8)	C(24)-C(26)	1.512(7)
C(5)-C(6)	1.381(7)	C(25)-C(26)	1.536(7)
C(5)-N(3)	1.477(6)	C(26)-C(27)	1.525(7)
C(6)-C(7)	1.389(7)	C(28)-C(29)	1.375(7)
C(8)-N(2)	1.357(6)	C(29)-C(30)	1.388(8)
C(8)-N(1)	1.357(6)	C(30)-C(31)	1.390(7)
C(8)-Au(1)	2.072(4)	C(31)-C(33)	1.516(7)
C(9)-C(10)	1.339(7)	C(32)-C(33)	1.532(8)
C(9)-N(2)	1.387(6)	C(33)-C(34)	1.526(8)
C(10)-N(1)	1.382(6)	C(35)-Cl(1)	1.744(7)
C(11)-C(19)	1.397(7)	C(35)-Cl(2)	1.776(8)
C(11)-C(12)	1.399(7)	Au(1)-O(1)	2.100(3)
C(11)-N(1)	1.469(6)	B(1)-F(7)	1.352(9)
C(12)-C(16)	1.395(7)	B(1)-F(4)	1.356(9)
C(12)-C(14)	1.514(7)	B(1)-F(5)	1.388(8)
C(13)-C(14)	1.539(7)	B(1)-F(6)	1.392(9)
C(14)-C(15)	1.536(8)	N(3)-O(2)	1.224(7)
C(16)-C(17)	1.384(8)	N(3)-O(3)	1.235(7)
C(17)-C(18)	1.376(8)		

F(1)-C(1)-F(2)	105.4(4)	C(24)-C(23)-N(2)	117.5(4)
F(1)-C(1)-F(3)	104.8(5)	C(31)-C(23)-N(2)	118.9(4)
F(2)-C(1)-F(3)	105.5(4)	C(23)-C(24)-C(28)	116.7(5)
F(1)-C(1)-Au(1)	112.3(3)	C(23)-C(24)-C(26)	123.5(4)
F(2)-C(1)-Au(1)	116.8(4)	C(28)-C(24)-C(26)	119.7(4)
F(3)-C(1)-Au(1)	111.2(3)	C(24)-C(26)-C(27)	110.3(4)

C(7)-C(2)-C(3)	121.2(4)	C(24)-C(26)-C(25)	112.6(4)
C(7)-C(2)-Au(1)	118.3(3)	C(27)-C(26)-C(25)	110.5(4)
C(3)-C(2)-Au(1)	120.4(3)	C(29)-C(28)-C(24)	121.3(5)
C(4)-C(3)-C(2)	118.7(5)	C(28)-C(29)-C(30)	119.9(5)
C(5)-C(4)-C(3)	119.1(5)	C(29)-C(30)-C(31)	121.8(5)
C(4)-C(5)-C(6)	122.7(5)	C(30)-C(31)-C(23)	116.7(5)
C(4)-C(5)-N(3)	119.0(5)	C(30)-C(31)-C(33)	121.2(5)
C(6)-C(5)-N(3)	118.3(5)	C(23)-C(31)-C(33)	122.0(4)
C(5)-C(6)-C(7)	118.2(5)	C(31)-C(33)-C(34)	109.8(4)
C(2)-C(7)-C(6)	120.1(5)	C(31)-C(33)-C(32)	112.7(5)
N(2)-C(8)-N(1)	105.6(4)	C(34)-C(33)-C(32)	111.0(5)
N(2)-C(8)-Au(1)	123.8(3)	Cl(1)-C(35)-Cl(2)	110.9(4)
N(1)-C(8)-Au(1)	128.3(3)	C(2)-Au(1)-C(1)	86.5(2)
C(10)-C(9)-N(2)	107.1(4)	C(2)-Au(1)-C(8)	94.9(2)
C(9)-C(10)-N(1)	107.5(4)	C(1)-Au(1)-C(8)	176.6(2)
C(19)-C(11)-C(12)	123.9(4)	C(2)-Au(1)-O(1)	177.1(2)
C(19)-C(11)-N(1)	118.8(4)	C(1)-Au(1)-O(1)	90.81(18)
C(12)-C(11)-N(1)	117.2(4)	C(8)-Au(1)-O(1)	87.85(16)
C(16)-C(12)-C(11)	116.4(4)	F(7)-B(1)-F(4)	110.5(7)
C(16)-C(12)-C(14)	120.2(4)	F(7)-B(1)-F(5)	107.7(6)
C(11)-C(12)-C(14)	123.3(4)	F(4)-B(1)-F(5)	110.2(6)
C(12)-C(14)-C(15)	110.0(5)	F(7)-B(1)-F(6)	108.2(6)
C(12)-C(14)-C(13)	114.2(4)	F(4)-B(1)-F(6)	110.2(6)
C(15)-C(14)-C(13)	108.8(4)	F(5)-B(1)-F(6)	109.9(6)
C(17)-C(16)-C(12)	121.7(5)	C(8)-N(1)-C(10)	109.9(4)
C(18)-C(17)-C(16)	119.8(5)	C(8)-N(1)-C(11)	124.0(4)
C(17)-C(18)-C(19)	121.8(5)	C(10)-N(1)-C(11)	124.9(4)
C(11)-C(19)-C(18)	116.3(5)	C(8)-N(2)-C(9)	109.9(4)
C(11)-C(19)-C(21)	124.0(5)	C(8)-N(2)-C(23)	123.7(4)
C(18)-C(19)-C(21)	119.5(4)	C(9)-N(2)-C(23)	125.3(4)
C(19)-C(21)-C(20)	112.1(5)	O(2)-N(3)-O(3)	124.8(5)
C(19)-C(21)-C(22)	109.6(5)	O(2)-N(3)-C(5)	118.3(5)
C(20)-C(21)-C(22)	111.1(4)	O(3)-N(3)-C(5)	116.9(5)
C(24)-C(23)-C(31)	123.6(5)		

Table 3.8 Crystal data and structure refinement for **7**-BF_4.

Identification code	sk_h070
Empirical formula	$C_{38}H_{52.73}AuBCl_2F_4N_4O_{7.37}$
Formula weight	1038.19
Temperature	100(2) K
Wavelength	0.71073 Å
Crystal system	Triclinic
Space group	P −1
Unit cell dimensions	a = 12.4200(6) Å α = 77.775(2)°.
	b = 2.6660(6) Å β = 89.028(2)°.
	c = 14.5678(8) Å γ = 86.844(2)°.
Volume	2236.3(2) $Å^3$
Z	2
Density	1.542 Mg/m^3
Absorption coefficient	3.475 mm^{-1}
F(000)	1043
Crystal size	0.24 × 0.08 × 0.04 mm^3
Theta range for data collection	1.430° to 25.404°
Index ranges	−14<=h<=14,
	−15<=k<=13,
	−16<=l<=17
Reflections collected	32879
Independent reflections	8124 [R(int) = 0.0325]
Completeness to theta = 25.000°	99.2 %
Absorption correction	None
Max. and min. transmission	1.000 and 0.6105
Refinement method	Full-matrix least-squares on F^2
Data / restraints / parameters	8124 / 0 / 569
Goodness-of-fit on F^2	1.051
Final R indices [I>2sigma(I)]	R1 = 0.0260, wR2 = 0.0551
R indices (all data)	R1 = 0.0308, wR2 = 0.0565

Extinction coefficient	n/a
Largest diff. peak and hole	1.018 and −0.838 e.Å^{-3}

Table 3.9 Atomic coordinates (Å x 10^4) and equivalent isotropic displacement parameters (Å^2 x 10^3) for **7**-BF_4. U(eq) is defined as one third of the trace of the orthogonalized U^{ij} tensor

	x	y	z	U(eq)
C(1)	2804(3)	2991(3)	8010(2)	18(1)
C(2)	2141(3)	1787(3)	6532(3)	23(1)
C(3)	1120(3)	1408(3)	6612(3)	28(1)
C(4)	937(3)	407(3)	6399(3)	34(1)
C(5)	1798(3)	-167(3)	6104(3)	33(1)
C(6)	2828(3)	197(3)	6006(3)	37(1)
C(7)	2992(3)	1186(3)	6220(3)	33(1)
C(8)	943(3)	3818(3)	4955(2)	23(1)
C(9)	934(3)	4143(3)	3899(3)	30(1)
C(10)	2111(3)	4366(3)	3635(3)	35(1)
C(11)	2718(3)	4021(3)	4549(3)	26(1)
C(12)	2980(3)	3273(3)	9468(2)	21(1)
C(13)	3724(3)	2502(3)	9360(3)	23(1)
C(14)	1466(3)	4324(3)	8538(2)	21(1)
C(15)	445(3)	3901(3)	8563(2)	25(1)
C(16)	-757(3)	2455(4)	8240(4)	54(1)
C(17)	300(3)	2699(3)	8656(3)	33(1)
C(18)	388(4)	2105(3)	9692(3)	44(1)
C(19)	-441(3)	4621(3)	8570(3)	31(1)
C(20)	-314(3)	5698(3)	8556(3)	32(1)
C(21)	703(3)	6096(3)	8523(3)	30(1)
C(22)	1629(3)	5418(3)	8517(2)	21(1)
C(23)	2839(3)	6899(3)	7750(3)	31(1)
C(24)	2735(3)	5874(3)	8525(3)	23(1)
C(25)	2962(3)	6125(3)	9487(3)	31(1)
C(26)	4180(3)	1439(3)	8142(2)	21(1)

C(27)	3830(3)	398(3)	8505(3)	24(1)
C(28)	2054(3)	-477(3)	8868(3)	38(1)
C(29)	2914(3)	166(3)	9212(3)	28(1)
C(30)	3333(4)	-433(4)	10175(3)	46(1)
C(31)	4400(3)	-454(3)	8218(3)	33(1)
C(32)	5268(3)	-272(3)	7603(3)	38(1)
C(33)	5590(3)	769(3)	7268(3)	36(1)
C(34)	5058(3)	1652(3)	7530(3)	27(1)
C(35)	5906(4)	2985(4)	6211(3)	51(1)
C(36)	5433(3)	2791(3)	7197(3)	30(1)
C(37)	6235(4)	3032(4)	7901(4)	57(1)
C(38)	1653(6)	1541(5)	2658(4)	88(2)
B(1)	6038(3)	6572(3)	8232(3)	27(1)
N(1)	1981(2)	3727(2)	5266(2)	19(1)
N(2)	2409(2)	3573(2)	8630(2)	18(1)
N(3)	3604(2)	2325(2)	8459(2)	19(1)
N(4)	1602(3)	-1207(3)	5842(3)	42(1)
O(1)	2684(2)	4936(2)	6589(2)	21(1)
O(2)	162(2)	3663(2)	5479(2)	26(1)
O(1W)	1875(2)	6270(2)	5142(2)	28(1)
O(3)	3677(2)	4007(2)	4683(2)	35(1)
O(2W)	4651(2)	5433(3)	6583(3)	40(1)
O(4)	736(3)	-1606(3)	6052(3)	67(1)
O(5)	2330(3)	-1613(2)	5425(2)	50(1)
F(1)	5468(2)	5646(2)	8274(2)	42(1)
F(2)	5574(2)	7185(2)	8823(2)	38(1)
F(3)	7103(2)	6256(2)	8495(2)	38(1)
F(4)	6029(2)	7163(2)	7309(2)	41(1)
Cl(1)	2030(2)	1057(3)	3786(1)	73(1)
Cl(2)	1449(3)	590(2)	2020(2)	90(1)
Au(1)	2401(1)	3315(1)	6637(1)	16(1)
Cl(2A)	805(7)	959(7)	1918(5)	54(2)
Cl(1A)	2024(8)	414(12)	3699(8)	73(1)
O(3W)	4972(10)	-1567(10)	5606(9)	101(6)

Table 3.10 Bond lengths [Å] and angles [°] for **7**-BF_4.

C(1)-N(3)	1.350(4)	C(24)-H(24)	1.0000
C(1)-N(2)	1.352(4)	C(25)-H(25A)	0.9800
C(1)-Au(1)	2.021(3)	C(25)-H(25B)	0.9800
C(2)-C(3)	1.374(5)	C(25)-H(25C)	0.9800
C(2)-C(7)	1.394(5)	C(26)-C(34)	1.397(5)
C(2)-Au(1)	2.018(3)	C(26)-C(27)	1.402(5)
C(3)-C(4)	1.399(5)	C(26)-N(3)	1.451(4)
C(3)-H(3)	0.9500	C(27)-C(31)	1.392(5)
C(4)-C(5)	1.374(6)	C(27)-C(29)	1.521(5)
C(4)-H(4)	0.9500	C(28)-C(29)	1.531(5)
C(5)-C(6)	1.378(6)	C(28)-H(28A)	0.9800
C(5)-N(4)	1.480(5)	C(28)-H(28B)	0.9800
C(6)-C(7)	1.380(5)	C(28)-H(28C)	0.9800
C(6)-H(6)	0.9500	C(29)-C(30)	1.531(5)
C(7)-H(7)	0.9500	C(29)-H(29)	1.0000
C(8)-O(2)	1.222(4)	C(30)-H(30A)	0.9800
C(8)-N(1)	1.364(4)	C(30)-H(30B)	0.9800
C(8)-C(9)	1.506(5)	C(30)-H(30C)	0.9800
C(9)-C(10)	1.531(5)	C(31)-C(32)	1.387(6)
C(9)-H(9A)	0.9900	C(31)-H(31)	0.9500
C(9)-H(9B)	0.9900	C(32)-C(33)	1.384(6)
C(10)-C(11)	1.512(5)	C(32)-H(32)	0.9500
C(10)-H(10A)	0.9900	C(33)-C(34)	1.387(5)
C(10)-H(10B)	0.9900	C(33)-H(33)	0.9500
C(11)-O(3)	1.209(4)	C(34)-C(36)	1.518(5)
C(11)-N(1)	1.382(5)	C(35)-C(36)	1.518(6)
C(12)-C(13)	1.339(5)	C(35)-H(35A)	0.9800
C(12)-N(2)	1.393(4)	C(35)-H(35A)	0.9800
C(12)-H(12)	0.9500	C(35)-H(35B)	0.9800
C(13)-N(3)	1.388(4)	C(35)-H(35C)	0.9800
C(13)-H(13)	0.9500	C(36)-C(37)	1.529(6)

C(14)-C(15)	1.400(5)	C(36)-H(36)	1.0000
C(14)-C(22)	1.406(5)	C(37)-H(37A)	0.9800
C(14)-N(2)	1.457(4)	C(37)-H(37B)	0.9800
C(15)-C(19)	1.391(5)	C(37)-H(37C)	0.9800
C(15)-C(17)	1.521(5)	C(38)-Cl(1)	1.692(6)
C(16)-C(17)	1.529(5)	C(38)-Cl(2)	1.701(7)
C(16)-H(16A)	0.9800	C(38)-Cl(2A)	1.810(10)
C(16)-H(16B)	0.9800	C(38)-Cl(1A)	1.893(12)
C(16)-H(16C)	0.9800	C(38)-H(38A)	0.9900
C(17)-C(18)	1.540(6)	C(38)-H(38B)	0.9900
C(17)-H(17)	1.0000	C(38)-H(38C)	0.9900
C(18)-H(18A)	0.9800	C(38)-H(38D)	0.9900
C(18)-H(18B)	0.9800	B(1)-F(2)	1.376(5)
C(18)-H(18C)	0.9800	B(1)-F(4)	1.393(5)
C(19)-C(20)	1.378(6)	B(1)-F(1)	1.393(5)
C(19)-H(19)	0.9500	B(1)-F(3)	1.396(5)
C(20)-C(21)	1.382(5)	N(1)-Au(1)	2.024(3)
C(20)-H(20)	0.9500	N(4)-O(4)	1.220(5)
C(21)-C(22)	1.398(5)	N(4)-O(5)	1.230(5)
C(21)-H(21)	0.9500	O(1)-Au(1)	2.088(2)
C(22)-C(24)	1.521(5)	O(1)-H(1)	0.94(4)
C(23)-C(24)	1.539(5)	O(1)-H(2)	0.94(5)
C(23)-H(23A)	0.9800	O(1W)-H(1WA)	0.92(5)
C(23)-H(23B)	0.9800	O(1W)-H(1WB)	0.79(5)
C(23)-H(23C)	0.9800	O(2W)-H(2WB)	0.80(5)
C(24)-C(25)	1.535(5)	O(2W)-H(2WA)	0.79(6)

N(3)-C(1)-N(2)	106.1(3)	H(25A)-C(25)-H(25C)	109.5
N(3)-C(1)-Au(1)	129.4(3)	H(25B)-C(25)-H(25C)	109.5
N(2)-C(1)-Au(1)	123.6(2)	C(34)-C(26)-C(27)	123.9(3)
C(3)-C(2)-C(7)	120.2(3)	C(34)-C(26)-N(3)	119.5(3)
C(3)-C(2)-Au(1)	121.1(3)	C(27)-C(26)-N(3)	116.6(3)
C(7)-C(2)-Au(1)	117.8(3)	C(31)-C(27)-C(26)	116.6(3)
C(2)-C(3)-C(4)	120.0(4)	C(31)-C(27)-C(29)	119.8(3)

C(2)-C(3)-H(3)	120.0	C(26)-C(27)-C(29)	123.5(3)
C(4)-C(3)-H(3)	120.0	C(29)-C(28)-H(28A)	109.5
C(5)-C(4)-C(3)	118.2(4)	C(29)-C(28)-H(28B)	109.5
C(5)-C(4)-H(4)	120.9	H(28A)-C(28)-H(28B)	109.5
C(3)-C(4)-H(4)	120.9	C(29)-C(28)-H(28C)	109.5
C(4)-C(5)-C(6)	123.2(3)	H(28A)-C(28)-H(28C)	109.5
C(4)-C(5)-N(4)	118.5(4)	H(28B)-C(28)-H(28C)	109.5
C(6)-C(5)-N(4)	118.3(4)	C(27)-C(29)-C(28)	111.4(3)
C(5)-C(6)-C(7)	117.8(4)	C(27)-C(29)-C(30)	111.2(3)
C(5)-C(6)-H(6)	121.1	C(28)-C(29)-C(30)	110.2(3)
C(7)-C(6)-H(6)	121.1	C(27)-C(29)-H(29)	107.9
C(6)-C(7)-C(2)	120.7(4)	C(28)-C(29)-H(29)	107.9
C(6)-C(7)-H(7)	119.7	C(30)-C(29)-H(29)	107.9
C(2)-C(7)-H(7)	119.7	C(29)-C(30)-H(30A)	109.5
O(2)-C(8)-N(1)	123.4(3)	C(29)-C(30)-H(30B)	109.5
O(2)-C(8)-C(9)	127.1(3)	H(30A)-C(30)-H(30B)	109.5
N(1)-C(8)-C(9)	109.5(3)	C(29)-C(30)-H(30C)	109.5
C(8)-C(9)-C(10)	104.1(3)	H(30A)-C(30)-H(30C)	109.5
C(8)-C(9)-H(9A)	110.9	H(30B)-C(30)-H(30C)	109.5
C(10)-C(9)-H(9A)	110.9	C(32)-C(31)-C(27)	121.1(4)
C(8)-C(9)-H(9B)	110.9	C(32)-C(31)-H(31)	119.4
C(10)-C(9)-H(9B)	110.9	C(27)-C(31)-H(31)	119.4
H(9A)-C(9)-H(9B)	109.0	C(33)-C(32)-C(31)	120.3(4)
C(11)-C(10)-C(9)	104.6(3)	C(33)-C(32)-H(32)	119.9
C(11)-C(10)-H(10A)	110.8	C(31)-C(32)-H(32)	119.9
C(9)-C(10)-H(10A)	110.8	C(32)-C(33)-C(34)	121.3(4)
C(11)-C(10)-H(10B)	110.8	C(32)-C(33)-H(33)	119.3
C(9)-C(10)-H(10B)	110.8	C(34)-C(33)-H(33)	119.3
H(10A)-C(10)-H(10B)	108.9	C(33)-C(34)-C(26)	116.8(3)
O(3)-C(11)-N(1)	122.8(3)	C(33)-C(34)-C(36)	121.7(3)
O(3)-C(11)-C(10)	128.7(3)	C(26)-C(34)-C(36)	121.5(3)
N(1)-C(11)-C(10)	108.5(3)	C(36)-C(35)-H(35A)	109.5
C(13)-C(12)-N(2)	107.3(3)	C(36)-C(35)-H(35B)	109.5
C(13)-C(12)-H(12)	126.4	H(35A)-C(35)-H(35B)	109.5

N(2)-C(12)-H(12)	126.4	C(36)-C(35)-H(35C)	109.5
C(12)-C(13)-N(3)	107.0(3)	H(35A)-C(35)-H(35C)	109.5
C(12)-C(13)-H(13)	126.5	H(35B)-C(35)-H(35C)	109.5
N(3)-C(13)-H(13)	126.5	C(35)-C(36)-C(34)	112.9(3)
C(15)-C(14)-C(22)	123.5(3)	C(35)-C(36)-C(37)	111.4(4)
C(15)-C(14)-N(2)	118.2(3)	C(34)-C(36)-C(37)	109.5(3)
C(22)-C(14)-N(2)	118.0(3)	C(35)-C(36)-H(36)	107.6
C(19)-C(15)-C(14)	116.9(3)	C(34)-C(36)-H(36)	107.6
C(19)-C(15)-C(17)	120.9(3)	C(37)-C(36)-H(36)	107.6
C(14)-C(15)-C(17)	122.0(3)	C(36)-C(37)-H(37A)	109.5
C(17)-C(16)-H(16A)	109.5	C(36)-C(37)-H(37B)	109.5
C(17)-C(16)-H(16B)	109.5	H(37A)-C(37)-H(37B)	109.5
H(16A)-C(16)-H(16B)	109.5	C(36)-C(37)-H(37C)	109.5
C(17)-C(16)-H(16C)	109.5	H(37A)-C(37)-H(37C)	109.5
H(16A)-C(16)-H(16C)	109.5	H(37B)-C(37)-H(37C)	109.5
H(16B)-C(16)-H(16C)	109.5	Cl(1)-C(38)-Cl(2)	115.6(4)
C(15)-C(17)-C(16)	113.4(4)	Cl(2A)-C(38)-Cl(1A)	106.1(5)
C(15)-C(17)-C(18)	110.4(3)	Cl(1)-C(38)-H(38A)	108.3
C(16)-C(17)-C(18)	110.1(4)	Cl(2)-C(38)-H(38A)	108.8
C(15)-C(17)-H(17)	107.6	Cl(1)-C(38)-H(38B)	108.5
C(16)-C(17)-H(17)	107.6	Cl(2)-C(38)-H(38B)	107.8
C(18)-C(17)-H(17)	107.6	H(38A)-C(38)-H(38B)	107.5
C(17)-C(18)-H(18A)	109.5	Cl(2A)-C(38)-H(38C)	108.7
C(17)-C(18)-H(18B)	109.5	Cl(1A)-C(38)-H(38C)	110.0
H(18A)-C(18)-H(18B)	109.5	Cl(2A)-C(38)-H(38D)	111.8
C(17)-C(18)-H(18C)	109.5	Cl(1A)-C(38)-H(38D)	111.4
H(18A)-C(18)-H(18C)	109.5	H(38C)-C(38)-H(38D)	108.8
H(18B)-C(18)-H(18C)	109.5	F(2)-B(1)-F(4)	110.3(3)
C(20)-C(19)-C(15)	121.3(3)	F(2)-B(1)-F(1)	110.0(3)
C(20)-C(19)-H(19)	119.4	F(4)-B(1)-F(1)	108.7(3)
C(15)-C(19)-H(19)	119.4	F(2)-B(1)-F(3)	110.3(3)
C(19)-C(20)-C(21)	120.6(3)	F(4)-B(1)-F(3)	108.9(3)
C(19)-C(20)-H(20)	119.7	F(1)-B(1)-F(3)	108.5(3)
C(21)-C(20)-H(20)	119.7	C(8)-N(1)-C(11)	112.8(3)

C(20)-C(21)-C(22)	121.2(4)	C(8)-N(1)-Au(1)	124.1(2)
C(20)-C(21)-H(21)	119.4	C(11)-N(1)-Au(1)	123.0(2)
C(22)-C(21)-H(21)	119.4	C(1)-N(2)-C(12)	109.6(3)
C(21)-C(22)-C(14)	116.5(3)	C(1)-N(2)-C(14)	128.5(3)
C(21)-C(22)-C(24)	119.7(3)	C(12)-N(2)-C(14)	121.6(3)
C(14)-C(22)-C(24)	123.8(3)	C(1)-N(3)-C(13)	110.1(3)
C(24)-C(23)-H(23A)	109.5	C(1)-N(3)-C(26)	127.3(3)
C(24)-C(23)-H(23A)	109.5	C(13)-N(3)-C(26)	122.1(3)
C(24)-C(23)-H(23B)	109.5	O(4)-N(4)-O(5)	124.3(4)
H(23A)-C(23)-H(23B)	109.5	O(4)-N(4)-C(5)	118.2(4)
C(24)-C(23)-H(23C)	109.5	O(5)-N(4)-C(5)	117.4(4)
H(23A)-C(23)-H(23C)	109.5	Au(1)-O(1)-H(1)	118(2)
H(23B)-C(23)-H(23C)	109.5	Au(1)-O(1)-H(2)	112(3)
C(22)-C(24)-C(25)	110.8(3)	H(1)-O(1)-H(2)	101(4)
C(22)-C(24)-C(23)	111.4(3)	H(1WA)-O(1W)-H(1WB)	108(4)
C(25)-C(24)-C(23)	109.9(3)	H(2WB)-O(2W)-H(2WA)	112(5)
C(22)-C(24)-H(24)	108.3	C(2)-Au(1)-C(1)	97.56(13)
C(25)-C(24)-H(24)	108.3	C(2)-Au(1)-N(1)	85.42(12)
C(23)-C(24)-H(24)	108.3	C(1)-Au(1)-N(1)	176.85(12)
C(24)-C(25)-H(25A)	109.5	C(2)-Au(1)-O(1)	173.85(12)
C(24)-C(25)-H(25B)	109.5	C(1)-Au(1)-O(1)	88.28(12)
H(25A)-C(25)-H(25B)	109.5	N(1)-Au(1)-O(1)	88.77(10)
C(24)-C(25)-H(25C)	109.5		